Herstellung und physikochemische Charakterisierung von planaren gestützten Lipid-Modellmembran Systemen

Dissertation zur Erlangung des Grades
„Doktor der Naturwissenschaften“

am Fachbereich Chemie und Pharmazie
der Johannes Gutenberg-Universität
Mainz

vorgelegt von
Tobias Baumgart
geboren in Osnabrück

Mainz 2001

Preparation and Physicochemical Characterisation of Planar Supported Lipid Model Membrane Systems

Thesis submitted to obtain the degree
„Doktor der Naturwissenschaften“

Fachbereich Chemie und Pharmazie
Johannes Gutenberg-Universität
Mainz

Tobias Baumgart
born in Osnabrück

Mainz 2001

ITHACA

When you set out on your journey to Ithaca,
pray that the road is long,
full of adventure, full of knowledge.
The Lestrygonians and the Cyclops,
the angry Poseidon -- do not fear them:
You will never find such as these on your path,
if your thoughts remain lofty, if a fine
emotion touches your spirit and your body.
The Lestrygonians and the Cyclops,
the fierce Poseidon you will never encounter,
if you do not carry them within your soul,
if your soul does not set them up before you.

Pray that the road is long.
That the summer mornings are many, when,
with such pleasure, with such joy
you will enter ports seen for the first time;
stop at Phoenician markets,
and purchase fine merchandise,
mother-of-pearl and coral, amber and ebony,
and sensual perfumes of all kinds,
as many sensual perfumes as you can;
visit many Egyptian cities,
to learn and learn from scholars.

Always keep Ithaca in your mind.
To arrive there is your ultimate goal.
But do not hurry the voyage at all.
It is better to let it last for many years;
and to anchor at the island when you are old,
rich with all you have gained on the way,
not expecting that Ithaca will offer you riches.

Ithaca has given you the beautiful voyage.
Without her you would have never set out on
the road.
She has nothing more to give you.

And if you find her poor, Ithaca has not
deceived you.
Wise as you have become, with so much
experience,
you must already have understood what
Ithacas mean.

Constantine P. Cavafy (1911)

Contents

1 SUMMARY 1

2 INTRODUCTION 3

3 METHODS 11

3.1 FLUORESCENCE RECOVERY AFTER PHOTOBLEACHING (FRAP) AND FLUORESCENCE MICROSCOPY 11
3.1.1 FRAP measurement principle 12
3.1.2 Setup 14
3.1.3 Measurement chamber for studying hydration effects in LB-films 18
3.2 FLUORESCENCE SPECTROSCOPY 20
3.2.1 Introduction 20
3.2.2 Setup 21
3.3 REFLECTION INTERFERENCE CONTRAST MICROSCOPY (RICM) 22
3.3.1 Introduction 22
3.3.2 Influence of illumination- and observation numerical aperture 24
3.3.3 Setup 25
3.4 ELLIPSOMETRY 28
3.4.1 Introduction 28
3.4.2 Setup 30
3.5 GENERATION OF CONTROLLED HUMIDITIES 31
3.5.1 Introduction 31
3.5.2 Methods for adjusting RH 33
3.6 IMPEDANCE SPECTROSCOPY 34
3.6.1 Measurement principle 34
3.6.2 Measurement setup 36
3.7 PH-MEASUREMENTS WITH FIELD-EFFECT TRANSISTORS (EOSFETS) 36
3.7.1 Introduction 37
3.7.2 Measurement setup 38
3.8 AFM-MICROSCOPY 39
3.9 ALPHA STEPPER 39
3.10 PREPARATION TECHNIQUES 40
3.10.1 Substrate cleaning and electrode production 40
3.10.2 Spin-coating 40
3.10.3 Langmuir-Blodgett-trough-techniques 41
3.10.4 Vesicle fusion 44
3.10.5 Preparation of giant multilamellar liposomes 44
3.10.6 Protein reconstitution 45

4 PREPARATION AND CHARACTERISATION OF THIN AND ULTRATHIN POLYSACCHARIDE FILMS 47

4.1 FILM THICKNESS 49
4.2 CHARACTERISATION OF THE FILM SURFACE BY MEANS OF AFM 52
4.3 CONTACT ANGLE MEASUREMENTS 55
4.4 SWELLING EXPERIMENTS 55
4.5 COVALENT COUPLING OF POLYMER LAYERS TO SUBSTRATES 61
4.6 CONCLUSION AND OUTLOOK 61

5 CHARACTERISATION OF SUPPORTED PHOSPHOLIPID MONOLAYER MEMBRANES 63

5.0.1 Forces involved in the membrane/substrate interaction 64
5.0.2 Research on phospholipid membrane hydration 72
5.1 EFFECTS OF THE CONDENSATION OF WATER DROPLETS AT HIGH HUMIDITIES 74
5.1.1 Glass surfaces 74
5.1.2 Chitosan surfaces 76
5.1.3 Conclusion 82
5.2 SPREADING OF LIPID MONOLAYERS ON HYDROPHILIC SUBSTRATES AT HIGH HUMIDITIES 84
5.2.1 Physics of spreading processes 85
5.2.2 Spreading of a Langmuir-Blodgett monolayer with defined lateral pressure 88
5.2.2.1 Spreading of DMPC on chitosan 90
5.2.2.2 Spreading of DSPC, DLPE and DMPC/cholesterol on chitosan 101

5.2.2.3 Spreading of DMPC on different substrates: agarose and glass 102
5.2.3 Spreading from a multilayer lipid reservoir *103*
5.2.4 Conclusion and outlook *105*
5.3 FLUIDITY OF SUPPORTED LIPID MONOLAYERS AS A FUNCTION OF AMBIENT HUMIDITIES AND SOLVENT VARIATION 107
5.3.1 Available theories for lateral self-diffusion in amphiphile membranes *108*
5.3.2 Preliminary experiments *111*
5.3.3 Lateral self-diffusion in phosphatidylcholine monolayers in different hydration states *113*
5.3.4 Variation of the lipid: DLPE and DMPC/cholesterol *125*
5.3.5 Variation of the substrate: agarose and glass *128*
5.3.6 Influence of non-aqueous solvents present in the surrounding gas phase *130*
5.3.7 Conclusion and outlook *132*
5.4 EFFECT OF AMBIENT HUMIDITIES ON THE FLUORESCENCE OF LABELLED LIPID MONOLAYERS 134
5.4.1 Environmental effects on fluorophores *135*
5.4.2 Preliminary remarks *137*
5.4.3 Fluorescence intensity measurements in partially hydrated lipid monolayers *143*
5.4.4 Humidity dependence of fluorescence spectra *150*
5.4.5 Conclusion, discussion and outlook *159*

6 CHARACTERISATION OF POLYMER-SUPPORTED PHOSPHOLIPID BILAYER MEMBRANES 163

6.1 LIPID BILAYER MEMBRANES SUPPORTED BY AGAROSE CUSHIONS 164
6.1.1 Preliminary experiments *165*
6.1.2 Bilayer lipid membranes on agarose cushions, deposited by LB/LS transfer *167*
6.1.3 Concepts to stabilise bilayer lipid membranes on an underlying support *173*
6.1.4 Interaction of the agarose surface with multilamellar giant liposomes *178*
6.1.5 Vesicle fusion experiments on agarose *179*
6.1.6 Spreading of lipid bilayer membranes from a lipid reservoir on agarose *180*
6.2 LIPID BILAYER MEMBRANES SUPPORTED BY CHITOSAN FILMS 181
6.2.1 Homogeneity of bilayers *181*
6.2.2 Lateral diffusion behaviour in chitosan-supported lipid bilayer membranes *184*
6.2.3 Interaction of the chitosan surface with multilamellar giant liposomes *187*
6.2.4 Spreading of lipid bilayer membranes from a lipid reservoir on chitosan *191*
6.2.5 Vesicle fusion experiments on chitosan *194*
6.2.6 Electrical properties of the bilayer lipid membrane/chitosan system *195*
6.3 CONCLUSION, DISCUSSION AND OUTLOOK 198

7 INCORPORATION AND EXAMINATION OF MEMBRANE PROTEINS IN SUPPORTED BILAYER LIPID MEMBRANES 203

7.1 INCORPORATION OF MEMBRANE PROTEINS: ADDITION OF CYTOCHROME C OXIDASE (COX) TO CHITOSAN LIPID MEMBRANES 203
7.2 ANALYSIS OF PROTEIN FUNCTIONALITY BY MEANS OF ION SENSITIVE FIELD-EFFECT TRANSISTORS 205
7.2.1 Self-healing and lateral fluidity of membranes deposited onto FETs *207*
7.2.2 Functional activity of nitrate reductase *208*
7.2.3 Functional activity of H^+-ATPase *210*
7.3 CONCLUSION AND OUTLOOK 212

8 MATERIALS 213

8.1 BILAYER SUPPORT 213
8.1.1 Substrates *213*
8.1.2 Polymers *213*
8.2 LIPIDS 215
8.2.1 Lipids with small headgroups *215*
8.2.2 Lipopolymers *220*
8.3 FLUORESCENCE DYES 221
8.4 PROTEINS 223

9 ABBREVIATIONS 225

10 TABLE OF FIGURES 229

11 LITERATURE 237

1 Summary

Thin polysaccharide films were prepared and characterised in terms of their thickness, roughness and swelling behaviour in humid air and under water. Substrate coating of surfaces by chitosan was shown to be an easy and effective strategy to decouple mono- and bilayer lipid membranes from the underlying support.

Self-repairing effects in supported lipid monolayers were observed and analysed at high humidities. For the first time, a detailed analysis of the spreading dynamics of lipid monolayers on hydrophilic supports at increased humidities was carried out. A simple model was derived which explained the observed time dependence of the spreading process.

Additionally, for the first time, a detailed analysis of the diffusional behaviour of amphiphile monolayers on water swellable substrates (polysaccharide cushions) with respect to the solvent content of the surrounding atmosphere (with an emphasis on water in air) was performed. A physical model was derived which explained the observed behaviour quantitatively.

Furthermore, for the first time, the known environmental sensitivity of the fluorescence probe NBD (7-nitrobenz-2-oxa-1,3-diazole) was used to probe local hydration changes in solid-supported phospholipid monolayer membranes upon changing the osmotic pressure. Variations in the hydration behaviour between different phospholipid headgroups could be resolved. Moreover, the technique allowed the analysis of the influence of the underlying support on the hydration of lipid headgroups. Different supports such as glass, agarose and chitosan were examined.

Polysaccharide cushions were coated with bilayer lipid membranes. Remarkable differences were found in membrane stability on varying supports. The different interactions between bilayer phospholipid membranes and substrates were further demonstrated by reflection interference contrast microscopy (RICM).

Successful bilayer preparations on chitosan polymer cushions were analysed in terms of fluidity of different lipid compositions. A comparison with bilayer membranes on glass revealed an increase of the phase transition temperature on chitosan, as compared to glass. The diffusion behaviour was significantly altered by addition of cholesterol. Bilayer

spreading from a lipid reservoir was observed on chitosan, which indicated self-healing properties of chitosan-supported bilayer lipid membranes.

The possibility to functionalyse chitosan-cushioned phospholipid bilayer membranes was demonstrated by incorporation of a fluorescently labelled integral membrane protein (cytochrome c oxidase, COX). COX was homogeneously incorporated and showed partial recovery after photobleaching of the attached fluorophores due to lateral diffusion.

However, an electrical analysis of protein functionality was complicated by the fact that the obtained membrane resistances were rather poor, while the membrane capacitancies were in the range of those usually obtained with black lipid membranes (BLMs).

The possibility of using ion sensitive field-effect transistors as a tool to determine membrane functionality was demonstrated. For the first time, the activity of H^+-ATPase in an eggPC bilayer membrane resting on the silicon oxide gate of a field-effect transistor was shown.

Additional results from the present work will not be presented in the following, because they have already been published or are about to be published elsewhere. These works include: the vesicle fusion onto laterally mixed thiolipopeptides and the subsequent characterisation by means of electrochemical and fluorescence methods [Baum, 2001]; the analysis of ATPase activity upon incorporation into peptide-supported bilayer membranes [Naum, 2001]; the preparation and characterisation of laterally patterned lithographically polymerised diacetylene lipids both on oxide supports [Mori, 2001b] and on polymer supports such as chitosan and poly(ethyleneimine) [Mori, 2001a] and the analysis of the structure and swelling behaviour of solid-supported lipids and lipopolymers by means of X-ray methods [Bolz, 2001].

The central part of the present work was carried out by means of a setup, which has previously been built by A. Sinner [Sinn, 1999]. This setup was enhanced in the present work by the incorporation of a reflection interference contrast microscope and a computer controlled shutter mechanism for the FRAP (fluorescence recovery after photobleaching) apparatus.

2 Introduction

It is a general aim of mankind to reduce the diversity and complexity of incidents and phenomena of living and inanimate nature by the invention of laws, which allow for the prediction of events by the knowledge of known parameters. In the natural sciences, these laws are parts of self-consistent theories, which rely on a few, appropriately chosen basic assumptions, which cannot be proved (axioms). An expressive metaphor describing the physical theory is that of an envelope, which is aimed to shape the complex appearance of nature [Duhe, 1954]. This envelope, designed by scientists to fit as closely as *currently* possible, based on the knowledge gained so far, can never be assumed to fit as closely as *ever* possible. In fact, it is generally agreed nowadays that the verification of a theory is not feasible: theories are invented and are to be regarded as useful until they are prone to falsification [Popp, 1994] and are replaced by more comprehensive theories.
In a similar way, biomimetic structures can be regarded as models, simplifying highly complex biological systems. Equivalent to the physical theory, the biomimetic model system allows for a comparison between the model invented by scientists on one hand, and phenomena observed in the biological system as found in nature, on the other hand. The model system may thus be analysed for its usefulness and – if necessary – be falsified and replaced by better-suited models, which are able to mimic more complicated biological phenomena.

Biological membranes

A biological structure of utmost importance is the membrane, which not only envelops the interior of animal, plant and bacterial cells, but also encloses functional units, like the cell nucleus, endoplasmatic reticulum, Golgi apparatus, lysosomes, endosomes, mitochondria, chloroplasts and peroxysomes, contained in the interior of biological cells [Albe, 1994]. Biomembranes therefore compartmentalise biological processes, but still allow for an exchange of both matter and information between different compartments. Figure 2.1 shows schematically the most important components of biomembranes. According to the fluid mosaic model [Sing, 1972], the main components are lipid molecules like phospholipids or cholesterol, and proteins. A structure universal to biomembranes is the lipid bilayer, self-assembled from amphipathic lipid molecules due to the hydrophobic effect [Tanf, 1980]. The lipid bilayer gives rise to the barrier property of the membrane towards water-soluble molecules and ions. It is important to note, however, that the bilayer lipid membrane can be crossed quite rapidly either by small hydrophobic molecules like

oxygen or carbon dioxide on one hand, and small uncharged polar molecules like water or ethanol, on the other hand.

Functionality is added to the membrane by proteins, which are either integral parts of the lipid bilayer or attached to the membrane on only one face, by covalent bonding to lipids or other proteins. Proteins enable the transport of matter across the membrane through channels or carriers, they allow for a linking between different proteins (e.g. integrines) and serve as receptors or enzymes for catalysing chemical reactions as a response towards extracellular signals [Albe, 1994].

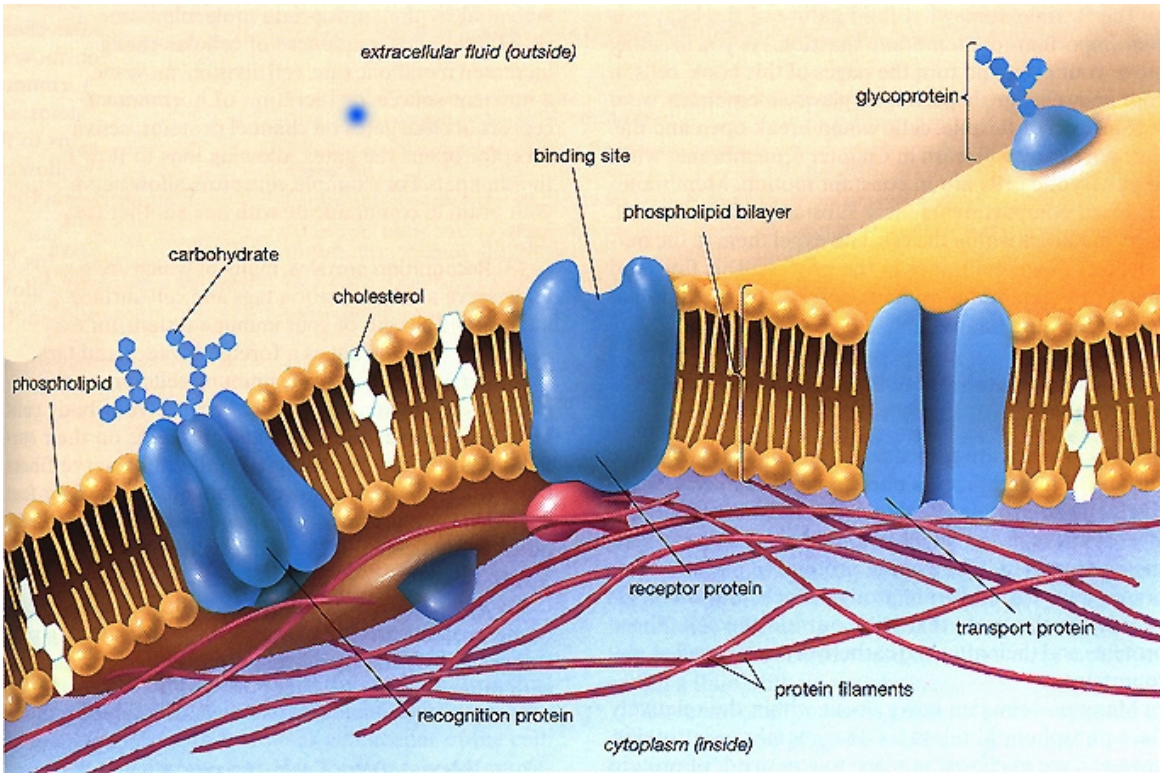

Figure 2.1: Schematic representation of a biomembrane according to the fluid mosaic model. Picture taken from [Chir, 1997].

The lipid composition in a biomembrane is usually asymmetric: while phosphoethanolamine and -serine are found mainly at the side facing the interior (cytoplasm) of the cell, phosphatidylcholine and sphingomyelin are mainly facing the extracellular fluid. The membrane is sandwiched between two different types of polymer networks, which consist of partially cross-linked oligo- and polysaccharides on the outside of the cell (glycocalix) and cross-linked protein filaments (cytoskeleton) extending through the cytoplasm.

Biomimetic model membranes

In order to reduce the obvious structural and functional complexity of biomembranes and to allow for systematic investigations, different model membrane systems have been developed. The main types are a) Langmuir films, b) Langmuir-Blodgett films on a solid support, c) solid-supported bilayer lipid membranes, d) liposomes, e) black lipid membranes (BLMs) and f) foam films (which may be regarded as the inverse of a lipid bilayer membrane), as shown in Figure 2.2.

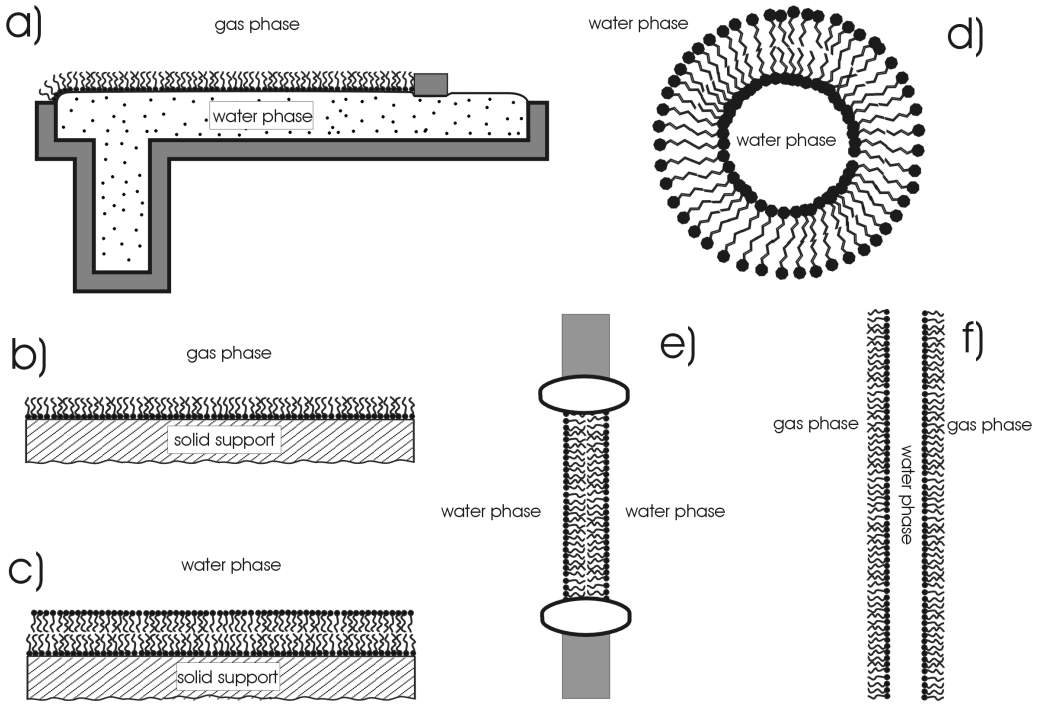

Figure 2.2: Lipid model membrane systems. a) Lipid monolayer at the gas/liquid interface on the Langmuir film balance. b) Lipid Langmuir-Blodgett film resting on a solid support, at the solid/gas interface. c) Solid-supported lipid bilayer membrane at the solid/liquid interface or separated from the support by an ultrathin water film. d) Spherical liposome separating two liquid compartments. e) Black lipid membrane (BLM) spanning an aperture usually in a teflon cup. The bilayer in the latter case is coupled to the hydrophobic teflon via a solvent enriched lipid reservoir. f) Soap film, a thin water phase is enclosed between two amphiphile monolayers.

Systems a), c), d) and e) allow for the study of lipid/protein interactions. The bilayer models c), d) and e) can be used for the incorporation and functional analysis of membrane spanning proteins.

Solid-supported mono- and bilayer membranes (b) and c)) potentially have a high long-term stability. Additionally, surface sensitive analysis techniques can be applied to study them. They therefore represent highly interesting systems both for basic research and practical applications e.g. in terms of biosensing [Sack, 1996]. Examples of these latter membrane models were developed and investigated in the present work.

The types of stabilisation of a model membrane by a solid support can be grouped into three different categories, with respect to the membrane/support interaction. A) pure physisorption, B) pure chemisorption and C) a combination of physi- and chemisorption i.e. the membrane is partially chemically coupled to the substrate and filling lipids make up the rest of the membrane [Corn, 1997], [Ragu, 1998], [Ling, 1998].

Lipids

Lipid molecules generally possess a polar part (head) and an apolar part (tail) and therefore are amphiphiles. Naturally occurring lipids may be grouped into two main classes: complex, hydrolysable lipids and simple, non-hydrolysable lipids. The former group comprises acylglycerides, phospholipids and sphingolipids. Terpenes, steroids and prostaglandines belong to the second group. Lipids most commonly used for building up model membrane systems are phospholipids and the steroid cholesterol. The basic structure of phospholipids is shown in Figure 2.3.

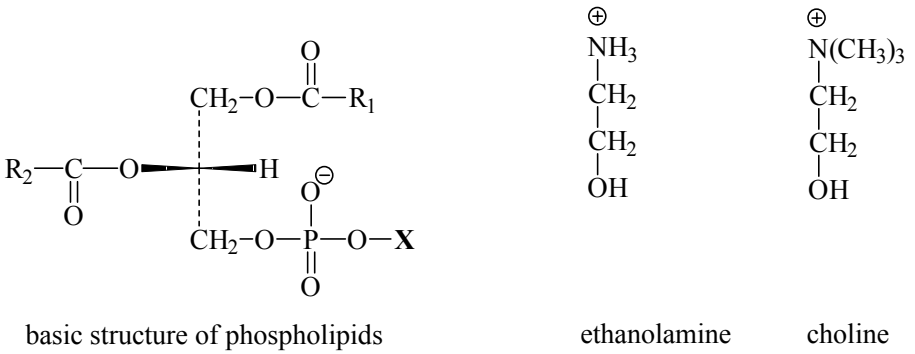

Figure 2.3: Basic structure of phospholipids. Common examples for the substituent X are the alcohols ethanolamine and choline. Both kinds of phospholipids are zwitterionic at a neutral pH. The substituents R_1 and R_2 are the hydrophobic tails of fatty acids (see text).

The core of a phospholipid is a glycerin-3-phosphate molecule. The phosphate group is linked to a polar molecule, like the alcohols ethanolamine (PE, cephalin) and choline (PC, lecithine), the aminoacid serin (PS), glycerol (PG) or sugars like inositol. The apolar part of phospholipids consists of the hydrocarbon tail of long chain fatty acids, which in most cases possess an even number of carbon atoms. The hydrophobic chain may be saturated or contain one or more double bonds. Common saturated fatty acids are (number of methylene groups in brackets): lauryl acid (10), myristic acid (12), palmitic acid (14), stearic acid (16) and arachidic acid (18). Besides these simplest fatty acids more than 100 more complex ones have been isolated from biological materials [Lehn, 1983].

Polymer-supported membranes

Important properties of biological membranes are lateral fluidity and a high water activity on both sides of the membrane. These key features must be retained in a substrate-supported membrane if the latter is to represent a suitable host for functionally active membrane proteins. This is firstly because reactions in membranes depend on lateral motion and the fluid dynamic properties of all membrane components [Wagn, 2000]. Secondly, the conformation ([Leik, 1993a] and references therein) and hence functional activity [Scar, 1996] of membrane proteins depends on the water activity of the surrounding. Water swellable hydrogels as membrane supports fulfil these requirements: they enable motional decoupling of the lipid membrane from an underlying substrate (such as oxide surfaces like glass and field-effect transistor gates, or metals). Moreover, they provide a hydrophilic, water-rich, soft environment for the embedding of voluminous peripheral parts of transmembrane proteins (see Figure 2.4 D)).

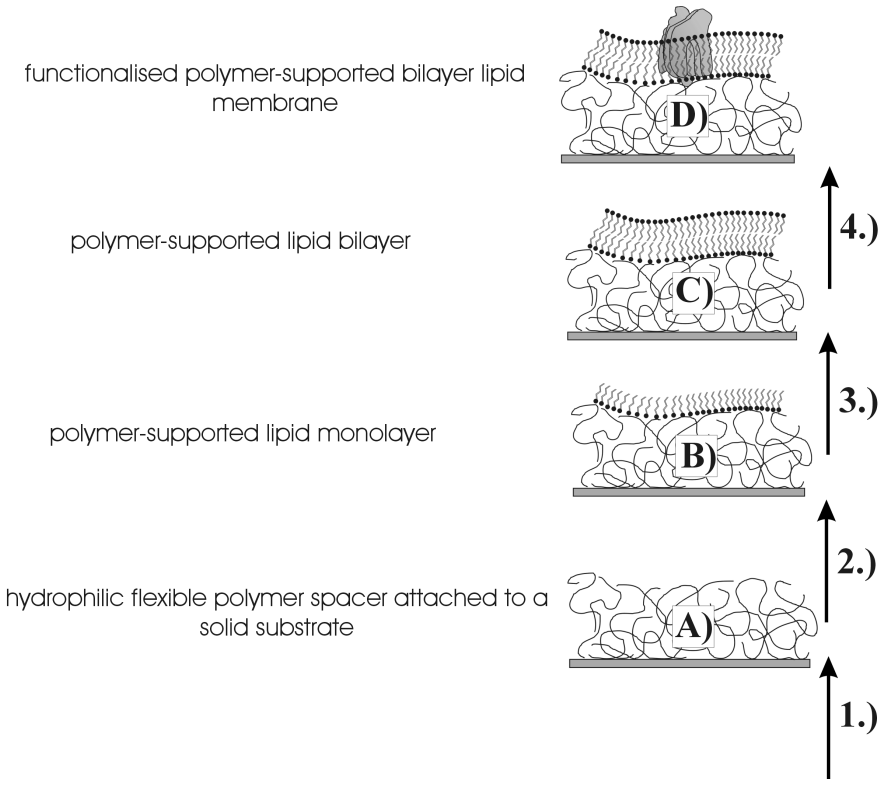

Figure 2.4: Hierarchy of structural complexity (capital letters), and fabrication steps (numbers) of functionalised polymer-supported model membranes.

The build-up of a functionalised solid-supported model membrane system from single components can be divided into several steps (Figure 2.4). The first step is a surface modification of a solid substrate, by the attachment of a hydrophilic, water swellable spacer by either physi- or chemisorption. The substrate may serve merely as a stabilising support, it may allow for fluorescence microscopy through transparent substrates by means

of high-aperture oil immersion objectives and/or serve as chemical or electrical transducer (e.g. metal electrodes, ion selective electrodes and field-effect transistors). The second step is the deposition of a lipid monolayer, which may be accomplished by Langmuir-Blodgett transfer. The deposition of a second monolayer leaflet, either by vesicle fusion or Langmuir-Schäfer transfer yields a polymer-supported bilayer. In a final step, proteins may be incorporated, e.g. by the method of detergent dilution of solubilised proteins.

The stepwise approach to the target structure (indicated by D) in Figure 2.4) allows for a systematic investigation and characterisation of the sub-structures of the target system, which was carried out in the present work. It must be mentioned, however, that it is often possible to combine two or more fabrication steps and thereby to reduce preparation effort and time. Step one and two may be combined by the self-assembly or Langmuir-Blodgett transfer of lipopolymers [Haus, 1998]. Step two and three may be linked by the fusion of vesicles onto a hydrophilic polymer cushion to yield a planar lipid bilayer [Hill, 1999]. The fusion of vesicles containing reconstituted trans-membrane proteins allows for the combination of step four with steps three [Naum, 1995b] and two. An alternative approach is to produce a freely suspended membrane (in terms of a black lipid membrane, E) in Figure 2.2) and to deposit it onto a polymer cushion afterwards [Ide, 1999]. Moreover, giant liposomes may be attached to the surface of a device coated by a thin polymer film [From, 1999].

Aim of the present work

The central aim of the present work was to elucidate features of the membrane/support interaction. A variety of common techniques with an emphasis on optical ones, were used. The focus of these investigations is to study the following key features of suitable biomimetic model membranes: lateral fluidity, hydration state, the stability of a membrane on a polymer support, self-healing properties, insulating properties, the possibility to incorporate membrane proteins in a laterally mobile state and the activity of incorporated membrane proteins. In order to be able to carry out extensive characterisations of polymer-supported membranes, two different polymer cushions, which are rather simple to prepare (without a chemical synthesis being involved) were developed.

The chapter structure of the present work follows exactly the hierarchy presented in Figure 2.4. Chapter four describes the preparation and characterisation of polymer cushions consisting of either agarose or chitosan. The fifth chapter is devoted to the analysis of polymer-cushioned lipid monolayers, with a special focus on the influence of water activity on membrane properties. The water activity is of significant biological relevance, due to its influence on the membrane hydration state, lateral fluidity and protein functionality. In chapter 6 the possibility to prepare stable bilayer lipid membranes on the

above mentioned polymer cushions will be discussed, successful preparations were further characterised. In chapter seven, the possibility of reconstituting integral membrane proteins will be examined. Finally, it was elucidated whether the activity of proton pumps like H^+-ATPase or nitrate reductase can be analysed by means of field-effect transistors. Transistor devices that allow for LB/LS-transfer were available just too late for use in the present work. Hence model membranes which were not separated from the oxide support by a polymer cushion were prepared by vesicle fusion, and served as a proof of principle for the electrochemical analysis of functional membrane proteins by means of field-effect transistors.

3 Methods

In the following, the physicochemical techniques that were applied in the present work will be introduced.

3.1 Fluorescence recovery after photobleaching (FRAP) and fluorescence microscopy

Fluorescence methods are utilised in an enormous extent for the analysis of structure, dynamics and a great variety of other properties of biologically relevant systems (for an overview see [Lako, 1983]). In the present work fluorescence labels were used which were covalently attached to membrane components like phospholipids, cholesterol or integral membrane proteins.

Fluorescence is the emission of a photon due to the return of an electron from a singlet excited state to the electronic ground state of a molecule (or of a lanthanide atom). Such transitions are quantum mechanically allowed and hence relatively fast (often in the range of several nanoseconds [Birk, 1970]. A second way of luminescence is the emission of a photon accompanying the decay of an excited triplet state to a singlet ground state involving a change of spin orientation. This leads to long lifetimes of the excited state, in the millisecond to second range (phosphorescence).

Whereas excitation leads to a population of higher vibrational levels of the first electronic excited state (due to the Frank-Condon principle), fluorescence emission usually occurs from the vibrational ground state of the first electronic excited state (Kasha rule). The relaxation of the initially excited state to the vibrational ground state of the electronic excited state occurs in a non-radiative way (internal conversion). Due to this process generally a shift of excitation and emission wavelength is observed (Stokes shift). The Stokes shift may be used in fluorescence microscopy: a combination of a band pass filter in the illumination light path and a higher wavelength cut-off filter in the observation light path allows for the observation of components bearing fluorescence labels with fluorescence properties corresponding to the particular filter set only.

The technique of fluorescence recovery after photobleaching (FRAP) was invented in the late nineteen seventies in order to analyse the lateral diffusion of bleachable fluorescence molecules embedded in thin films [Axel, 1976]. The method is based on the fact that fluorescence probes oxidise in a photoreaction, particularly when they are subject to intense illumination. Lateral exchange of bleached and unbleached molecules by diffusion

or flow then leads to a recovery of the measured fluorescence. In the following, the basic principle of the FRAP method shall be described.

3.1.1 FRAP measurement principle

Originally, FRAP (fluorescence recovery after photobleaching) was developed for analysing the lateral self-diffusion of fluorescence labels in lipid membranes, but is currently used for determining the mobility of a variety of other biological or pharmaceutical components [Meyv, 1999]. Fluorophores commonly employed include fluorescein derivatives like fluorescein isothiocyanate (FITC), diphenylhexatriene derivatives (DPH), nitrobenzoxadiazole derivatives (NBD) or dialkylcarbocyanine derivatives (DiI) [Meyv, 1999]. The bleaching of these fluorophores is usually performed by means of intense laser light.

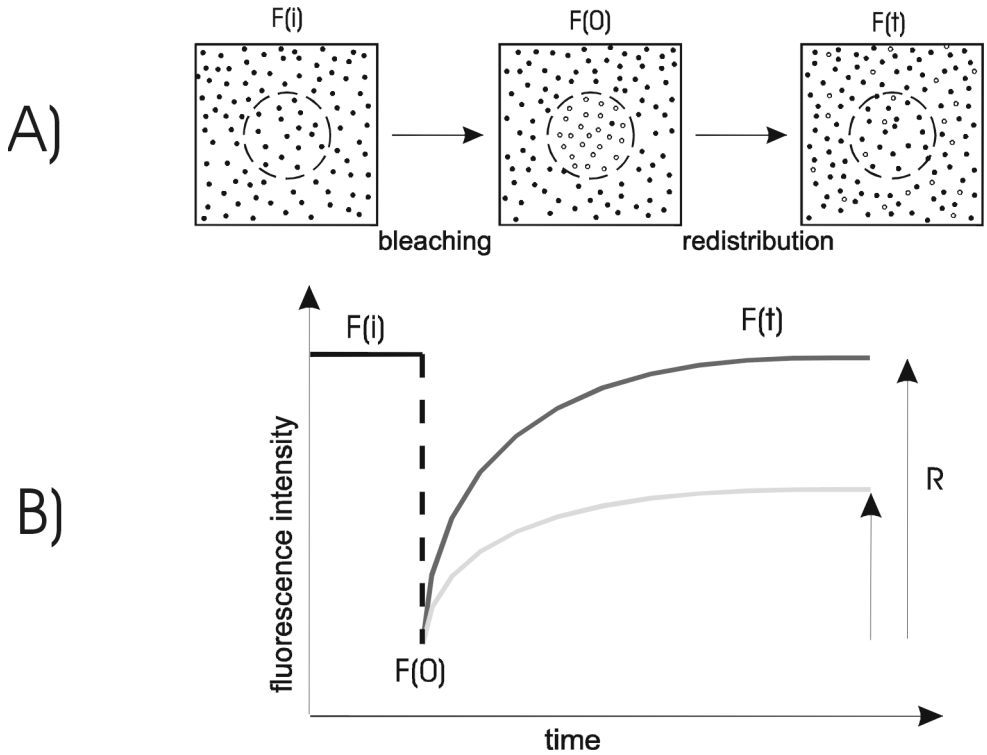

Figure 3.1: Basic principle of the FRAP method. A) Fluorescence labelled lipid molecules are added in a low concentration to a lipid membrane. The membrane is illuminated in a circular region and the fluorescence intensity, $F(i)$, is observed. Switching to a high illumination intensity during a short time interval leads to complete or partial bleaching of the fluorescence labels (fluorescence intensity, $F(t = 0)$). Provided the membrane is laterally fluid, bleached membrane labels are replaced by unbleached labels leading to a fluorescence recovery. B) Time dependence of the fluorescence recovery, $F(t)$, after photobleaching. The recovery curve, $F(t)$, is a function of the lateral diffusion coefficient, D, and the relative recovery, R.

Different bleaching geometries have been used. The simplest one is spot bleaching [Axel, 1976] with a uniform or a gaussian profile. The analysis of the time dependence of fluorescence recovery yields a diffusion coefficient, D, and relative recovery, R (see below). Pattern bleaching is valuable for identifying flow or anisotropic diffusion, by changing the pattern orientation. Additionally, fringe pattern bleaching in combination with a Fourier transform of the measured time development of the bleached pattern allows for a determination of diffusion coefficient distributions [Auch, 2000]. In the present work, spot bleaching in terms of a uniform bleach profile was applied (see Figure 3.1). The prerequisites of a successful data analysis are a linear relation between fluorescence intensity and probe concentration (which is the case only in a limited concentration range [Lako, 1983]) and that bleaching is irreversible. The latter, however, has only to be considered when studying very fast diffusion, with characteristic diffusion times, τ_D, in the range of ms [Meyv, 1999], where

$$\tau_D = \frac{w^2}{4D} \tag{3.1}$$

with the radius of the bleach spot, w. It was shown in [Soum, 1983] that the time dependent fluorescence intensity, $F(t)$, (see Figure 3.1) can be fitted by analysing the time dependence of the concentration profile of the bleached molecules, ${}^*C(r,t)$, where r is the distance from the centre of the bleach spot. The overall number of molecules equals at every time t the overall number of molecules at time t_0, i.e. before bleaching, according to

$$C(r,t) + {}^*C(r,t) = C(r,t_0) \tag{3.2}$$

The diffusion equation

$$\frac{\partial {}^*C(r,t)}{\partial t} = D\nabla^2 {}^*C(r,t) \tag{3.3}$$

(see chapter 5.3.1) is solved with the following initial and boundary conditions:

$${}^*C(r,t_0) = C(r,t_0) \qquad r \le w \tag{3.4}$$

$${}^*C(r=\infty,t) = 0 \qquad r > w \tag{3.5}$$

(3.4) is valid only in the case of complete bleaching. Partial bleaching leads to a smaller initial concentration of bleached molecules. The following equation is obtained, which can be fitted to the experimental data:

$$F(t) = \{F(\infty) - F(0)\}\left\{1 - \exp\left(-\frac{2\tau_D}{t}\right)\left[\mathrm{I}_0\left(\frac{2\tau_D}{t}\right) + \mathrm{I}_1\left(\frac{2\tau_D}{t}\right)\right]\right\} \quad \textbf{(3.6)}$$

where I_0 and I_1 are modified Bessel functions of zeroth and first order. Furthermore, the relative recovery, R, is obtained from the fit of (3.6) to the data and the measurement of the initial fluorescence intensity, $F(i)$, according to

$$R = \frac{F(\infty) - F(0)}{F(i) - F(0)} \quad \textbf{(3.7)}$$

3.1.2 Setup

The setup used for fluorescence microscopy and FRAP measurements has been described in detail previously [Sinn, 1999], so only the very basic parts shall be reviewed here. However, this setup was further characterised and improved in the present work as will be shown below. The central part of the FRAP apparatus was an inverted microscope (IX-70, Olympus). A mercury burner (HBO 100, Olympus, 100 Watt) allowed for illumination of the whole observation field. For fluorescence microscopy, a fluorescence cube consisting of an excitation bandpass filter (BP 470 – 490, Olympus, Hamburg) and a barrier filter (BA 515, fluorescence cube U-MNIB, Olympus, Hamburg) was used. FRAP experiments were performed with an argon ion laser (Innova 90/4, Coherent, Dieburg), which was operated at a wavelength of 488 nm (at a power of 1.2 Watt). A combination of three pockels cells and four linear polarisers (Gsänger, München) in an alternating arrangement permitted beam attenuation by a factor of 10^6.
Changing the pockels cell voltage provided adjustment of the observation intensity (see Figure 3.2), which is necessary in order to avoid photobleaching during intensity measurements.

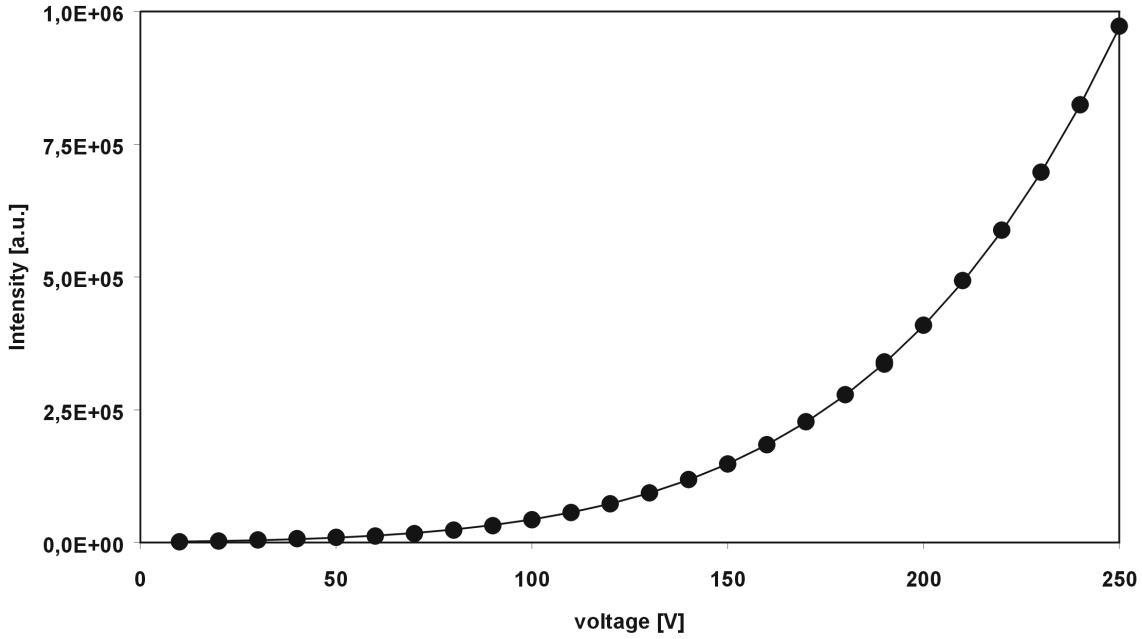

Figure 3.2: Laser intensity (measured by means of a photomultiplier tube) as a function of pockels cell voltage.

The intensity ratio, I/I_0, corresponding to the beam attenuation of a combination of a pockels cell and two linear polarisers can be calculated according to

$$\frac{I}{I_0} = \rho \cos^2\left[\frac{\pi}{2} - \delta + \frac{U}{U_{\lambda/2}}\right] \tag{3.8}$$

where ρ and $U_{\lambda/2}$ are material constants (loss coefficient and half wave voltage) and δ takes into account misalignment or stray light effects. In the case of a series of modulators, the overall attenuation is a result of the multiplication of the contrast ratio for each single modulator, given by (3.8). The bold line in Figure 3.2 corresponds to the fitting of (3.8) to the data, taking into account three modulators. A successful fit was obtained with parameters in good agreement with those provided by the manufacturer (Gsänger, München).

Probably as a result of thermal effects, the laser output was not constant with respect to the light intensity (see Figure 3.3).

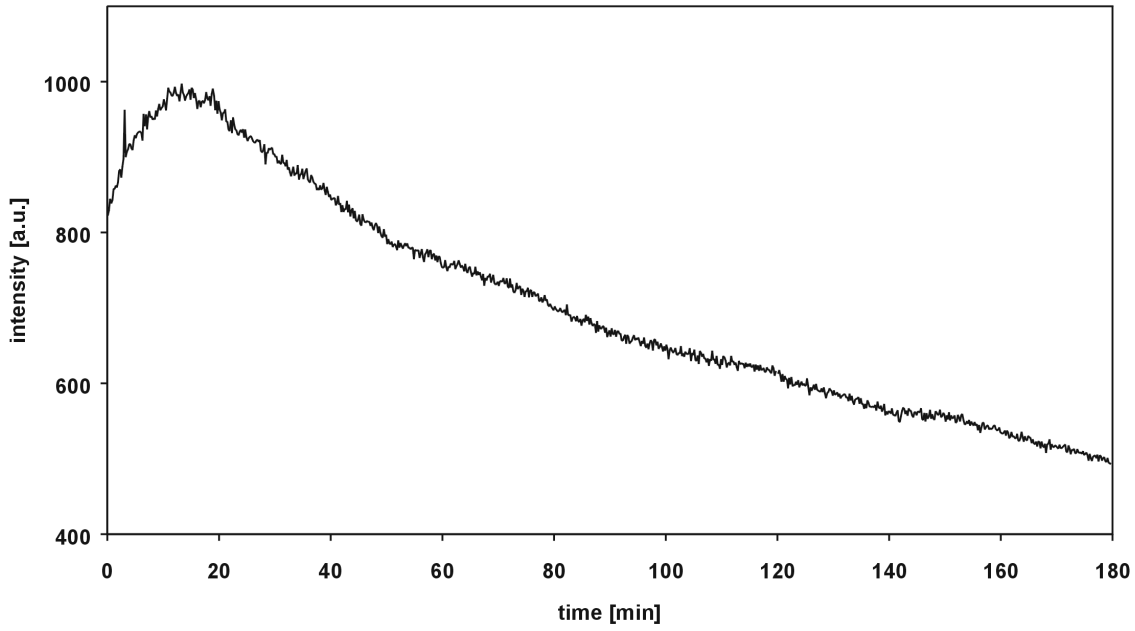

Figure 3.3: Laser intensity as a function of observation time (the measurement was started directly after switching-on the laser).

According to Figure 3.3, the laser should be switched on at least 30 min before starting FRAP experiments. The laser instability has to be considered when measuring extremely small diffusion coefficients. In the present work, fluorescence recovery was measured in a time interval shorter than 5 min, which in a usual FRAP experiment leads to errors in the estimation of $F(\infty)$ of much less than 1 %. Bleaching was performed by a high voltage switch (Solatron, Warsaw), with switching times smaller than 60 µs. The bleaching time was adjustable and was usually set to 40 ms. This bleach interval is a compromise between a time long enough for strong bleaching and a time short enough not to allow significant diffusion during bleaching. The measurement of the fluorescence intensity was performed by means of a photomultiplier tube (9893/100, Thorn EMI, England). During bleaching, the photomultiplier was gated. Gating, high voltage switching, photomultiplier counting and shutter control (see below) were performed with the help of a real time card (Adwin 4ld, Jäger) which allowed for the communication between PC and measurement hardware by means of the software Adbasic (Jägersoftware). The software Testpoint (Keithley) provided a user interface for device control and data representation.

Focus adjustment (and fluorescence microscopy) could be performed by means of a light enhancing camera (extended ISIS, Photonic Sciences). Fluorescence images were digitised by a frame grabber card (AG-5, Scion, USA) and could be processed using the program SCION image (SCION, USA) or Image Pro Plus (Media Cybernetics, Leiden, Netherlands).

Since in the present work small diffusion coefficients of partially dehydrated lipid membranes were measured, care had to be taken to avoid bleaching through the observation beam, i.e. prior to exertion of the bleach pulse or after bleaching. Accordingly, a mechanical shutter was inserted into the illumination pathway, which allowed for illumination of the sample during defined observation intervals only. By an additional panel, which was introduced in the present work into the FRAP control program (originally written by A. Sinner [Sinn, 1999] with the help of the software Testpoint), the number of observation intervals, the length of an observation interval and the distribution of data points along the time axis could be varied (see Figure 3.4).

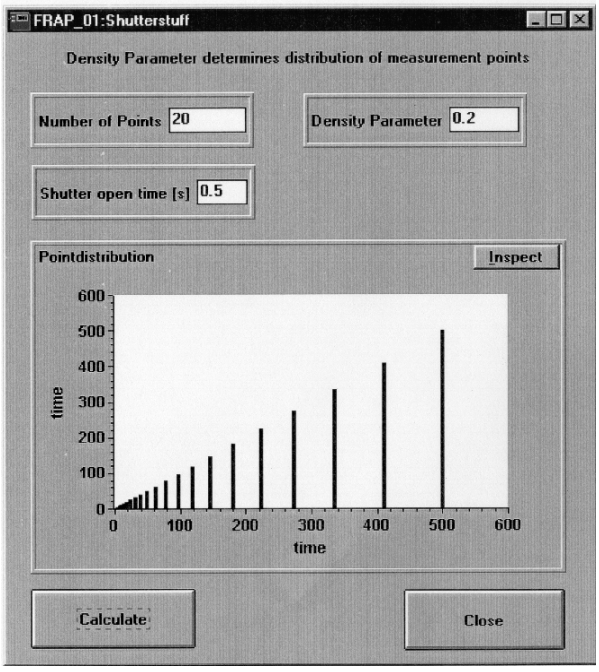

Figure 3.4: Message box of the shutter panel in the FRAP data acquisition and setup control program.

The data point density was chosen to increase exponentially with shorter observation time, since according to Figure 3.1, accurate determination of $F(t)$ requires a higher number of data points at shorter observation times. A density parameter, τ, allowed for changing the data point distribution from an even distribution on the time axis to a maximal density increase at lower observation times. The data point distribution was calculated as follows. A total number of data points, N, and a total measurement time, t_N, were chosen. The time, Δt, between single data point readings was varied exponentially with the data point index, n, (with $1 \leqslant n \leqslant N$), according to

$$\Delta t(n) = t_n - t_{n-1} = c \cdot \exp(\tau \cdot n) \qquad \textbf{(3.9)}$$

where c is a constant to be determined. The time, t_n, at which the data point, n, is read is calculated by

$$t_n = \sum_{i=1}^{n} \Delta t_i = c \sum_{i=1}^{n} \exp(\tau \cdot i) \quad \textbf{(3.10)}$$

The parameter c is calculated from the requirement

$$t_N = c \sum_{i=1}^{N} \exp(\tau \cdot i) \quad \textbf{(3.11)}$$

which finally leads to

$$t_n = \frac{t_N}{\sum_{i=1}^{N} \exp(\tau \cdot i)} \sum_{i=1}^{n} \exp(\tau \cdot i) \quad \textbf{(3.12)}$$

From (3.12) it follows that a value of $\tau = 0$ results in an even data point distribution and a positive value leads to a data point density which decreases with increasing data point index (see Figure 3.4).
The data fitting to Equation (3.6) was performed by the program Frapfit, which was developed in the present work, in cooperation with J. Worm, MPIP Mainz. The program was written in C++ using the Simplex algorithm for data fitting.

3.1.3 Measurement chamber for studying hydration effects in LB-films

Supported lipid monolayers allow for the osmotic stress method (see chapter 5.0.2) to be applied in the form of varying water vapour pressures in the surrounding gas phase. The obvious advantage of this method is the possibility to very rapidly change between different water activities over a wide and continuous range [Baek, 1995].
The schematic composition of the humidity chamber for microscopic observation of supported monolayers is depicted in Figure 3.5.

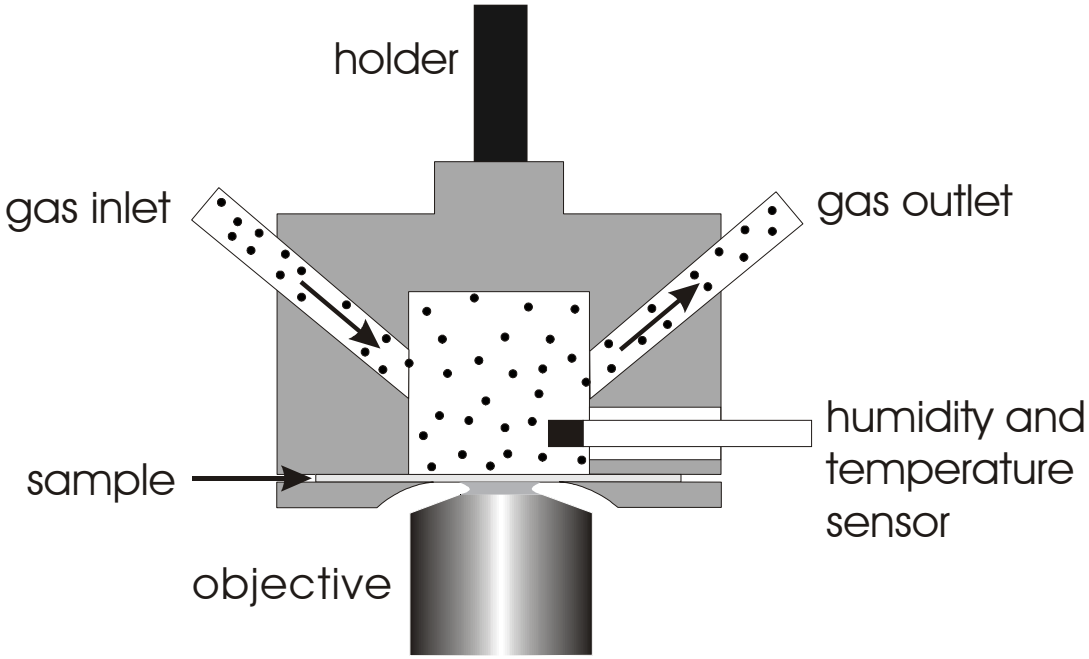

Figure 3.5: Humidity chamber for microscopic observation and FRAP measurements on supported lipid monolayers. The chamber walls were temperature-controlled by a water circle. The temperature and humidity sensor was thermally isolated from the chamber walls by a Teflon capsule. Prior to gluing the objective to the sample backside (microscopic coverglass), lipid on the backside of the coverglass was thoroughly wiped off with isopropanol.

The humidity sensor (see chapter 3.5) was thermally isolated from the chamber wall by a Teflon capsule. The wall temperature of the humidity chamber (brass) was controllable by flowing water through the chamber walls.

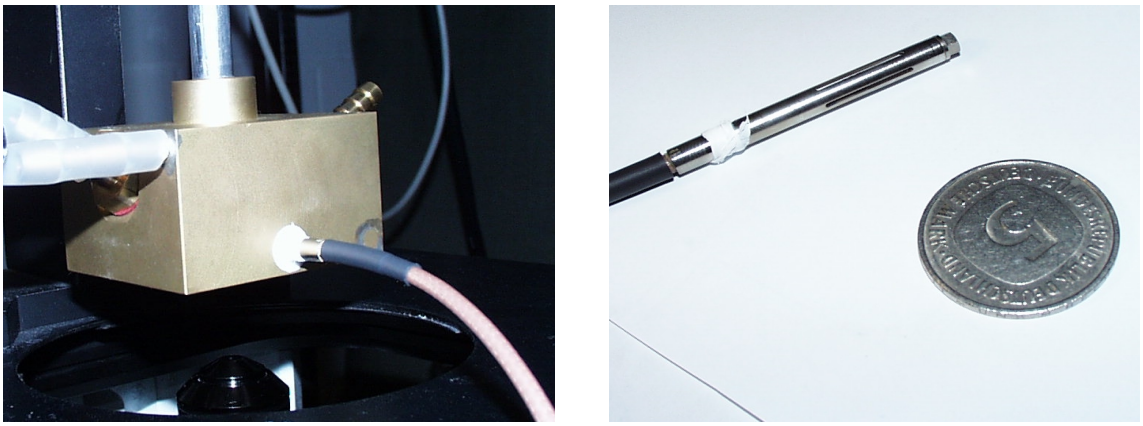

Figure 3.6: Left: photograph of the humidity chamber depicted in Figure 3.5, mounted on the microscope stage. Lateral position adjustments were performed by micrometer screws moving the microscope stage. Focus control was performed by moving the objective in the z-direction. Right: photograph of the humidity and temperature sensor.

The gas tubes and the inlet were surrounded by a jacket maintained at the same temperature. The humidity chamber had a volume of approximately 14 cm^3. The water activity in the nitrogen stream was controlled as described in chapter 3.5.2.

The preparation of the supported monolayer was in all cases performed by LB-transfer (see chapter 3.10.3). Prior to optical coupling of the microscope objective to the sample backside by means of immersion oil, the monolayer transferred to the backside of the microscopic coverglass was thoroughly wiped off by means of isopropanol.

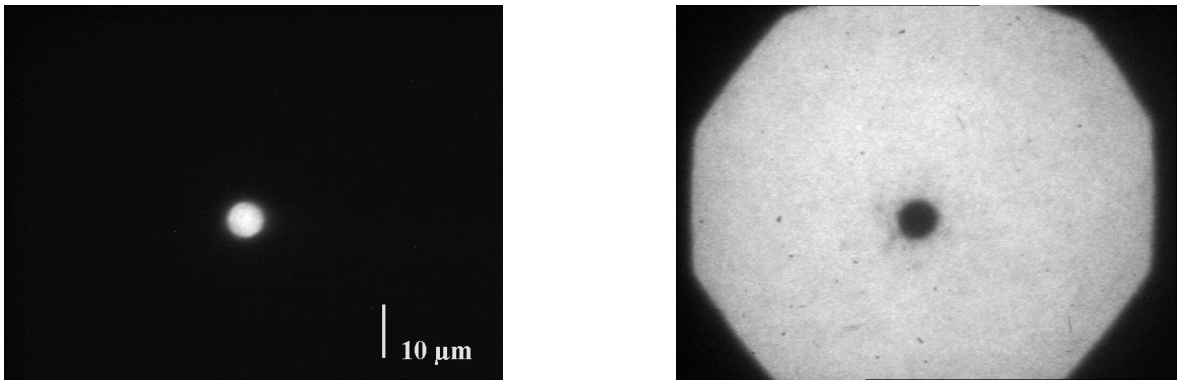

Figure 3.7: Fluorescence micrographs of a supported lipid monolayer mounted into the humidity chamber. Illumination by laser light (prior to bleaching, left) and the mercury burner (after bleaching, right) insured a homogenous, circular illumination by the laser without severe reflections.

Before raising the humidity inside the chamber, the sample was allowed to thermally equilibrate.

Microscopic observation by laser light and the bleached area by illumination with a mercury burner, revealed no significant reflections inside of the humidity chamber, which would distort the circular profile of the laser spot (Figure 3.7). The absence of reflections is of relevance in case of FRAP experiments.

3.2 Fluorescence spectroscopy

3.2.1 Introduction

Fluorescence spectroscopy is used in order to obtain information about spectral positions, shapes and relative intensities of transitions of electronically excited fluorescent particles. An emission spectrum is the wavelength distribution of the emission measured at a single, constant excitation wavelength. An excitation spectrum, on the other hand, is recorded using a single observation wavelength and varying the excitation wavelength. Consequently, the emission spectrum reflects the vibrational levels of the ground electronic state, while the excitation spectrum reflects the vibrational levels of the electronically excited states. Often, excitation and emission spectra obey the mirror image rule, i.e. the emission spectrum appears to be a mirror image of the excitation spectrum, which is a

result of the similarity of vibrational levels of excited state and ground state. However, there are many exceptions from this rule. Generally, emission spectra are red shifted with respect to the excitation spectra (Stokes shift, see above).

3.2.2 Setup

The spectrofluorometer Fluorolog 2 F212, Spex, USA, with two monochromators was used. The light source was a xenon-arc lamp (XBO 450 W, Osram). Fluorescence was detected by single photon counting with the help of a photomultiplier tube (PMT R928, Hamamatsu, cooled to –30 °C). A reference detector photomultiplier tube (PMT R508, Hamamatsu) allowed for the wavelength correction of the lamp intensity. The instrument was controlled by the software Datamate DM1B, Spex.

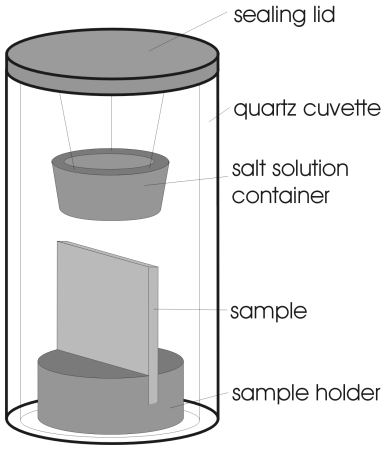

Figure 3.8: Measurement chamber used for fluorescence spectroscopy with substrate-supported lipid monolayers. The chamber consisted of a quartz cuvette, which was sealed by an airtight lid. The relative humidity was adjusted by means of a saturated salt solution.

All spectra were obtained in a quantum corrected form, i.e. were corrected for wavelength dependent distortions due to the components of the spectrofluorometer. The illumination and detection pathways were orientated at an angle of 90°. In order to keep the reflected excitation beam from entering the emission monochromator, the sample surface normal was oriented at 22.5° with respect to the illumination pathway. A cylindrical quartz cuvette was used which allowed for adjusting the relative humidity by means of a container filled with saturated salt solutions (see Figure 3.8).

3.3 Reflection interference contrast microscopy (RICM)

3.3.1 Introduction

An important part of the present work was the assembly of a reflection interference contrast microscope. Therefore in the following the underlying principle as well as the experimental realisation are described. The interference reflection microscopy method was first used in 1964 by Curtis [Curt, 1964] in order to study the adhesion of living cells to glass surfaces. Currently, reflection interference contrast microscopy is widely used in order to study the interaction of both biological cells, model membranes [Rädl, 1993b] and colloidal probes [Rädl, 1992] with surfaces. Both the experimental technique [Ploe, 1975], [Bere, 1979], [Rädl, 1993b] and the theory of data analysis [Ging, 1979], [Kühn, 1996b], [Wieg, 1998] have been improved considerably during the past years.

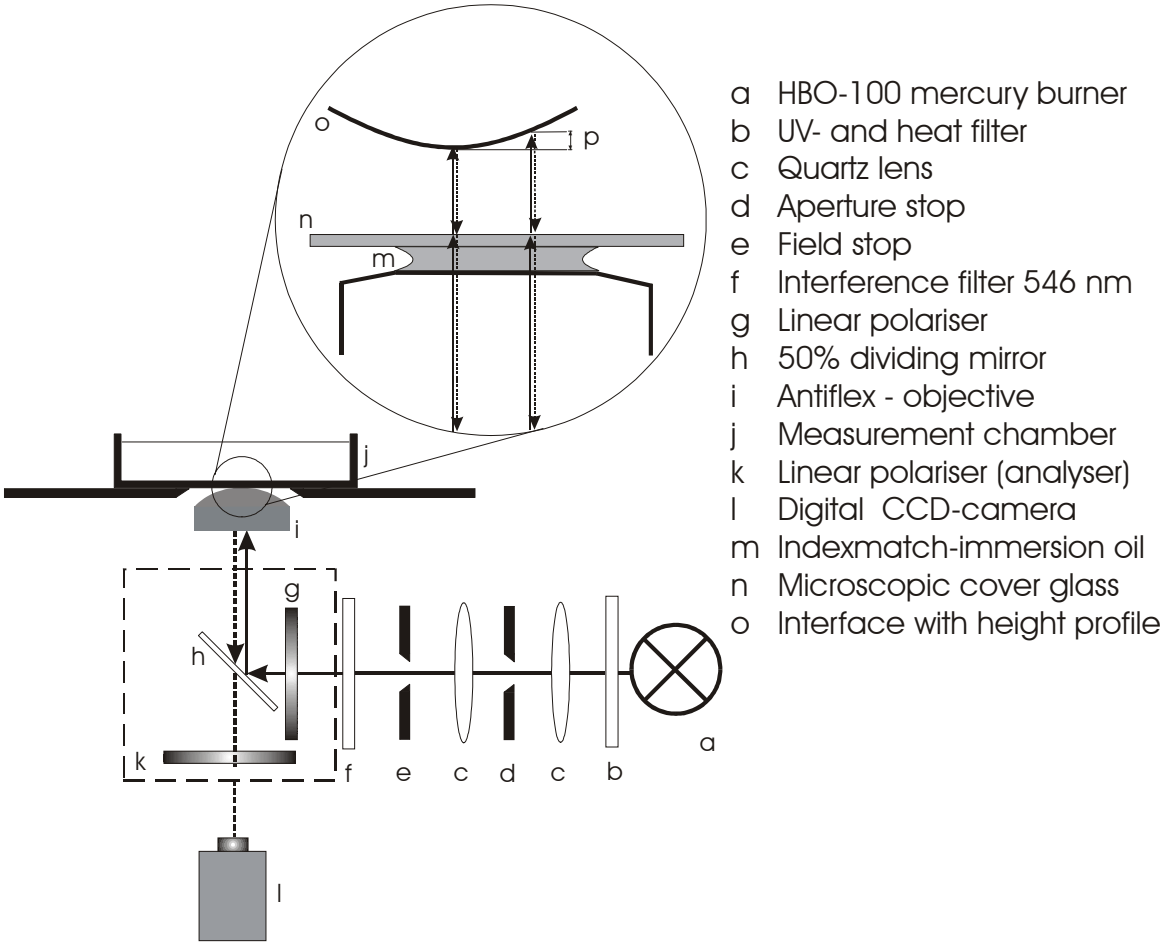

Figure 3.9: Principle and experimental realisation of a reflection interference contrast microscope.

The basic principle of the technique as well as the setup are depicted in Figure 3.9. A sample is illuminated with monochromatic light by epi-illumination through a thin

microscopic coverglass. Ideally, for obtaining an optimal interference contrast, illumination should be performed by normal incidence of the incoming light. This means that the illumination numerical aperture INA, defined by

$$INA = n_1 \sin(\alpha) \tag{3.13}$$

(with n_1 being the refractive index of the medium and α is the maximum illumination angle measured towards the surface normal) should be zero.
Reflection takes place both at the glass/medium interface (intensity I_1) and at the medium/object interface (intensity I_2). The reflectivity, R, of an interface (like for example the glass (g)/medium (m) interface) is given by

$$R_{gm} = \frac{I_1}{I_0} = \left(\frac{n_g - n_m}{n_g + n_m} \right)^2 \tag{3.14}$$

where I_0 is the illumination intensity and n is the refractive index of the particular medium.
To a first approximation (by assuming zero INA) the intensity distribution function of the interferogram *I(x,y)* can be calculated as

$$I(x,y) = I_1 + I_2 + 2\sqrt{I_1 I_2}\cos[2k(g(x,y)+h)+\delta] \tag{3.15}$$

g(x,y) denotes the surface contour of the object, h is the minimum vertical object/substrate distance, $k = 2\pi n/\lambda$ is the wave vector (with n being the refractive index of the medium and λ is the wavelength of the illuminating beam). δ is a phase shift which occurs at the medium/object-interface, if the object has a higher refractive index than the medium, which is usually the case. From (3.15) it follows that the intensity, $I(x,y)$, increases in case of $0 < h < (\lambda/4n)$, which means that separation distances can unambiguously be determined in this distance regime only.
The term reflection-contrast microscopy was first used by Ploem [Ploe, 1975], who significantly improved the technique by inventing a special method of contrast enhancement which shall be described in the following. As the intensity of the reflected light is small compared to the illuminating beam, the contrast of the interferogram often suffers from scattered light, stemming from straying at the interfaces of the optical system. The stray light can be reduced considerably by the so-called antiflex technique. The principle of this method is shown in Figure 3.9: a polariser produces linearly polarised

light in the illumination pathway. After passing the microscope objective, which is covered with a $\lambda/4$-plate (antiflex-objective), the light becomes circular polarised. After having been reflected above the objective the light passes through the quarter wave plate a second time and becomes linearly polarised again, but with a polarisation plane which is rotated by 90°. By using a second linear polariser, the position of which is chosen to be 90° with respect to the first linear polariser, light that stems from reflection above the objective can be selectively transmitted. However, stray light from reflections below the $\lambda/4$-plate is diminished.

3.3.2 Influence of illumination- and observation numerical aperture

In reality, illumination always occurs with a finite aperture. The control of the illumination numerical aperture is essential for a reflection interference contrast microscope. The determination of cell attachment to surfaces demands a high INA, since interference patterns arising from reflection at surfaces above the contact plane have to be suppressed [Bere, 1979]. On the other hand, in order to determine surface profiles of objects in the illumination space, the INA has to be minimised. With increasing distance, h, of an object from the glass substrate, the contrast of interference extrema (see chapter 6.2.3), defined by

$$K = \frac{I_{\max} - I_{\min}}{I_{\max} + I_{\min}} \tag{3.16}$$

decays with $\sin(y)/y$ [Rädl, 1993a] according to

$$K = \frac{2\sqrt{I_1 I_2}}{I_1 + I_2} \frac{\sin(y)}{y} \tag{3.17}$$

where y is defined as

$$y = 2kh \sin^2 \alpha / 2 \tag{3.18}$$

While the illumination numerical aperture INA has to be maximised or minimised according to experimental requirements, the observation numerical aperture NA generally needs to be maximised, since the resolution limit of the microscope is inversely proportional to NA.

3.3.3 Setup

The experimental setup, which was realised in the present work, is depicted in Figure 3.9. The central part was an inverted microscope (IX 70, Olympus, the same microscope allowed for fluorescence microscopy and FRAP with the same sample). A high-pressure mercury burner (HBO 100) served as light source. A band-pass filter (546 nm, Zeiss, Göttingen) allowed for the selection of the intense line at 546.1 nm of the mercury lamp. A modified DIC cube (U-MDIC, Olympus, Hamburg) was equipped with two rotatable linear polarisers (see the dashed square in Figure 3.9). The microscope objective was a Neofluar 63/1.25 Antiflex objective (Zeiss, Göttingen).

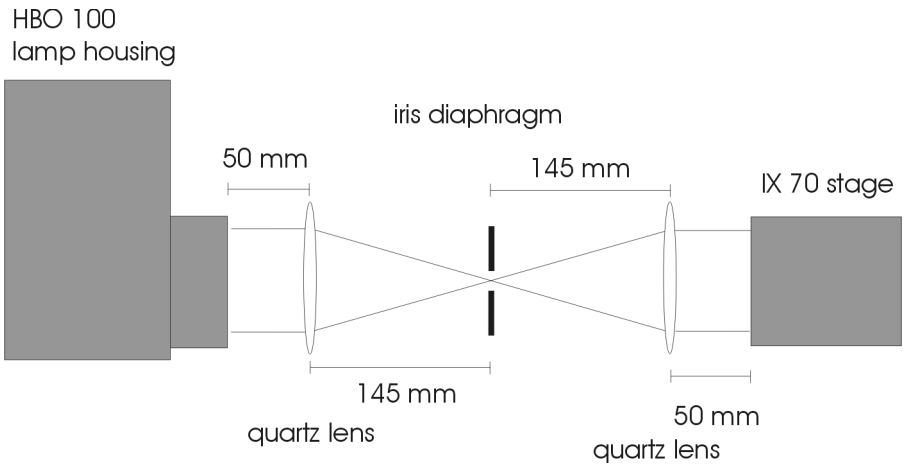

Figure 3.10: Schematic depiction of the home built aperture stop. Lamp housing and microscope (grey parts) were separated and two quartz lenses and an iris diaphragm aperture stop inserted.

Originally, the IX 70 did not allow for control of INA. Therefore an aperture stop had to be built as follows. Two quartz lenses (Spindler & Hoyer, Göttingen) were inserted into the illumination light path with focal lengths of 150 mm and a diameter of 50 mm. The lenses and an iris diaphragm, which served as aperture stop were arranged according to Figure 3.10. The configuration shown in Figure 3.10 was kindly provided by Y. Kitagawa, Olympus.

The aperture stop provided adjustment of INA between 0.15 and approximately the maximum numerical aperture of the Antiflex objective (1.2). The INA could be obtained by the measurement of the width of a section through the illumination cone, which appeared on the roughened surface of a 1 cm thick quartz block on top of the objective.

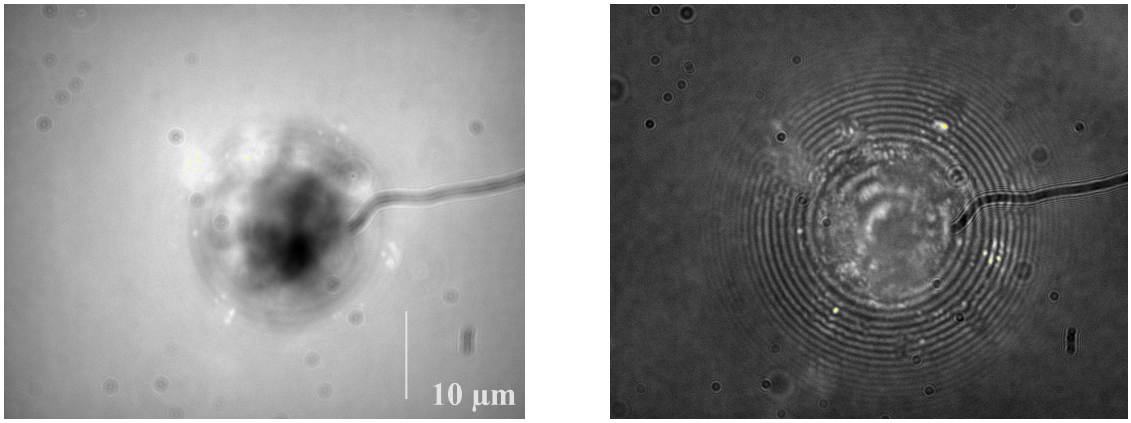

Figure 3.11: Influence of the aperture stop opening (Figure 3.10) on the contrast of interferograms of a glass bead (radius 73 µm) on a microscopic coverglass in air. Left: aperture stop completely opened. Right: INA reduced to 0.15.

Figure 3.11 demonstrates the gain in contrast of the interference fringes of a glass bead (Newtonian rings) by reducing the illumination numerical aperture of the microscope setup.

The alignment of the reflection interference contrast microscope was performed as follows. With a standard oil immersion objective the surface of a microscopic coverglass (in air) was viewed. The linear polariser next to the light source was rotated to the position of maximum reflected light intensity (as measured by a digital camera). Subsequently, the second linear polariser was mounted into the light path and rotated until the observed reflected intensity was minimised. Finally, the Antiflex objective was switched into the light path and the quarter wave plate (of the Antiflex objective) turned until the light intensity reached a maximum. Since the modified DIC cube was mounted into the fluorescence revolver of the IX 70, turning the revolver (and shifting the excitation filter slide) allowed for a convenient exchange of RICM or fluorescence microscopy mode. RICM images were recorded by means of a digital CCD camera (C 4742-95-12-NR, 1280x1024 pixels, Hamamatsu, Germany) which was controlled by the software HiPic 32 (Hamamatsu, Germany).

In order to test the assembled setup, negatively charged glass beads (Bangs Laboratories, Fishers, USA) were immersed in MilliQ water and examined by RICM. According to [Rädl, 1992], negatively charged colloidal particles over glass surfaces show thermally activated changes of the sphere-to-substrate distance which can be analysed by RICM. Figure 3.12 shows a picture of a hovering glass bead with a radius, R, of 33 µm.

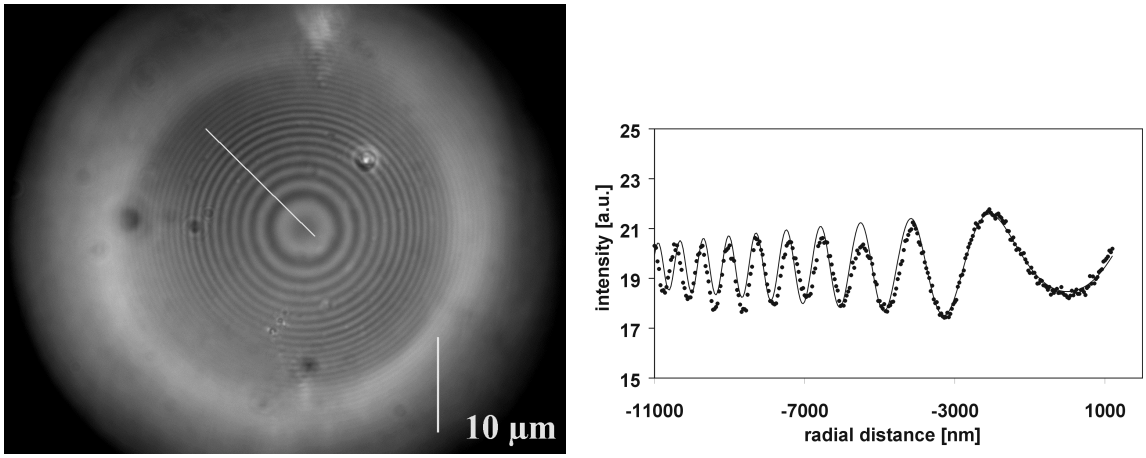

Figure 3.12: Glass bead hovering over a microscopic coverglass in MilliQ water. Left: RICM image. Right: Line profile drawn from the centre of the sphere. The bold line corresponds to a fit of (3.15) to the data.

The line profile drawn from the centre of the particle could be fitted successfully to (3.15), taking into account the surface profile of a sphere:

$$g(x) = R - \left(R^2 - x^2\right)^{1/2} \tag{3.19}$$

From the fit shown in the right part of Figure 3.12 a momentary separation distance of 35 nm was obtained. Furthermore, Figure 3.13 demonstrates the sensitivity of the RICM setup.

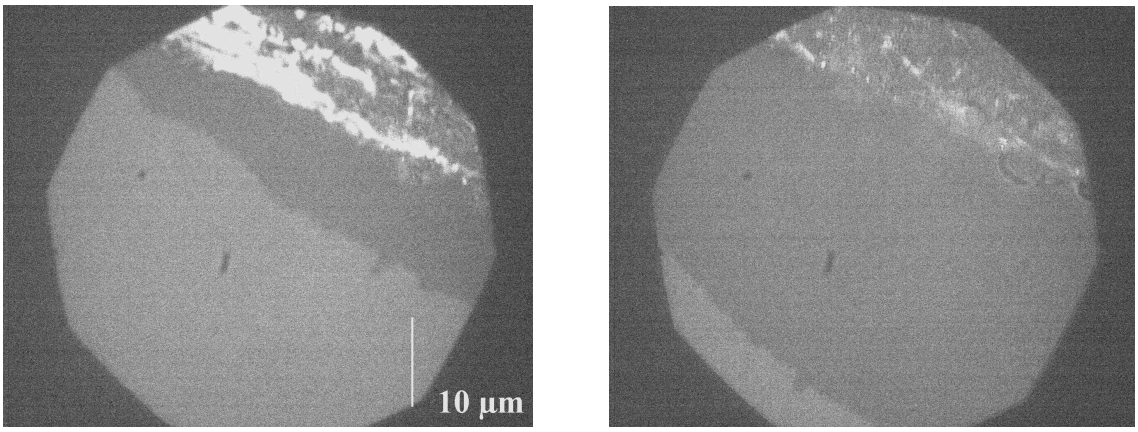

Figure 3.13: Spreading of a single bilayer from a lipid reservoir deposited onto a microscopic coverglass. The latter was covered by a layer of 45 nm MgF_2 for contrast enhancement and an additional layer of 5 nm SiO_2. The right picture was taken several minutes after the left one.

A 45 nm MgF_2 film was deposited onto a microscopic coverglass by evaporation. The MgF_2 film served as a contrast enhancement layer [Rädl, 1993b] (n (MgF_2) = 1.386 and n (Lipid) ≈ 1.5, which is close to glass (n = 1.532)). A SiO_2 layer (5 nm) was deposited onto

the MgF_2 film in order to increase the hydrophilicity of the surface [Wieg, 1998]. A lipid reservoir was deposited onto the SiO_2 surface [Rädl, 1995a] and thoroughly dried. According to Figure 3.13, the sensitivity of the RICM setup was high enough to allow for the observation of a single bilayer membrane spreading from a lipid reservoir.

3.4 Ellipsometry

Ellipsometry is one of the most popular methods for the determination of thicknesses and refractive indexes of thin films on planar substrates [Azza, 1977]. The method makes use of the fact that during the reflection of light at an interface of media with different refractive indices, a change in polarisation state and phase shift of s- and p-polarised light occurs. From the measurement of the change in polarisation state and phase shift, and the assumption of a particular layer system, the thickness or refractive index of a layer may be determined. In the following paragraph the basics of the technique will be explained. In a subsequent section, the setups for null-ellipsometry with internal and external reflection will be described.

3.4.1 Introduction

A light beam directed to a surface at an incidence angle, Θ_1, (see Figure 3.14), is partially reflected and partially transmitted.

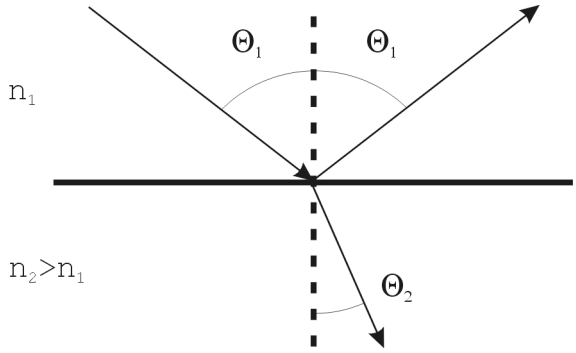

Figure 3.14: Reflection and refraction of light at an interface of two media with refractive indices n_1 and n_2.

The angles of reflected and refracted beams are correlated to the refractive indices n_1 and n_2 of the two media according to

$$n_1 \cdot \sin\Theta_1 = n_2 \sin\Theta_2 \qquad \textbf{(3.20)}$$

From (3.20) it follows that a corresponding transmitted beam is not found for every incidence angle, Θ_1. At an incidence angle greater than the critical angle, Θ_c, total reflection occurs. The ratio of the amplitudes of the reflected and incident beams is called the reflection coefficient, R. Unpolarised light can generally be represented as a sum of two linear polarised waves with field vectors orthogonal toward one another. In the case where the field vector is directed along the plane containing incoming and reflected beams, the wave is p-polarised. If the field vector is orthogonal to the plane made up by incoming and reflected beam, the light is s-polarised. Reflection coefficients for s- and p-polarised light are generally different. In case of a three layer system (where the media 1 and 3 are semi-infinite half spaces), the reflection coefficients for s- and p-polarised light ($R^{s,p}$) are defined as

$$R^{s,p} = \frac{r_{12}^{s,p} + r_{23}^{s,p} \cdot \exp(-2i\beta)}{1 + r_{12}^{s,p} r_{23}^{s,p} \exp(-2i\beta)} \tag{3.21}$$

where the reflection coefficients at single interfaces are given by

$$r_{ij}^{s} = \frac{n_i \cos\Theta_1 - n_j \cos\Theta_2}{n_i \cos\Theta_1 + n_j \cos\Theta_2}, \qquad r_{ij}^{p} = \frac{n_j \cos\Theta_1 - n_i \cos\Theta_2}{n_j \cos\Theta_1 + n_i \cos\Theta_2} \tag{3.22}$$

In (3.21), the parameter β is a phase shift due to passing through the layer, given by

$$\beta = 2\pi\left(\frac{L}{\lambda}\right) \cdot n_2 \cdot \cos\Theta_2 \tag{3.23}$$

where L is the thickness of layer 2 and λ the wavelength of the light. The fundamental equation of ellipsometry is given by

$$\frac{R^p}{R^s} = \tan\Psi \exp(i\Delta) \tag{3.24}$$

Δ is the change in the phase shift difference between s- and p-polarised light of incoming and outgoing wave and Ψ is defined by

$$\tan\Psi = \frac{|R^p|}{|R^s|} \tag{3.25}$$

The parameters Ψ and Δ are the quantities measured by an ellipsometer. Two different ellipsometer setups (see below) were applied in the present work: the configuration using external reflection served as a standard way for determining film thicknesses, while internal reflection allowed for a convenient alteration of the environment of the sample.

3.4.2 Setup

In Figure 3.15, the setup of a null-ellipsometer with external reflection is depicted.

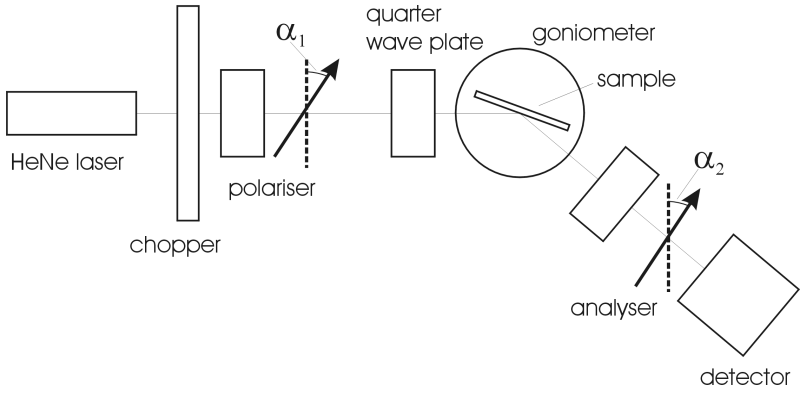

Figure 3.15: Schematic setup for a null-ellipsometer with external reflection.

A sample is illuminated by elliptically polarised light and the angular position, α_1, of the polariser is varied until light that is reflected from the sample, is linear polarised and can be extinguished by the analyser at an angle α_2. From α_1 and α_2, the ellipsometrical parameters Ψ and Δ are obtained, which allow for a determination of film thickness or refractive index of a layer.

Alternatively, thicknesses were determined in an internal reflection mode. The same ellipsometer setup was used as shown in Figure 3.15, with the important difference that the film under investigation was deposited onto a LaSFN9 prism. Both incoming and outgoing beams must pass through the prism, according to Figure 3.16. The setup such modified allows for multiple angle internal reflection ellipsometry (MAIRE), i.e. the parameters Ψ and Δ are determined as a function of the internal reflection angle Φ, which is related to the outer angle, Θ_1, by

$$\sin\Phi = \sin\Theta_1 \frac{n_{air}}{n_{prism}} \tag{3.26}$$

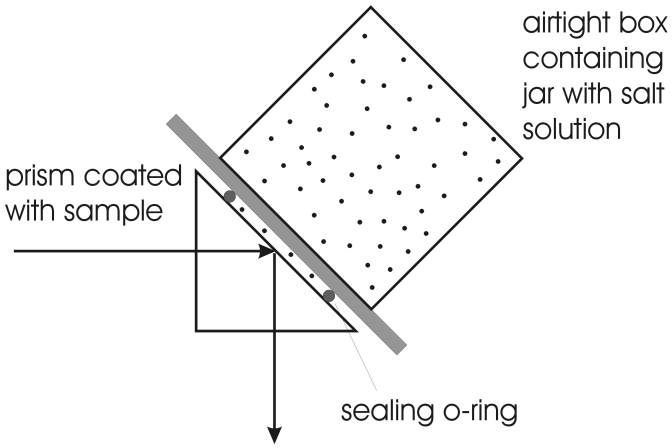

Figure 3.16: Configuration used for MAIRE-measurements of film thicknesses as a function of relative humidity.

Provided the film of interest is in the range of the optical wavelength, both film thickness and refractive index of the film may be determined in parallel. An advantage of MAIRE is that films in different environments may be examined, using a minimised number of reflecting interfaces. The experimental data sets $\Psi(\Phi)$ and $\Delta(\Phi)$ were fitted by a program written in Fortran by D. Johannsman, MPIP, Mainz. The laser for ellipsometry measurements had a wavelength of 632.8 nm (Uniphase, 5 mW).

3.5 Generation of controlled humidities

Two different methods were applied for adjusting relative humidities *RH* in gas phases. Firstly, *RH* was changed by equilibrating the atmosphere with different saturated salt solutions at a constant temperature. Secondly, *RH* could be altered by changing the mixing ratio of a dry and a water-saturated gas stream. In the following, a theoretical overview will be provided. Subsequently, the two above-mentioned methods will be described in more detail.

3.5.1 Introduction

The partial water pressure, *p*, and the total pressure, *P*, which is the sum of *p* and the partial pressure of the remaining gas (e.g. N_2) can be expressed by [Moor, 1973]

$$p = p_0 \cdot \exp\left(\frac{v}{kT}(P - p_0)\right) \tag{3.27}$$

where v is the volume of a water molecule, p_0 is the water vapour pressure without external pressure. The relative humidity is defined by

$$RH = \frac{N}{N_0} \cdot 100\% = \frac{p}{p_0} \cdot 100\% = a_w \cdot 100\% \tag{3.28}$$

where N is the total amount of water in the gas phase and a_w is the water activity (in the gas phase). According to (3.28), the water activity in a water-saturated gas phase corresponds to the water activity in bulk water (a_w = 1, in equilibrium).

At atmospheric pressure, the partial water pressure at saturation may be calculated according to the Magnus formula:

$$p = C_1 \exp\left(\frac{C_2 T}{C_3 + T}\right) \tag{3.29}$$

with the empirical constants C_1 = 6.11, C_2 = 17.62 and C_3 = 243.12, which are valid for vapour above liquid water in a temperature range from –45 to 50 °C [Sonn, 1966]. With (3.29), RH may be expressed by:

$$RH = \frac{C_1 \exp\left(\frac{C_2 T_s}{C_3 + T_s}\right)}{C_1 \exp\left(\frac{C_2 T}{C_3 + T}\right)} \cdot 100\% \tag{3.30}$$

where T_s is the saturation temperature at the particular relative humidity (dew point). Due to the temperature dependence of the maximum water content of the gas phase, temperature gradients between temperature sensor and sample can lead to large errors in RH. As the error increases with increasing relative humidity, in the present work the humidity range above RH = 90 % was omitted in most cases.

3.5.2 Methods for adjusting *RH*

One of the simplest ways for controlling the relative humidity of a gas phase is to equilibrate the latter with a saturated salt solution. At saturation, the solution possesses a well-defined concentration. Due to the temperature dependence of *RH* (and the maximum salt content of the water phase), temperature control is necessary. The presence of salt reduces the water vapour pressure according to Rault's law of vapour pressure lowering [Moor, 1973]. The following salt solutions were employed:

salt solution	**relative humidity (T = 22 °C)**
LiBr	12 %
$CaCl_2$	35 %
K_2CO_3	43 %
KI	70 %
NH_4Cl	78 %
$ZnSO_4$	87 %
KNO_3	93 %

Table 3.1: Relative humidities measured over saturated salt solutions in sealed compartments at a temperature of 22 °C [Bies, 1999].

The advantage of the above-mentioned method is its relative simplicity. On the other hand, since water transfer occurs across a smooth (and hence relatively small) water surface, the establishment of equilibrium is time consuming. A convenient alternative approach is the mixing of a dry and a water saturated gas stream [Wolf, 1998]. In the present work the water-rich gas was produced by bubbling nitrogen through a series connection of two water filled bottles, the dry gas was obtained by passing a nitrogen gas stream through a series connection of two silica gel filled bottles. Computer controlled valves (MKS Instruments, Germany, type 1259C-10000SV) allowed for changing the mixing ratios at a constant total flow. Mixing of the two gas streams occurred shortly before the gas stream entered the measurement chamber (see Figure 3.5, chapter 3.1.3). Care had to be taken to avoid water droplets from creeping along the gas tubes and entering the measurement chamber. Therefore a water trap was inserted into the wet gas tube and the final part of the mixed gas tube was filled with cotton wool. *RH* was determined by measuring both temperature and gas phase water content in the measurement chamber, as depicted in Figure 3.5, chapter 3.1.3. The humidity and temperature sensor was a Hygroclip miniature air probe with A1H interface, Rotronic, Germany. The transducer was equipped with an

RS 232 interface, which enabled data readout by a PC. A feedback loop allowed for adjusting *RH* to the desired value.
Figure 3.17 demonstrates that switching to any desired value of *RH* could be accomplished within less than 5 min.

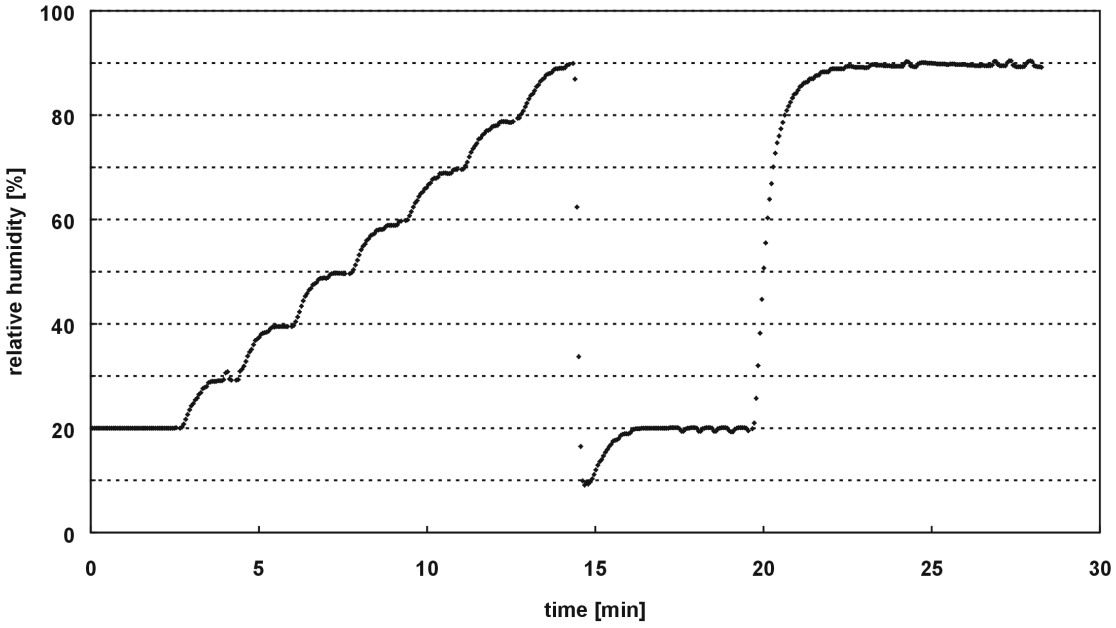

Figure 3.17: Velocity of humidity changes detected in the measurement chamber shown in Figure 3.5, chapter 3.1.3.

3.6 Impedance spectroscopy

Impedance spectroscopy is a versatile tool for the determination of the electrical properties of complex materials. Both interface and bulk properties, solid and liquid systems, conducting, non-conducting and semi-conducting samples may be examined [MacD, 1987].

3.6.1 Measurement principle

The method is based on the determination of the system's response towards a periodic sinusoidal perturbation in terms of a voltage, $U(t)$, with a frequency, ν, and a maximum amplitude, U_0, according to

$$U(t) = U_0 \cdot \sin(\omega t) \qquad \text{with} \quad \omega = 2\pi\nu \tag{3.31}$$

The time-dependent current, $I(t)$, is generally phase shifted with respect to the applied voltage:

$$I(t) = I_0 \sin(\omega t + \delta) \tag{3.32}$$

The impedance, Z, is calculated from

$$Z = \frac{U(t)}{I(t)} = |Z|(\cos\delta + i\sin\delta) = |Z| \cdot \exp(i\delta) = Z' + iZ'' \tag{3.33}$$

Z is a complex number with a real part, Z', and an imaginary part, Z'',. Z may be represented as a vector with polar coordinates, where the length of the vector is given by

$$|Z| = \frac{U_0}{I_0}\sqrt{(Z')^2 + (Z'')^2} \tag{3.34}$$

and the phase angle is obtained from

$$\tan\delta = \frac{Z''}{Z'} \tag{3.35}$$

Furthermore, the inverse of the complex impedance is called admittance, Y:

$$Y = \frac{1}{Z} = Y' + iY'' \tag{3.36}$$

Generally, impedance and admittance are frequency dependent (except from a system which can be represented by a pure ohmic resistance). With impedance spectroscopy the frequency dependence of these parameters is determined. The raw data may conveniently be represented in a number of different ways [Lind, 1996], the most commonly used ones being the Bode-plot ($|Z|$ and δ against ν), the Nyquist plot (Z'' against Z') and the complex frequency reduced admittance plot (Y''/ω against Y'/ω). As an example, Figure 3.18 shows the frequency reduced admittance plot of a system, which may be characterised by the equivalent circuit shown in the inset. From the width of the semi-circle the capacitance may directly be determined.

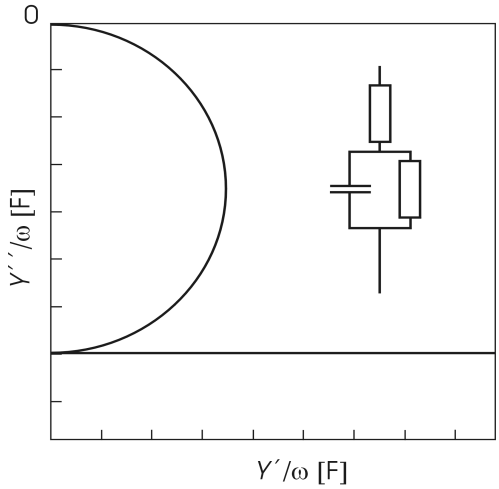

Figure 3.18: Complex frequency reduced admittance plot for a resistor connected in series with a RC element consisting of a resistor and capacitor in parallel.

The series connection of a resistor and a parallel connection of a further resistor and a capacitor is the simplest equivalent circuit representing a model membrane in an electrolyte solution.

3.6.2 Measurement setup

Impedance spectroscopy was performed with a frequency-generator-analyser (Zahner, type IM6) in the frequency range 10^{-2} to $5 \cdot 10^{4}$ Hz at an amplitude of 20 mV. Two electrodes were used (an Ag/AgCl reference electrode and a gold film evaporated onto a glass plate, which served as sample substrate). Data fitting was accomplished with the program Zview (Scribner Associates Inc., version 2.1b).

3.7 pH-measurements with field-effect transistors (EOSFETs)

Ion sensitive field-effect transistors (ISFETs) were first described in 1970 [Berg, 1970] and have since then been used for sensing purposes in numerous scientific fields. In the present work, electrolyte-oxide-semiconductor field-effect transistors (EOSFETs) were applied, which served as a pH-sensitive ISFET. In the following, a very basic introduction into the principle of EOSFETs will be provided. More detailed treatises are to be found in [Berg, 1970], [Sprö, 1997a], [Krau, 2000] and [Inge, 2001].

3.7.1 Introduction

Generally, field-effect transistors are semiconductor devices with three different connections called source, drain and gate. The electric current through a channel between source and drain may be controlled by an electric field between gate electrode and semiconductor surface. In the present work, n-channel FETs were used. In the case of n-channel FETs, source and drain consist of n-doped silicon. Source and drain are separated by p-doped silicon (see Figure 3.19). In classical MOSFETs (metal-oxide-semiconductor field-effect transistors) the gate consists of a metal contact, which is separated from the p-doped zone by a thin isolating oxide layer (e.g. SiO_2). In the interface region between semiconductor and oxide, a conducting channel forms upon applying a source/gate voltage. The conductivity of the channel depends on the magnitude of the source/gate voltage. In case of EOSFETs the metal layer above the gate oxide is omitted and the latter is contacted through the electrolyte solution by means of an Ag/AgCl reference electrode (bath electrode, see Figure 3.19).

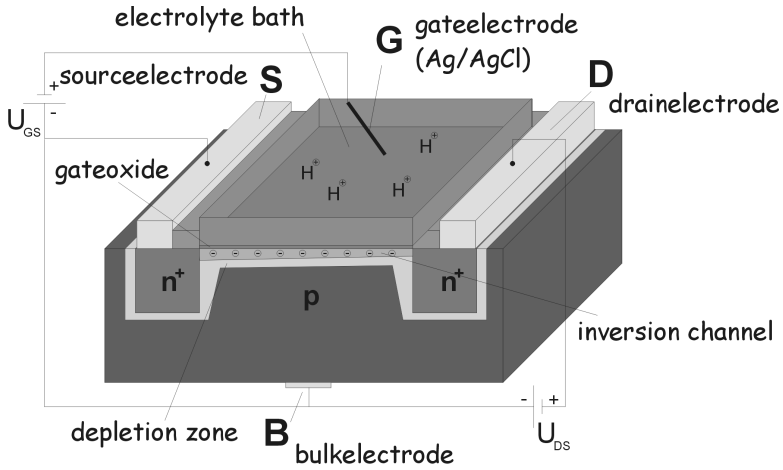

Figure 3.19: Schematic depiction of an n-channel FET. The gate oxide is contacted by an electrolyte solution. The gate-source voltage leads to a conducting n-channel, through which a current may flow due to the drain-source voltage. The drain current depends on the gate oxide surface charges, which are influenced by pH.

In that case, the channel conductivity is influenced by the potential drop Ψ_E across the electrolyte/oxide interface, which depends on the surface charge of the gate oxide. According to the site-binding model [Yate, 1974], the charge of a SiO_2 surface immersed in an electrolyte is controlled by the proton concentration $[H^+]$, and the dissociation constants K_a and K_b of SiOH moieties, which refer to the following reactions, which take place at the SiO_2-surface:

$$\equiv SiO^- + H^+ \leftrightarrow \equiv SiOH \qquad with \qquad K_a = \frac{[SiO^-][H^+]}{[SiOH]}$$

$$\equiv SiOH + H^+ \leftrightarrow \equiv SiOH_2^+ \quad with \qquad K_b = \frac{[SiOH_2^+]}{[SiOH][H^+]} \tag{3.37}$$

The pH-sensitivity of the EOSFETs used in the present work was determined to be linear with $\Delta\Psi_E = 34 \pm 2$ mV/ΔpH, which holds at least in the pH-regime from pH = 5 to pH = 13 [Sprö, 1997a].

3.7.2 Measurement setup

N-channel EOSFET 4x4 arrays were developed by M. Krause, MPIP Mainz [Krau, 2000]. The transistor arrays were mounted onto a standard 28-pin DIL ceramic carrier for integrated circuits, as described in [Sprö, 1997a]. A glass ring (with a diameter of 16 mm and a height of 3 mm) in combination with a silicon funnel served as an electrolyte container (with a volume of 400 µl) above the EOSFET array (see Figure 3.20).

Figure 3.20: Photo of an EOSFET array chip mounted onto a DIL ceramic carrier. The chip contacts were sealed by a silicon funnel surrounded by a glass ring, which served as a container for the electrolyte bath.

A combination of a low-noise pre-amplifier and a subsequent amplifier with power supply was used for signal processing as described in [Sprö, 1997a]. A 12 bit A/D converter (Jäger, Adwin 4) allowed for data-readout by a PC, supported by a program written by means of the software TestPoint (Keithley, version 3.0) [Sprö, 1997a]. Lipid bilayer membranes were deposited onto the EOSFET surfaces by vesicle fusion as described below. Obviously, the front-side contacted EOSFETs depicted in Figure 3.19 do not allow for a membrane deposition by Langmuir-Blodgett transfer (see below), which would be helpful for building more complicated model membrane systems. However, the backside-

contacted EOSFET chips developed by S. Ingebrandt [Inge, 2001] offer a promising route to EOSFET-supported model membrane systems, which can be prepared by Langmuir-Blodgett trough methods.

3.8 AFM-microscopy

Atomic force microscopy (AFM) was developed in 1986 [Binn, 1986] and has found a widespread use in a variety of surface science areas. Basically, a cantilever tip consisting of Si, SiO_2 or Si_3N_4 is moved over the sample surface by piezoelectric scanners. The deflection of the cantilever is detected by the reflection of a laser beam (see Figure 3.21). The tip deflection may either be kept constant by a feedback loop (constant force mode) or allowed to vary with the surface topology (deflection mode). Furthermore, three different methods for obtaining information about the topology of a substrate can be distinguished. Firstly, the tip is in contact with the sample during the whole scanning process (contact mode). Secondly, the tip may be oscillated at a defined frequency and only allowed to tap the surface (tapping mode) which permits the analysis especially of soft materials. Thirdly, the tip may be oscillated without contacting the surface. By the influence of surface forces on the probe deflection extremely smooth surfaces may be examined in particular. In the present work, the tapping mode was used for obtaining topography images of hydrogel films, in air and in water.

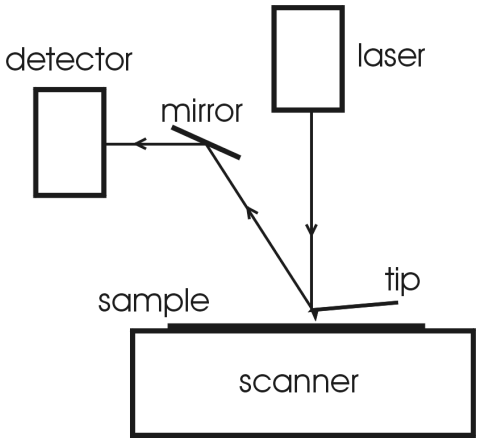

Figure 3.21: Schematic setup of an atomic force microscope.

3.9 Alpha stepper

Thickness measurements with an alpha stepper were performed by scratching the film with a sharp needle and measuring the step height between scratched and un-scratched areas. The instrument was an alpha-step 200, Tencor instruments, Mountain View, California.

3.10 Preparation techniques

In the following, the methods used for substrate cleaning, polymer film formation, membrane formation and membrane functionalisation shall be described.

3.10.1 Substrate cleaning and electrode production

Glass substrates were throughout cleaned by means of the following procedure:

- 15 min ultrasonication in a Hellmanex solution
- 10 times rinsing with MilliQ water
- 15 min ultrasonication in MilliQ water
- 10 times rinsing with MilliQ water
- 15 min ultrasonication in MilliQ water
- 10 times rinsing with MilliQ water
- 15 min ultrasonication in ethanol
- subsequent drying in a N_2-stream

A Hellmanex solution of a concentration of 2 % was used (Helma, Helmanex II). Ultrasonication was carried out at a temperature of 35 °C. The ultrasonication bath was a Sonorex, type Super RK510 H. MilliQ water was obtained from a Millipore water purification system ($R \geq 18.2$ MΩcm^{-1}, Millipore, Eschborn, Germany).
Gold electrodes were prepared by evaporation of 2 nm Cr (Balzers, 99.9 %) and subsequently 50 nm Au (Balzers 99.99 %) in a vacuum chamber at a pressure of $5 \cdot 10^{-6}$ mbar (Balzers, type BAE 250).

3.10.2 Spin-coating

Spin-coating was performed with the spin-coater EC101D, Headway research, which allowed for an adjustment of the spinning speed up to 10000 rpm.

3.10.3 Langmuir-Blodgett-trough techniques

Amphiphilic molecules spread at the air/water interface to form a monomolecular layer, when being applied to the water surface from a solution in a water insoluble volatile solvent. On a Langmuir-trough, the monolayer pressure, which acts against a lateral compression performed by a barrier, may be varied by changing the trough area [Pett, 1996].

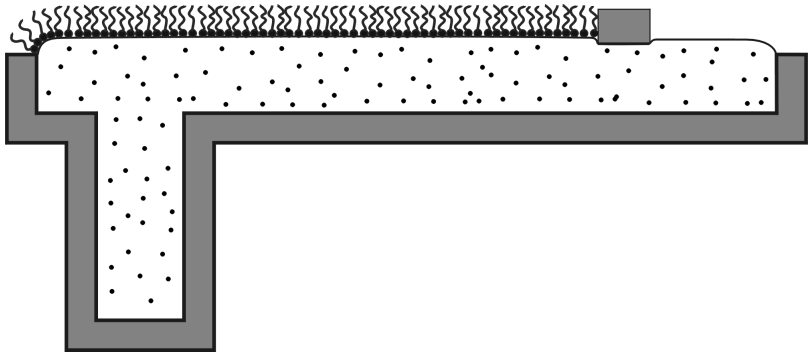

Figure 3.22: Langmuir-Blodgett trough with a single moveable barrier. The trough possesses a well to allow for substrate immersion during or prior to vertical monolayer transfer.

There are several ways to measure the lateral pressure of an amphiphile monolayer. The most popular ones are the Langmuir balance and the Wilhelmy plate method. By means of the latter method, which was applied in the present work, the surface tension, γ, of the monolayer-covered gas/liquid interface is measured. The lateral monolayer pressure is equal to the reduction of surface tension by the monolayer film, according to

$$\pi = \gamma_0 - \gamma \tag{3.38}$$

where γ_0 corresponds to the surface tension of pure water (72.8 mN/m at 20 °C). The Wilhelmy plate is a thin sheet of completely wettable material (generally filter paper is used) with a thickness, d, and an horizontal width, w. The plate is partially immersed into the trough and the vertical force acting on the plate suspension is measured by a balance. Provided that gravity and buoyancy can be neglected (which is the case for small pieces of filter paper) this force, F, amounts to

$$F = 2\gamma(d + w)\cos\Theta \tag{3.39}$$

where Θ is the contact angle at the triple line (plate, liquid and gas). For completely wettable plate materials and sufficiently thin plates ($d << w$) the change in surface tension, $\Delta\gamma = \pi$, is simply given by

$$\Delta\gamma = \frac{\Delta F}{2w} \tag{3.40}$$

The monolayer undergoes several phase transitions upon compression on the liquid surface. Analogous to three-dimensional systems gaseous, liquid and solid phase may be distinguished as shown in a typical pressure/area isotherm depicted in Figure 3.23.

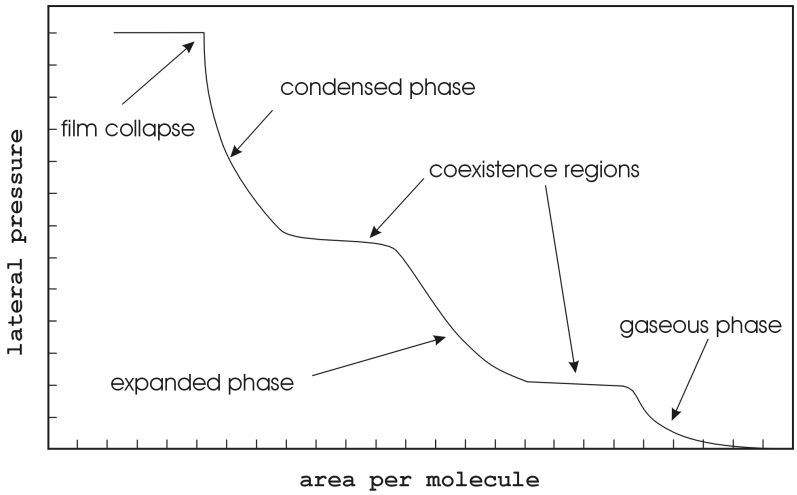

Figure 3.23: Schematic representation of a typical isotherm for a monolayer at the air/water interface.

Transitions between the gaseous and liquid expanded (fluid) phase and from the liquid expanded to the liquid condensed (solid) phase are first order transitions. Moreover, numerous higher order transitions exist, both in the expanded and more so in the condensed phase [Albr, 1978], [Pett, 1996]. Above a certain lateral pressure the monolayer collapses and multilayer structures are formed. The shape of pressure/area isotherms strongly depends on temperature, the properties of the trough subphase and the nature of the particular amphiphile. Regarding the latter, the length of the hydrophobic chain strongly influences transitions temperatures (in case of fatty acids reducing the hydrocarbon chain length by one methylene group is roughly equivalent to a temperature increase of 5 to 10 °C). Moreover, the kind of the lipid headgroup influences transition temperatures: e.g. in case of phosphoethanolamines higher transition temperatures are found compared to phosphatidylcholines, since in the former case lipid headgroups interact more strongly (via H-bonding). It must be noted that depending on the particular

temperature of the isotherm with respect to critical temperatures, the first order transitions schematically depicted in Figure 3.23 are not necessarily observed [Albr, 1978].
Amphiphile monolayers may be deposited by a vertical transfer both to hydrophilic or hydrophobic substrates, as shown in Figure 3.24.

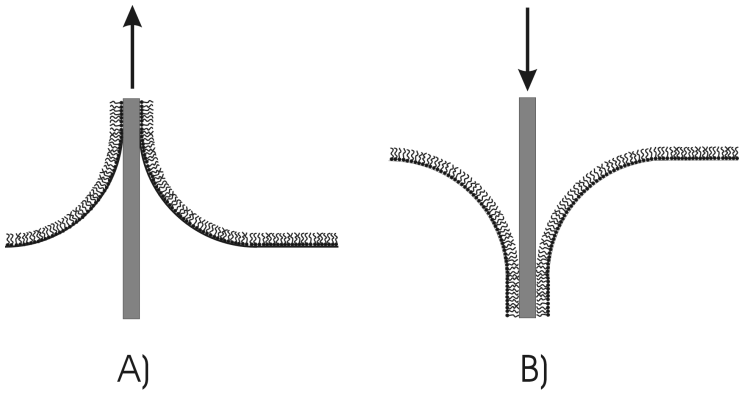

Figure 3.24: Langmuir-Blodgett transfer of an amphiphile monolayer onto A) a hydrophilic substrate by an upstroke and B) onto a hydrophobic substrate by a downstroke.

The deposition type as depicted in Figure 3.24 is called Y-type. In case of multilayer formation by Y-type transfer the alternating monolayers are faced head-to-head or tail-to-tail. However, deposition types are observed where monolayer transfer occurs only at a downstroke (X-type) or upstroke (Z-type). However, it is often not possible to fabricate a phospholipid bilayer by a Y-type deposition mode, since upon transfer of the second monolayer by a downstroke the membrane floats from the surface. This problem can be circumvented by a so-called Langmuir-Schäfer (or Schäfer) transfer. This approach consists of pressing a monolayer-coated substrate horizontally through the monolayer-covered air/water interface, which leads to the formation of a substrate-supported bilayer membrane, to be seen in Figure 3.25.

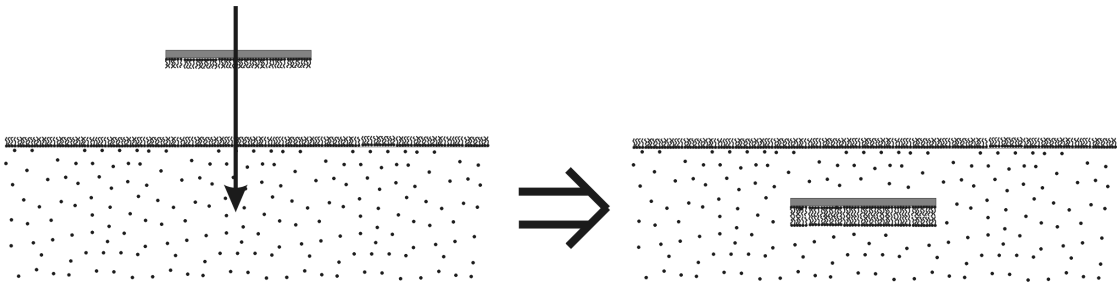

Figure 3.25: Langmuir-Schäfer transfer to obtain a substrate-supported bilayer. A monolayer-covered substrate is horizontally pressed through a monolayer at the air/water interface.

In the present work, the substrate could be stored and transported in a specially built small glass tub [Sinn, 1999], which was inserted into the trough subphase before spreading of the

monolayer. The glass bowl allowed for transferring the bilayer-coated sample to the measurement chamber (e.g. of the FRAP apparatus). In every case lipid monolayers were compressed at a barrier speed of 20 cm^2/min. Langmuir-Blodgett transfer was performed at a dipper speed of 4 mm/min.

3.10.4 Vesicle fusion

Besides the above-mentioned Langmuir-Blodgett/Langmuir-Schäfer (LB/LS-) transfer, bilayer [Bria, 1984] (or monolayer [Kalb, 1992]) membranes may be prepared by the fusion of small unilamellar vesicles (SUVs) onto hydrophilic (or hydrophobic) surfaces. While LB/LS transfer allows for an adjustment of lateral transfer pressure and moreover for the preparation of asymmetric bilayer membranes, vesicle fusion is a relatively simple method. Another advantage of the latter is the possibility to prepare functionalised substrate-supported bilayer lipid membranes in one step, by the fusion of protein-containing vesicles (see below).
SUVs may be formed by ultrasonication of a lipid dispersion [Bria, 1984], extrusion of a lipid dispersion through a filter with small pore size [MacD, 1991] or injection of an isopropanol lipid solution into the aqueous phase (e.g. [Wied, 2000]). In most cases during the present work the first method was applied. Lipid dissolved in chloroform was filled into test-tubes and the solvent was evaporated while rotating the test-tube so as to cover the inner walls by a thin lipid film. Subsequently, the lipid was thoroughly dried under vacuum over night. Afterwards, MilliQ water (or an aqueous solution) was added to the test-tube and the lipid was allowed to rehydrate for at least 3 *h* at 40 °C. Sonication was performed by means of a the tip sonicator Sonifier 250 Branson, at a power of 30 W for 30 min, using a water bath for cooling. The clear dispersion was centrifuged (Labofuge 200, Haraeus) at 5300 rpm for 15 min, in order to remove sonicator debris. The vesicle dispersion was used directly after preparation.
Alternatively, functionalised lipid bilayer membranes were obtained by the fusion of protein-containing SUVs (see below). Prior to vesicle fusion, the dispersion was freshly extruded 20 times through polycarbonate membranes with a pore size of 100 nm. The extruder was a LiposoFast Basic, Avestin, Canada.

3.10.5 Preparation of giant multilamellar liposomes

Lipid from a stock solution in chloroform was dried on a teflon disk and desiccated under vacuum over night. Subsequently, 100 mM sucrose solution was added to the teflon disk

placed at the bottom of a glass beaker and left for at least 12 h at 40 °C. During this time, the lipid swelled and formed closed vesicles. A few ml of this vesicle dispersion was transferred into a measurement chamber filled with 100 mM inositol. The vesicles sedimented slowly to the bottom of the chamber due to the difference in density of sucrose inside the vesicle and inositol outside. In the case of experiments with giant multilamellar vesicles (liposomes), the measurement chamber consisted of a teflon frame (10 × 30 × 40 mm) into which a hole was drilled (∅ 8 mm). The teflon frame was closed at the bottom by a glass cover slip.

3.10.6 Protein reconstitution

Membrane proteins isolated from biological sources and solubilised by means of detergent may be reconstituted into artificial bilayer lipid membranes. It is necessary, however, to remove most of the detergent present in the protein preparation since high amounts of detergent may substantially decrease the bilayer membrane quality (detergent stabilises membrane defects and causes the lipid membranes to become leaky or even to decompose). Detergent removal may be performed by gel filtration, dialysis or the use of polystyrene beads. Two general categories for reconstitution may be distinguished [Genn, 1989]. In one case, most of the detergent is removed before applying the protein to lipid membranes. In the second case, proteins and lipids are mixed together in the presence of detergent, which is then removed to yield proteoliposomes.

H^+-ATPase (ATPase CF_0F_1 from chloroplasts) containing eggPC vesicles (10 protein molecules per vesicle) used in the present work were a gift from P. Gräber, Freiburg. Nitrate reductase from “Pseudomonas Stutzeri” reconstituted into DMPC/POPC (1:1) vesicles were kindly provided by P. Steinrücke, Jena. In both cases, protein reconstitution had been performed by the second strategy mentioned above, the detergent was removed by dialysis [Rich, 1990], [From, 1992].

Reconstitution of solubilised (fluorescence labelled) cytochrome c oxidase (COX) by detergent dilution was performed as described in [Naum, 1999]. The fluorescence labelled COX was kindly provided by A. Aagaard, Göteborg. The labelling of the protein with fluoresceine isothiocyanate was performed as described in [Mara, 1998]. The protein was solubilised by dodecylmaltoside.

4 Preparation and characterisation of thin and ultrathin polysaccharide films

In chapter 2 it was pointed out that polymer interlayers have a great potential for effectively decoupling lipid membranes and the peripheral parts of integral membrane proteins from supports such as gold, glass, indium tin oxide (ITO) or silicon devices. Therefore numerous efforts have been made to prepare suitable polymer cushions, physisorbed or chemically coupled to an underlying support, as well as physisorbed or chemically coupled to the lipid membrane on top.

Regarding chemisorbed lipid membranes as target structures, two main approaches can be distinguished, depending on the order of layer preparations [Knol, 2000]. The first is the synthesis/attachment of a polymer cushion on/to a solid substrate and the subsequent deposition of a lipid monolayer with reactive headgroups (bottom-up concept) [Beye, 1996b], [Heib, 1998]. The second one is the synthesis of co- or terpolymers (top-down process), consisting of a hydrophobic lipid (or lipid-like) part, a hydrophilic spacer and in some cases a reactive anchor group, followed by transfer to the substrate [Spin, 1992], [Corn, 1997], [Ragu, 1998], [Haus, 1998], [Heib, 1998], [Sinn, 1998], [Thea, 1999], [Shen, 2000].

The stabilisation of a lipid membrane on a polymer cushion by strong electrostatic binding can be regarded to be intermediate between chemi- and physisorption, on the one hand no chemical bond is formed, but on the other hand lateral fluidity is decreased drastically [Cass, 1999], [Jenk, 2000].

Whereas lipid membranes, which are either completely or partially chemically coupled to the polymer cushion, are regarded to be advantageous to membrane stability, they increase the synthetic expense and considerably reduce membrane fluidity. The latter is generally assumed to be favourable, if not essential for the activity of membrane proteins. In the present work, however, membranes were prepared which were (predominantly) purely physisorbed to the polymer cushion. This was due to the easier preparation and higher fluidity compared to chemisorbed membranes and because of the fact that the focus of this work was to characterise the membrane/polymer interface in terms of dynamics and water content. Clearly, for this purpose purely physisorbed membranes are more suitable.

The first reports on physisorbed polymer-supported lipid monolayers on a solid substrate probably were published by the Ringsdorff group [Chi, 1992a], [Chi, 1992b], [Chi, 1993], [Chi, 1994]. In these works, polyethyleneimine (PEI) was used as an interlayer between a solid support and an amphiphile membrane (see also [Wong, 1999a] and [Wong, 1999b]). Additionally the polysaccharides dextran and cellulose [Elen, 1996], [Raed, 1997], [Györ,

1999], [Niss, 1999], [Hill, 1999], [Wieg, 1997a] and polyacrylamide [Arya, 1985], [Kühn, 1994] were applied to prepare polymer-supported mono- and bilayer lipid membranes.

While each of the above mentioned systems has its advantages and disadvantages, all of those systems have in common the fact that it is difficult or impossible to control or alter the membrane/substrate spacing by varying the thickness of the interlayer polymer cushion. The latter is of importance for surface sensitive techniques (see below). Additionally, the electrical analysis of single membrane channels requires a large ionic reservoir (i.e. a polymer cushion of sufficient thickness) [Cost, 1998]. The use of polymers, which are soluble under particular conditions and otherwise form a water insoluble gel is a way to avoid these problems. In combination with dip-coating or spin-coating an extremely wide range of polymer thicknesses can be obtained readily (see below). Additionally, this approach offers a very simple and time-saving access to ready-to-use polymer cushions for the preparation of supported lipid membranes, which is favourable for extensive physico-chemical investigations (as carried out in the present work). Agarose and chitosan are polysaccharides, which can be dissolved under special conditions (see chapter 8.1.2), and are insoluble under the conditions used for membrane preparation and analysis.

Probably due to the simple fabrication of the polymer cushion, agarose has been used extensively for supporting membranes, which were obtained by the thinning of a lipid solution, painted across a small aperture. These BLM-like membranes were formed either on top of an agarose cushion exposed to electrolyte [Hong, 1987], [Uto, 1994], [Hian, 1996], [Lu, 1996], [Novo, 1997], [Ide, 1999], or sandwiched between two agarose sheets [Cost, 1998], [Cost, 1999], [Cost, 2000]. Additionally, monolayer lipid membranes were transferred to agarose by means of Langmuir-Blodgett transfer [Diet, 1995]. In chapter 6.1, the stability of lipid bilayer membranes will be examined, which were prepared by LB/LS-transfer onto thin agarose films.

The use of chitosan as a polymer cushion to support planar bilayer lipid membranes, as described in chapter 6.2, has (to the best of the author's knowledge) not been reported so far. However, chitosan has been utilised to coat liposomes with a monomolecular layer (so called "chitosomes"), leading to an enhanced liposome stability [Henr, 1994], [Henr, 1996], [Take, 1996], [Henr, 1997]. In chapter 6.2 it will be shown that in comparison to agarose, chitosan polymer cushions, which are as easy to prepare as agarose films, have major advantages for preparing homogeneous and stable bilayer lipid membranes by LB-methods.

4.1 Film thickness

Surface techniques to study biomaterial/host interfaces (see [Chit, 1998b] and references therein) require control of the film thickness of adhesion layers, or layers which render a surface bio-compatibel. Included in these surface techniques are methods using evanescent waves (in the infrared or visible wavelength range), such as total internal reflection fluorescence (TIRF) [Murm, 1998], [Robe, 1998], attenuated total reflection Fourier transform infrared spectroscopy (ATR/FTIR) [Chit, 1998a], waveguide spectroscopy [Plow, 1998] and surface plasmon resonance spectroscopy (SPS) [Kamb, 1999]. Furthermore, interference reflection microscopy methods [Rädl, 1993b], are used to characterise the biomaterial/support interface. Common to all these techniques is the necessity that the interface of interest must be at an optimal distance from the surface of the support. Both the evanescent and interference techniques have a limited distance range and the contrast obtained using reflection interference techniques critically varies with the distance between the reflecting interface of interest and the support (see chapter 6.2.3). Furthermore, epi-fluorescence microscopy, which was used extensively in the present work for a variety of purposes including FRAP (see chapter 3.1), requires (in case of high-magnification and high-resolution images) oil immersion objectives with a large numerical aperture and hence small working distance. For these reasons, an adjustment of polymer film thickness was of utmost importance for the techniques used and aims followed in the present work.

A reliable procedure to adjust the thickness of physisorbed polymer films is to coat the sample with a polymer solution, while vigorously spinning the substrate (spin-coating) [Wals, 1999]. This procedure, however, was not feasible in case of thin agarose films because agarose is water-soluble only at elevated temperatures. Reflection interference contrast microscopy revealed that spin-coated agarose films were rather inhomogeneous, possibly due to the gelation occurring during spin-coating (picture not shown). Therefore, agarose films were prepared by dip-coating, i.e. the substrate was immersed into a hot agarose solution of defined concentration and quickly withdrawn. A thin polymer film remained on the glass [de Ge, 1986] and formed a thin gel film upon cooling [Diet, 1995]. The concentration of the polymer solution allowed to reliably control the film thickness (Figure 4.1). The resulting film thickness depends on the viscosity and surface tension of the polymer solution, as well as on the velocity with which the substrate is withdrawn from the solution (see (4.1)). It must be mentioned, however, that the viscosity of the solution is time dependent. Prolonged heating of the polymer solution in absence of buffer results in autocatalytic chain cleavage, accompanied by a reduction of viscosity and gelling ability

[Hick, 1968]. Samples were therefore prepared immediately after complete dissolution of the polymer.

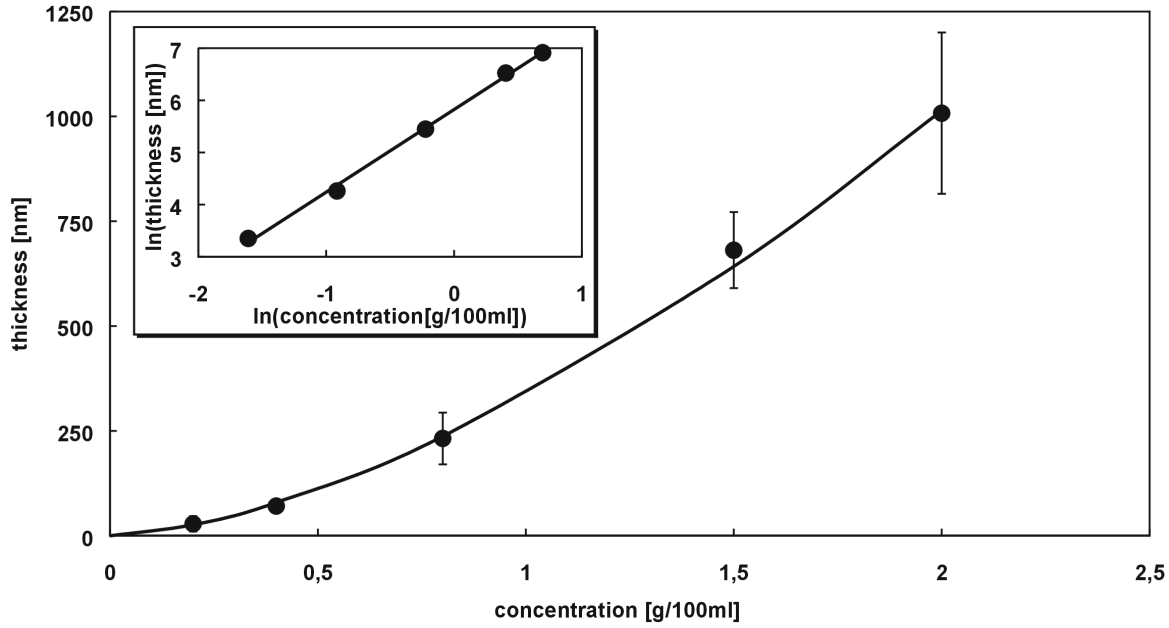

Figure 4.1: Thickness of agarose films as measured by an α-stepper. The films were prepared by dip-coating from a hot solution. Thicknesses were measured after gelation and drying the film at ambient conditions.

In principle, according to the Landau-Levich theory [Land, 1942], the thickness e of the fluid film, which remains on a quickly withdrawn substrate, can be calculated by

$$e = 0.94 \frac{(\eta v)^{2/3}}{\gamma_{LV}^{1/6} (\rho g)^{1/2}}, \tag{4.1}$$

where η is the viscosity of the solution, v is the velocity with which the substrate is withdrawn from the solution, γ_{LV} is the surface tension of the solution, ρ is the density of the solution and g is gravity. The unknown parameters in (4.1) are the viscosity and surface tension of the coating solution. Both parameters are concentration dependent and as this dependence is not known, the thickness/concentration relationship shown in Figure 4.1 is only empirical[1)]. On the other hand, the empirically found thickness/concentration correlation can be used as a calibration curve to control the film thickness of dip-coated agarose layers.

[1)] In principle, the concentration dependence of the viscosity can be calculated by means of the Huggins equation and the Mark-Houwink equation [Elia, 1990]. These equations, however, contain empirical parameters, which were unknown in the present case.

While in the case of agarose the film forming methods to produce layers with a thickness in the sub-micrometer range were limited to dip-coating, in the case of chitosan thin films could be prepared in three different ways. Molecularly thin films could be prepared by adsorption from an acetic acid solution onto a glass, mica or SiO_2 surface [Clae, 1992]. Besides physisorption from solution and dip-coating (see above), spin-coating from an acetic acid solution led to high-quality films (see chapter 4.2). These films were stable on glass and gold substrates upon immersion in pure water or electrolyte.

By varying both spinning speed and concentration of the coating solutions, spin-coated films as thin as only a few nm could be prepared (Figure 4.2). Tapping mode AFM microscopy revealed a homogeneous deposition and the absence of dewetting under the preparation conditions shown in Figure 4.2. On the other hand, thick chitosan films (in the µm range) prepared by dip-coating, were prone to develop cracks during the drying process, as was observed by optical microscopy.

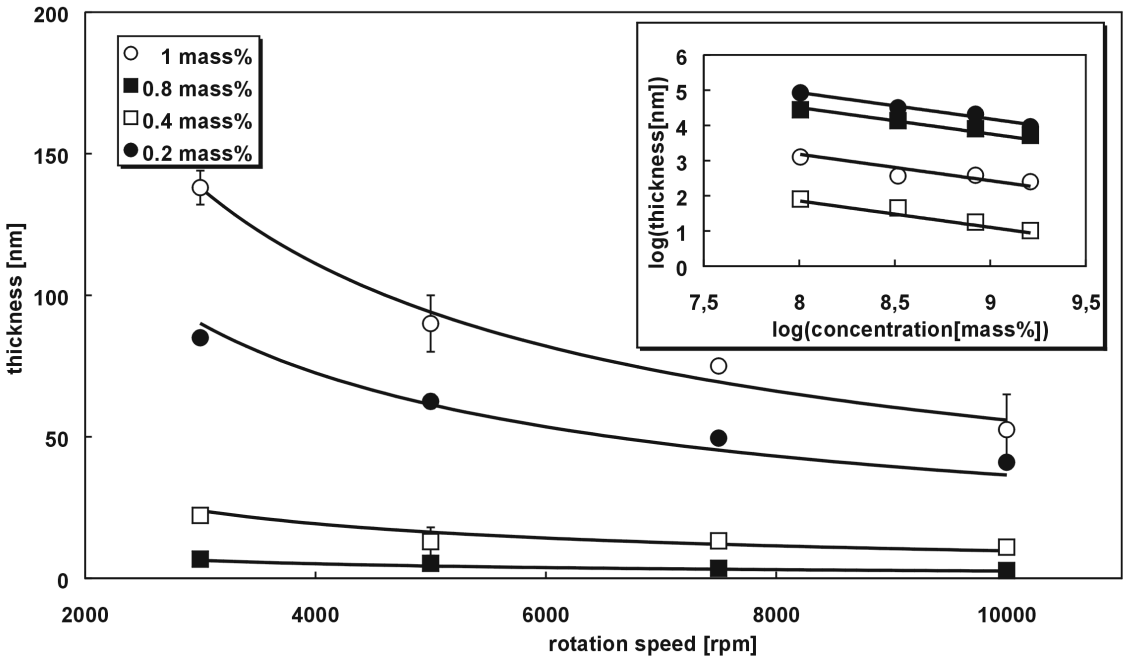

Figure 4.2: Thickness of chitosan films prepared by spin-coating as measured by ellipsometry. Both spinning speed and concentration of the chitosan solution was varied. The lines result from a simultaneous fit of (4.2) to the whole data set.

Due to the influence of numerous parameters, the spin-coating process is rather difficult to describe theoretically, and the equations are of little relevance for practical use [Lawr, 1988], [Born, 1989], [Shim, 1989]. However, often an empirical relation of the form

$$d = Ac^{\alpha}\omega^{\beta} \qquad \textbf{(4.2)}$$

can be found, where d is the final thickness of the dry film, c is the concentration of the spinning solution, ω is the spinning velocity and A, α and β are empirical parameters. The parameter α was often found to be greater or equal to one, and β equalled in many cases – 0.5 (see [Wals, 1999] and references therein).

The bold lines in Figure 4.2 result from a simultaneous least squares fit of the master equation (4.2) to the whole data set. From the fit, the following master equation for spin-coating of dilute chitosan solutions was obtained:

$$d = 5.6 \cdot 10^4 c^{1.91} \omega^{-0.75} \tag{4.3}$$

where the unit of the thickness is in nm, the concentration is in mass% and the spinning speed rotations per minute (rpm). According to Figure 4.2, a satisfactory agreement between (4.3) and the experiment was found over the whole range of concentrations and spinning speeds. Generally, the film quality in terms of surface roughness and homogeneous coverage depends on the parameters of the spin-coating procedure, such as the concentration of the solute, the choice of solvent and the spinning speed [Zieg, 2000]. Homogeneity and low surface roughness of the polymer film are a requirement for a successful deposition of lipid membranes onto polymer cushions [Kühn, 1994]. Therefore, agarose and chitosan films were further analysed by AFM, both directly after the preparation in air and subsequently in a water-swollen state.

4.2 Characterisation of the film surface by means of AFM

Figure 4.3 reveals, that agarose cushions had a pronounced roughness in the dry state already (the root mean square value (RMS) measured over an area of 50 μm^2 was 13.6 nm). Upon addition of MilliQ water, swelling of the polymer led to an expansion of the surface structures, both laterally and normal to the surface (Figure 4.3), and the RMS value increased to 29.4 nm. In contrast to agarose films, thin chitosan polymer films were rather smooth after spin-coating (Figure 4.4). The root mean square roughness measured in a square region of 1 μm^2, was found to be 0.26 nm. This is even lower than the roughness of the underlying glass support (RMS = 0.30 nm). No influence of the film thickness, i.e. spinning speed and concentration of the polymer solution on the quality of the films in terms of surface roughness, was found.

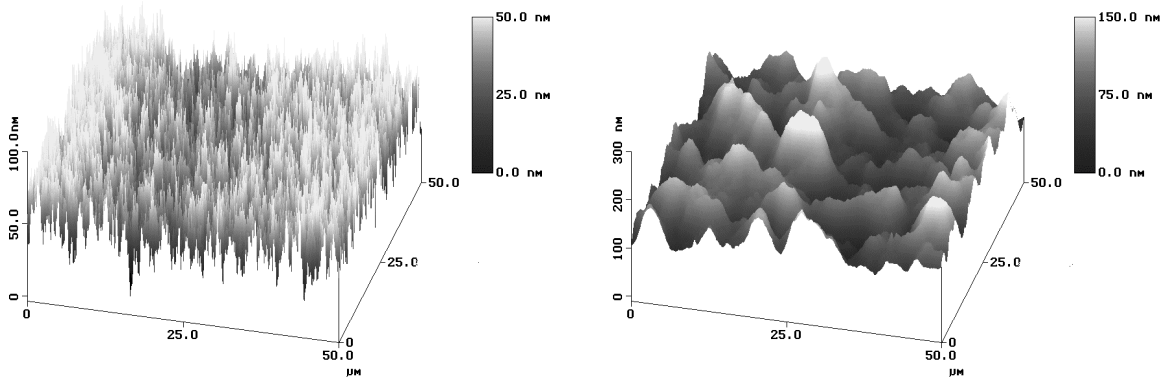

Figure 4.3: AFM topogram (tapping mode) of agarose in a dry (left) and water swollen (right) state (the right picture was taken while imaging under water).

Orange-Peel effects, frequently observed in the case of spin-coating of solutions with volatile solvents [Wals, 1999], were absent in all cases, indicating that water (in terms of a dilute acetic acid solution) is a favourable chitosan solvent to produce spin-coated films with high quality.

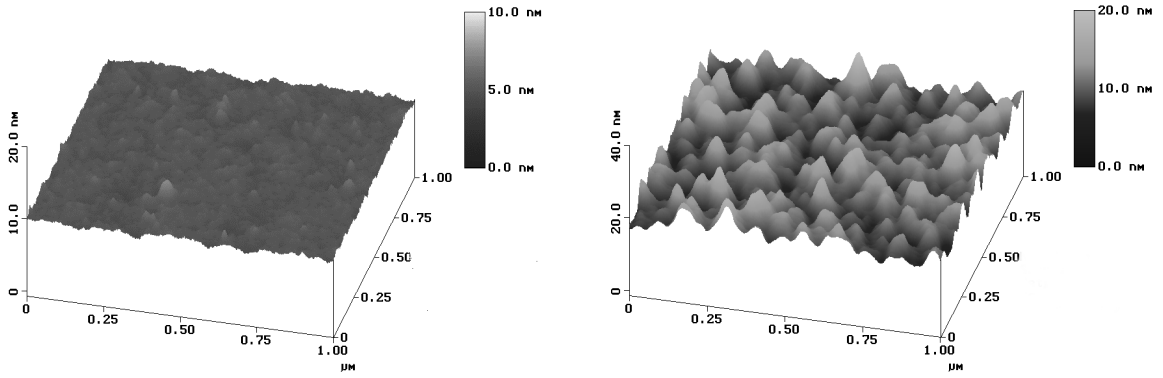

Figure 4.4: Tapping mode AFM pictures of chitosan in a dry (left, before neutralising) and water swollen (right, after neutralising) state.

Figure 4.4 reveals that films immersed in water after neutralising (chitosan was formed from acetic acid solutions, see chapter 8.1.2), showed an increased roughness (RMS = 2.17 nm) compared to the initial film. Moreover, the increased roughness of a neutralised, water swollen chitosan film could be shown to be mainly due to the neutralisation procedure. The roughness increase due to neutralising the polymer film can be seen by comparing Figure 4.5, where the topography of a neutralised chitosan film is shown (which was analysed after re-drying the film and imaging in air) with Figure 4.4 (left part). A RMS value of 1.32 nm was found for a neutralised chitosan film imaged in air. Without neutralising, the films seemed to be rather soft upon hydration in MilliQ water. Especially in case of thick films,

which were not neutralised, delamination was frequently observed. The AFM image revealed a relatively inhomogeneous surface (Figure 4.5, right). The vertical lines are imaging artefacts, indicating a very soft structure, difficult to image. The elevations found in the topography images of chitosan in the dry (Figure 4.5, left) and water swollen (Figure 4.4, right) state show quite regular diameters of (68 ± 11.7) nm and (154 ± 16.9) nm.

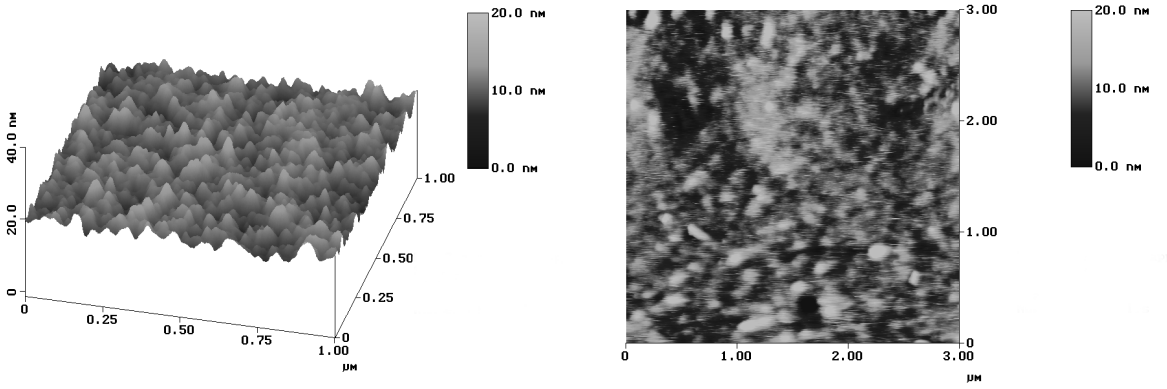

Figure 4.5: Tapping mode AFM topography images of spin-coated chitosan films. Left: film after neutralising the polymer, imaged in the dry state (in air). Right: chitosan film immersed and imaged in MilliQ water without neutralising prior to addition of MilliQ water. Due to the imaging artefacts in the right picture, the image was not converted into a surface profile plot.

These diameters possibly correspond to individual chitosan coils. From the ratio of diameters corresponding to water-swollen and dry state (which is 154/68 = 2.28), a volumetric swelling ratio may be calculated according to $2.28^3 = 11.85$, which is much higher than the swelling ratio of the bulk film (which is 3.1) as measured by ellipsometry (see chapter 4.4). A lower swelling ratio of the bulk film is reasonable because of stronger steric interactions in the bulk film than at the surface.

The roughness of a dry, neutralised chitosan film (RMS = 1.32 nm) may be compared with the values found for other polymer layers, which have been prepared to cushion lipid membranes so far. In the case of hairy rod cellulose derivatives, a roughness of 0.8 nm (measured by X-ray reflectometry) was obtained after the regeneration of cellulose [Scha, 1993]. In [Beye, 1996b], an oxide surface was modified with a copolymer, leading to a roughness of 1.33 nm [Beye, 1996a]. A lipopolymer described in [Shen, 2000], showed a RMS roughness of 1.39 nm in the dry state. Thus the roughness of neutralised chitosan films – although prepared in a simple manner – is comparable to those found for other polymers, which have been used to cushion lipid membranes. On the other hand, for the purpose of vesicle fusion (see chapter 6.2.5), a roughness as low as possible is favourable. Probably, the roughness of spin-coated chitosan films can be further reduced by cross-linking the polymer after spin-coating but before neutralising. This could be performed by

coupling photo-linkers to the polymer chain before spin-coating, and photo cross-linking the polymer layer afterwards.

4.3 Contact angle measurements

Contact angle measurements on chitosan films were performed by means of the sessile drop method (using pure water). For freshly spin-coated films, prior to neutralising an advancing value of 65° was found, which is in agreement with published values [Chen, 2000]. After neutralisation, however, the value decreased to 25°, which is probably due to the substitution of acetate by the more polar borate (used in the neutralisation procedure). In both cases, a considerable contact angle hysteresis was observed, receding angles were difficult to measure due to the fact that the contact line hardly receded upon reduction of the droplet volume. Such behaviour is usually found with water swellable hydrogels with variable surface configurations and has been explained by the concept of surface-state-equilibration. The latter assumes a reorientation of hydrophilic and more hydrophobic moieties upon putting a water droplet on the gel surface (see [Yasu, 1994] and references therein). In the case of agarose, an advancing contact angle of 20° and a receding angle of approximately 10° was found, indicating a lower contact angle hysteresis as compared to chitosan.

4.4 Swelling experiments

Important functions of suitable membrane cushions are to provide a stabilising support on the one hand, and a water-rich cushion on the other hand. Highly water-swollen supports are advantageous to the lateral fluidity of the bilayer and to keep the membrane in a well hydrated state, on both sides of the bilayer (see chapter 5.4). Both conditions are necessary to ensure the functioning of integral membrane proteins. Therefore, water uptake by the polymer cushion upon immersion in buffer solution is favourable. The amount of water incorporated can be monitored by the swelling of the polymer, either in water, or in humid air.

In the case of agarose films, precise ellipsometry measurements were not possible because of the high roughness and heterogeneity of the polymer film. Unreasonable values were obtained from data fitting. The water uptake of the polymer cushion, however, may be inferred indirectly from the structural rearrangements of the agarose film upon swelling, as observed by AFM (see Figure 4.3). Chitosan films, on the other hand, were suitable substrates for optical thickness measurements (for an introduction into multi-angle

ellipsometry see chapter 3.4). In all cases (representative examples are shown in Figure 4.6), the ellipsometry data could be fitted by means of a box model, i.e. assuming the refractive index of the polymer film to be a step function. The assumption of a diffuse polymer/water interface [Habi, 1999] did not improve the fit quality, hence all data were fitted by the box model.

In Figure 4.6, the angle resolved ellipsometry data for a chitosan film in the dry state and the water-swollen state are shown.

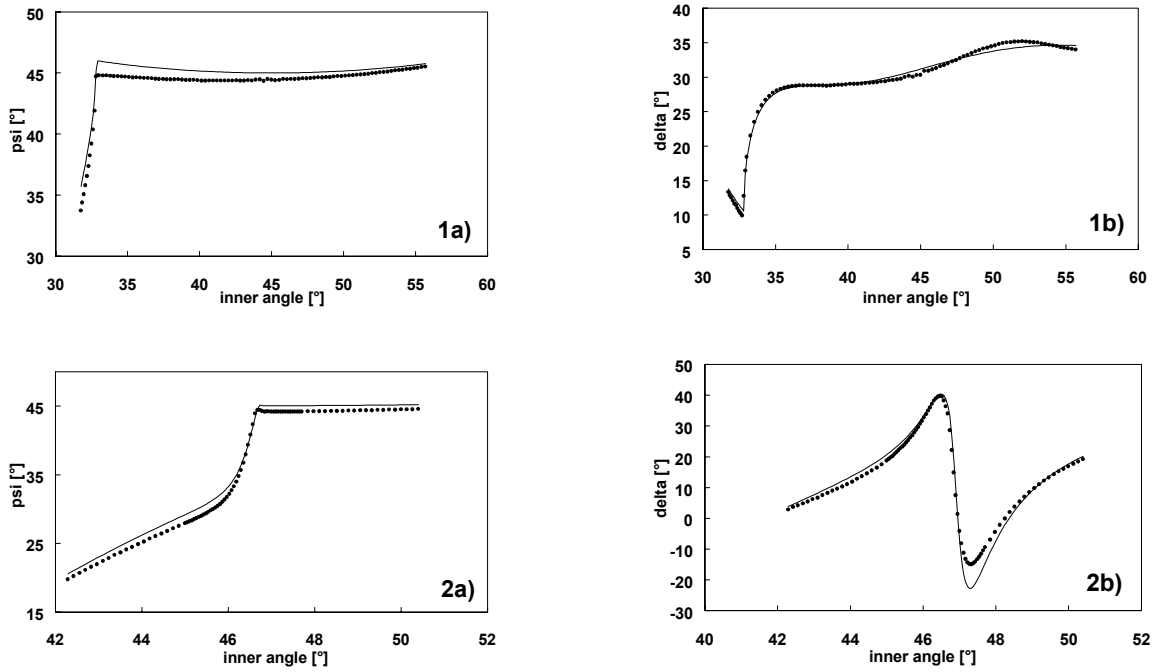

Figure 4.6: Psi (1a) and 2a)) and delta (1b) and 2b)) curves of a chitosan film in a dry (1a) and 1b)) and in a water swollen state (2a) and 2b)).

Simultaneous fitting of the Ψ and Δ curves (see chapter 3.4) yielded a dry film thickness (i.e. measured in air at ambient conditions, with a relative humidity of approximately 50 %) of 155 nm and a refractive index of 1.52. The refractive index of the dry film was slightly lower compared to the value for glucose (1.56, [Elen, 1996]), which is probably due to the fact that the polymer contained a residual amount of water (see below). Upon addition of MilliQ water (pH = 5.5), the polymer swelled to a thickness of 481 nm, i.e. by a factor of 3.1. A comparable swelling ratio was found in [Khal, 1999].

No thickness changes were observed during storage in MilliQ water over several weeks, indicating a stable film. Moreover, no significant thickness changes were observed upon addition of monovalent salt (NaCl) up to a concentration of 3 mol/l. This indicates that the slight protonation of the polymer (the pK_s value of chitosan is in the range 6.3 – 7 [Clae, 1992]) at pH = 5.5 does not influence the film thickness significantly.

Additionally, the swelling of a chitosan film with an initial thickness (of 198 nm) not much smaller than the wavelength of the laser beam used for ellipsometry measurements was analysed while increasing the relative humidity. The thickness increase upon swelling can be seen in Figure 4.7. Due to the relatively large thickness of the polymer cushion, both refractive index (see Figure 4.9) and film thickness could be fitted independently. As shown in [Bies, 2000], the swelling of hydrophilic polymers can be fitted by the Flory-Huggins equation:

$$\ln\frac{p}{p_0} = \ln\phi_1 + (1-\phi_1) + \chi(1-\phi_1)^2 \qquad \textbf{(4.4)}$$

where p and p_0 are the partial water pressures at the particular relative humidity and in case of water saturation, ϕ_1 is the volume fraction of solvent molecules in the polymer matrix (which can be calculated from the measured dry and swollen film thicknesses d_0 and d, respectively, according to $\phi_1 = 1\text{-}d_0/d$) and χ is the Flory-Huggins interaction parameter.

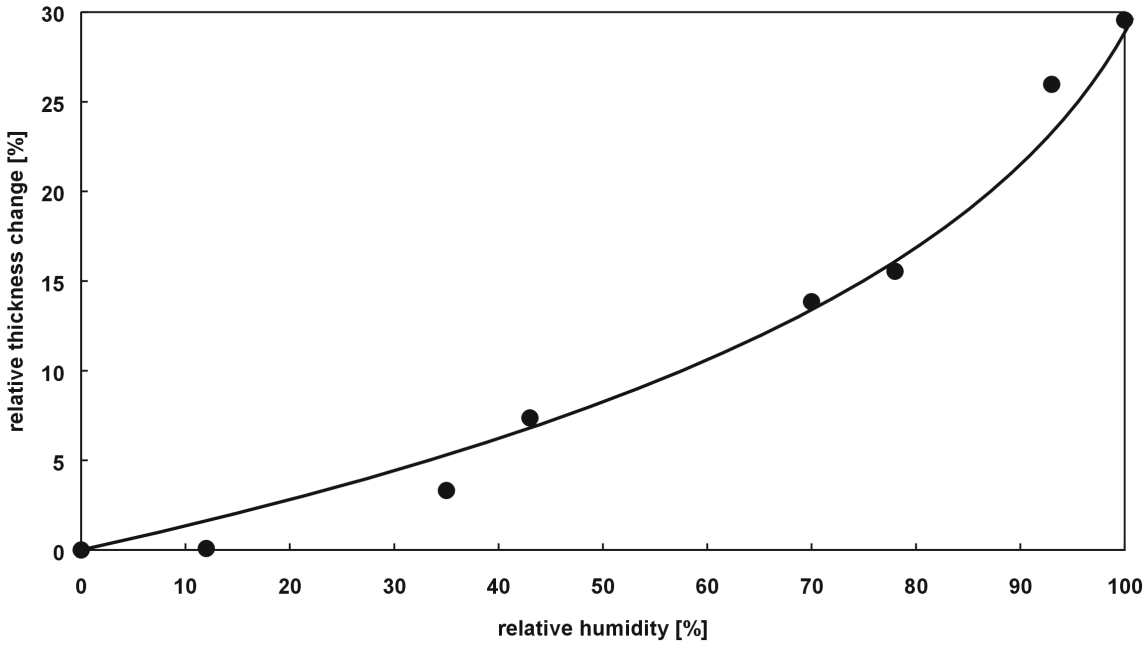

Figure 4.7: Relative humidity variation experiments on a chitosan film. The initial film thickness was 198nm. The bold line is a fit of the Flory-Huggins equation with the Flory-Huggins interaction parameter of 1.05.

According to Figure 4.7, the swelling of chitosan can be fitted successfully assuming a Flory-Huggins type swelling using an interaction parameter χ = 1.05. Values for χ in a comparable range are found in cases where the interactions of the solvent molecules are strong compared to the interactions between solvent and polymer [Bies, 2000]. As the

chitosan film at a pH value close to neutral can be described as an entanglement network, the Flory-Rehner model (4.5), which describes the swelling of polymer networks (taking into account an elastic resistance against swelling) should more accurately quantify the swelling behaviour of chitosan [Flor, 1953].

$$\ln\frac{p}{p_0} = \ln\phi_1 + (1-\phi_1) + \chi(1-\phi_1)^2 + \frac{\rho V_1\left(1-\frac{2M_c}{M_n}\right)}{M_c}\left((1-\phi_1)^{1/3} - \frac{1-\phi_1}{2}\right) \qquad \textbf{(4.5)}$$

In (4.5), ρ is the density of the dry polymer, V_1 is the molar volume of the solvent, M_n is the number-average molecular weight of the polymer and M_c is the effective molecular weight between two cross-linking points. However, a two parameter fit in terms of the Flory-Rehner model did not significantly improve the fit, hence the parameter M_c could not be determined. According to (4.5), the swelling process is independent of M_c if it is large, which means that the entanglement density is small. This is reasonable for a polymer spin-coated from a dilute solution.

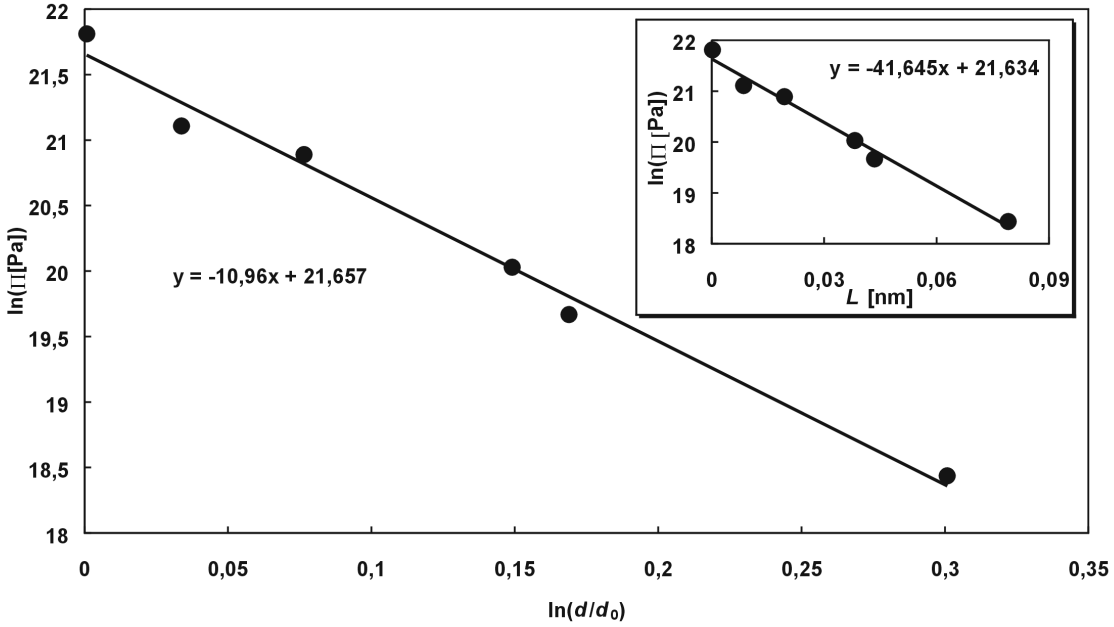

Figure 4.8: Logarithm of disjoining pressure and swelling ratios of chitosan films, as determined from relative humidities and film thicknesses shown in Figure 4.7. An alternative data representation in terms of plotting ln(Π) against the distance *L* between monomer units (see text) is shown in the inset.

The data shown in Figure 4.7 can be represented in an alternative way [Math, 1999] by plotting ln(Π), where Π is the disjoining pressure of the film against $\ln(d/d_0)$. This procedure allows for a further classification of the swelling process. The disjoining

pressure (see chapter 5.0.1) is calculated from the relative humidity $RH = p/p_0 \cdot 100$ according to

$$\Pi = \frac{kT}{\nu} \ln \frac{p_0}{p} \tag{4.6}$$

where k is Boltzmann's constant, T is the temperature and ν is the volume of a water molecule. The result of the axis transformation is shown in Figure 4.8.

According to [Math, 1999], a scaling law $\Pi \sim (d/d_0)^{-9}$, corresponds to a swelling process dominated by a hardcore potential. In [Math, 1999] exponents varying between -9 and -10 were found for the swelling of dextran and hyaluronic acid films, in case of small swelling ratios. A linear fit to the data shown in Figure 4.8 yielded an exponent of -11, which is only slightly exceeding the range found in [Math, 1999]. The discrepancy might be explained by a leaky measurement chamber in the present case. A lower relative humidity than the theoretical value (as valid for a completely closed cell) leads to a lower swelling ratio and hence to a smaller (i.e. more negative) slope in Figure 4.8.

For dextran and hyaluronic acid [Math, 1999], at higher humidities a crossing-over from hard-core repulsion to a regime dominated by hydration forces (4.7) was found. Due to the smaller swelling of chitosan, this cross-over is not observed in the present case.

Assuming hydration forces (4.7) to dominate the swelling process (see chapter 5.0.1), a data representation according to a plot of $\ln(\Pi)$ against the distance, L, between neighbouring monosaccharide units should yield a straight line.

$$\Pi = \Pi_0 \exp(-L/\lambda_w) \tag{4.7}$$

In (4.7), Π_0 is an internal pressure and λ_w is a decay constant (for the terminology concerning surface *forces* and disjoining *pressures* see chapter 5.0.1). The distance, L, may be calculated from the swelling ratio and the molecular size of a monosaccharide unit, approximately given by $a_0 = 0.75$ nm [Math, 1999]:

$$L = a_0 \left((d/d_0)^{1/3} - 1 \right) \tag{4.8}$$

From the fit parameters obtained from a linear fit to the data shown in the inset of Figure 4.8, the parameters $\Pi_0 = 2.4 \cdot 10^9$ Pa and $\lambda_w = 0.024$ nm were calculated. The decay constant is much too small as compared to cases where hydration forces dominate the swelling process (see chapter 5.0.1). Additionally, the relatively small distance L in the whole

swelling regime rules out the domination of hydration forces, since these are usually found in a distance regime between 1 and 3 nm (see chapter 5.0.1).

As mentioned above, an independent determination of film thickness and refractive index of chitosan films was possible. The refractive indices thus obtained are shown in Figure 4.9. According to the Garnet equation (4.9), the refractive index n_f of the water swollen polymer may be calculated from the refractive index n_0 of the dry film (1.58, see Figure 4.9), the refractive index of water n_w = 1.33, and the volume fraction of the polymer $\phi = d_0/d$ (Figure 4.7) [Baek, 1995].

$$\frac{n_f - n_w}{n_f^2 + 2n_w^2} = \phi \frac{n_0 - n_w}{n_0^2 + 2n_w^2} \tag{4.9}$$

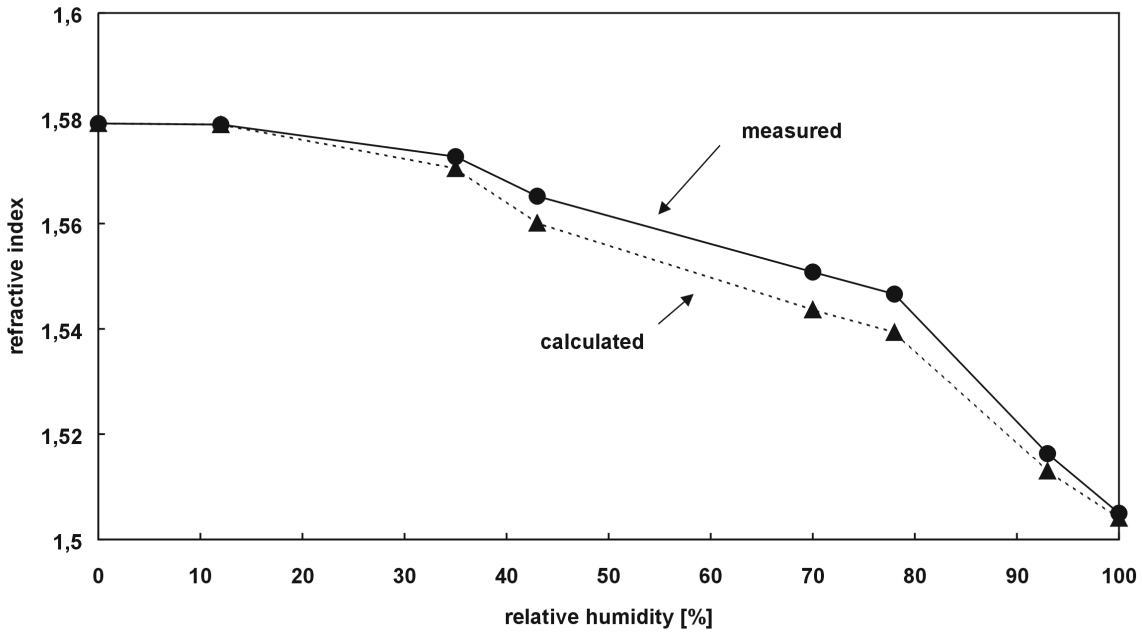

Figure 4.9: Measured and calculated refractive indices as determined by ellipsometry, in parallel to the film thicknesses shown in Figure 4.7.

According to Figure 4.9, a reasonable agreement between refractive indices calculated by (4.9) and those determined directly from the two parameter fits of the ellipsometry data is obtained, which underlines the reliability of the measurements. Moreover, the applicability of (4.9) allows determining film thicknesses during the swelling of chitosan films with a thickness much smaller than the wavelength of the laser beam, which was used for ellipsometry. These films are too thin for an independent determination of film thickness

and refractive index, but the film thicknesses may be obtained by applying (4.9) [Baek, 1995].

4.5 Covalent coupling of polymer layers to substrates

Chitosan films were chemically coupled to oxide substrates by means of a photo-linker. For this purpose, a benzophenone derivative was immobilised on the surface (see Figure 4.10).

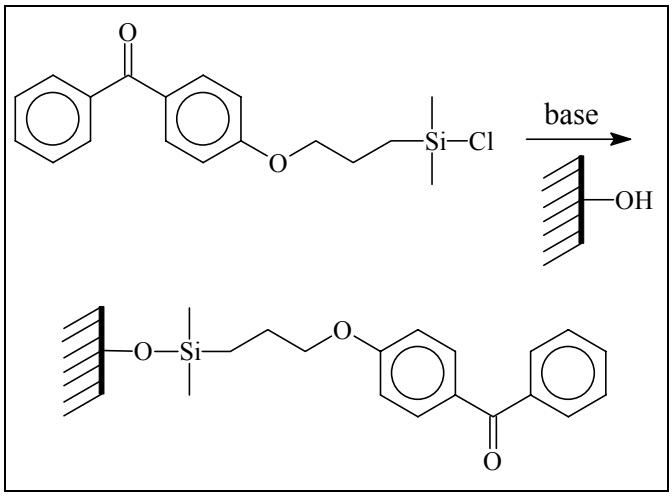

Figure 4.10: Immobilisation of a photo-reactive benzophenone derivative, used to chemically attach chitosan films to oxide surfaces.

Afterwards, a chitosan film was spin-coated onto the modified surface and irradiated with UV light (see [Pruc, 1999]), which leads to a radical reaction involving the carbonyl moiety and C-H-bonds of the spin-coated polymer. The successful coupling to the underlying surface could be observed by an increased resistance to vigorous rinsing. Under the conditions chosen for the experiments in this work, however, a physical adsorption was found to be sufficient.

4.6 Conclusion and outlook

Thin physisorbed polysaccharide films from agarose and chitosan were prepared by simple, time-saving but yet reliable procedures. Agarose was dip-coated and chitosan mainly spin-coated. While agarose films showed a pronounced surface roughness, chitosan films were relatively smooth initially. In the latter case, the roughness increased significantly upon neutralising the polymer film, but was comparable to the roughness of other polymer cushions, which – as described in the literature – were used to cushion lipid

bilayers. Swelling in water – a favourable, if not essential feature of suitable model membrane cushions – was observed for both polymers. In case of chitosan films, a quantification of the water incorporation was possible.

Both polymers have been used extensively in the past to support biomaterials. Chitosan, for example, is considered to be a suitable substrate for the bio-modification of implant surfaces and therefore receives considerable attention from medical sciences (e.g. [Suzu, 1999] and references therein). The thin films produced and characterised in the present work allow the use of surface sensitive analysis techniques. In the following chapters, these polysaccharide thin films will be used to cushion lipid mono- and bilayer membranes.

5 Characterisation of supported phospholipid monolayer membranes

The present chapter describes the characterisation of lipid monolayers, which were deposited onto the thin polysaccharide films examined in the previous chapter. For comparison, monolayers were also transferred to and analysed on glass supports. The substrate-supported lipid monolayer represents an intermediate stage in the fabrication of functionalised model membrane systems (see chapter 2) and therefore needs to be properly understood. Additionally, the monolayer stage allows for physicochemical studies, which would be more complicated, if not impossible, in case of a lipid bilayer.

The phospholipid monolayer represents one half of the bilayer, which is regarded to constitute, among other components, the compartmentalising part of biological membranes [Sing, 1972] (see chapter 2). The monolayer itself is for the biophysicist the simplest, most model like approach to the analysis of lipid membranes. It allows for the analysis of properties of the monolayer itself (for a review see: [Möhw, 1990]) and also the interaction of the monolayer with substances (e.g. proteins) present in the underlying subphase [Möhw, 1990] can be studied.

Direct biological relevance of monolayer studies arises from the fact that lung alveoli bear a thin liquid linen layer, composed of an aqueous subphase covered by a layer of pulmonary surfactant [Borg, 1988].

While the physicochemical parameters of phospholipid monolayers (more generally: Langmuir monolayers) at the air-water interface have been systematically and intensively studied for several decades [Möhw, 1990] and are currently relatively well understood [McCo, 1991], studies of substrate-supported phospholipid monolayers (more generally: Langmuir-Blodgett films) are relatively scarce [Fisc, 1984] so far. However, recently interest has particularly grown, partially due to upcoming technical applications [Swal, 1987] and partially due to the invention of new approaches, especially the scanning probe techniques [Ivan, 1997] like STM (scanning tunneling microscopy) [Smit, 1987], AFM (atomic force microscopy) [Chi, 1993], NSOM (near-field scanning optical microscopy) [Hwan, 1995], and related methodologies. Interest has especially been paid to the microscopic structure of supported phospholipid films. Both the film morphology directly after LB-transfer and lateral reorganisations upon storage have been examined [Chi, 1993], [Shik, 1998]. For the latter to take place, it has been observed that an increased relative humidity (*RH*) or the presence of other solvents is favourable [Chen, 1989], [Chi, 1992a], [Berm, 1997], [Shik, 1998].

However, "*surprisingly few studies have been made on the effects of humidity or other vapours on monolayer-coated surfaces exposed to ambient conditions*" [Chen, 1989]. Moreover, even the few works available in most cases only qualitatively describe the effects of changing ambient humidity – quantitative assessments of the effect of *RH* on dynamic parameters of supported phospholipid monolayers are rare.

The aim of the present chapter is to reduce this lack of information. The first part (chapter 5.1) deals with the distortion of monolayer structure by the condensation of water droplets on the monolayer film and the subsequent recovery of the homogeneous appearance at moderate humidities due to lateral spreading. This self-repairing effect will then be analysed quantitatively in chapter 5.2, in terms of the determination of spreading velocities of monolayers on various supports, depending on ambient humidity. While this effect will be shown to be due to convection driven by a Marangoni-force, and not due to surface diffusion of a two dimensional gas or liquid, the latter process, in particular the lateral self-diffusion of membrane probes due to thermally driven in-plane motions of lipid molecules, will be examined in chapter 5.3, with a special emphasis on the influence of humidity on the fluidity of the monolayer membrane. Finally, in chapter 5.4, it will be shown that the same fluorescence membrane probe (NBD-PE) which in the preceding chapters was used for examining dynamic properties of monolayer membranes, can be used to investigate local hydration changes in the headgroup region of phospholipid monolayers as a result of alterations of ambient humidity. However, before turning to the experimental results, a brief introduction concerning the surface forces determining the membrane/substrate interaction will be provided.

5.0.1 Forces involved in the membrane/substrate interaction

It is common practice ([Isra, 1992a]), to combine the contributions of different forces acting at the interface between two bulk phases in the disjoining pressure model. Note that in surface physics, forces are normalised with respect to the area of the interface. "Surfaces force" and "disjoining pressure" therefore are terms used for describing the same physical quantity [Isra, 1992a]. The term "disjoining pressure", for which the thermodynamic definition reads:

$$\Pi = -\frac{1}{A} \cdot \left. \frac{\partial G}{\partial d} \right|_{A,T,V} \qquad \textbf{(5.0.1)}$$

was introduced by Derjaguin [Derj, 1936]. The quantities in Equation (5.0.1) are as follows: Π is the disjoining pressure, A is the surface area, G is the Gibbs free energy, d is the separation distance between the two surfaces, T is the temperature and V is the volume of the bulk phases. The contributions to the total disjoining pressure in case of a substrate-supported lipid monolayer are:

$$\Pi(d) = \Pi_{dl}(d) + \Pi_{vw}(d) + \Pi_{hyd}(d) + \Pi(d)_{other} \qquad \textbf{(5.0.2)}$$

where Π_{dl} is the double layer repulsion, Π_{vw} is the van der Waals interaction and Π_{hyd} is the hydration repulsion. Additional forces, which often contribute to $\Pi(d)$ are the gravitational force, capillary forces and other forces (see below). In the following, the forces occurring in (5.0.2) shall be described separately.

Double layer forces

The basis for the calculation of the electrostatic contribution to the disjoining pressure is the diffusive double layer model (Gouy-Chapman-model [Gouy, 1917]), which allows to calculate the electrical potential, Ψ, at a certain distance from a surface, with the surface potential, Ψ_1. The surface potential and surface charge, σ_1, are interrelated by the Grahame equation [Grah, 1947]:

$$\sigma_1 = \sqrt{8\varepsilon_0 \varepsilon n k T}\,\sinh\left(\frac{e\Psi_1}{2kT}\right) \qquad \textbf{(5.0.3)}$$

with ε_0 being the electrical permittivity of free space, ε is that one of the medium, n is the salt concentration (expressed as particles/m^3, here for a 1:1 electrolyte), k is the Boltzmann-constant and e is the elementary charge.

In the case of small potentials, Ψ_1, below about 25 mV, the Grahame equation reduces to:

$$\sigma_1 = \varepsilon\varepsilon_0\kappa\Psi_1 \qquad \textbf{(5.0.4)}$$

The electrostatic pressure (force per unit area) in the gap with permittivity ε between two media 1 and 2 can be expressed as [Verw, 1948]:

$$\Pi_{el} = 64nkT \tanh\left(\frac{e\Psi_1}{4kT}\right)\tanh\left(\frac{e\Psi_2}{kT}\right)\exp(-\kappa d) \qquad \textbf{(5.0.5)}$$

In (5.0.5), k is defined as

$$\kappa = \left[\sum_i \frac{n_i z_i^2 e^2}{\varepsilon_0 \varepsilon kT}\right]^{0.5} \qquad \textbf{(5.0.6)}$$

where the ions, i, bear the charge, z_i. The inverse value, $l = 1/k$, is called the Debye length, or screening length. The Debye length directly yields the thickness of the electric double layer and can be used to calculate its capacitance.

van der Waals forces

In addition to electrostatic double layer forces present between charged or dipolar molecules, there is a further kind of force which acts between all types of atoms or molecules, be they charged, dipolar or neutral. Between *two* polar molecules at a distance, r, three distinct types of forces contribute to the total, attractive interaction, which are collectively known as van der Waals force. The interaction energy w_{vw} may therefore be written as [Isra, 1992a]:

$$w_{vw}(r) = -\frac{C_{vw}}{r^6} = -\frac{C_{orient} + C_{ind} + C_{disp}}{r^6} \qquad \textbf{(5.0.7)}$$

The three types of forces, derived from the interaction energies, are namely the orientation or Keesom force, the induction or Debye force and the dispersion or London force. Whereas the former two are due to the interaction of two permanent dipoles (Keesom force) or a permanent and an induced dipole (Debye force), the dispersion force is an induced dipole – induced dipole interaction and is essentially quantum mechanical in nature. The dispersion force often dominates the two other components.

In reality, often the interaction of surfaces consisting of many molecules rather than the two-molecule interaction described by (5.0.7) is of interest. The power laws describing the distance dependent interaction energy between macroscopic bodies of course depend on the actual geometry. For two flat surfaces interacting across a medium, the interaction energy per unit area W, yields

$$W_{vw} = -\frac{H}{12\pi d^2} \tag{5.0.8}$$

H is the so-called Hamaker constant [Hama, 1937], which is most accurately calculated by the Lifshitz theory [Lifs, 1955]. The Lifshitz theory – rather than additivity of pair interactions – takes into account the influence of neighbouring atoms on the interaction between any pair of atoms. The Hamaker constant for three media 1, 2 and 3 can be expressed as

$$\begin{aligned} H &= H_{\nu=0} + H_{\nu>0} \\ &\approx \frac{3}{4}kT\left(\frac{\varepsilon_1-\varepsilon_3}{\varepsilon_1+\varepsilon_3}\right)\left(\frac{\varepsilon_2-\varepsilon_3}{\varepsilon_2+\varepsilon_3}\right) \\ &+ \frac{3h\nu_e}{8\sqrt{2}}\frac{\left(n_1^2-n_3^2\right)\left(n_2^2-n_3^2\right)}{\left(n_1^2+n_3^2\right)^{1/2}\left(n_2^2+n_3^2\right)^{1/2}\left\{\left(n_1^2+n_3^2\right)^{1/2}+\left(n_2^2+n_3^2\right)^{1/2}\right\}} \end{aligned} \tag{5.0.9}$$

The zero frequency term $H_{\nu=0}$, where ν is frequency, includes the Keesom and Debye terms. The second term is the London force, with ε_i and n_i being dielectric permittivity and refractive index of medium i, h is Planck's constant and ν_e is an absorption frequency, which is assumed to be equal for all the three media.

From (5.0.9) it follows that the van der Waals force between identical macroscopical bodies in a medium is always attractive, whereas the van der Waals force between bodies of different material can be attractive or repulsive. The latter occurs, when the refractive index of a medium across which two different media are interacting is intermediate between these two media.

Furthermore, if two media, like a lipid membrane and a substrate like glass interact through water, the dielectric constant of the latter results in a large zero frequency contribution to the Hamaker constant which leads to the following approximation:

$$H \approx H_{\nu=0} \approx \frac{3}{4}kT \tag{5.0.10}$$

In contrast to the double layer interaction, the van der Waals potential is nearly insensitive to variations in electrolyte concentration and pH.

Combination of double layer and van der Waals forces: DLVO theory

The combination of double layer force and van der Waals forces is performed in the DLVO theory of colloidal stability, after Derjaguin and Landau [Derj, 1941], and Verwey and Overbeek [Verw, 1948].

An example representing a configuration studied in the present chapter, consisting of the media glass, water, lipid and air (in a sandwich geometry), where the water layer thickness is varied, is shown in Figure 5.1. The surface of glass is negatively charged and a zwitterionic phospholipid membrane bears a slightly negative surface charge also [Marr, 1996]. The double layer term in Equation (5.0.2) is therefore repulsive, but is overpowered by the van der Waals term. Adding negatively charged lipid to the membrane or using pure charged lipid increases P_{dl} and can lead to a secondary minimum, which has been observed experimentally [Schn, 1986].

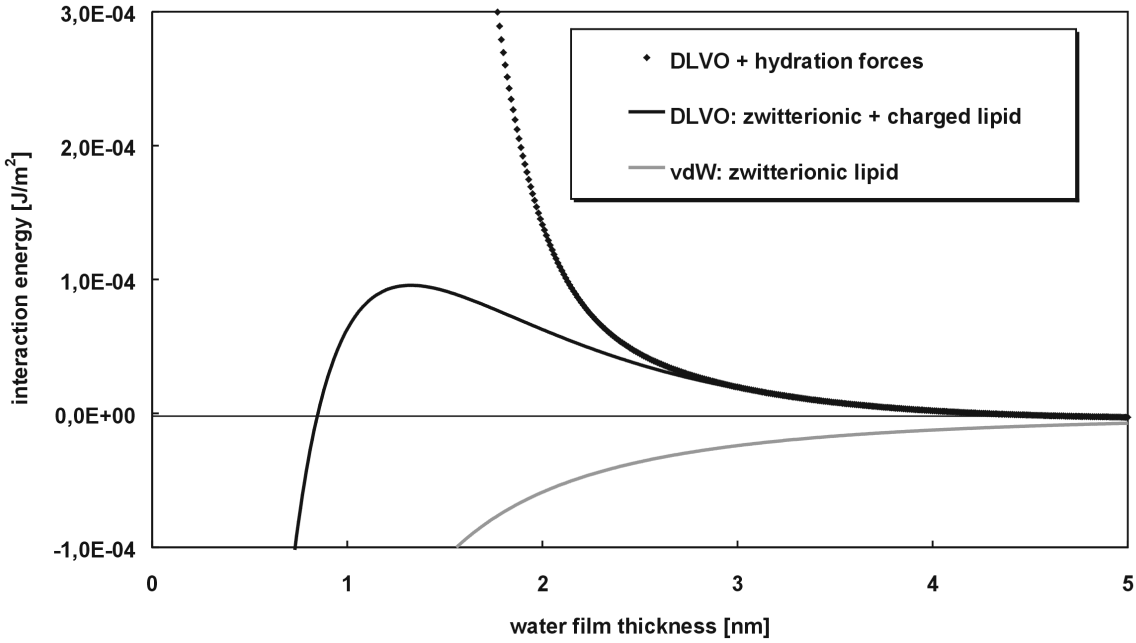

Figure 5.1: Energy per area versus distance profiles of surface interactions for the four-layer system glass, water, lipid and air. For the simulation the parameter were as follows: non-retarded Hamaker constant $5 \cdot 10^{-21}$ J [Frey, 1995], Ψ_{glass} = 70 mV, Ψ_{lipid} (zwitterionic) = 0.5 mV, Ψ_{lipid} (zwitterionic + small amount of negatively charged lipid) = 5mV, λ = 900 nm (pure water), $\Pi_0 = 3.16 \cdot 10^9$ N/m², λ_w = 2.2 Å (see [Iono, 1996] and chapter 5.3).

At small separations, the van der Waals interaction always exceeds the double layer force, which is due to the power law dependence of the former, whereas P_{dl} at small distances converges to a finite value. Also shown in Figure 5.1 is the contribution of a non-DLVO force, which shall be described in the next section.

Non-DLVO forces, the hydration force

From Figure 5.1 it follows that with the DLVO theory only, such phenomena like the swelling of lipid bilayers [Rand, 1989], the stability of vesicle dispersions of lecithins, or the thickness increase of amphiphilic monolayers on a support [Chen, 1989] upon increasing relative humidity, cannot be explained. In fact it can be assumed that without the existence of additional, repulsive forces, life would not be possible.

The breakdown of the DLVO theory at small distances can partially be explained by the breakdown of the continuum theories underlying both contributions. However, there are several additional phenomena, which give rise to further forces.

In general non-DLVO forces can be attractive or repulsive and at small separations they can be much stronger than either of the two DLVO forces.

In aqueous environments, the so-called hydration force [Lang, 1936], is responsible for large deviations from DLVO theory when hydrophilic surfaces approach each other to less than approximately 3 nm [Rand, 1989]. The origin and nature of these forces has been and is still controversially discussed [Isra, 1990], [Marr, 1993], [Leik, 1993a], [Isra, 1996]. It has been stated that the hydration force "*is probably the most important, yet the least understood of all the forces in liquids*" [Isra, 1992a].

Empirically, it was found that the repulsive hydration force decays exponentially with a decay constant often close to the dimension of a water molecule. This fact had led to the concept of water structuring by hydrophilic surfaces [Marc, 1976], which, however, later turned out to be – at least partially – erroneous [Isra, 1990]. In fact it has been stated that water structuring effects at surfaces actually lead to *attractive* forces [Isra, 1996].

Two main contributions to the hydration force may be identified. The first can be regarded as a solvation force (Israelachvili refers to this contribution as *the* hydration force [Isra, 1992a]). It arises whenever water molecules strongly bind to hydrophilic groups. The strength of this force depends on the energy needed to disrupt the hydrogen bonding network and/or dehydrate two mutually approaching surfaces. The range of this kind of hydration force is usually approximately 3 – 5 nm and it decays exponentially with distance [Rand, 1989].

Oscillatory forces, which have a mainly geometric origin, may result, if solvent molecules are forced into quasi-discrete layers between two lattice-like surfaces. In the case of lipid membrane surfaces, however, these oscillatory forces are smeared out due to the roughness of the headgroups on the scale of a water molecule and the thermal mobility of the surfaces.

The second type of hydration force arises between fluid-like amphiphilic molecules and is due to the suppression of thermally excited protrusions of the amphiphile from the fluid-like surface [Isra, 1990] when these surfaces approach (or one fluid-like surface

approaches a solid surface). This force is also called protrusion or steric force. It is easily shown [Isra, 1990] that the protrusion force per unit area obeys:

$$F = \frac{\left(n\alpha^2\, d/kT\right)e^{-\alpha d/kT}}{\{1-\left(1+\alpha d/kT\right)e^{-\alpha d/kT}\}} \qquad \textbf{(5.0.11)}$$

where $n = 1/s^2$ is the number of protrusion sites per unit area, with s being the lateral dimension (diameter) of a protrusion. In the case of a lipid membrane, s corresponds to the headgroup area of the lipid molecule. The parameter a is explained below. In the derivation of (5.0.11) it is assumed, that the density $r(z)$ of protrusions, extending a distance z (protrusion length) from the surface decays exponentially according to

$$\rho(z) = \rho(0)e^{-\upsilon_i(z_i)/kT} \qquad \textbf{(5.0.12)}$$

with the protrusion potential, $\eta_i(z_i)$, of the surface, i, being linearly approximated by

$$\upsilon_i(z) = \alpha\ z_i \qquad \textbf{(5.0.13)}$$

The interaction parameter, a, is calculated by multiplying the excess area, psz, created by a protrusion, by the interfacial energy, g:

$$\alpha \approx \pi\sigma\gamma \qquad \textbf{(5.0.14)}$$

(5.0.11) can be approximated by

$$F = C \cdot e^{-\frac{d}{\lambda}} \qquad \textbf{(5.0.15)}$$

with a decay length of

$$\lambda \approx \frac{kT}{\alpha} \approx \frac{kT}{\pi\sigma\gamma} \quad \text{for} \quad d > \lambda \qquad \textbf{(5.0.16)}$$

and an only weakly distance-dependent preexponential factor

$$C \approx 2.7 n\alpha \qquad \textbf{(5.0.17)}$$

The range of the protrusion force measured between surfactant and lipid bilayers is about 1 – 3 nm, with decay lengths varying between 0.08 to 0.64 nm [Rand, 1989]. Below a separation of 3 to 5 Å an upward break from this exponential law is predicted and has been found experimentally [Leik, 1993a].

Both contributions to the hydration force are therefore exponential with decay lengths and preexponential factors that are often comparable.

Due to their short range, it is usually not possible to experimentally distinguish between contributions arising from pure hydration (solvation) effects and thermal fluctuation (steric or protrusion) forces. In some cases, however, it is possible to regulate the hydrophilicity of molecules (e.g. by binding of counterions) and to identify a solvation force [Isra, 1992a].

In the calculation leading to (5.0.11), it was assumed, that only one protrusion mode contributes. In addition to these molecular scale protrusions, however, all fluid-like structures also undergo collective thermal fluctuations at the macroscopic level, which can be calculated by continuum theories. Among these are undulations (out of plane motions due to a finite bending modulus) and peristaltic motions (squeezing fluctuations due to a finite area expansion modulus). Repulsive forces arise whenever these motions are confined due to the approach of another surface. The distance dependence of the latter two forces obeys power laws, and therefore does not reflect the experimentally observed exponential decay of the disjoining pressure, at small separation distances.

Furthermore, when two lipid bilayers are brought into a short distance from each other their headgroups overlap, which yields an exponentially decaying force-law. This kind of repulsive force is dominant for separation distances below 0.5 nm [Marr, 1996].

Attractive hydrophobic forces are conventionally thought to arise because the orientation of water molecules in contact with a hydrophobic molecule is entropically unfavourable. Two such molecules therefore attract each other, since upon approaching, water is expelled to the adjacent bulk water, which is entropically favoured. However, the hydrophobic force at the current stage of research is not well understood theoretically [Isra, 1992a], [Finn, 1996].

Further non-DLVO forces can arise from bridging effects as induced by the presence of Ca^{2+} and from the disruption of the liquid hydrogen-bonding network between two surfaces.

In addition to these non-specific interactions, especially in biological systems, specific forces can be identified. These include such important phenomena like lock-and-key or ligand-receptor interactions, as for example found in the case of biotin and streptavidin [Wilc, 1990].
In summary, it can be stated that the hydration force, which is important for the understanding of the experiments described in the present chapter, consists of a very complex interplay between different contributions [Marr, 1996], which act either in parallel or against each other. Contrary to this complexity of forces is the empirical observation, that many biological surfaces like phospholipid membranes [Rand, 1989], polysaccharides [Rau, 1990], even DNA [Rau, 1984] and proteins [Leik, 1993b] show a mono-exponential variation of the disjoining pressure with respect to the separation distance. This empirical relation depends negligibly on the ionic strength and composition of the bulk solution.
The present chapter focuses on hydration effects of supported phospholipid monolayers at distances where the hydration forces dominate any contribution of DLVO forces. In the following paragraph, a brief overview about present and past research in this field is presented.

5.0.2 Research on phospholipid membrane hydration

Hydration effects in biological systems in general [Finn, 1996] and in biological membranes in particular [Jend, 1996] are a matter of intense scientific interest for several decades. This is due to the tension between the enormous importance of water in structural and dynamic aspects of animate nature on the one hand, and the poor understanding of water itself and its influence on biological processes and structures of biomolecules and their aggregates on the other hand [Finn, 1996].
Perhaps the earliest works directly studying phospholipid hydration date back to 1961 [Elwo, 1961]. Gravimetric techniques were used to study the water uptake of phospholipids at different stages of hydration. Since then, numerous techniques have been applied to study water uptake, pressure-distance relationships during swelling and structural transitions accompanying hydration. These techniques include microbalance [Arig, 1994], electrical [Piss, 1993], x-ray diffraction [Rand, 1989] and surface force measurements [Isra, 1987], nuclear magnetic resonance (NMR) [Bech, 1991], infrared spectroscopy [Bind, 1999], neutron reflectometry [Naum, 1995a] and several other methodologies.

Different methods have been applied to alter physical parameters that lead to hydration changes. Perhaps most common is the osmotic stress method (OSM) [Pars, 1979], [Rand, 1989]. Here, the water activity of a second phase is controlled and brought into equilibrium with the lipid membrane. Water activity is usually tuned by means of polymer solutions or by changing the relative humidity of a vapour phase, as described in chapter 3.5. The distance between two opposing lipid membranes can be varied more directly by the surface force apparatus. The agreement with the OSM is in most cases acceptable [Rand, 1989].
In addition to these experimental approaches to study biomembrane/water interactions, simulations on the basis of Monte Carlo [Gall, 1995] and molecular dynamics calculations have been carried out [Pere, 1996], [Marr, 1993], [Marr, 1996].
Not only has the amount of adsorbed water and its influence on static properties and property changes of lipid membranes been a matter of concern but also the dynamics of bound and unbound water at and near the surface of model and biological membranes.
Both simulations and experimental works concerning the influence of hydration forces on the dynamics of *lipid* molecules in lipid membranes, however, are relatively scarce. The former derives from the fact that at the present stage, computer power does not allow to simulate a hydrated lipid membrane for observation times, which are sufficient to allow for the calculation of reliable diffusion coefficients. The latter situation might be due to the strong frictional coupling of solid-supported monolayers to the underlying support, which slows down lateral translational dynamics considerably and phenomena like monolayer spreading and diffusion are difficult to analyse. In the present work, however, water swellable hydrogels were employed to reduce the friction between membrane and support [Sack, 1996].

5.1 Effects of the condensation of water droplets at high humidities

In the following chapter, supported phospholipid monolayers were subjected to an oversaturated vapour stream. This was performed by setting a temperature gradient over the microscopic coverglas. This could be accomplished by contacting the coverglass with a cold microscope objective. Condensation subsequently occurred below 100 % relative humidity, as measured by the chamber sensor. Presumably, condensation started at inhomogeneities of the lipid monolayer, such as defects, which acted as nucleation centres. The shape of the resulting water droplets, the influence of droplet formation on the lipid layer, and the behaviour of the distorted monolayer after reducing *RH* to a value just below the dew point were studied by means of RICM (reflection interference contrast microscopy) and fluorescence microscopy. In these experiments the support, as well as the monolayer lipid and the fluorescence probe were varied.

5.1.1 Glass surfaces

On lipid monolayers transferred onto thoroughly cleaned, bare microscopic coverglasses, water droplets appeared perfectly circular. The density of the interference fringes indicated a high contact angle (compare e.g. Figure 5.4), which can be seen in the following reflection contrast interferogram (Figure 5.2). The addition of fluorescence dyes to the monolayer did not influence the interference pattern. Therefore it can be concluded that the droplets were resting above the lipid layer, on the low energy surface of the lipid tails.

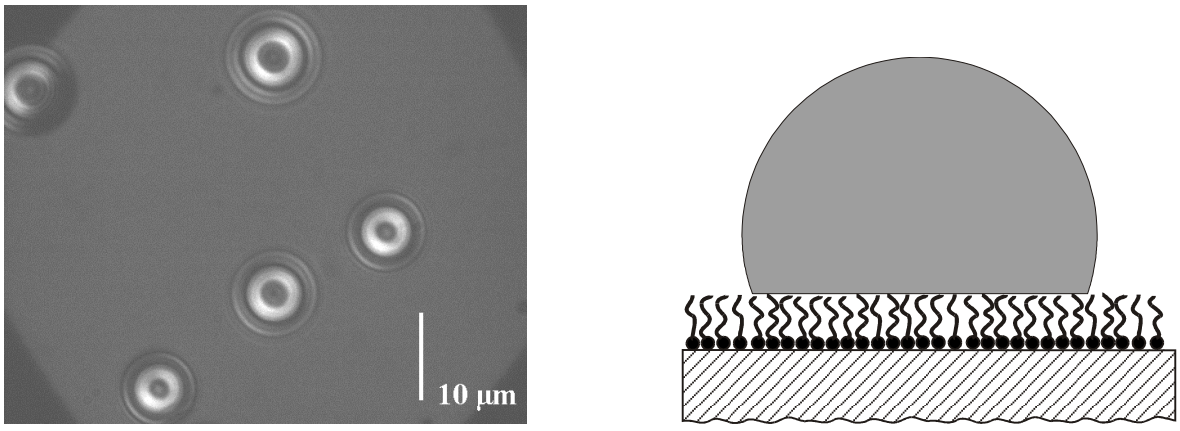

Figure 5.2: Left: interference fringes of water droplets, freshly condensed on a DMPC monolayer (lateral pressure 35 mN/m,) on a glass surface, right: schematic drawing of the configuration observed in the left image.

Theoretically, from interferograms obtained by RICM the contact angle of the water droplets can be calculated [Rädl, 1995b]. However, due to the following reasons such a calculation was not performed.

First of all, the Young equation (5.1.1), which describes the contact angle of a liquid droplet resting on an interface as a function of the surface energies of the relevant media, applies only in equilibrium.

$$\gamma_L \cdot \cos\Theta = \gamma_S - \gamma_{SL} \qquad \textbf{(5.1.1)}$$

In (5.1.1), γ_L, γ_S, and γ_{SL} are the free energies per unit area of the liquid-vapour interface, the solid-vapour interface and the solid-liquid interface respectively and Θ is the contact angle. The equilibrium condition requires:

$$\left.\frac{\partial G}{\partial A}\right|_{T,P} = 0 \qquad \textbf{(5.1.2)}$$

where A is the contact area between liquid droplet and the solid. While the droplet volume scales with the third power of the radius, the droplet surface is proportional to r^2. Very small droplets therefore occupy a relatively large area compared to macroscopical droplets and to fulfil the equilibrium condition (5.1.2) is difficult because of non-constant droplet areas due to evaporation/condensation. Second, for very small droplets, the contribution of Laplace pressure, Δp, (5.1.3) which due to the small droplet radius is not negligible changes during spreading.

$$\Delta p = \gamma_{WV} C \qquad \textbf{(5.1.3)}$$

In (5.1.3), γ_{WV} is the surface tension of water and C is the curvature, which for a spherical droplet corresponds to the inverse of its radius r.

Third, the analysis of RICM images of curved surfaces is not straightforward and practically, only contact angles below 40° can be determined accurately [Wieg, 1997b].

While contact angles were not explicitly computed, the interferogram of a water droplet resting on a lipid monolayer on glass (Figure 5.2) served as a reference for comparing contact angles *qualitatively* with other supports.

The influence of droplet condensation on monolayer homogeneity was analysed by fluorescence microscopy. In the experiment depicted in Figure 5.3, after the first droplets appeared, the humidity was switched back to a value below, but close to, the dew point.

Clearly, the monolayer was partially destroyed due to forces acting at and near the three phase (glass, vapour, water) line. On the other hand, monolayers totally immersed in water, by carefully pouring pure MilliQ water on top of them, were metastable [Yami, 1997] (Figure 5.46), which was also observed by others [Auch, 2000].
The exposure of the distorted monolayer to a relative humidity just below the dew point first caused the water droplets to evaporate and yielded a subsequent recovery of the homogeneous monolayer.

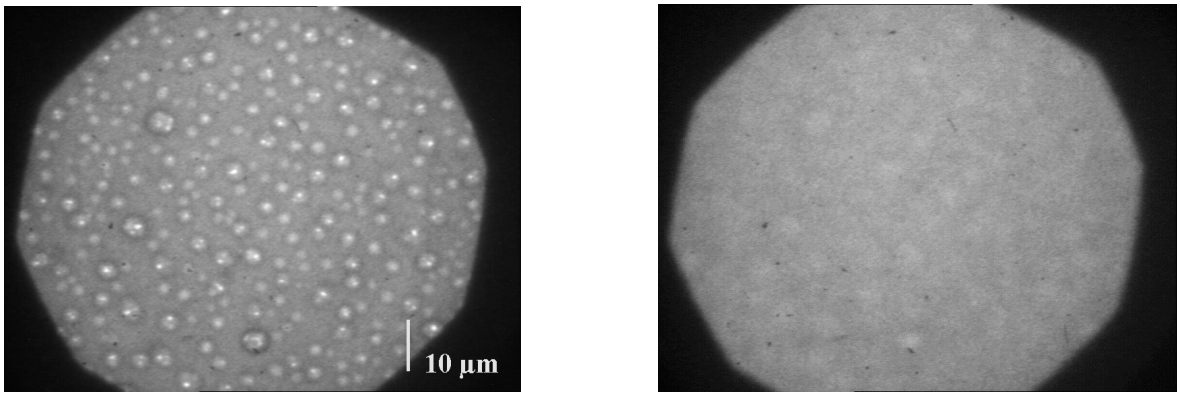

Figure 5.3: Fluorescence pictures of DMPC monolayers (lateral pressure 35 mN/m, fluorescence probe NBD-PC) on a glass surface. Left picture: structure of the monolayer upon condensation of water droplets, right picture: recovery of a homogeneous structure after 17 min of storage at a relative humidity near condensation.

This "self-repairing" effect was slow on glass surfaces: it took more than half an hour for defects over a range of not more than some µm to be healed. However, already this simple experiment provides a method to at least qualitatively compare the influence of the underlying support on dynamic properties of a supported model membrane. Following the main path of the present work, which is to characterise polymer/lipid interactions, a hydrogel was employed in order to reduce membrane coupling to the support.

5.1.2 Chitosan surfaces

It has been shown in chapter 4.4, that chitosan swells when being exposed to water with increasing activity. Furthermore, as will be shown in chapter 6.2, chitosan was used to successfully cushion fluid bilayer model membranes. As an attempt to study the influence of a polymeric support on the strength of lipid/support interactions, DMPC monolayers were transferred onto a thin chitosan cushion (with a typical thickness of 150 nm in the dry state). In the following part the fluorescence probes NBD-PC and NBD-PE were used. Additionally, as an alternative to choline headgroups, the lipid DLPE with a phosphoethanolamine headgroup, was transferred.

I) DMPC + NBD-PC

In Figure 5.4, the RICM image of water droplets on a DMPC covered chitosan film is shown. In order to perform fluorescence microscopy simultaneously, the monolayer was stained by adding 1 mol% of the fluorescent phospholipid NBD-PC, which possesses a choline headgroup.

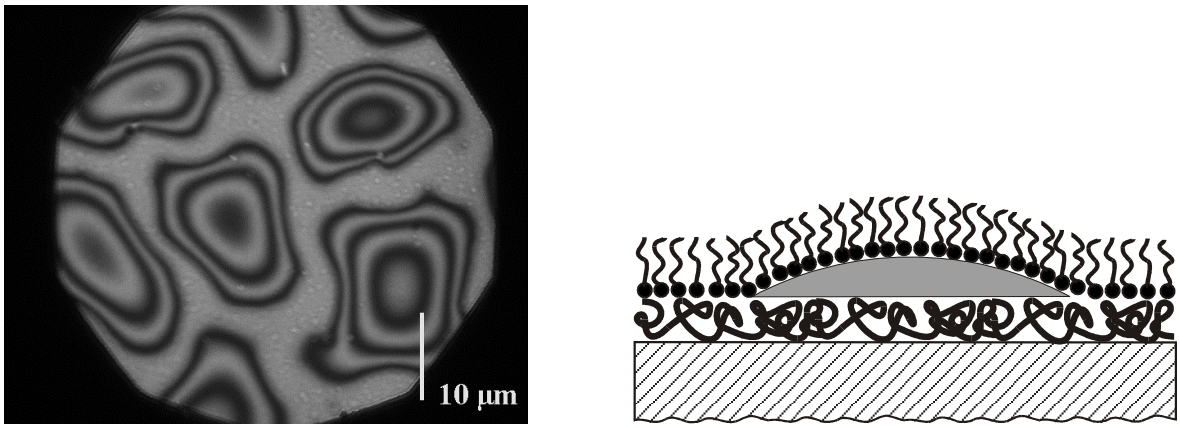

Figure 5.4: Left: RICM image of water droplets on a DMPC monolayer on a chitosan film (lateral pressure 35 mN/m) and an additional fluorescence probe (NBD-PC), right: schematic drawing of the configuration observed in the left image.

Clearly, the spacing of the interference fringes is much larger as compared to DMPC monolayers on glass (see Figure 5.2), which indicates a smaller contact angle. Additionally, the line tension seemed to be reduced because of the non-circular appearance of the water droplets, caused by pinning centres.

In the situation depicted in the right part of Figure 5.4, the contact angle for a macroscopic droplet in equilibrium, according to the Young equation, can be written as

$$\gamma_{WL}\cos\Theta = \gamma_{PL} - \gamma_{PW}\,, \qquad \textbf{(5.1.4)}$$

with γ_{WL}, γ_{PL} and γ_{PW} being the interfacial energies of the water-lipid, polymer-lipid and polymer-water interface, respectively. The first value is known from the lateral pressure of the lipid layer ρ (which is assumed to be constant), since

$$\pi = \gamma_{WV} - \gamma_{WL} \qquad \textbf{(5.1.5)}$$

with the surface tension of water being γ_{WV}. The equilibrium contact angle in this kind of experiment is therefore determined by the interfacial energy of the polymer-lipid interface. The Young equation, however, as mentioned above, only applies to macroscopic droplets. In this case macroscopic means firstly, that the droplet radius is large enough to allow for

neglecting the influence of Laplace pressure changes, and secondly that forces between the surfaces such as van der Waals or hydrophobic interactions, can be neglected. Both conditions, however, were not fulfilled in the present case.

Fluorescence microscopy revealed that – as in the case of glass – condensation of water droplets caused heterogeneities to appear at the position where water droplets developed. However, contrary to glass-supported monolayers, these heterogeneities appeared as black spots in the fluorescence pictures, and did not grow further after having reached a certain dimension, while the water droplets still grew. Therefore the defects, observed in Figure 5.5, are much smaller compared to the water droplets seen in Figure 5.4.

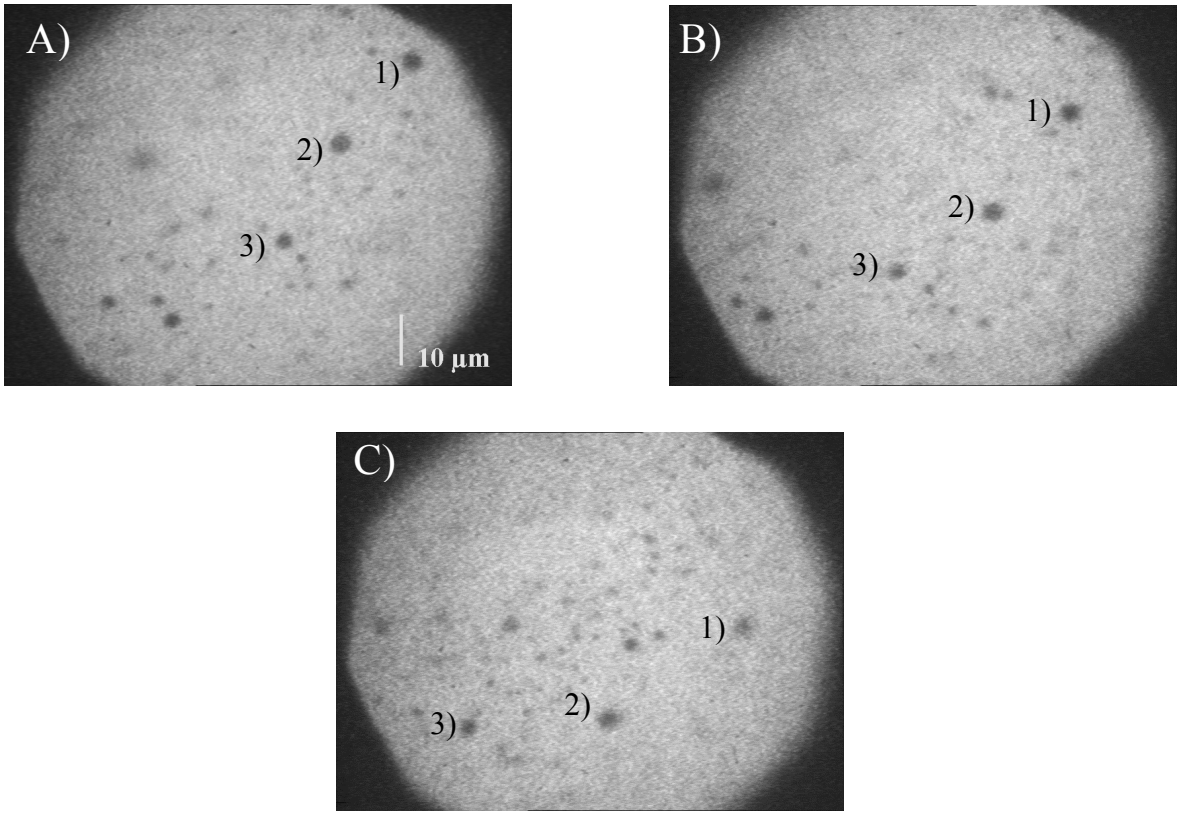

Figure 5.5: Fluorescence images: observation of the flow of monolayer defects on a DMPC monolayer (lateral pressure 35 mN/m, fluorescence probe NBD-PC) on chitosan. The monolayer was detached from the surface and was subject to convection, as can be seen by the movement of heterogeneities (for the sake of a simple assignment, the same defects were numbered in each image). The pictures were taken at a time interval of approximately 5 s.

Moreover, the lipid monolayer detached from the chitosan support in the droplet regions and was subject to convection (probably due to the nitrogen gas stream caused by the humidity setup), as can be observed in the time sequence, depicted in Figure 5.5. The partial detachment of the polymer cushion from the glass substrate (which would lead to a RICM image similar to Figure 5.4) could be ruled out, since such an effect was not observed with polymer cushions, which were not covered by monolayers. Monolayer detachment was inferred from a shift of the focal plane and an increased variability of the latter (see the rims of the field stop, Figure 5.5). Clearly, the comparison of this experiment

with the case of a glass-supported DMPC monolayer demonstrates that by use of a polymer cushion, the adhesion of a lipid monolayer to the support can be lowered considerably.
Generally, regions of reduced or no fluorescence intensity are due to either holes in the lipid monolayer, or regions with a different phase state. In case of the latter, the contrast arises because of lower dye solubility in regions of a higher lipid density [Möhw, 1990]. The size and geometry of the observed defects, however, did not change when the same experiment was carried out at slightly different temperatures. Therefore, the black spots seen in Figure 5.5 are due to areas, which are not covered by a lipid film.
The spreading power of the lipid layer can be expressed in terms of a spreading coefficient, *S*,

$$S = \gamma_{WV} - \gamma_{WL} - \gamma_{LV} \qquad \textbf{(5.1.6)}$$

Clearly, this spreading coefficient is positive and, therefore, spreading should be favoured. However, the holes can be kinetically hindered from closing.

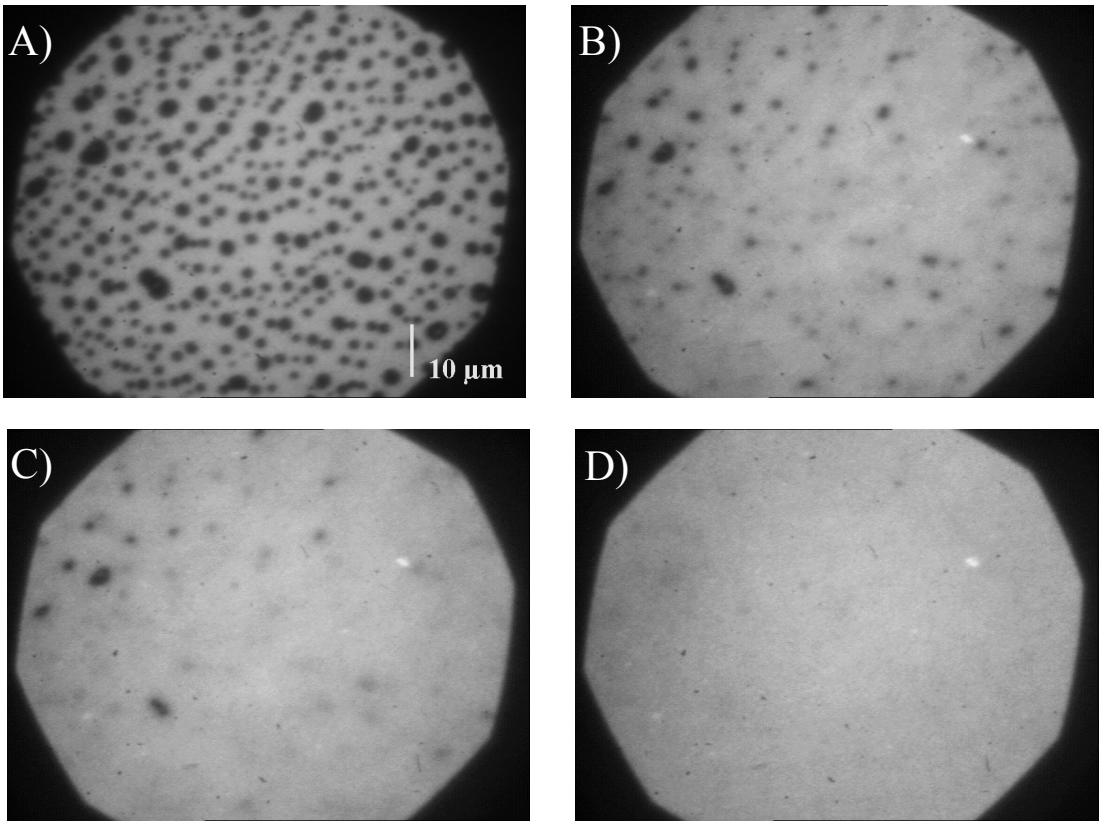

Figure 5.6: Fluorescence images showing A) the structure of a lipid monolayer (DMPC, lateral pressure 35 mN/m, fluorescence probe NBD-PC) which had been subject to a condensation of water droplets, and which had been dried rapidly afterwards, B) – D) the same location on the same monolayer as in A), after switching to a high (near condensation) humidity. The time interval between each picture was approximately 1 minute.

Nevertheless, line tension at the film/defect boundary forces the defects into a circular geometry (Figure 5.6 A)).

After switching *RH* quickly to approximately 5 %, the water droplets disappeared rapidly, while the defects in the monolayer were „frozen in“, as can be seen in Figure 5.6 A). After switching to a high (near condensation) humidity, kinetic hindrance of spreading was overcome and the defects healed to yield a perfectly homogeneous fluorescence image (Figure 5.6 B) – D)). The healing of these defects was much quicker as compared to the case of a glass-supported monolayer (see Figure 5.3). In fact, the spreading of lipid monolayers on polymer supports was fast enough to be analysed quantitatively by depositing a monolayer onto only one half of the substrate and observing the subsequent growth of the monolayer covered surface at higher humidities (see chapter 5.2).

The self-healing properties of supported phospholipid *bilayers* due to the spreading of hydrated excess lipid were first found by Rädler et al. [Rädl, 1995a]. Self-annealing or self-repairing properties of Langmuir-Blodgett *monolayers*, however, are also considered to be of substantial importance [Swal, 1987].

II) DMPC + NBD-PE

As an alternative to NBD-PC, the negatively charged phospholipid probe NBD-PE was employed to stain DMPC monolayers. Contact angles in this case, as observed in the interferogram (Figure 5.7), were considerably lower compared to glass-supported monolayers.

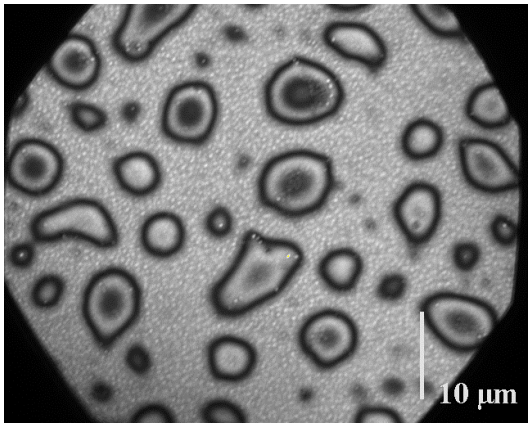

Figure 5.7: RICM image of water droplets on a DMPC monolayer-supported by a chitosan cushion (lateral pressure 35 mN/m, fluorescence probe NBD-PE).

However, when the negatively charged dye was used the coupling to the polymer support was stronger, as a detachment of the lipid layer from the polymer support was not observed by fluorescence microscopy. This stronger coupling can be explained by an electrostatic contribution. Due to the amino groups, chitosan is positively charged at pH values below

about 6.5 [Clae, 1992] which leads to a positive Zeta-potential in case of pure MilliQ water [Mino, 1998].

Instead of a complete detachment, the monolayer became partially covered by a water droplet (Figure 5.8). The reduced fluorescence intensity in the water covered areas in Figure 5.8 can be explained by two effects. One is a reduction of the quantum yield of the fluorophor due to the interaction with water molecules (this effect is examined in detail in chapter 5.4).

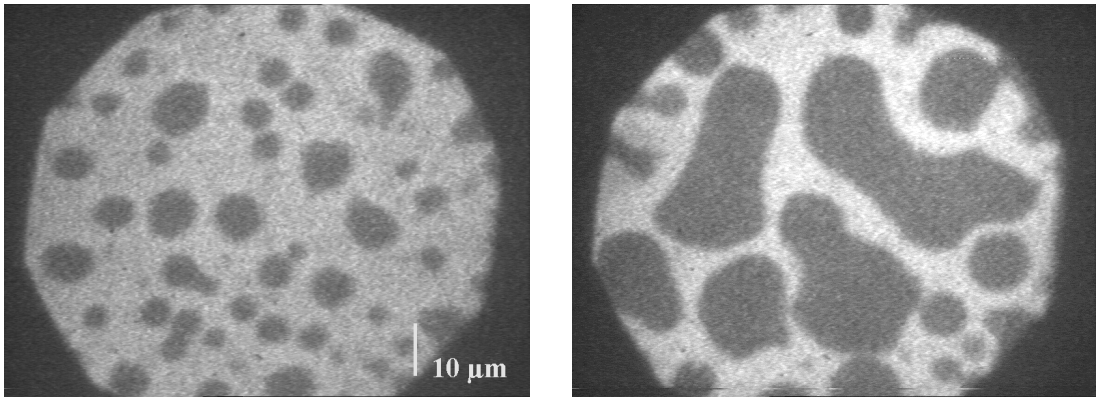

Figure 5.8: Fluorescence image: water droplets on a DMPC monolayer (lateral pressure 35 mN/m, fluorescence probe NBD-PE) resting on chitosan. The right picture was taken approximately five seconds after the left picture. Note: a) defects did not change position but could fuse to yield bigger ones, b) the fluorescence intensity of areas between the droplets is increased in the right picture compared to the left one (both pictures were taken at exactly the same conditions), c) water-covered regions showed a faint fluorescence.

A second reason is a partial detachment of lipid molecules in water-covered areas, and an enrichment in areas free from bulk-water, by the piston effect of the moving droplet front [Yami, 1997]. The latter fact explains the observation of small contact angles of water droplets (compared to the case of lipid monolayers on glass) and a higher fluorescence intensity in the areas which are not covered by the droplet, compared to the intensity prior to condensation.

III) DLPE

DLPE monolayers, stained with NBD-PE were even more stable against water droplet condensation. No detachment was observed, the fluorescence intensity was only slightly reduced and the interferograms indicated higher contact angles (Figure 5.9) compared to chitosan-cushioned DMPC monolayers. These observations indicate that in the case of DLPE, water droplets were resting on an almost undistorted monolayer.

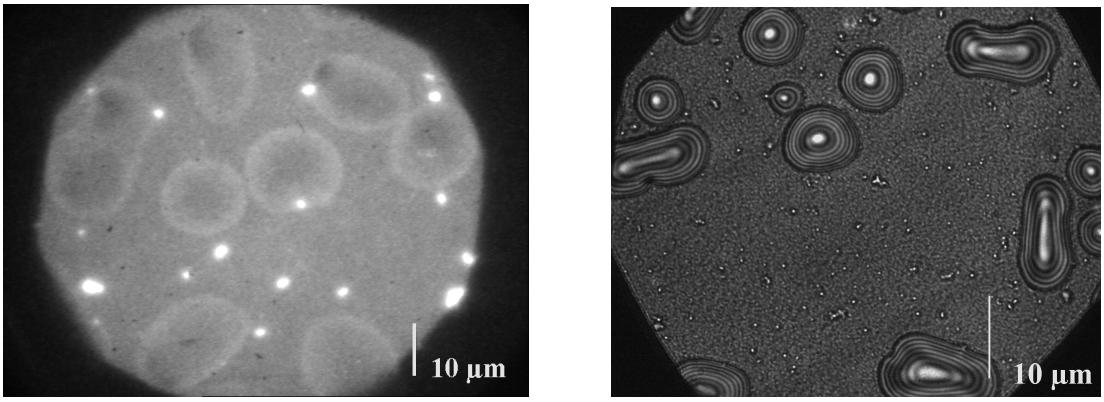

Figure 5.9: Water droplets on a DLPE monolayer on chitosan (left: fluorescence, right: RICM), fluorescence probe NBD-PE. Note: the bright spots in the left picture are regions where droplets have dried previously.

The higher stability of DLPE layers can at least partially be explained by the lower tendency to be hydrated. Another reason could be the lower roughness of the hydrophilic surface of the DLPE monolayer, compared to the case of DMPC [Damo, 1994]. The latter could possibly render it more difficult for a water droplet to creep under the monolayer and lift it from the polymer surface. It cannot be totally ruled out, however, that DLPE, although transferred in a fluid state, was subject to a phase transition induced by substrate mediated condensation [Rieg, 1992]. This question will be further addressed in the following two chapters (5.2 and 5.3).

5.1.3 Conclusion

Reflection interference contrast microscopy and fluorescence microscopy were applied in parallel to qualitatively analyse the strength of the adhesion of phospholipid monolayers. The strength of adhesion was described through the resistance of monolayers against distortion by water droplets and the contact angle of the droplets. Furthermore, fluorescence microscopy revealed that the condensation of water droplets on a monolayer/hydrogel-support system could cause the monolayer to lift off from the substrate completely and float on the water droplet. Additionally, it was observed that monolayer distortions, caused by growing water droplets, could heal after droplet evaporation and by keeping the monolayer at a high relative humidity. Monolayer stability was found to be influenced by (I) the nature of the underlying substrate, (II) the kind of fluorescence probe used to dye the monolayer, and (III) the nature of the lipid headgroup and/or the phase state of the lipid layer.

From the qualitative analysis performed in the present chapter it can be concluded that the stability of a lipid monolayer, when subjected to a condensation of water droplets, increases in the following order: DMPC (NBD-PC) on chitosan < DMPC (NBD-PE) on

chitosan < DLPE (NBD-PE) on chitosan ≈ DMPC on glass. The observations leading to this order are summarised in Table 5.1.

monolayer	**RICM (contact angle)**	**fluorescence in the region of microdroplets**
DMPC on glass	high	slight distortion
DLPE (NBD-PE) on chitosan	moderate – high	slight distortion
DMPC (NBD-PE) on chitosan	small	compression of the monolayer in water-free regions by a piston effect of growing droplets
DMPC (NBD-PC) on chitosan	small	complete detachment of the whole monolayer from the support

Table 5.1: Summary of the results from water droplet condensation experiments on supported lipid monolayers, obtained by RICM and fluorescence microscopy. The monolayers are ordered with decreasing stability from top to bottom.

The self-repairing effect of Langmuir-Blodgett films, in terms of the spreading of supported monolayers, which has qualitatively been shown in Figure 5.6, shall be analysed quantitatively in the following chapter.

5.2 Spreading of lipid monolayers on hydrophilic substrates at high humidities

Generally, biosensor applications based on model membrane systems demand a highly insulating membrane [Stel, 1993]. The structure of an initially deposited monolayer significantly influences the characteristics of the second monolayer deposited onto the first [Merk, 1989], and therefore determines the quality of the resulting bilayer. Several processes can lead to film defects. Monolayer quality might be reduced due to mechanical distortions during the transfer process. Furthermore, deposition by Langmuir-Blodgett transfer inevitably comprises a drying step. If a polymer cushion is used as a membrane support, during the drying step, thinning of the cushion might result in local, transient area changes, which could be inscribed into the lipid layer permanently due to reduced dynamics of lipid molecules in the dry state.

Obviously, an increased humidity will lead to a reduced motional coupling of the lipid layer to the hydrogel support, which leads to enhanced diffusion and increased spreading velocity. Positive influences of the exposure of the monolayer to increased humidities are possibly the levelling out of local density gradients and the healing of voids or cracks in the monolayer film. The latter two types of defects have been observed by electron microscopy [Fisc, 1984] and scanning probe microscopy techniques, e.g. [Sike, 1996]. The healing of monolayer defects after increasing monolayer mobility can be assumed to be due to either surface diffusion or a collective transport by spreading, and a combination of both transport mechanisms [Gave, 1990].

The topic of the present chapter is to study the possibility of phospholipid monolayer spreading and the spreading characteristics upon exposure to a high ambient humidity. The influence of the substrate, the humidity and the lateral pressure within the monolayer on the spreading behaviour will be analysed. Additionally, as an alternative to preparation of a lipid source for spreading by LB-transfer, spreading from a multilayer stack will be examined.

Effects of ambient humidity on lateral self-diffusion within lipid monolayers, however, will be treated explicitly in chapter 5.3. In the following part, a brief overview of important aspects of spreading processes, with an emphasis on the dynamics of spreading, will be provided.

5.2.1 Physics of spreading processes

The spontaneous spreading of liquids on solid surfaces is controlled by the competition between driving terms and dissipative processes [Vali, 1999].
The dynamics of a macroscopic droplet spreading on a solid can often be described by

$$R \propto \Omega^{3/10}\left(\gamma\frac{t}{\eta}\right)^{1/10} \qquad \textbf{(5.2.1)}$$

where R is the time-dependent droplet radius, W is the droplet volume, g and h are the surface tension and viscosity of the liquid. Equation (5.2.1), which is valid for small droplets, i.e. gravitation can be neglected [Lope, 1976], is known as Tanner law [de Gen, 1985]. From this equation it follows that the velocity of the droplet front, dR/dt, is essentially independent from the spreading power S, which is the driving term for droplet spreading:

$$S = \gamma_S - \gamma_L - \gamma_{SL} \qquad \textbf{(5.2.2)}$$

with g_S, g_L and g_{SL} being the interfacial tensions of the solid and liquid surface, and the solid-liquid interface, respectively.
However, it has long been known, that the spreading of a macroscopic liquid droplet on a solid is preceded by a very thin, invisible film [Hard, 1919], which occurs even when condensation from a vapour phase can be neglected [Bang, 1938]. Whereas the shape of the macroscopic droplet is a thermodynamic, macroscopic property [Isra, 1992a], the surface profile of the precursor film is controlled by long-range surface forces (between approximately 30 Å and 1 µm, see chapter 5.0.1). Where evaporation can be neglected, the thickness of the "completely" spread droplet is above the value of a monolayer, even in case of a zero (macroscopic) contact angle. In case of dominant van der Waals forces the maximum height e of the spread droplets can be expressed as [Joan, 1984]:

$$e = \left(\frac{H}{4\pi S}\right)^{1/2} \qquad \textbf{(5.2.3)}$$

H is the Hamaker constant and S is the spreading coefficient. In case of a dominant double layer force, e depends on the reciprocal of the logarithm of S. Due to (5.2.3), liquids with

large S spread more efficiently than liquids of small S. The independence of droplet spreading velocity on the spreading power can be explained by complete consumption of the free energy (per unit area) S through dissipative processes in the precursor film [de Gen, 1985].

Spreading films in the range of the thickness e are mesoscopic films [Vali, 1999] which can be described by continuum theories both in terms of statics (DLVO theory) and dynamics (hydrodynamics: Navier-Stokes equations).

Wetting of molecularly thin liquid films, however, is often accompanied by structuring effects. In fact, the films advance as a series of distinct molecular layers [Hesl, 1989], or – in later spreading stages – as a single monomolecular layer. While for macroscopic and mesoscopic films a no-slip boundary at the solid-liquid interface applies (the dissipation occurs in the bulk liquid, quantified by means of the viscosity η), in the case of molecularly thin layers dissipation occurs by friction at the solid support, on the molecular scale.

The monolayer growth of a simple liquid, extending from a straight reservoir or from a droplet of radius R_0, has been studied experimentally, mainly by means of spatially resolved ellipsometry [Hesl, 1988], [Fray, 1993], [Caza, 1994], [Vali, 1999], [Voue, 1999], [Blak, 1999], in combination with AFM [Vill, 1997] or by spatially resolved surface plasmon spectroscopy [Luch, 2000]. Numerous theoretical investigations have been carried out [Abra, 1990], [Coni, 1993], [Burl, 1996a], [Burl, 1996b], [Osha, 1998b]. In parallel, computer simulations [De Co, 1993] have been performed.

In most of the above-mentioned works monolayer spreading was found to follow a square-root behaviour with respect to the time dependence of the spreading distance. In particular, the model developed in [Burl, 1996a], [Burl, 1996b], [Osha, 1998b] leads to the following equation for a monolayer spreading from a bulk droplet with a radius R_0:

$$R(t) = R_0 + A\sqrt{D_0 t} \qquad \textbf{(5.2.4)}$$

In (5.2.4), A is a parameter which may be positive (wetting), zero, or negative (dewetting), and depends on temperature and particle/particle and particle/substrate interactions. D_0 is the diffusion coefficient of an isolated liquid molecule on the surface. Interestingly, A depends mainly on liquid-liquid interactions and is almost independent of the spreading power [Burl, 1996b].

Apart from pure simple liquids, wetting of solids often occurs by or in the presence of surface-active compounds like surfactants and lipid molecules. Wetting by amphiphiles is highly facilitated in the presence of water films ranging in thickness from the molecular to the macroscopic scale. The kinetics of spreading in these cases are accompanied by

additional phenomena like superspreading [Hill, 1998]), fingering instabilities [Troi, 1989], [Troi, 1990], [Elen, 1994] or solitary waves [Borg, 1988], [Jens, 1992], [Frey, 1992].

The spreading dynamics of amphiphile monolayers on water films can be complex and the form of the spreading law depends on film thickness and monolayer geometry as well as on the ratio of the Marangoni driving term (surface tension gradient) to the diffusion coefficient (5.2.13). In case of a constant film thickness, a constant spreading velocity proportional to the surface pressure gradient and the film thickness was found [He, 1998], according to:

$$\frac{\Delta\pi}{l} = \frac{\eta_w v}{d} \qquad \textbf{(5.2.5)}$$

where π is the surface pressure, l is the length of the spreading film, η_w is the water viscosity, v is the spreading velocity and d is the film thickness.

The spreading of a lipid monolayer on top of a thin water film results in an attractive van der Waals interaction [Frey, 1995]: the water film collapses if it is sufficiently thin and if the van der Waals force is not balanced by a repulsive double layer force [Schn, 1986], [Birc, 1995], [Elen, 1994].

The spreading of monomolecular amphiphile films on solids was analysed in [Tibe, 1994b], [Tibe, 1994a], [Vill, 1996] and [Luch, 2000]. Generally, a square root behaviour of precursor film radius growth with a very sharp spreading front and a dense monolayer was found. Studies on the spreading behaviour of trisiloxane oligo(ethyleneoxide) surfactants revealed that the ambient humidity influenced the spreading rates remarkably.

The spreading of phospholipid membranes on solid substrates thus far was analysed in terms of the spreading of bilayers deposited onto hydrophilic substrates [Rädl, 1995a], [Niss, 1999]. The spreading of a single bilayer was observed, with a spreading front displacement following a square root behaviour with respect to the observation time.

The spreading of Langmuir-Blodgett monolayers (and of phospholipid monolayers in particular) on solid supports to the best of the author's knowledge so far has not been examined. This might partially be due to the fact that spreading on typical supports such as silicon oxide, glass or mica is too slow. In order to circumvent this problem, in the present study, a water swellable hydrogel was used for supporting the monolayer.

5.2.2 Spreading of a Langmuir-Blodgett monolayer with defined lateral pressure

In order to examine the spreading behaviour of a phospholipid monolayer supported by a thin polymer film, Langmuir-Blodgett films were prepared by immersing the substrate only half into the subphase [Berm, 1997]. Prior to spreading the lipid solution, the substrate was equilibrated in the trough (for approximately half an hour) to allow for a smooth three-phase line to be established. Omitting the latter resulted in a final monolayer edge line with a pronounced roughness due to an inhomogeneous wetting of the polymer film, as can be seen in Figure 5.16. After spreading the lipid solution the solvent was allowed to evaporate (for a quarter of an hour) and the film was finally compressed. In order to allow for visualisation of the deposited monolayer by fluorescence microscopy the lipid solution was doped by the addition of 1 mol% of the lipid fluorescence probe NBD-PE.
The water film height profile close to the three-phase line at a partially immersed substrate is shown schematically in Figure 5.13.

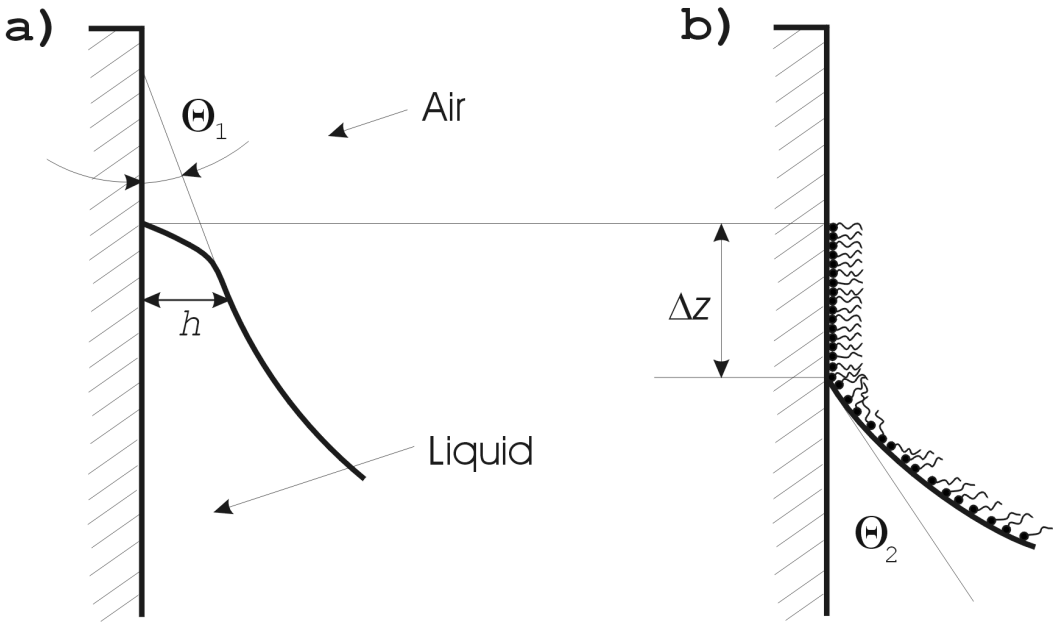

Figure 5.13: Height profile of the water film near a substrate prior (a), and after (b) spreading lipid solution on the trough subphase *before* compression of the monolayer film. Due to a local collapse of the water film at the leading edge and possibly a substrate induced dehydration of lipid headgroups, the initial three phase line retracts upon spreading lipid solution, indicated by a height difference, D*z*. During the retraction, lipid is deposited at a higher lateral pressure compared to the uncompressed monolayer. The retraction of the initial wetting front during spreading is assumed to being grossly reduced, if not diminished, due to the presence of a hydrated polymer cushion.

Prior to spreading the lipid solution a macroscopic contact angle Θ_1 is observed. The film profile significantly differs at the leading edge of the water film. The edge height, *h*, is controlled by (repulsive) van der Waals and/or double layer forces [de Gen, 1985]. The

width of the distorted region is by far below the resolution of the optical microscope. The situation becomes more complicated when applying the lipid solution onto the subphase. As already mentioned, a substrate/water-film/lipid-layer system leads to van der Waals attraction above a certain lateral pressure of the monolayer. By the collapse of the initial water film, a retraction of the three-phase line can occur.

The development of the meniscus at the three-phase line after spreading the lipid solution on the subphase (but *before* compression) was analysed by Yaminsky et al. [Yami, 1997]. These authors found that the three-phase line at a mica substrate, half immersed into a pure water subphase, retracts several hundreds of micrometers upon spreading of lipid solution (DSPE) onto the subphase (see Figure 5.13b)). Upon retraction, the contact angle increased due to the deposition of lipid onto the solid, at a pressure of several mN/m, although the lateral pressure within the monolayer on the subphase was still below 0.1 mN/m. The contact angle (and therefore the lateral pressure of the monolayer deposited during meniscus retraction) depended on the amount of lipid solution initially loaded onto the subphase.

The pressure difference between a monolayer deposited onto a substrate and that one remaining on the LB-trough subphase depends on the strength of the head group – substrate interaction [Yami, 1997]. As in the present case a hydrogel was used as a substrate, it can be assumed that the retraction of the initial three-phase line is grossly reduced, if not diminished completely. Even if a slight retraction occurred, the final monolayer density distribution was homogeneous (see Figure 5.14 and Figure 5.16) up to the monolayer leading edge, for the following reason.

The polymer dries slowly upon retraction of the meniscus, at least when in contact with a nearby water bulk phase and in an environment with an increased relative humidity. Therefore, a distinct border between swollen and unswollen polymer cushion remains until the compression of the monolayer (by closing the barrier) is finished. The monolayer mobility on the swollen polymer is high, hence compression of the lipid layer on the swollen polymer film is still possible (see chapter 5.1.2, Figure 5.8). Therefore, it is reasonable to assume that the edge of the monolayer *after* compression is still approximately located at the initial wetting front of the water subphase before spreading of the lipid solution. This is the case even though the subphase could slightly retract after it was loaded with lipid solution. It will be shown below (Figure 5.20) that the spreading velocity of the monolayer at increased *RH* depends remarkably on the lateral pressure of the monolayer on the subphase of the LB-trough, i.e. the pressure before deposition onto the polymer support. If, however, no compression of the lipid deposited during retraction of the subphase shortly after spreading the lipid solution was possible (as in the case of a mica support [Yami, 1997]), the spreading front velocity of the advancing monolayer at

increased humidities would depend on the amount of lipid solution deposited onto the subphase [Yami, 1997], and not on the lateral monolayer pressure obtained after compression.

In cases where the lipid solution was deposited rapidly after immersing the substrate a rough monolayer edge was observed (Figure 5.16). On the other hand, equilibrating the substrate with the subphase prior to the deposition of lipid solution led to smooth monolayer edges. This clearly indicates that the position of the monolayer edge is defined by the position of the initial three-phase line prior to adding lipid solution onto the LB-subphase.

After completion of compression the film was deposited without further delay in order to avoid significant spreading of the monolayer on the polymer support. The halfway covered substrate was finally mounted into the humidity chamber and observed by means of a fluorescence microscope.

5.2.2.1 Spreading of DMPC on chitosan

Observation of the monolayer at *RH* = 50 % revealed a sharp monolayer edge and no mobility (Figure 5.14, left).

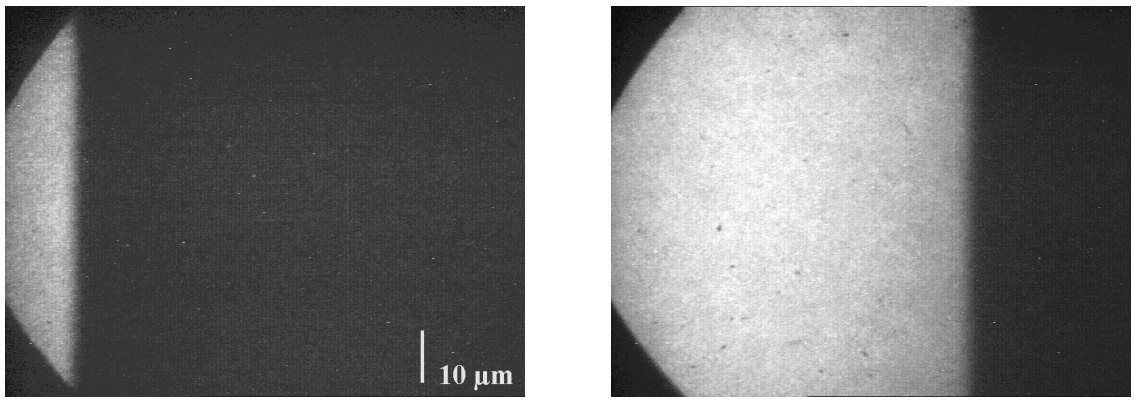

Figure 5.14: DMPC monolayer on a chitosan film, lateral pressure 50 mN/m, relative humidity 90 %, left picture: beginning of the spreading experiment, right picture: 9 min later. Note: the broadening of the spreading front during the spreading process was negligibly small.

From the intensity profile past the initial monolayer edge (Figure 5.15) it can be deduced that the edge width (about 1 µm) was in the range of the resolution of the optical microscope.

Switching to *RH* = 90 % substantially increased the monolayer mobility, which resulted in a movement of the spreading front.

Accompanying the monolayer edge displacement, a broadening of the edge width occurred, as deduced from the intensity profiles shown in Figure 5.15. This subtle

broadening could either be due to a slight increase of the edge roughness or a small density gradient induced by spreading. It cannot be totally ruled out, however, that the reduced fluorescence intensity of the monolayer edge was due to a higher friction of the fluorescence probe with the underlying support, compared to the unlabelled lipid molecules.

From the sharp spreading front observed directly after film deposition, it can be concluded that monolayer spreading before completion of the deposition process, while the substrate was partially immersed in the subphase of the LB-trough, was negligible. Also, the intensity distribution over the whole spreading distance did not change significantly during spreading, which is contrary to the diffusion model developed in [Burl, 1996a], where an s-shaped intensity profile was found in the spreading region, $x(t)$, (compare Figure 5.19).

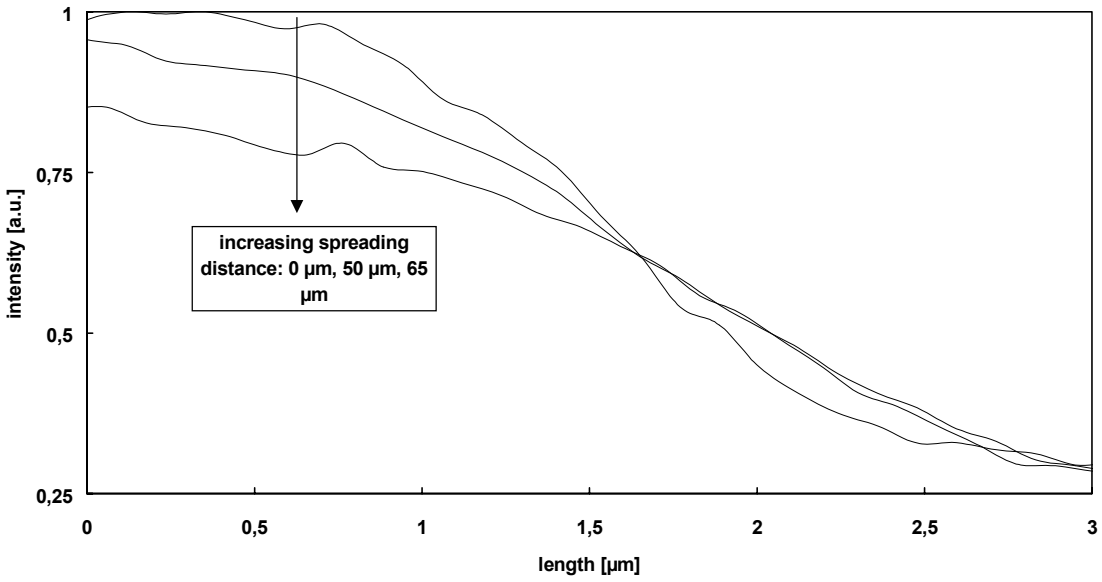

Figure 5.15: Intensity profiles of the monolayer edge (along a line orthogonal to the edge) during spreading. Note: the width of the edge prior to spreading is comparable to the resolution of the optical microscope. The intensity profiles have been shifted arbitrarily with respect to the length axis. Profiles were examined directly after deposition (0 µm), and after spreading over distances of 50 µm and 65 µm.

As has been mentioned already, insufficient equilibration of the polymer cushion in the aqueous subphase led to a rough monolayer edge. However, during the spreading process at an increased *RH* the roughness levelled out (Figure 5.16) while spreading over a distance much less than 100 µm, which is a further indication that spreading before completion of the LB-transfer process was negligible. Also in Figure 5.16, it can clearly be seen that the intensity of the spreading monolayer is constant before and after spreading over a distance of dozens of micrometers.

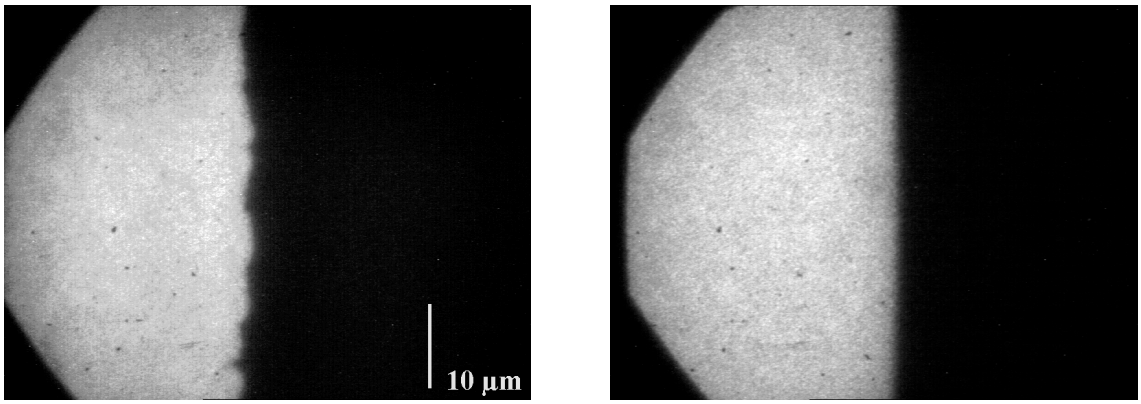

Figure 5.16: DMPC monolayer on a chitosan film, lateral pressure 20 mN/m, relative humidity 90 %, left picture: prior to increasing humidity, right picture: 50 min later. In the case of the right picture, the sample had been shifted in order to compensate for the movement of the spreading front (approximately 40 µm).

In order to compare the spreading front before and after spreading at increased humidities, the former was extracted from the fluorescence micrographs by digital image processing. The result of this procedure can be seen in Figure 5.17. Note that for the sake of easier comparison, the two edge lines have been shifted arbitrarily relative to each other and rotated by 90° with respect to the fluorescence image (Figure 5.16).

Clearly, it can be seen that the spreading line became much smoother, during the spreading process. On the other hand, the low scale roughness seemed to be increased. This may, however, have been an artefact due to a different signal to noise ratio, since the low scale roughness is below the resolution of the optical microscope.

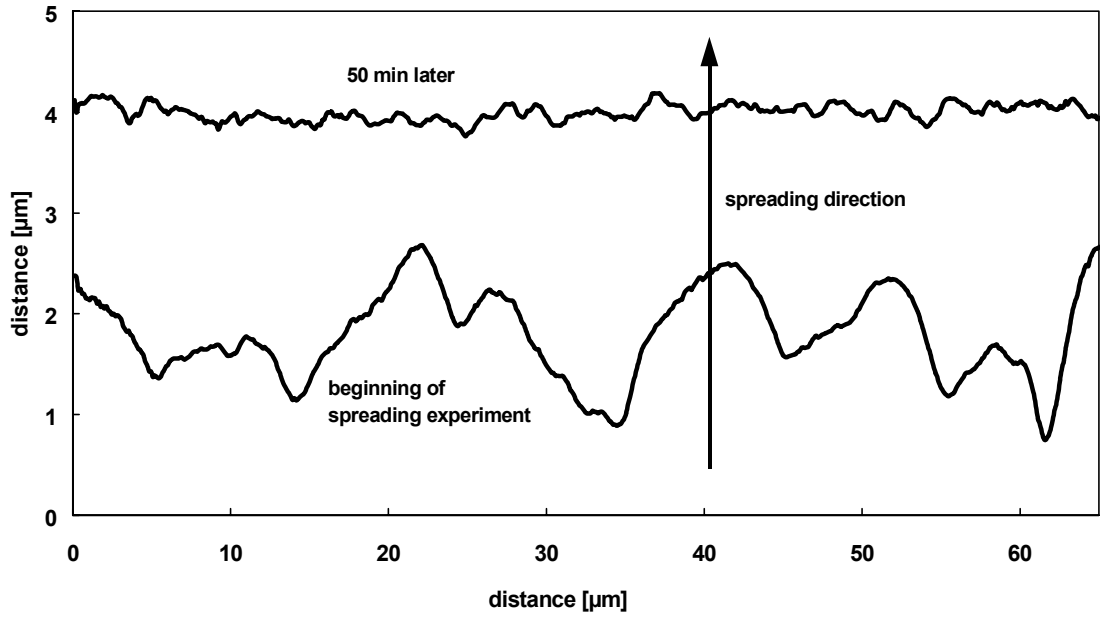

Figure 5.17: Development of the spreading front of a lipid monolayer spreading from a Langmuir-Blodgett film (see Figure 5.16). The spreading fronts have been turned by 90° with respect to Figure 5.16. Note: a) the two lines have been shifted arbitrarily towards each other in the y-direction, b) x- and y-axis are scaled differently.

The smooth spreading front of lipid monolayers is in contrast to the spreading of phospholipid bilayers on hydrophilic surfaces, where a steady roughening during spreading was observed [Rädl, 1995a]. The latter was explained by a percolation process: smooth spreading is obstructed by pinning centres at low spreading velocities.

As the spreading coefficient in case of monolayer spreading is much higher compared to bilayer spreading [Sack, 1996], percolation due to pinning centres is likely to be reduced considerably.

Spreading experiments for time dependent quantitative measurements were performed with samples where the spreading front appeared smooth right from the start. Monolayers were transferred at different lateral pressures and the displacement of the spreading front relative to the starting position was determined at different spreading times. Figure 5.18 shows a typical development of the spreading front. In that experiment, a DMPC monolayer was transferred at a lateral pressure of 20 mN/m. The position of the monolayer edge was determined and afterwards, *RH* was set to 90 %.

An almost perfectly linear relation between spreading front displacement and time (Figure 5.18) was found for all lateral pressures, π, and relative humidities, *RH*. The final spreading distance was in all cases below 90 µm, which is small compared to the initial total length (1,8 cm) of the monolayer. Hence the monolayer in this case can be regarded as an infinite lipid reservoir.

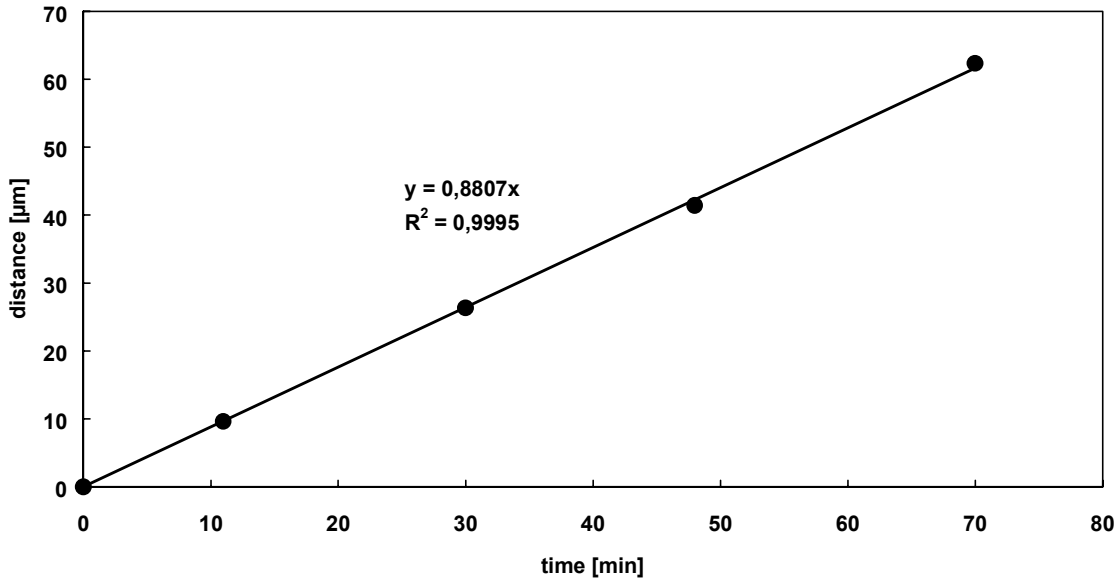

Figure 5.18: Spreading front displacement of a DMPC monolayer on chitosan, lateral pressure 20 mN/m, relative humidity 90 %. The slope of a linear fit yielded a velocity of 0.88 µm/min, corresponding to 0.015 µm/s.

The physical analysis of the spreading of a quasi two-dimensional layer on a solid can be reduced to a one-dimensional problem [Burl, 1996a], as depicted in Figure 5.19.

In [Burl, 1996a] and [Osha, 1998a], particle dynamics were modelled as an activated random hopping transport constrained by hard-core (short-range) interactions between the local minima of potential wells in a square lattice (Figure 5.19). The wells are deep with respect to desorption, but act as a much lower barrier against the movement across the surface. Hops of diffusors only take place if the neighbouring well is vacant. All particles, except those located at the film boundary, have isotropic transition rates: the probability to hop in any of the four directions is 1/4. However, at the film boundary transition rates are different: the probability, q, for a boundary particle to hop in the direction of the film exceeds the probability, p, to move towards the free surface. Advancement of the film, however, occurs because vacancies created by a boundary particle, while hopping towards the free surface, are filled by "bulk" monolayer particles.

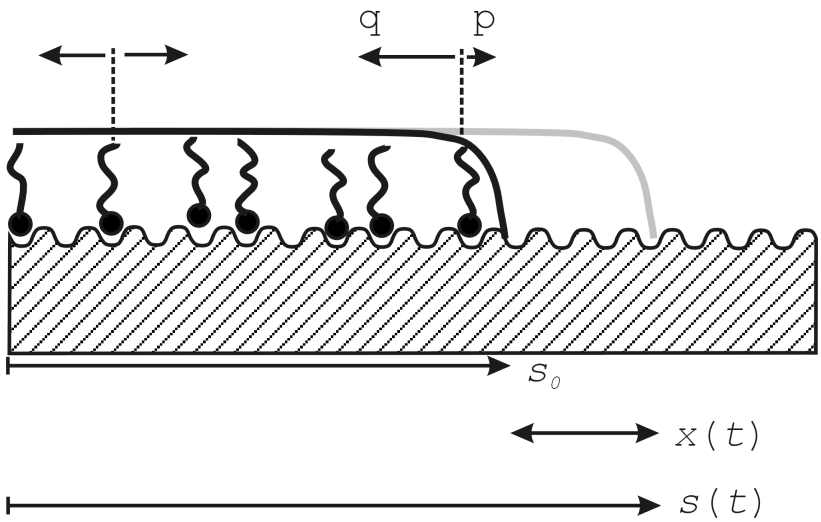

Figure 5.19: Spreading of a lipid monolayer initially confined to a fraction of the whole substrate area. Molecules in the "bulk" film have the same transition probabilities in each direction. Boundary particles, however, have a higher tendency, $q > p$, to jump into the direction of the film, due to long-range attractive forces on the particle exerted by the monolayer. s_0: initial length of the monolayer film, $s(t)$: total length of the film at time, t, $x(t)$: spreading distance at time, t. The polymer supporting the lipid monolayer has been omitted for clarity.

The asymmetry of transition rates at the boundary arises because of long-range (van der Waals) attractions. Thus, the "bulk" monolayer exerts a force on boundary particles, which drags them towards the film, and monolayer spreading can be regarded as liquid-like.

The hopping model proposed in [Burl, 1996a] and [Burl, 1996b] for monolayer spreading from an infinite bulk-liquid reservoir and applied to the spreading of a semi-infinite monolayer in a refined form in [Osha, 1998b] and [Osha, 1998a], is mathematically quite elaborate.

Here, a much simpler approach proposed in [Rädl, 1995a] for the analysis of the spreading of a lipid bilayer on a solid substrate from an infinite reservoir will be adapted.
In [Rädl, 1995a], a stationary equilibrium is assumed, i.e. the gain in free energy per area, W_A, by bilayer spreading is equal to the energy dissipation by friction:

$$W_A \mathrm{d}A = (f \mathrm{d}y)\mathrm{d}s \qquad \textbf{(5.2.6)}$$

where $\mathrm{d}A = \mathrm{d}y\mathrm{d}s$ is the area covered by the spreading film element (y is the width of the proceeding rim) and f is the viscous force per unit length of the proceeding rim. Further, a linear dependence of f on sliding velocity, $v(s,t) = \mathrm{d}s/\mathrm{d}t$, as well as on the total length of the bilayer film is assumed:

$$f = \zeta \frac{\mathrm{d}s(t)}{\mathrm{d}t} s(t) \qquad \textbf{(5.2.7)}$$

Combining (5.2.6) and (5.2.7) then leads after integration to the spreading law:

$$v(t) = \sqrt{\frac{W_A}{2\zeta}} \frac{1}{\sqrt{t}} \qquad \textbf{(5.2.8)}$$

and hence to a $t^{-1/2}$ dependence of the spreading velocity. z is a viscous drag coefficient [Rädl, 1995a] which was interpreted in terms of a linear velocity gradient in the water film between solid support and lipid membrane. Assuming no-slip boundaries at membrane and solid surface yields $z = h_w/d$, where h_w is the bulk water viscosity and d the thickness of the water film. Furthermore, dehydration of the membrane/substrate gap due to the presence of moderate amounts of cholesterol was found to lower bilayer spreading significantly [Niss, 1999]. In that case, z was interpreted as describing the friction between two monolayers, the first one (proximal layer) being fixed and the second one (distal layer) sliding over the first one. The meaning of z in case of films with a thickness in the molecular range, however, is not obvious. In fact, what friction means at the molecular scale and which parameters are relevant is currently still a matter of debate [Vali, 1999].
In the following, a model will be derived which follows closely the argumentation provided in [Rädl, 1995a]. The main difference lies in the fact that in [Rädl, 1995a], the spreading reservoir was a hydrated bilayer stack, whereas in the present case, the spreading reservoir is the monolayer itself. In the case of small spreading distances ($x(t) << s_0$, see Figure 5.19), the monolayer acts as an infinite reservoir. In the configuration depicted in

Figure 5.19, the monolayer is initially confined to an area defined by length s_0 (and width y). Hence, the viscous force per unit length (5.2.7) yields:

$$f = \zeta \frac{\mathrm{d}s(t)}{\mathrm{d}t} s(t) = \zeta \frac{\mathrm{d}s(t)}{\mathrm{d}t} \left(s_0 + x(t)\right) \qquad \textbf{(5.2.9)}$$

where the monolayer is assumed to behave rheologically as a Newtonian interface [Scri, 1960], which is also assumed to be the case for direct friction with a solid support [Evan, 1988]. Additionally, it is supposed that dissipation occurs in the whole film with an initial length, s_0. This assumption can in principle be proofed by examining monolayer films with different initial lengths, which, however, was not carried out in the present work.
The parameter z in the present experimental configuration quantifies the viscous friction at the monolayer/substrate interface. Possibly, there might be an additional contribution of the dilational viscosity of the monolayer [Borg, 1988], [Hirs, 1997], [Wüst, 1999]. Combination of (5.2.9) and (5.2.6) yields:

$$\left(s_0 + x(t)\right)\mathrm{d}s(t) = \left(s_0 + x(t)\right)\mathrm{d}x(t) = \frac{W_A}{\zeta}\mathrm{d}t \qquad \textbf{(5.2.10)}$$

and after integration:

$$s_0 x(t) + \frac{1}{2} x(t)^2 = \frac{W_A}{\zeta} t \qquad \textbf{(5.2.11)}$$

Since $s_0 >> x(t)$, (5.2.11) reduces finally to

$$\boxed{x(t) = \frac{W_A}{\zeta s_0} \cdot t} \qquad \textbf{(5.2.12)}$$

From (5.2.12) it follows that the spreading front displacement is proportional to the energy per unit area W_A gained by spreading, and inversely proportional to the friction coefficient ζ and the length s_0 of the region in which dissipation occurs. Possibly, s_0 might correspond to a region with a smaller length than the initial film length. However, this does not effect the derivation of (5.2.12), as long as s_0 is much smaller than $x(t)$. W_A is the difference in surface energy of the monolayer-covered and the monolayer-free area and may therefore be approximated by the monolayer film pressure π (compare (4.1.5)). The spreading described by (5.2.12) therefore is driven by a Marangoni force, i.e. a surface tension

gradient. Note that the time derivative of (5.2.12) closely resembles (5.2.5) which, however, was derived by means of hydrodynamics.

Thus for small spreading distances $x(t)$, in contrast to (5.2.8), a constant velocity is obtained, as far as W_A/z is constant. The latter condition is fulfilled if the monolayer density variation at the monolayer edge is small. This condition is expected to be valid because of the strong attraction of boundary particles at the monolayer edge. This attraction possibly causes the dilution of vacancies in the monolayer, i.e. the distribution of additional free area due to monolayer dilation, to be fast compared to the advancement of the monolayer edge. Hence, dissipation is distributed over a large length of the spreading film. The absence of significant density gradients is in contrast to the microscopic (diffusion) model derived in [Osha, 1998a] and [Osha, 1998b], where in the spreading region of length $\sim x(t)$ an s-shaped concentration profile develops. Both $x(t)$ and the mass of monolayers in the region $x(t)$ grow proportional to $t^{-1/2}$. Dissipation is restricted to this region of length $\sim x(t)$.

On the other hand, Borgas and Grotberg [Borg, 1988] theoretically predicted that monolayer velocity on a thin film is constant in the steady state (in case of a constant monolayer length). In [Elen, 1994] and [He, 1998], a constant spreading velocity for monolayer spreading on a thin (mesoscopic) water film was found experimentally. He and Ketterson [He, 1998] studied the rate of lipid exchange between monolayers at different lateral pressures on two LB-troughs, connected by a glass bridge covered by a thin water film. A linear dependence of monolayer velocity on the surface pressure difference, Δp, was found (5.2.5)) in the case of low velocities.

Figure 5.20 shows the influence of the lateral film pressure on spreading velocities of chitosan-supported monolayers at two different relative humidities. The error bars were calculated from the error of linear fits to the data series (Figure 5.18) and do not include error estimates from repeated measurements.

From the diagram, the following conclusions can be drawn: (I) *RH* showed a strong influence on the spreading velocity. In the case of a DMPC monolayer of 50 mN/m, a change of *RH* from 85 % to 90 % led to an increase of the spreading velocity from 5.3 µm/min to 25 µm/min, i.e. a factor of 4.7. (II) The lateral pressure set on the LB-trough during monolayer deposition strongly influenced the spreading velocity. At a relative humidity of 90 %, a change from p = 10 mN/m to 50 mN/m, increased the spreading velocity from 0.1 µm/m to 25 µm/min, i.e. by a factor of 250. (III) The most interesting finding is that the relation between spreading velocity and lateral monolayer pressure $\pi = W_A$ was non-linear, which is contrary to spreading of lipid on a water film of mesoscopic thickness [He, 1998]. Instead, the slope of an arbitrary fit to the data increases monotonously. At a lateral pressure of 50 mN/m at 25 °C, the DMPC monolayer was just

in the coexistence region, which, however, did not seem to influence the spreading velocity.

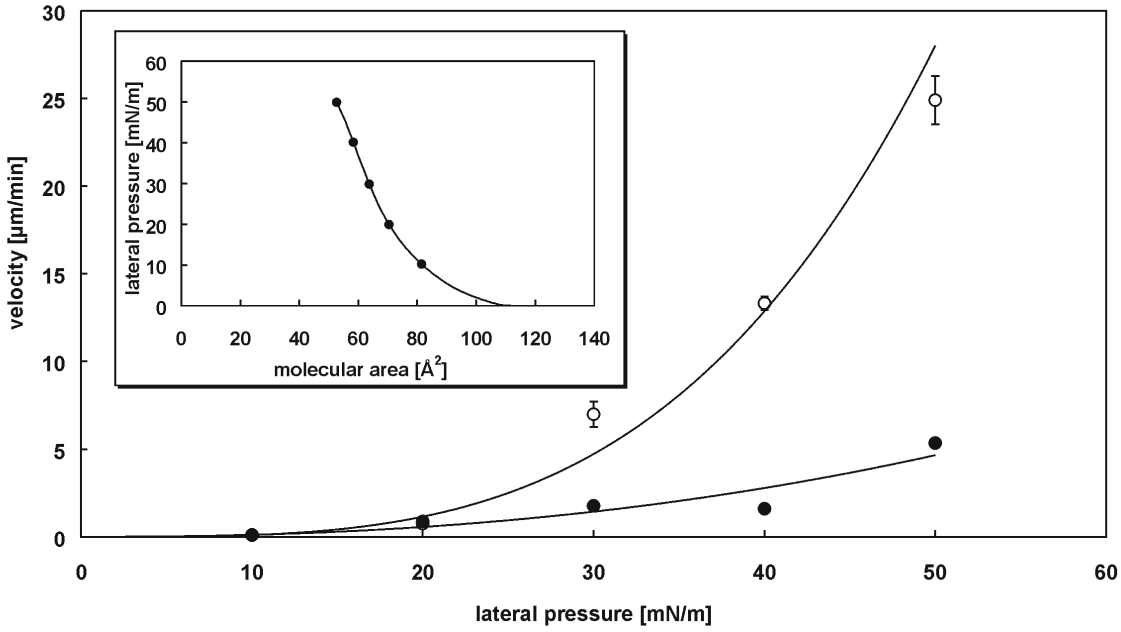

Figure 5.20: Comparison of the spreading velocities of DMPC monolayers transferred at different lateral pressures at two different relative humidities. Closed circles: *RH* = 85 %, open circles: *RH* = 90 %. The lines are guides to the eyes. Inset: pressure/area isotherm of DMPC at 25 °C, the dots refer to the transfer pressures.

For a given monolayer, W_A should not depend remarkably on humidity, thus the viscous drag coefficient z is the value responsible for changing spreading velocities with varying humidities.

The strong influence of the lateral pressure is in contrast to the diffusion model developed in [Burl, 1996b], where a negligible influence of the spreading power (which is proportional to the lateral monolayer pressure, see (5.2.2) and (5.1.5)) on the rate of monolayer growth was found. Thus, besides the constant velocity during spreading, the strong influence of the spreading power on the spreading velocity also favours the model developed above (5.2.12).

In all cases, monolayer dilation was below 0.5 % of its original density. Hence the influence of a shrinking monolayer reservoir, which becomes more pronounced for monolayers with an initially low density, can be neglected. The observed non-linearity can be explained by means of (5.2.12) by assuming that ζ depends on the lateral film pressure. One could argue that a change in headgroup density is accompanied by a change in the friction coefficient z. In fact a hydrodynamic relation between z and the self-diffusion coefficient exists [Evan, 1988], [Merk, 1989], [Niss, 1999]. The self-diffusion coefficient, however, increases with decreasing monolayer density [Pete, 1983]. This effect would

accelerate spreading at lower lateral pressures, which is not consistent with the data. The influence of *RH* on z is possibly due to a change of the monolayer/substrate disjoining pressure, which in the present case is dominated by hydration forces. It could be the case that the hydration force is dependent not only on *RH* but also on p. In the case of protrusion forces [Isra, 1990], the pre-factor of the exponential relation between disjoining pressure and separation distance depends on the protrusion site density (5.0.17). A reduced lateral pressure leads to a reduced protrusion site density, which could possibly result in a smaller hydration force leading to increased friction in case of monolayers with small lateral pressures. In principle, the drag coefficient ζ can be determined by diffusion measurements (see chapter 5.3) and compared to those found from spreading experiments [Niss, 1999]. In the present case, however, the contribution of the dilational viscosity of the lipid monolayer to the dissipation is unknown. Furthermore, in order to be able to calculate ζ from spreading experiments, the length of the dissipation region must be known. Therefore a comparison of friction coefficients obtained from spreading and diffusion experiments was not carried out.

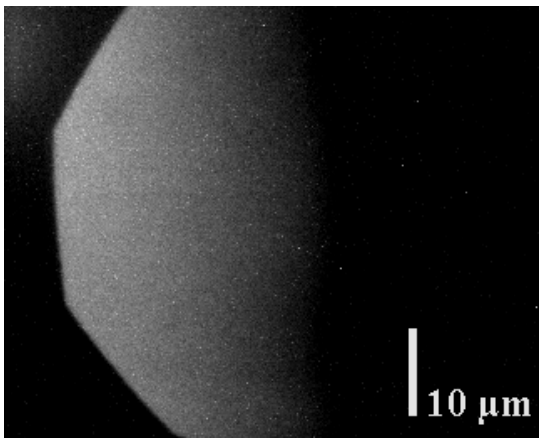

Figure 5.21: DMPC monolayer on a Chitosan film, lateral pressure 50 mN/m. The picture was taken at *RH* = 50 %, after 2 min exposure to a humidity near condensation (> 98 %).

At extremely high values of *RH* close to the dew point, contrary to the case of moderate humidities, a pronounced decrease of fluorescence intensity near the monolayer leading edge was observed (Figure 5.21) during spreading over a distance of approximately 40 µm. The edge became diffuse and curvy.

The remarkably reduced sharpness of the spreading front is also depicted in an intensity profile past the monolayer leading edge (Figure 5.22).

Following [Gave, 1990], the ratio between advection-like spreading and spreading by diffusion is described by a surface Peclet number, which in the present case reads:

$$Pe = \frac{W_A}{\zeta D} \qquad \textbf{(5.2.13)}$$

D is the diffusion coefficient of an isolated molecule. Note that the definition of the Peclet number is lent from hydrodynamics, and for the quantity z, the already mentioned restrictions hold.

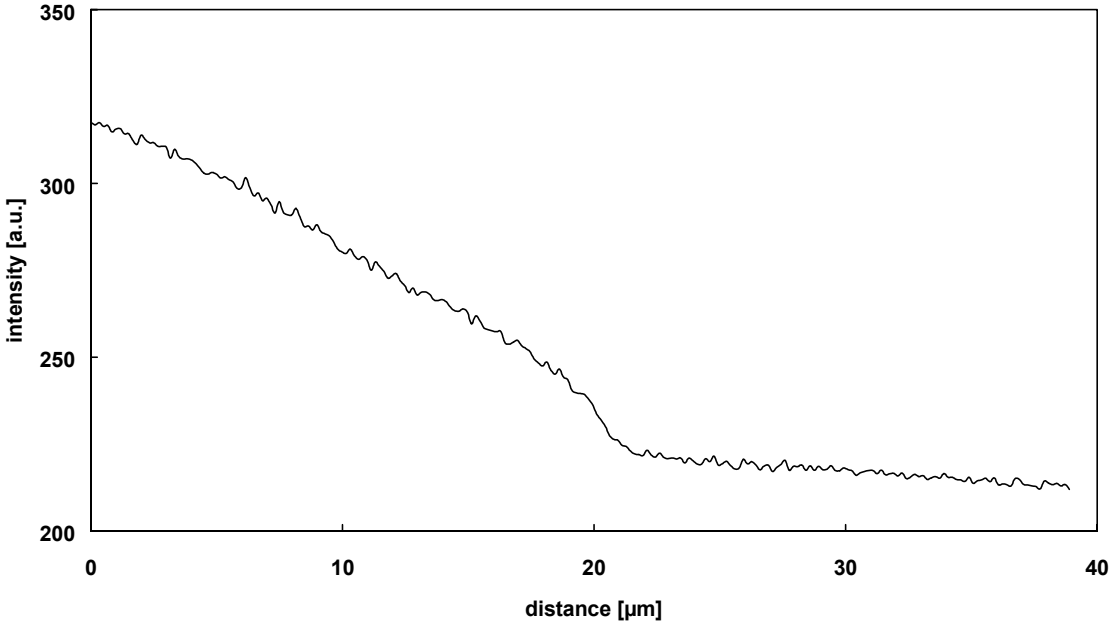

Figure 5.22: Line profile indicating the intensity distribution along the horizontal axis of Figure 5.21. Note: the picture was taken without background subtraction, hence the non-zero intensities in the right tail of the curve.

In case of high Peclet numbers spreading by advection is favoured. Increasing *RH* will both decrease z and increase D. It could be the case, however, that the diffusion coefficient *at the leading edge* is influenced by *RH* more strongly than z, the friction coefficient observed in the bulk film. This can be expected since the properties of a monolayer coated chitosan surface and a free chitosan surface are likely to be different in terms of roughness and polarity, due to a smoothing effect induced by a relatively smooth monolayer surface and due to the polarity of the monolayer headgroups. In the case of spreading by advection, since dissipation is distributed over a large monolayer area, the spreading dynamics will be governed by the average monolayer/polymer distance regulated by hydration forces. At least partially, the disjoining pressure in the monolayer/polymer interface is influenced by protrusion forces [Isra, 1990], a phenomenon which is likely to be reduced for a diffusor at the leading edge of a spreading monolayer, i.e. a boundary particle (Figure 5.19).

At a humidity very close to the dew point, however, it is possible that a thin, interconnected water film develops on the free polymer surface, which allows for diffusion

to take place, at least in case of a monolayer which is diluted enough that van der Waals attraction is too weak to force the water layer to collapse. This effect might explain the diffuse spreading front observed at extremely high humidities (Figure 5.22).
It cannot be totally ruled out, however, that the reduced fluorescence intensity at the leading edge of the monolayer film is an artefact due to the reduced mobility of the fluorescence labelled lipid in comparison to unlabelled lipids.
In order to clarify this uncertainty, the use of non-probe techniques, such as spatially resolved ellipsometry [Hesl, 1989], reflection interference contrast microscopy [Rädl, 1993b] or surface plasmon microscopy [Luch, 2000] is necessary.

5.2.2.2 Spreading of DSPC, DLPE and DMPC/cholesterol on chitosan

In order to analyse the influence of the phase state on the spreading behaviour, a DSPC monolayer was transferred to a chitosan cushion at a lateral pressure of 40 mN/m, where DSPC is completely in the liquid condensed state. Figure 5.23 shows, that contrary to a fluid monolayer (Figure 5.14), a relatively diffuse monolayer edge was obtained. Moreover, the film was rather inhomogeneous. It showed holes and cracks, which stem from the brittle condition of a condensed monolayer, in combination with a highly reduced mobility. In fact, raising *RH* even to values close to the dew point could not induce any observable spreading during the time of several hours. Obviously, according to (5.2.12), the friction coefficient z is highly increased. Thus the magnitude of friction on the solid support is connected to the lateral fluidity of the monolayer membrane, which in the solid and in the fluid state can differ by several orders of magnitude [Pete, 1983].

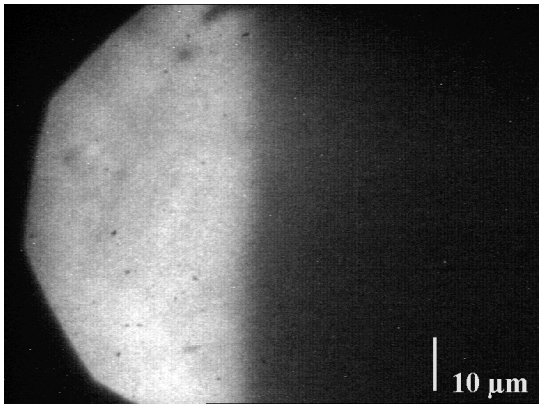

Figure 5.23: Monolayer edge of DSPC on Chitosan, lateral transfer pressure 40 mN/m.

Furthermore, the influence of the nature of the phospholipid headgroup was studied by transferring a DLPE monolayer at a lateral pressure of 40 mN/m at 25 °C, where it is in the liquid expanded state. At a relative humidity of 90 % a spreading velocity of 1.31 ± 0.033

µm/min was found. This may be compared to the spreading velocity of a DMPC monolayer under the same conditions, for which a value of 13.3 ± 0.37 µm/ min was obtained. The higher spreading velocity of DMPC is likely to be at least partially due to the lower hydration of PE headgroups [Rand, 1989]. Taking into account the results from complementary methods to study membrane/substrate interactions presented in chapter 5.1 and 5.3, it is likely that during the transfer of DLPE at a lateral pressure of 40 mN/m a phase transition (substrate mediated condensation) occurred [Rieg, 1992]. This seems to be in accordance with the monolayer stability analysed in chapter 5.1 and the much reduced fluidity as described in chapter 5.3. In fact a temperature increase was found to raise the lateral mobility of chitosan-supported DLPE monolayers drastically, indicating that a phase transition was involved (chapter 5.3.4). The reason for the higher influence of chitosan on the phase state of DLPE compared to DMPC is the different composition of their corresponding headgroups. The nature and difference of the substrate/lipid interaction, however, is not known so far.

Finally, the influence of the presence of cholesterol was examined. A DMPC monolayer with an additional amount of 30 mol% cholesterol was transferred onto a chitosan cushion at a lateral pressure of 40 mN/m at 25 °C. A spreading velocity of 0.16 ± 0.009 µm/min was found at 90 % *RH*. Thus the spreading velocity is reduced considerably compared to the value found for a pure DMPC monolayer. The influence of cholesterol on supported membrane dynamics is manifold. Cholesterol reduces the diffusion coefficients in phospholipid membranes considerably (see chapter 5.3.4). Additionally, the presence of cholesterol leads to a dehydration of the membrane substrate gap [Niss, 1999] which results in a further decrease in spreading velocity.

5.2.2.3 Spreading of DMPC on different substrates: agarose and glass

In order to demonstrate the influence of the nature of the monolayer substrate on spreading velocities, a DMPC monolayer with a lateral transfer pressure of 40 mN/m was deposited onto agarose and in a different experiment directly onto glass. In case of the former, the spreading velocity at *RH* = 90 % was 1.00 ± 0.020 µm/min, hence considerably lower as compared to a DMPC monolayer on chitosan prepared and analysed under the same conditions. One reason for such an increase in ζ is the pronounced roughness of agarose in comparison to chitosan. As was mentioned in chapter 4.4, the swelling of agarose could not be analysed by means of ellipsometry, so the swelling state of the two polymer cushions cannot be compared with each other.

On glass, the situation for a DMPC monolayer, lateral pressure of 40 mN/m at 25 °C and relative humidity of 90 % was similar to that of a DSPC monolayer on chitosan, exposed to the same conditions. On the one hand, a clearly visible boundary between covered and uncovered substrate surface was observed (fluorescence picture not shown). On the other hand, no displacement of the spreading front was observed during several hours of exposure to extremely high relative humidities.

5.2.3 Spreading from a multilayer lipid reservoir

As an alternative to spreading from a lipid reservoir which consists of the deposited Langmuir-Blodgett monolayer itself, a multilayer stack was deposited onto a chitosan cushion from a chloroform solution [Rädl, 1995a]. A straight edge was formed by coating the rim of a microscopic coverglass with a very concentrated, viscous lipid solution and stamping the latter onto the polymer. Afterwards, the substrate was dried in vacuo over night. The sample was then mounted into the humidity chamber and subjected to RH = 90 %. Hydration of the multilayer lipid reservoir led to increased lipid mobility and a lipid layer spread out (Figure 5.24). At the top of Figure 5.24 the brightly shining reservoir can be observed. Seemingly, spreading already occurred before drying the substrate in vacuo, i.e. with chloroform still present, because a faintly fluorescent film (compared to the reservoir) was found in all cases already before increasing RH.

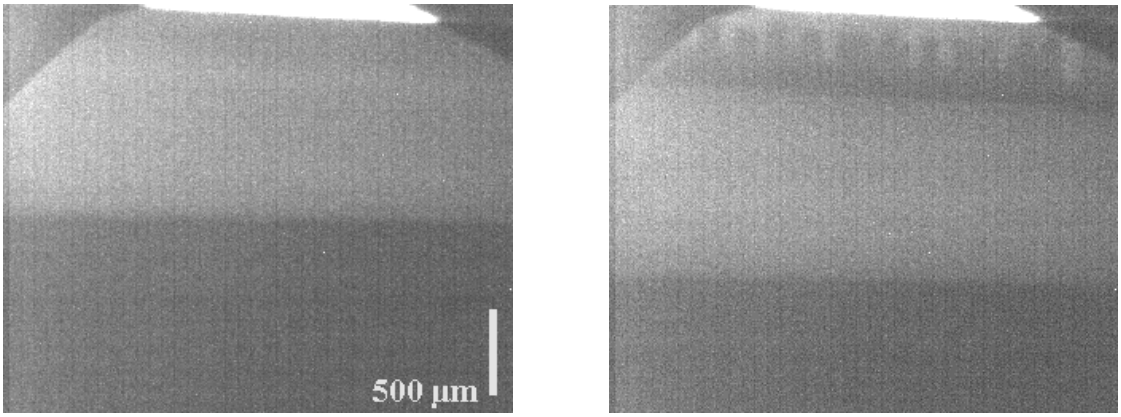

Figure 5.24: Spreading from a lipid reservoir deposited from a chloroform solution onto a chitosan film, left picture: 5 min after increasing *RH*, right picture: 25 min later.

In principle, the latter effect could be avoided by depositing the lipid from a stamp, which had been completely dried before the stamping procedure [Niss, 1999]. This, however, bears the danger of partially destroying the polymer cushion.

It can clearly be deduced from Figure 5.24, which has a significantly lower resolution compared to e.g. Figure 5.14 that no detectable density gradients in the film developed. Instead, the film became inhomogeneous near the reservoir, which is further proof, that the film is moving as a whole and not in the diffusion like fashion assumed by Oshanin et al. [Osha, 1998b]. The spreading distance in the above mentioned experiment was measured relative to the lipid reservoir (Figure 5.25). The spreading velocity was found to be not constant. However, the spreading front displacement did not obey a square root law with respect to the spreading time. Clearly, spreading from a multilayer stack at partial hydration is a much less defined experiment than spreading from a homogeneous lipid monolayer, therefore the latter was examined in much more detail.

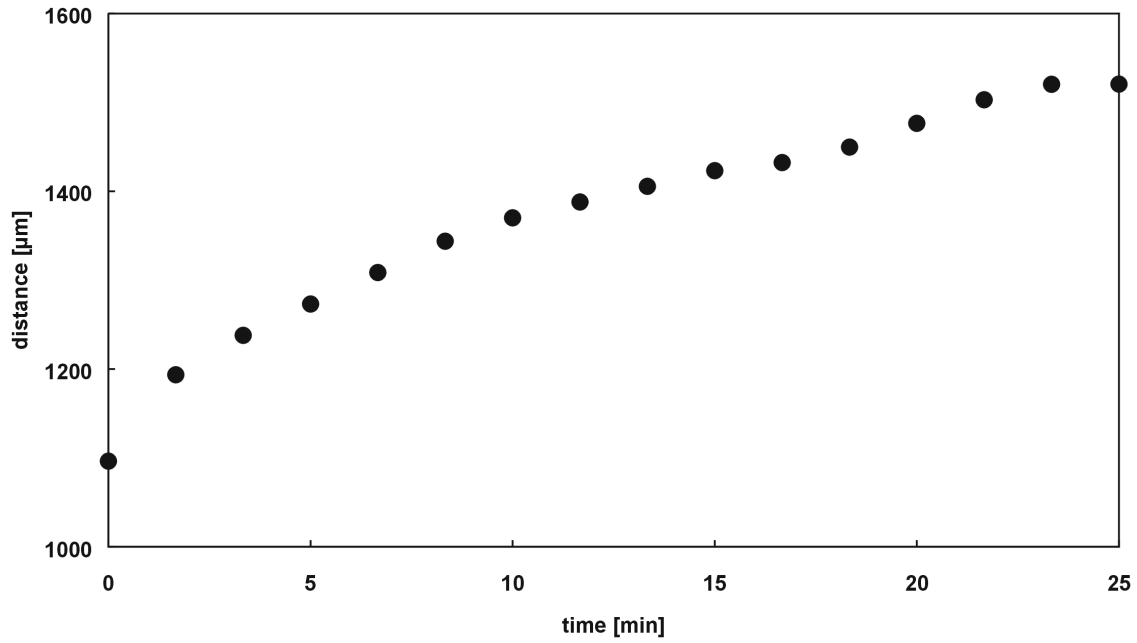

Figure 5.25: Spreading front displacement obtained by spreading from a multilayer reservoir deposited onto a chitosan cushion at a relative humidity of 90 %.

It is uncertain whether the reservoir can be regarded as a lipid source on the time scale of the spreading experiment. Instead, it might be the case that the hydration of the source is a much slower process than the expansion of the initial precursor film. Furthermore, it is not known whether a monolayer or multilayer spreads on the chitosan cushion. The latter has indeed been observed in case of thermotropic liquid-crystals [Luch, 2000]. In order to clarify this matter height sensitive techniques such as spatially resolved ellipsometry [Hesl, 1989], surface plasmon microscopy [Luch, 2000] or reflection interference contrast microscopy [Rädl, 1993b] have to be applied.

5.2.4 Conclusion and outlook

A self-repairing ability of physisorbed amphiphile monolayers on hydrophilic substrates was observed and quantitatively analysed by covering one half of a hydrogel surface with a Langmuir-Blodgett film, raising the relative humidity considerably and examining the spreading kinetics of the monolayer onto the uncovered area. Directly after the transfer a very sharp and linear monolayer edge was observed, provided the hydrogel was equilibrated sufficiently with the trough subphase. In case of film edge distortions being observed right after the transfer, these healed out quickly during the spreading process to yield a straight and sharp monolayer edge. This is in contrast to bilayer spreading, which was explained by the much higher spreading power in case of monolayer spreading. A spreading front displacement linear with time was found for a lateral expansion of the monolayer less than 0.5 %. This was explained by assuming an expansion over a large film area and balancing the resulting dissipation by friction at the monolayer substrate interface with the driving force, the high surface energy of a free hydrogel surface. A simple model was derived which describes the dependence of the spreading velocity on the system parameters. The following features were found to influence the spreading dynamics: (I) the transfer pressure of the monolayer, (II) the relative humidity, (III) the phase state of the monolayer, (IV) the nature of the lipid headgroup, (V) the cholesterol content of the monolayer, (VI) the nature of the substrate.

The dependence of the spreading velocity on the driving force was found to be non-linear, in contrast to the spreading velocities obtained on a thin water film sublayer [He, 1998], which could be explained by assuming that the friction at the monolayer/substrate interface varies with the monolayer density.

It is important to note that a retraction of the monolayer leading edge while *reducing* the value of *RH* was never observed. In fact, in multibilayer stacks changing *RH* leads to an additional effective lateral pressure [Pars, 1979], which compresses the bilayer and can therefore induce phase transitions (e.g. [Bind, 1998]). In case of a substrate-supported lipid monolayer, however, a lateral compression, which would be caused by a dehydration of the monolayer headgroups, would indeed be accompanied by a dewetting process. It is likely that (due to the much higher spreading power compared to a bilayer on a bilayer) dewetting is energetically so unfavourable that lateral compression and humidity induced phase transitions in solid-supported monolayers are frustrated. This question will be further addressed in chapter 5.3.

As already mentioned in the introduction, the self-healing properties of Langmuir-Blodgett films might be of considerable importance for practical applications. The spreading power of bilayers on solid substrates is much lower compared to monolayers, therefore the

healing of monolayer defects *before* depositing a second monolayer could be important for fabricating highly insulating bilayers.

Many additionally important aspects of monolayer spreading could not be examined in the present work. Among these are a much more refined analysis of the quantitative influence of relative humidity on spreading velocity, the use of solvent gases different from water, and a deeper analysis of roughness effects on spreading velocities.

Due to the asymmetric monolayer/support interface, the effect of monolayer hydration could not be distinguished from the swelling of the polymer support. Additionally, the monolayer/substrate separation in a hydrogel-supported membrane is difficult to determine, due to the swelling of the polymer cushion over length scales much larger than the monolayer/substrate interface. These disadvantages could possibly be circumvented by spreading of a lipid monolayer on top of another monolayer, as depicted in Figure 5.26 for example. A hydrophobised substrate would be partially coated by Langmuir-Blodgett transfer. Subsequent withdrawing of the substrate would then result in an inverse bilayer (a solid-supported "foam film") with a defined bilayer edge. Substantially increasing *RH* should lead to a precisely measurable (e.g. by ellipsometry or surface plasmon resonance spectroscopy) change in the water layer thickness *d* (amounting to up to 3 nm [Rand, 1989]). Provided that the spreading front displacement is small compared to monolayer expansion, the spreading velocity should be determined by friction in the lipid/lipid interface lowered by repulsive hydration forces, and the spreading power. The water layer thickness in case of monolayers with low lateral pressure, however, is determined not only by repulsive hydration forces but also by attractive hydrophobic forces as has been shown in the case of partially depleted bilayers by Helm et al. ([Helm, 1989]), so additional phenomena can be studied.

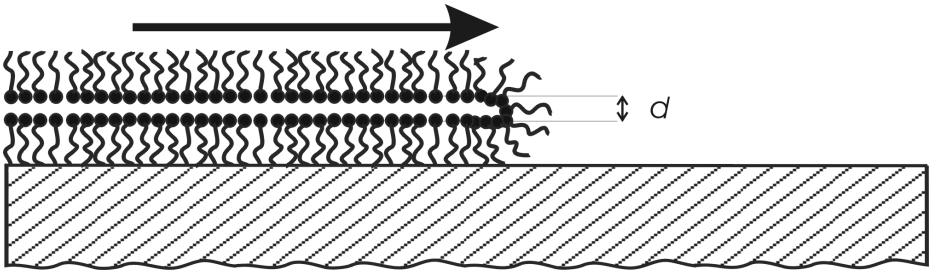

Figure 5.26: Possible experimental configuration for correlating monolayer spreading with the water content of the lipid/lipid interface, i.e. the thickness of the water layer *d*. Spreading is due to the advancement of the upper monolayer, while the lower one is fixed on the substrate.

While in the present chapter collective monolayer motions in terms of advection induced by surface energy gradients were analysed, the next chapter will be concerned with Brownian motion, i.e. entropically driven dynamics of solid-supported monolayers.

5.3 Fluidity of supported lipid monolayers as a function of ambient humidities and solvent variation

While vast literature exists concerning diffusion of lipid molecules in free and supported model and biological *bilayer*-membranes [Cleg, 1985], [Alme, 1995], and in monolayers at the air water interface (e.g. [Pete, 1983]), experimental data concerning the fluidity of *supported monolayers* of amphiphiles in general, and phospholipids in particular, are relatively scarce.

The lateral diffusion of fully hydrated monolayers on hydrophobic supports was measured in [Merk, 1989] using FRAP. In other studies hydrogels were employed as a hydrophilic support for phospholipid monolayers and were found to enhance monolayer fluidity compared to glass supports in a water-saturated atmosphere [Kühn, 1994], [Diet, 1995]. Furthermore, polyelectrolytes were coated with a planar lipid monolayer and fluidity was determined by a fringe pattern photobleaching technique after immersing the substrate in different solvents and in air [Auch, 2000].

Several authors point to the influence of humidity on the dynamics of supported amphiphile monolayers [Chen, 1989], [Chi, 1992a], [Chen, 1992], [Berm, 1997], [Shik, 1998]. During the exposure of a supported lipid monolayer to a high humidity atmosphere, water permeates the hydrophobic part [Vand, 1985] and the headgroups become hydrated, as observed for example by a thickness increase of the monolayer [Chen, 1992], [Bolz, 2001] accompanied by a weakening of the monolayer substrate interaction [Yami, 1997]. A systematic study of the effects of humidity changes on supported monolayer dynamics, however, to the best of the author's knowledge, is missing completely.

This is not the case for bilayers: McCown et al. [McCo, 1981] analysed the influence of humidity changes on the lateral diffusion of membrane probes added to a multibilayer stack. The decrease of fluidity at lower humidities (even though the acyl chains remained in the fluid state) was assumed to be due to (I) the smaller area per lipid headgroup and (II) the smaller volume fraction of the polar headgroup in the aqueous region. The latter influences lipid mobility due to the proximity of the opposing headgroup. Galle et al. developed a simple model which includes influences of temperature and humidity based on the Arrhenius expression for activated diffusion [Gall, 1995]. Again, the influence of humidity was assumed to be due to its influence on the lipid headgroup area, hence on the free area available for diffusion (see below). The mobility of surfactant monolayers deposited onto silica surfaces was analysed in [Neum, 1994], however, the authors used a rather special setup, resembling a surface force apparatus, and performed bleaching experiments in the contact zone of two monolayer coated surfaces only.

The aim of the present chapter is to characterise the lipid-membrane/substrate interface with respect to its influence on membrane mobility. Supported lipid monolayers are particularly well suited for this purpose due to their robustness and insensitivity towards substrate inhomogeneities compared to supported bilayers [Kühn, 1994], and the fact that the disjoining pressure may be changed readily over a wide range by adjusting the ambient humidity. Before proceeding to the experimental details, a brief introduction into presently available theories describing diffusion in amphiphile membranes will be given.

5.3.1 Available theories for lateral self-diffusion in amphiphile membranes

The solution of the diffusion equation

$$\frac{\partial C(r,t)}{\partial t} = D\nabla^2 C(r,t) \qquad \textbf{(5.3.1)}$$

where D is the diffusion coefficient, ∇^2 is the Laplacian operator and $C(r,t)$ is the Gaussian probability distribution of displacements, r, can be written as:

$$C(r,t) = \frac{1}{4\pi Dt}\exp\left(-\frac{r^2}{4Dt}\right) \qquad \textbf{(5.3.2)}$$

(5.3.2) follows from the assumption of an instantaneous unit source at the origin at $t = 0$. From (5.3.2) it follows that the second momentum of this distribution, $\langle r^2 \rangle$, can be written as

$$\left\langle r^2 \right\rangle = 4Dt \qquad \textbf{(5.3.3)}$$

which can be used as a definition of the diffusion coefficient in a two-dimensional homogeneous medium [Alme, 1995]. D is a function of the friction coefficient, f, by the well-known Einstein relation

$$D = \frac{kT}{f} \qquad \textbf{(5.3.4)}$$

The friction coefficient can be calculated by solving the Navier-Stokes equations and taking into account the frictional coupling to the boundary liquids. Saffman and Delbrück [Saff, 1975] arrived at the following expression for the friction coefficient

$$f = 4\pi\eta h\left(\ln\frac{\eta h}{\eta_w R} - \gamma \right)^{-1} \qquad \textbf{(5.3.5)}$$

with the membrane viscosity, η, and membrane thickness, h, water viscosity, η_w, radius, R, of the diffusor and γ is the Euler constant. (5.3.5) is valid in case of

$$\varepsilon \equiv \frac{2\eta_w R}{\eta h} \le 0.1 \qquad \textbf{(5.3.6)}$$

i.e. for large diffusors (like integral membrane proteins) and low viscosity of the surrounding medium. An expression for $\varepsilon \ll 1$ was derived in [Hugh, 1981]. Evans and Sackmann [Evan, 1988] examined the effect of weak dynamic coupling of a membrane to an adjacent support and found

$$f = 4\pi\eta h\left(\frac{(\varepsilon')^2}{4} + \frac{\varepsilon' \mathrm{I}_1(\varepsilon')}{\mathrm{I}_0(\varepsilon')} \right)^{-1} \qquad \textbf{(5.3.7)}$$

I_0 and I_1 are modified Bessel functions of the second kind, orders zero and one, and

$$\varepsilon' = R\left(\frac{b_s}{\eta h} \right)^{0.5} \qquad \textbf{(5.3.8)}$$

The friction coefficient, b_s, in case of a membrane floating on an ultrathin water film, can be calculated by assuming a linear velocity gradient in the water film: $b_s = \eta_w/d$, where d is the thickness of the water film.

In case of very weak frictional coupling ($\varepsilon' \ll 1$), (5.3.7) reduces to (5.3.5), whereas in case of strong coupling ($\varepsilon' \gg 1$) [Kühn, 1994]:

$$D = \frac{kT}{\pi b_s R^2} \qquad \textbf{(5.3.9)}$$

Refined calculations of the flow fields revealed that the Evans-Sackmann equation may be used even for not particularly thin water layers, e.g. a monolayer on the Langmuir film balance [Ston, 1998].

Although the Evans-Sackmann model was used for determining frictional coefficients of lipid probes [Merk, 1989], it is questionable if the diffusion of lipids may be characterised by the continuum models described above, which neglect the discreteness of the lipid matrix, which may only be valid for large membrane proteins [Alme, 1995].

Alternatively, a free area model based on the free volume theory [Cohe, 1959] was derived in order to calculate diffusion coefficients based on the microstructure of a two-dimensional system [Gall, 1979]:

$$D = D(a^*)\exp\left(-\frac{\gamma a^*}{a_f}\right) \qquad \textbf{(5.3.10)}$$

In this expression a^* is a critical free area available for a diffusor, below which no diffusion takes place, $D(a^*)$ is the diffusion coefficient in a free area, $a_f = a_f(T)$ is the average free-area in the system and g is a geometric factor. In more general expressions an activation term $-E_a/kT$ is added to the argument of the exponential [Chun, 1966]. A similar expression will be used in chapter 5.3.3 to describe the dependence of the diffusion constant on relative humidity. In addition to these models numerous computer simulations have been performed based on two-dimensional Ising spin-lattice models, e.g. [Pink, 1983], [Pink, 1993], the success of which underlines the applicability of lattice models for analysing lateral lipid diffusion in lipid membranes.

All the diffusion theories mentioned so far are valid only in homogeneous systems. Theories valid for heterogeneous systems, i.e. where domains with different mobilities are present, can be divided into effective-medium and percolation theories [Saxt, 1982]. In case of the former, the most useful form [Saxt, 1982] is the Bruggeman-Landauer equation [Tama, 1993]:

$$\frac{D}{D_f} = \left(x-\frac{1}{2}\right)(1-r) + \left[\left(x-\frac{1}{2}\right)^2(1-r)^2 + r\right]^{0.5} \qquad \textbf{(5.3.11)}$$

In this equation D is the measured diffusion coefficient, D_f is the diffusion coefficient in the fluid phase, x is the phase fraction of the fluid phase, r is called relative permeability and is defined as

$$r = K\frac{D_d}{D_f} = \frac{[A]_d}{[A]_f}\frac{D_d}{D_f} \qquad \textbf{(5.3.12)}$$

where K is the partition coefficient expressed by the concentration of diffusing species in the solid domain $[A]_d$ and that one in the fluid phase $[A]_f$ and D_d and D_f are the diffusion coefficients in the solid domain and the fluid phase respectively. In case $r < 10^{-3}$ the effective medium theory is no longer applicable, and the solid domains can be regarded as impermeable domains (archipelago [Saxt, 1982]). In that case a critical fluid phase fraction, x_c, exists (percolation threshold), below which diffusion can essentially be neglected. Above the percolation threshold the diffusion coefficient follows a power law:

$$D \approx D_f (x - x_c)^t \qquad \textbf{(5.3.13)}$$

where t is a critical exponent.
In chapter 5.3.3 the applicability of the theories that have been introduced above to the problem of humidity dependent lateral self-diffusion in hydrogel-supported phospholipid monolayers will be discussed and a modified free volume model will be presented. In the next section, however, the measurements will first be described in detail.

5.3.2 Preliminary experiments

Thin chitosan films (approximately 150 nm in the dry state) were prepared as described in chapter 4 and coated with lipid monolayers. The monolayers were stained with a fluorescence dye and deposited by Langmuir-Blodgett transfer as described in chapter 3.10.3. The substrate was mounted into the humidity chamber, lipid on the backside of the substrate was thoroughly wiped off with an isopropanol-soaked tissue, the oil immersion objective was optically coupled to the substrate by means of immersion oil and the setup was allowed to equilibrate at RH = 50 % for at least half an hour. The relative humidity was then appropriately increased. After performing an alteration of RH, the sample was allowed to equilibrate for 5 min before starting diffusion measurements. If not indicated otherwise, all diffusion experiments were performed at 26 °C, which was equal to the ambient temperature. At least five bleaching experiments were performed on different locations of the sample to allow for appropriate error estimation and averaging. The diffusion coefficient was found to be highly dependent on ambient humidity, however, complete reversibility was found while changing RH between 70 % and 85 % (Figure 5.33). Furthermore, pronounced drying at $RH \geq 4$ %, which was the lower limit of the

humidity setup, did not lead to irreversible changes of the diffusion coefficient (data not shown). From the reversibility of the monolayer fluidity, it can thus be concluded that harsh changes in *RH* did not lead to irreversible morphological distortions in the monolayer or at the polymer surface. Moreover, while diffusion coefficients where depending on *RH*, the relative recovery, *R*, was in all cases of the experiments described in the following close to or equal to one. This indicates a complete fluorescence recovery, in the whole accessible humidity range.

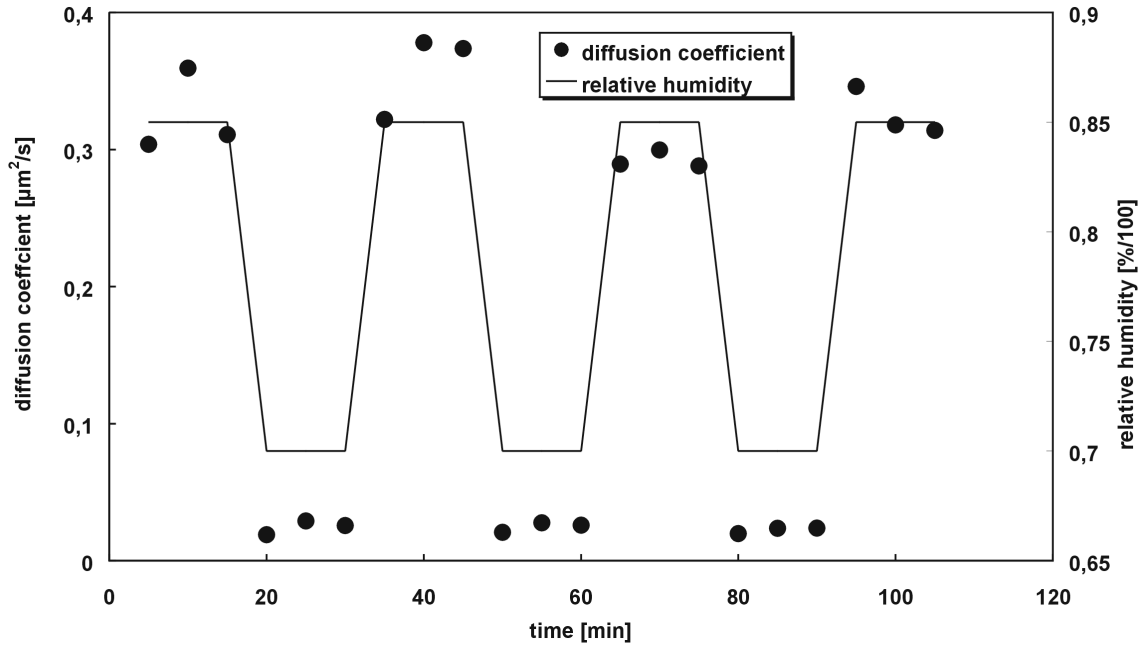

Figure 5.33: Reversibility of changes of the diffusion coefficient (dots) upon switching between different ambient humidities (line), in a DMPC monolayer on chitosan, lateral pressure 35 mN/m, fluorescence probe NBD-PE.

Prolonged annealing times at high humidities revealed that the monolayer fluidity did not increase after further annealing, i.e. after reaching a certain humidity, which took seconds to minutes depending on the direction and steepness of the jump, no further swelling at the monolayer/polymer interface occurred. The diffusion constant decreased by a factor of 14 while decreasing the relative humidity from 85 % to 70 %. This decrease is much stronger compared to humidity dependent diffusion measurements in multibilayer stacks [McCo, 1981]. These authors found an eight-fold decrease while reducing *RH* from approximately 100 % to 50 %. This clearly indicates a higher adsorption of diffusors in a partially dried monolayer system compared to partially dried bilayers.

Figure 5.34 shows the influence of temperature on the diffusion constant, in an interval between 20 °C and 30 °C, at *RH* = 80 %. From the slope of the Arrhenius plot an apparent activation energy of 416 ± 33 kJmol^{-1} may be calculated, which is about a factor of ten higher compared to the value found for glass-supported DMPC bilayers in the completely

hydrated and fluid state (54 ± 10 kJ/mol [Merk, 1989]), indicating an additional energetic barrier for diffusion. It cannot be ruled out completely, however, that the large slope is partially due to a temperature difference between humid gas inside of the cell and the sample itself, due to an influence of the room temperature of 26 °C. At a cell temperature higher than room temperature, the humidity directly above the sample could be higher than in the rest of the measurement cell and vice versa. This effect would induce a larger temperature dependence caused by different humidities at different temperatures. Due to this uncertainty, detailed studies of the influence of temperature changes could not be performed.

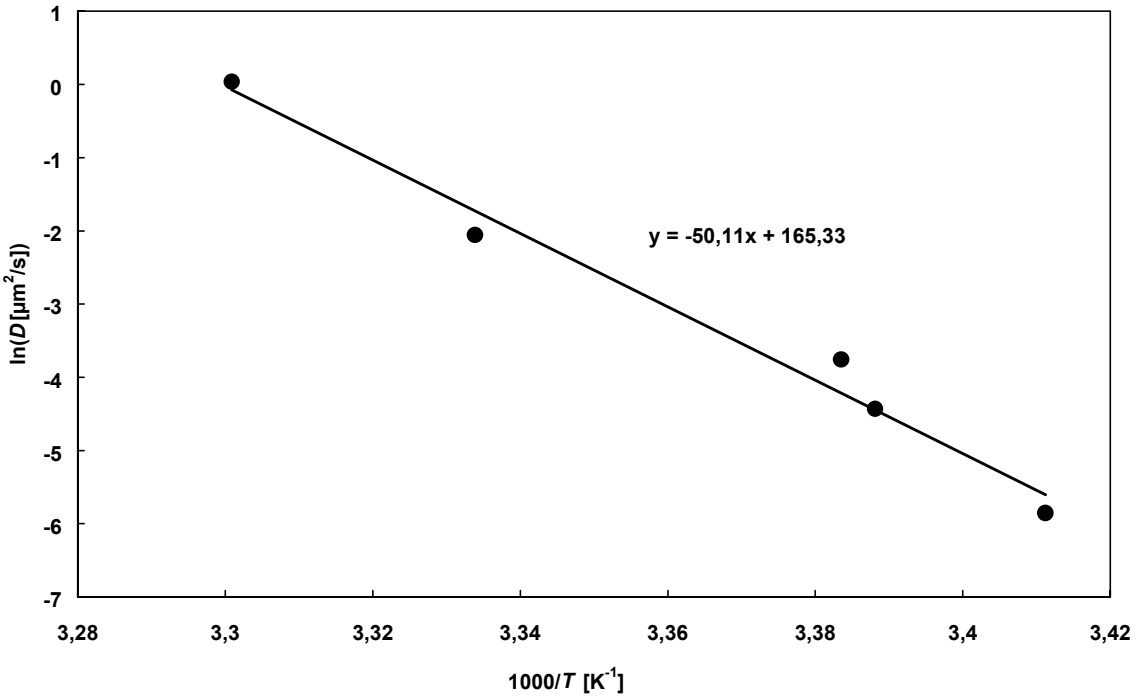

Figure 5.34: Temperature dependence of diffusion coefficients on chitosan-cushioned monolayers, lateral pressure 35 mN/m, fluorescence probe NBD-PE, at a relative humidity of 80 %.

5.3.3 Lateral self-diffusion in phosphatidylcholine monolayers in different hydration states

Detailed studies concerning the influence of humidity on lipid self-diffusion in monolayers were carried out in a humidity range of 90 % down to 65 % to 50 %, depending on the mobility found for low hydration states. The upper value was chosen because, as described in chapter 3.5, the error in determining *RH* largely depends on the magnitude of the relative humidity; at high humidities small temperature gradients can produce large differences in *RH*. At the lower boundary the resolution limit of the FRAP setup was encountered, which is determined by laser stability, mechanical stability of the setup, and

probe stability. The lower boundary for the diffusion coefficient in the case of the present setup was found to be around a value of 10^{-3} $\mu m^2/s$. In the range of this value, data scattering became too high and recovery times became too long to be reasonable from a practical point of view. As reversibility of diffusion coefficient changes was found, the measurements were always begun at RH = 90 %, upon which the relative humidity was lowered in steps of DRH = 2.5 %. At each value of RH at least five measurements at different positions on the sample were performed. In order to avoid significant bleaching during the observation of fluorescence recovery in case of small diffusion coefficients, the laser beam was temporarily shut off by means of a mechanical shutter. As the switching of the mechanical shutter was too slow in case of fast diffusion, the shutter mechanism was activated at RH around 80 %.

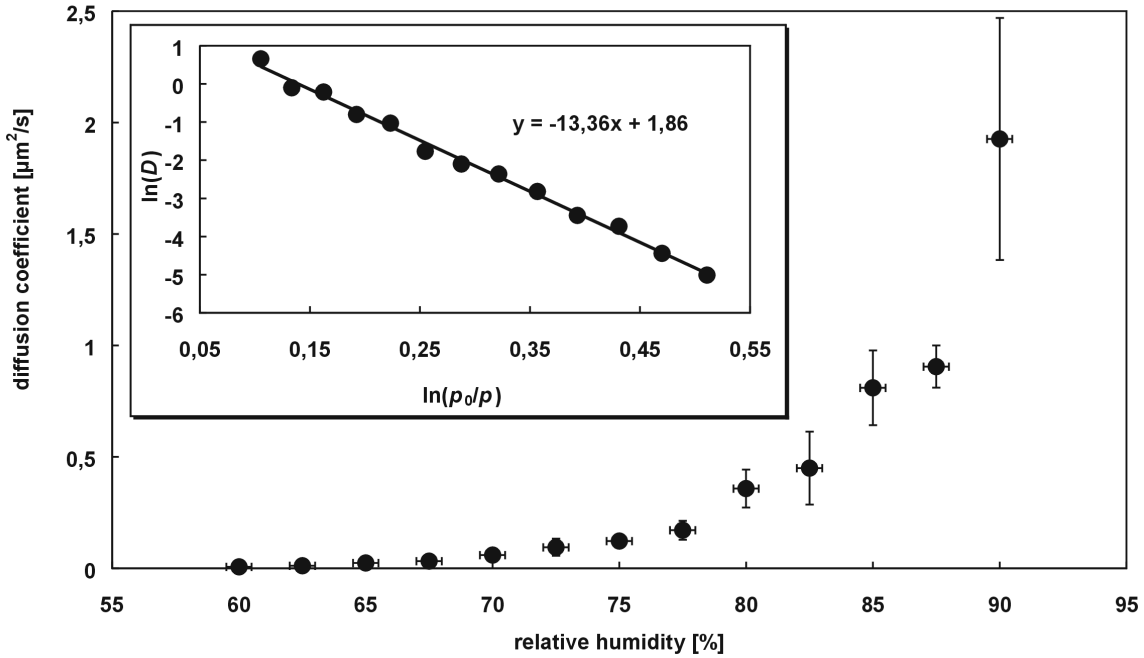

Figure 5.35: Diffusion coefficients of a chitosan-cushioned DMPC monolayer, lateral pressure 35 mN/m, fluorescence probe: NBD-PE, temperature 26 °C. The inset shows an axis transformation of the same data set, the natural logarithm of *D* is plotted against the natural logarithm of $p_0/p = 100/RH$.

Figure 5.35 shows the reduction of the diffusion coefficient in a DMPC layer which was stained with the headgroup labelled membrane probe NBD-PE and transferred at a lateral pressure of 35 mN/m (the influence of labelling at the headgroup on the reporter ability of the probe will be analysed below). Additionally, from the inset in Figure 5.35 it can clearly be deduced that an axis transformation in terms of a double logarithmic plot of the diffusion coefficient against the ratio of the partial water pressures p_0/p, leads to an essentially straight line. The partial pressure p_0 refers to water saturation, and p is the value

at the humidity $RH = 100 \cdot p/p_0$. The quantity $\ln(p_0/p)$ is proportional to the pressure difference, Π, (osmotic pressure) with respect to water saturation, according to:

$$\Pi = (kT/\upsilon)\ln\left(\frac{p_0}{p}\right) \qquad \textbf{(5.3.14)}$$

where υ is the volume of a water molecule and k is Boltzmann's constant. (5.3.14) follows from the equality of the chemical potential differences μ in the water film $\mu = -\Pi\upsilon$ and in the gas phase $\mu = kT\ln(p/p_0)$ with respect to a water bulk phase [Derj, 1987]. In the following a simple model shall be derived which explains the observations. Before proceeding to the derivation of this model, however, it shall be examined, to what extent the Evans-Sackmann theory (5.3.7) can be used to describe the friction in the monolayer/support interface.

According to (5.3.7), in order to calculate the friction coefficient, b_s, the parameters η, h and R have to be determined. The membrane thickness, h, and radius of the lipid probe, R, are known from literature [Merk, 1989]. The membrane viscosity, η, can be calculated by diffusion measurements in freely suspended bilayers or in monolayers at the air/water interface, by means of the Saffmann-Delbrück equation (5.3.5). Using a monolayer surface viscosity of $1.65 \cdot 10^{-10}$ Ns/m [Merk, 1989], which is valid for monolayers of DMPC at 25 °C, at a lateral pressure corresponding to the monolayer pressure in a free bilayer, the dependency of the diffusion coefficient on b_s can be calculated according to (5.3.7) (Figure 5.36). The membrane viscosity is supposed to be independent of RH. This assumption is justified by the fact that no indications for humidity induced lateral compression of the monolayer were found (see below). Assuming, furthermore, a linear velocity gradient in a thin lubricating water film between monolayer membrane and polymer cushion and a no-slip boundary at the surface of the polymer cushion, it turned out that the reduction of the diffusion coefficient was much too high to be describable by dissipation in a water layer (Figure 5.36). The lubrication layer thicknesses were calculated according to $b_s = \eta_w/d$, where η_w is the bulk water viscosity, and d is the thickness of the water film. For example, at a relative humidity of 77.5 %, a diffusion coefficient of $D \approx 0.17$ µm^2/s was found (Figure 5.35) which according to Figure 5.36 would correspond to a water layer thickness of ≈ 0.01 Å. As this value is smaller than a water monolayer, the assumption of a continuous water layer between lipid monolayer and underlying substrate is not justified.

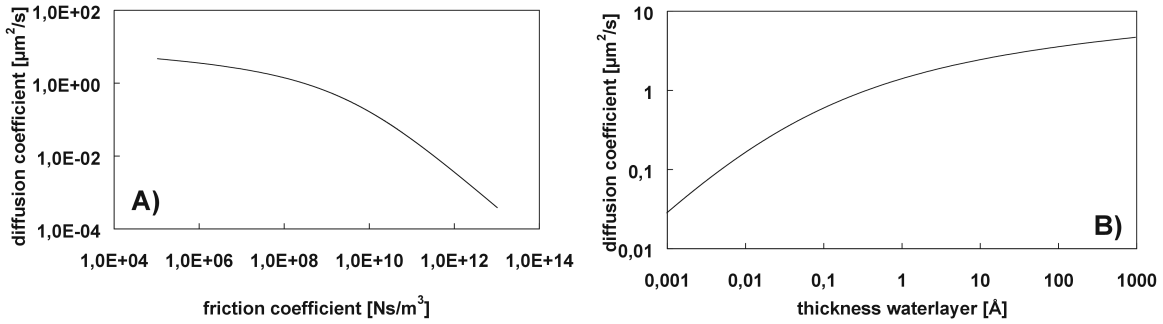

Figure 5.36: A) Relation between the measured diffusion coefficient in a substrate-supported monolayer membrane and the corresponding friction coefficient, b_s, calculated by means of (5.3.7), i.e. the Evans-Sackmann theory. B) Relation between measured diffusion constant and lubrication layer thicknesses calculated from the friction coefficients in A), according to $b_s = \eta_w/d$ (see text).

Molecularly thin water films have certainly different properties than bulk water [Marr, 1993], e.g. the viscosity for the first three molecular layers of water on a surface is increased. On the other hand, it is likely that the no-slip boundary condition in the experiment presented in Figure 5.35 does not apply, and that direct friction between diffusors and the substrate has to be assumed. According to [Vaz, 1985], it can be doubted if continuum models like the Evans-Sackmann model can be applied to study diffusion in model membranes, where the diffusors (in this case lipid molecules, contrary to comparably large membrane proteins) "see" the discreteness of their matrix. Instead microscopic models have to be used. Such a microscopic model will be derived in the following, similar to the free area model (5.3.10).

A basic assumption of the model is that diffusion can be regarded as an activated hopping process, which results in an Arrhenius-type diffusion behaviour:

$$D = D_0 \cdot \exp\left(-E_a/kT\right) \tag{5.3.15}$$

Hopping thus takes place in a two-dimensional, triangular [Pink, 1983] lattice, with an activation energy, E_a, to perform a hopping step. The diffusion coefficient may therefore be expressed as [Gall, 1979]:

$$D = \frac{1}{4} \nu_i \lambda^2 \tag{5.3.16}$$

where ν_i is the number of diffusional steps per second (jump frequency) and λ is the average jump length, which corresponds to the average distance of the lipid lattice and is a function of the headgroup area and hence the lateral pressure of the membrane. On the one

hand, data presentation in terms of jump frequencies allows for a ready comparison between different headgroup sizes and monolayer densities, but on the other hand, diffusion coefficients are the direct FRAP results, hence all data sets were expressed in terms of the latter.

Furthermore, it is assumed, that the diffusional activation energy is related to the adsorption energy [Clar, 1970], [Adam, 1990]. In order to derive an appropriate model which focuses on the influence of hydration on lateral diffusion, all parameters which are, in a first approximation, independent of the relative humidity, are assumed to define the pre-exponential factor in (5.3.15). In particular, it is assumed that the free area available for diffusion is independent of *RH*, therefore the relevant parameters (5.3.10) can be incorporated into D_0. The latter assumption will be rationalised further below. Thus D_0 is the diffusion coefficient found for a particular substrate-supported monolayer in the fully hydrated state. The adsorption energy is dependent on *RH* and the hydration pressure contribution can be calculated by an integration of the disjoining pressure along the surface normal [Rand, 1989]. A correlation between *RH* and the activation energy for diffusion has previously been assumed in [Berm, 1997].

The lipid layer may be regarded as being partially fixed in a periodic lattice of potential wells [Osha, 1998b], [Auch, 2000], the depths of which are dependent on the state of hydration in the monolayer/polymer interface (Figure 5.37). The depth is very deep concerning desorption to the gas phase, but allows for lateral jumps [Osha, 1998b].

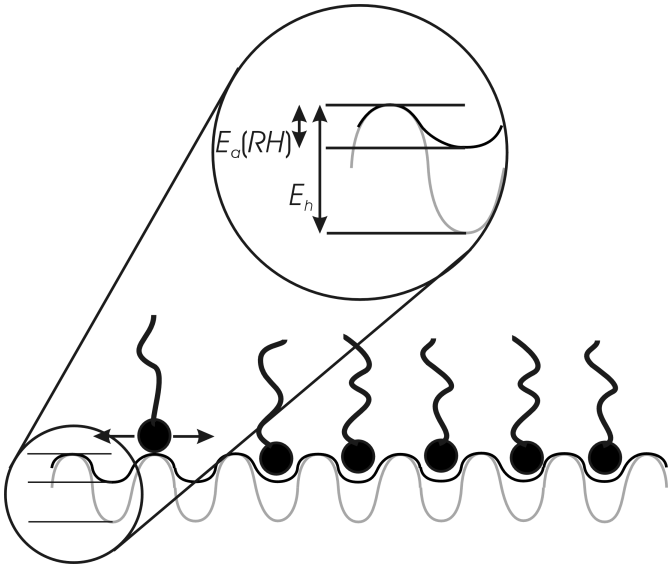

Figure 5.37: Lattice model for humidity dependent activated diffusion in a substrate-supported lipid monolayer. Grey line: depth of potential wells (E_h) in the completely dry state. Black line: depth of the potential wells ($E_a(RH)$) at the relative humidity *RH*.

While the forces which contribute to the experimentally observed hydration force are to date poorly understood, simple empirical relations exist in most cases (see chapter 5.0.1 for

details). In order to calculate the activation energy change by alteration of *RH*, the empirical exponential relation between disjoining pressure, Π, and distance, *d*, (5.3.17) is used (compare Equation 4.0.15), which holds for the swelling of lipid bilayers [Rand, 1989] and numerous other biological compounds [Leik, 1993a] (see chapter 5.0.1).

$$\Pi = \Pi_0 \exp(-d/\lambda_w) \tag{5.3.17}$$

Π_0 is an internal pressure, which is obtained by extrapolation to $d = 0$ and λ_w is a decay length. In the pressure range, where (5.3.17) holds, i.e. in a distance regime between 0.5 and 3 nm, the disjoining pressure is equal to the osmotic pressure [Pars, 1979].
Combination of (5.3.17) and (5.3.14) yields for the equilibrium distance:

$$d\left(\frac{p_0}{p}\right) = -\lambda_w \ln\left(\frac{\Pi}{\Pi_0}\right) = -\lambda_w \ln\left(\frac{kT}{\Pi_0 \upsilon} \ln\left(\frac{p_0}{p}\right)\right) \tag{5.3.18}$$

(5.3.18) again is valid only in the distance regime between 0.5 and 3 nm, where the hydration force dominates the surface forces. In the completely dry state, the hydration pressure contribution E_a to the activation energy corresponds to the energy E_h necessary to dehydrate a lipid headgroup, which can be approximated according to

$$E_h = a \int_{d=0}^{\infty} \Pi \delta d = \lambda_w a \Pi_0 \tag{5.3.19}$$

where *a* is the area of a lipid headgroup. In fact (5.3.19) slightly underestimates the hydration energy, due to an upward deviation of Π at distances below 0.5 nm [Isra, 1990]. In a partially hydrated state, E_h is reduced (lower depth of potential wells) by the humidity dependent disjoining pressure, i.e.

$$E_a = E_h - a \int_{d=0}^{d\left(\frac{p_0}{p}\right)} \Pi \delta d = \lambda_w a \Pi_0 - a \cdot \Pi_0 \cdot (-\lambda_w) \cdot \exp\left(-\frac{1}{\lambda_w} d(p_0/p)\right) \Bigg|_0^{d\left(\frac{p_0}{p}\right)} \tag{5.3.20}$$

Substitution for E_a in (5.3.15) yields:

$$\ln D = \ln D_0 - 1/(kT)\cdot\lambda_w \cdot a \cdot \Pi_0 \exp(-d(p_o/p)/\lambda_w) \qquad \textbf{(5.3.21)}$$

and with (5.3.18) it follows:

$$\ln D = \ln D_0 - 1/(kT)\cdot\lambda_w \cdot a \cdot \Pi_0 \exp\left(\lambda_w \ln\left(\frac{kT}{\Pi_0 \upsilon}\ln\left(\frac{p_0}{p}\right)\right)\Big/\lambda_w\right) \qquad \textbf{(5.3.22)}$$

which can be written in the final form:

$$\boxed{\ln D = \ln D_0 - C\ln\frac{p_0}{p}} \qquad \textbf{(5.3.23)}$$

with

$$C = \frac{a\cdot\lambda_w}{\upsilon} \qquad \textbf{(5.3.24)}$$

According to (5.3.23), a plot of ln(D) versus ln(p_0/p) should result in a straight line with the slope -C and an intercept of ln(D_0). Comparing (5.3.23) with the inset of Figure 5.35, a nice qualitative agreement between the model and experiment is found. In the following, the assumptions, limitations and the information, which can be drawn from the model, shall be examined.

According to (5.3.24), a correlation between the slope, -C, obtained by humidity dependent diffusion measurements and the decay parameter, l_w, of the hydration force exists, which is the basic conclusion to be drawn from the model. In order to calculate λ_w, the following parameters were used. The volume of a water molecule is n = 30 Å^3, which may be obtained from the molarity of water (55 mol/l). Furthermore, the area a was approximated according to the area of a fully hydrated DMPC headgroup a = 60 Å^2, which corresponds both to a fully hydrated headgroup in a bilayer [Pere, 1996], and to the molecular area at the transfer pressure of the monolayer (see chapter 8.2.1). By means of these parameters, from the slope C = -13.4 obtained from Figure 5.35, a decay constant l_w = 6.7 Å can be calculated. Experimentally determined values for the decay constant of the hydration force (determined in bilayers) lie in the range of 0.8 to 6.4 Å [Rand, 1989], [Mars, 1989]. The highest values are found for lysolipids. In the case of DMPC bilayer swelling, a value of

2.2 Å was measured [Iono, 1996]. The discrepancy is partially due to the different systems studied, here a solid-supported monolayer and there a multibilayer stack. Furthermore, the difference may be due to the apparent over-simplifications of the model. First, the actual cross-sectional area of the lipid headgroup in a partially dehydrated monolayer is smaller compared to the value measured by means of the film-balance in the completely hydrated state, which, according to (5.3.24) will lead to a lower decay parameter. Second, in the derivation of (5.3.22) the swelling of the polymer cushion was completely neglected. As described in chapter 4.4, the chitosan cushion swells in humid air, which reduces the density of binding sites. Third, the inter-particle interactions within the lipid monolayer, which may vary upon changing *RH*, were neglected also.

From the linear fit to the data shown in the inset of Figure 5.35, a diffusion coefficient D_0 = 6.4 $\mu m^2/s$ was obtained, which is considerably smaller compared to diffusion coefficients measured at the air/water interface (in the case of e.g. DLPC monolayers at a lateral pressure of 35 mN/m at room temperature a value of D = 20 $\mu m^2/s$ was found [Pete, 1983]). The smaller value in the present case indicates viscous friction in the lubrication layer between monolayer and polymer support [Evan, 1988].

(5.3.23) is valid only for not too high disjoining pressures, due to the non-convergence of (5.3.14) with respect to a zero relative humidity, contrary to (5.3.17), which converges for zero distance. This condition is fulfilled in the present experiments, since *RH* in no case was smaller than 50 %. In the completely dry state, however, diffusion can be assumed to be approximated by

$$\ln D = \ln D_0 - E_h / kT \qquad \textbf{(5.3.25)}$$

where E_h is given by (5.3.19). From E_h, the maximal reduction of fluidity due to dehydration can be calculated. According to [Rand, 1989], the energy to dehydrate the phospholipid headgroups lies in the range of 8.4 to 42 kJ/mol. Correlating E_h with the work to dehydrate lipid headgroups then for the fluidity enhancement by hydration leads to a range of 30 to $2 \cdot 10^7$, which covers the range found experimentally (Figure 5.35).

In order to test for a possible influence of the fluorescence label on the humidity dependence of diffusion constants, besides NBD-PE, the tail-labelled phospholipid NBD-PC was used (Figure 5.38).

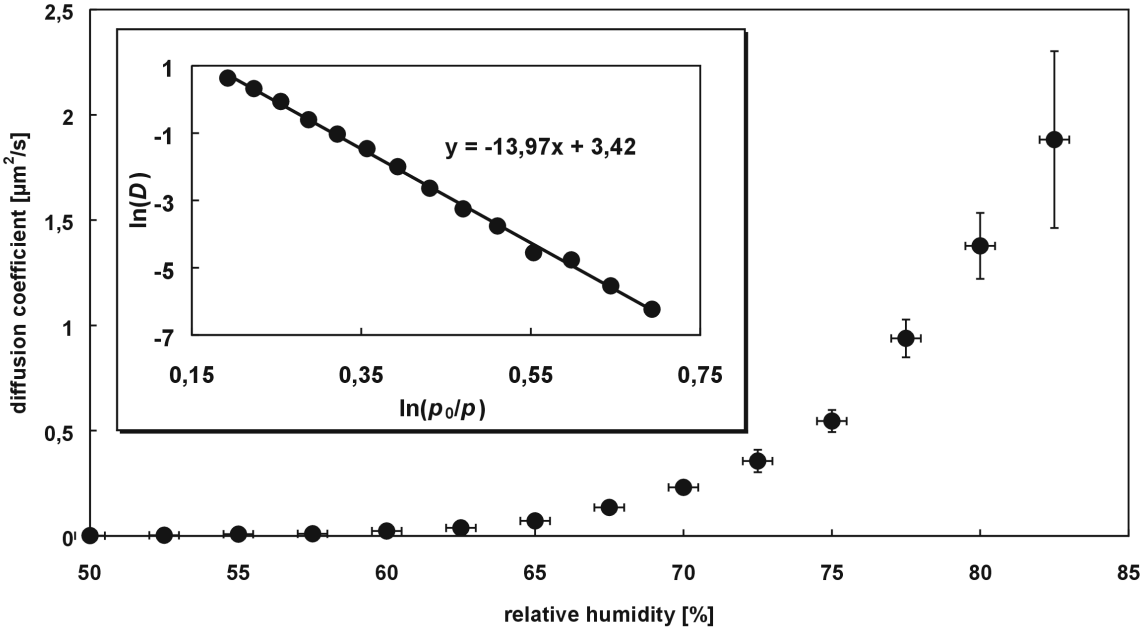

Figure 5.38: Diffusion coefficients in a chitosan-cushioned DMPC monolayer, lateral pressure 35 mN/m, fluorescence probe: NBD-PC, temperature: 30 °C. The inset shows an axis transformation of the same data set.

Within the experimental error, the same slope as in the case of NBD-PE labels was found. Due to the higher temperature (30 °C compared to 26 °C in the case of NBD-PE) the intercept is higher as compared to Figure 5.35 (see also the discussion concerning the temperature influence in chapter 5.3.2). It is known that the fluorescence label NBD in the case of NBD-PC stained, completely hydrated lipid bilayers is located in the polar region of the membrane, although the fluorescence probe is attached to the unpolar tail of the lipid molecule [Chat, 1990]. This, however, must not necessarily refer to a partially dehydrated solid-supported monolayer also. However, in order to further prove that a disturbing effect of the fluorescence probe can be neglected in the present kind of experiment, NBD-labelled cholesterol (NBD-Chol) was used. The label of the latter is known to be located in the non-polar region of completely hydrated lipid bilayers [Chat, 1999a]. As shown in Figure 5.39, the measured slope and intercept (at a temperature of 26 °C) are in accordance (within the experimental accuracy) with the values found for NBD-PE labelled DMPC monolayers. This fact clearly indicates that all the three probes essentially monitor the lateral fluidity of the host matrix. It is known for hydrophobic probe molecules that independently of their size, the lateral fluidity of the lipid matrix is probed [Balc, 1993], hence the values found for NBD-Chol refer to those which were obtained using NBD-PE.

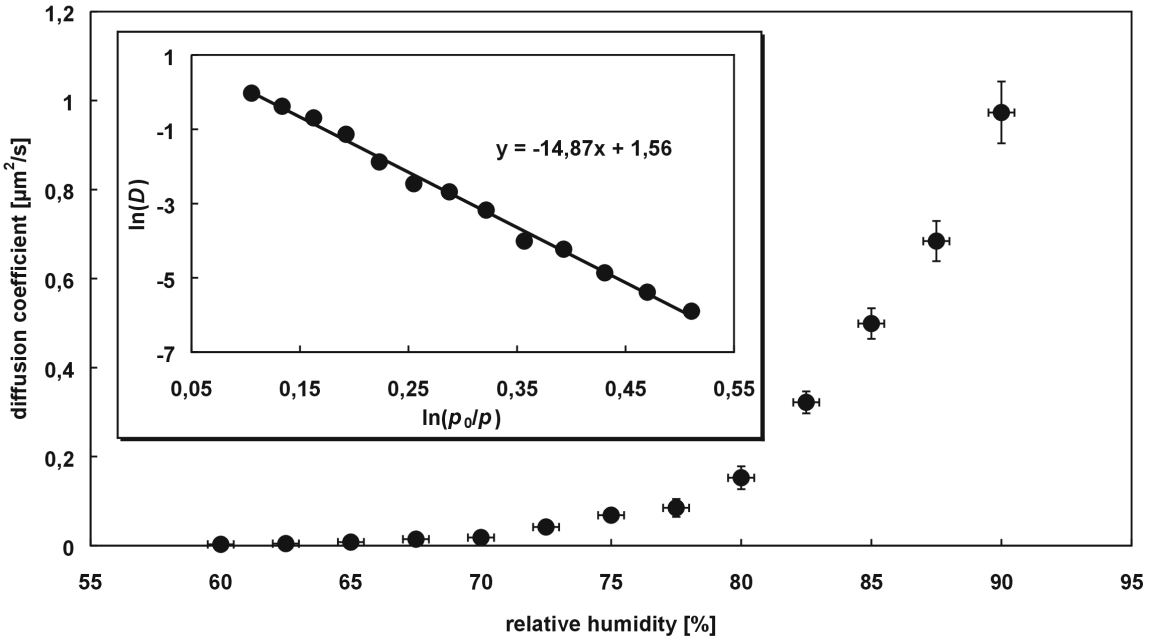

Figure 5.39: Diffusion coefficients in a chitosan-cushioned DMPC monolayer, lateral pressure 35 mN/m, fluorescence probe: NBD-Chol, temperature 26 °C. The inset shows an axis transformation of the same data set.

As has already been mentioned, in multibilayer stacks, the reduction of *RH* exerts an effective lateral pressure, which compresses the membrane and induces phase transitions [Siro, 1988]. However, in the monolayer studies carried out in the present work, no discontinuities were found in the examined data range. In order to elucidate a possible contribution of humidity induced phase changes, monolayers of DPhyPC were prepared, which were stained with NBD-PE. The lipid DPhyPC does not show phase transitions in bilayers, down to a temperature of –120 °C [Lind, 1979]. As by dehydration the same transitions can be induced like by temperature reduction, DPhyPC is assumed to remain in the fluid state upon dehydration.

Apart from a slightly higher slope compared to DMPC monolayers subject to corresponding conditions, the same relation between lateral diffusion and relative humidity was found (Figure 5.40). This result underlines the assumption made in the derivation of (5.3.23) that lateral pressure changes during partially dehydrating the supported lipid monolayer can be neglected. The latter hypothesis is also strongly supported by the fact, that a variation of the monolayer density (during LB transfer) did not lead to significant changes in the observed behaviour (linearity throughout the examined humidity range, Figure 5.41).

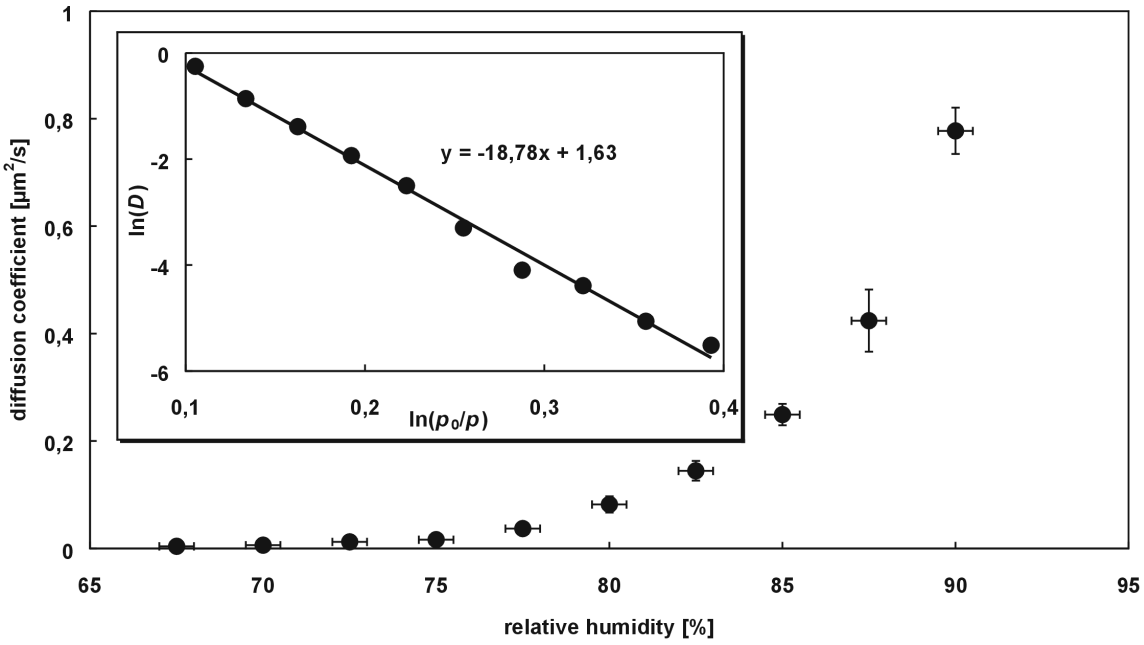

Figure 5.40: Diffusion coefficients in a chitosan-cushioned DPhyPC monolayer, lateral pressure 35 mN/m, fluorescence probe: NBD-PE, temperature 26 °C. The inset shows an axis transformation of the same data set.

At high hydration levels, the fluidity increased with decreasing lateral pressure (compare the intercepts of the linear fits in Figure 5.41). This is readily explained by the free area theory (5.3.10): the higher the lateral pressure, the lower is the average free area available for diffusion, hence the diffusion coefficient drops [Gall, 1979].

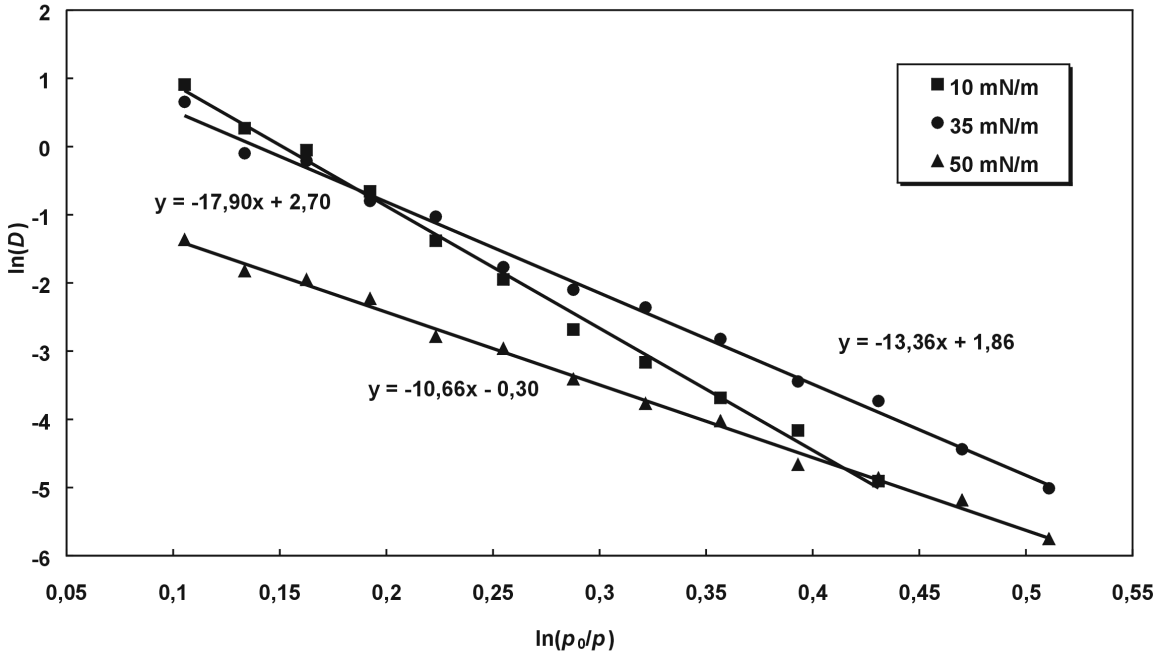

Figure 5.41: Double logarithmic plots of diffusion constants measured in DMPC monolayers on chitosan, transferred at the lateral pressures of 10, 35 and 50 mN/m, fluorescence probe NBD-PE, temperature 26 °C.

Additionally, with a higher lateral pressure, the slopes of the linear fits decrease, which – according to (5.3.24) – corresponds to a decrease in l_w. While to the best of the author's knowledge no analysis concerning the lateral pressure dependence of the hydration force of solid-supported monolayers exists (see also [Wenn, 2001]), generally lipid bilayers in the gel phase show smaller decay constants compared to those in the fluid state [Isra, 1992b], [Mars, 1989]. If the trend concerning the decay constants in Figure 5.41 can be explained by a higher area fraction of solid condensed domains with increasing lateral pressure (see also [Pink, 1995]), can only be assumed, however.

From the fact that in no case a discontinuity (in terms of a deviation from linearity of the double logarithmic plot) was observed, it can clearly be deduced that sharp first-order transitions induced by dehydration were not present in the hydrogel-supported monolayers examined in the present work. As already mentioned, this observation is contrary to the case of multibilayer stacks. In the following paragraph, this difference shall be discussed and phase transitions of solid-supported monolayers will be examined in the light of observations to be found in literature.

It has been pointed out by a number of authors that monolayers deposited onto a solid substrate by LB-transfer, can possess a higher lateral pressure on the support as compared to a floating monolayer on the trough subphase [Rieg, 1988], [Rieg, 1992], [Spra, 1994b], [Sike, 1996], [Sike, 1997], [Yami, 1997]. The solid-supported monolayer may even be in a different phase state. This phenomenon is known as substrate-mediated condensation and occurs in the meniscus region during transfer [Rieg, 1988]. It is due to either the interaction between headgroups and the solid surface (e.g. [Sike, 1996]), or to different pH values in the thin meniscus compared to the bulk water phase (e.g. [Rieg, 1988]). All of the above-cited works deal with phase transitions, which occur *during* the LB-transfer. Other groups reported morphological changes during storage, i.e. *after* the transfer. Chi et al. observed ageing effects of polymer-supported stearic acid monolayers [Chi, 1993], [Chi, 1994]. It was assumed that water is transported together with the monolayer onto the solid substrate and that subsequent dehydration would increase the phase transition temperature of the monolayer, causing more molecules to be involved in a phase transition to a more condensed phase. In other works, phase transitions of polymer-supported, charged monolayers were observed by fluorescence microscopy and the transition temperatures were found to be increased with respect to monolayers at the air/water interface [Chi, 1992a], [Chi, 1992b] and further increased in case of glass-supported monolayers. Again, the change in the phase transition temperature was attributed to be influenced by changes in the hydration state of the polar headgroups, modulated by different supports (water, hydrophilic polymers or glass) and ambient humidity. Fluorescence microscopy allows to follow phase transitions in amphiphile membranes, because the dye solubility is usually

lower in condensed phases [Möhw, 1990] (provided that the domains have a size above the resolution of the optical microscope). However, in the present work, in no case the formation of domains upon dehydrating the monolayer was found in fluorescence micrographs. Moreover, contrary to the works cited above, Shiku and Dunn [Shik, 1998] found no evidence for phase transitions in solid-supported DPPC monolayers, deposited in the coexistence region, upon varying *RH*.

A first order fluid/solid transition is necessarily accompanied by a lateral compression. As the surface area of the support is fixed, such a lateral compression would involve a partial dewetting of the monolayer. In this case, monolayer mobility would have to be analysed in terms of percolation models (see chapter 4.3.1) and a percolation threshold would exist. Such a dewetting is, however, energetically unfavourable due to the high spreading power of lipid monolayers on substrates with high surface energies. This is contrary to the case of lipid bilayer stacks, where the spreading parameter (for a bilayer spreading on top of another bilayer) in case of completely hydrated choline headgroups is even negative, as only a single bilayer spreads on hydrated solid surfaces [Rädl, 1995a]. Therefore, the influence of relative humidity on the phase behaviour of monolayers on high surface energy substrates on the one hand, and multibilayer stacks on the other hand, cannot be directly compared. It is likely that phase transitions in solid-supported monolayers cannot be described by a unique, effective lateral pressure, caused by dehydration of lipid headgroups as in the case of multibilayer stacks [Pars, 1979]. On the contrary, in case of a solid-supported monolayer, the special and complex monolayer/support interactions have to be taken into account, which includes electrostatic interactions and surface roughness effects. Clearly, further examinations are needed to analyse the transition orders, and parameters, which influence humidity induced phase transitions in solid-supported monolayers.

5.3.4 Variation of the lipid: DLPE and DMPC/cholesterol

It is a well-known fact that bilayers with PE headgroups hydrate to a lower extent compared to PC headgroups [Rand, 1989], [Jend, 1996], [Sell, 1999]. This leads to a higher fusion tendency of liposomes with PE headgroups compared to PC headgroups, and a higher tendency of the former to built multi-bilayers. PE headgroups form hydrogen bonds with neighbour lipids, which leads to a smaller headgroup size and higher main phase transition temperatures, T_r. For diffusion experiments, DLPE is well suited because

of its relatively small value of T_r = 29 °C[2)] in bilayers [Mars, 1990]. Additionally, DLPE was chosen because its hydration properties were analysed by computer simulations [Pere, 1996] and directly compared to DMPC [Damo, 1994].

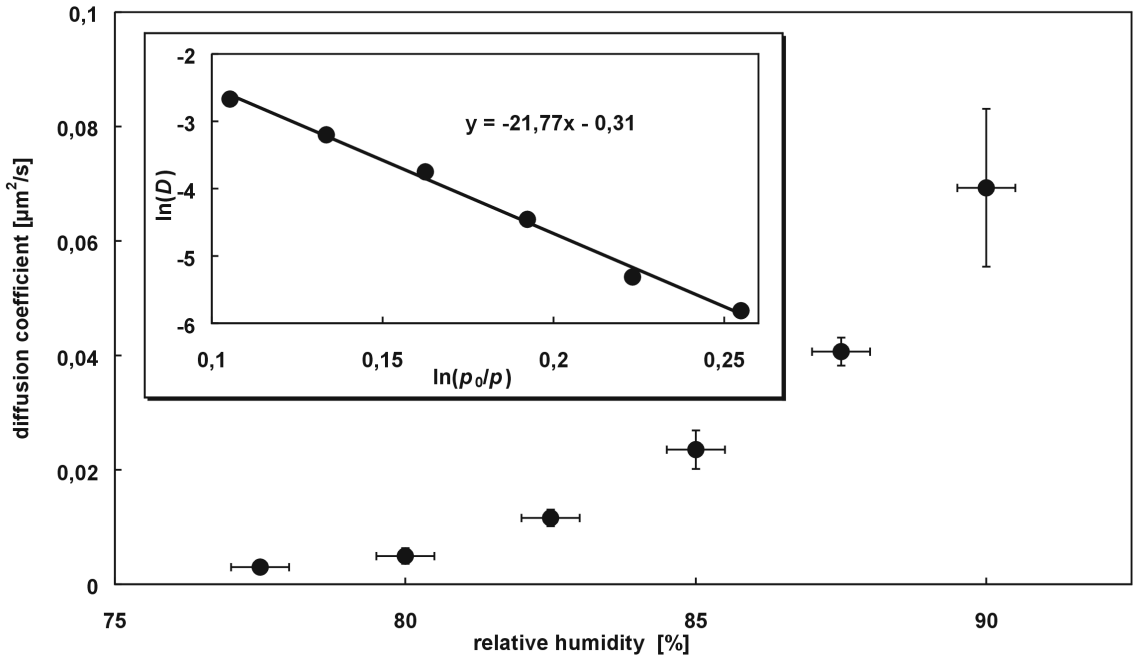

Figure 5.42: Diffusion coefficients in a chitosan-cushioned DLPE monolayer, lateral pressure 35 mN/m, fluorescence probe: NBD-PE, temperature 26 °C. The inset shows an axis transformation of the same data set.

DLPE monolayers were stained with NBD-PE and transferred at a lateral pressure of 35 mN/m at a temperature of 25 °C. At these conditions, the monolayer is in the liquid expanded state (see chapter 8.2.1). A linear relationship between the osmotic pressure and the diffusion coefficient (in a double-logarithmic plot) was found (Figure 5.42). Surprisingly, a very low fluidity was obtained, even at high hydration levels (compare e.g. Figure 5.35 and Figure 5.42). However, slightly increasing the temperature at which diffusion experiments were carried out from 26 to 30 °C, led to a diffusion coefficient at *RH* = 90 % (Figure 5.43), which was comparable to the value found for DMPC monolayers at 30 °C (compare Figure 5.38). The big difference at the two temperatures can be explained by assuming, that the DLPE monolayer is in different phase states at 26 and 30 °C. This would imply that during the transfer of the DLPE monolayer, the latter was subject to a substrate-mediated condensation. Indications for this assumption have already been found while comparing the monolayer stability against condensation of water droplets

[2)] Note that while the main phase transition in phospholipid monolayers and bilayers in principle is physically an identical process, the transition *temperatures* are different, even in case of the same lateral pressure in a single monolayer and a monolayer in a bilayer membrane. The difference is due to energetic coupling between the two leaflets in a bilayer [Pink, 1983].

(chapter 5.1), and the spreading kinetics (chapter 5.2). Heating to a temperature of 30 °C could then have caused a phase transition, which would explain the much increased fluidity at that temperature. The slope of the linear fits is nearly identical at the two temperatures, which was also observed in case of DMPC monolayers at different temperatures (compare Figure 5.35 and Figure 5.38).

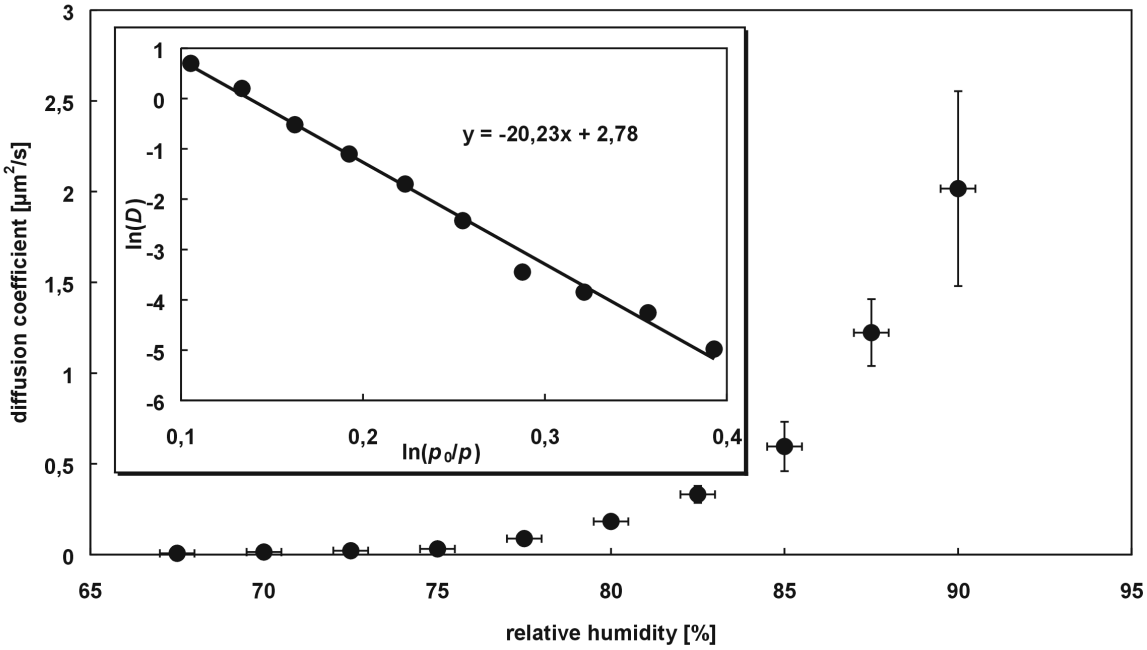

Figure 5.43: Diffusion coefficients in a chitosan-cushioned DLPE monolayer, lateral pressure 35 mN/m, fluorescence probe: NBD-PE, temperature 30 °C. The inset shows an axis transformation of the same data set.

In the case of multibilayer stacks, however, for fluid bilayers higher decay constants of the hydration force are found compared to those in the solid state [Rand, 1989]. The difference may be due to different inter-membrane interactions in the solid and fluid state, which are absent in case of supported monolayers. The same reason is likely to be responsible for the fact that higher slopes were found for DMPE monolayers compared to DMPC monolayers. In multibilayers with PE headgroups, however, a decay constant of a significantly shorter range is found (e.g. [Rand, 1989]). This difference was shown to be due to interactions between the R-NH_3^+ headgroups with the nonesterified oxygens of the phosphate group in an opposing leaflet [Damo, 1994]. Clearly, in the light of this finding, in case of polysaccharide-supported monolayers a different range of the decay constant is expected.

A further important component of biomembranes is cholesterol, which was added to DMPC at a concentration of 30 mol%. The presence of cholesterol considerably reduced the fluidity of the supported monolayer (compare e.g. Figure 5.35 and Figure 5.44). This is also found in case of free bilayers [Alme, 1992], where the fluidity reduction can be shown to be due to the occupation of free volume by cholesterol. In case of polysaccharide-

supported membranes, an additional interaction of the cholesterol headgroup with the support is assumed [Elen, 1996].

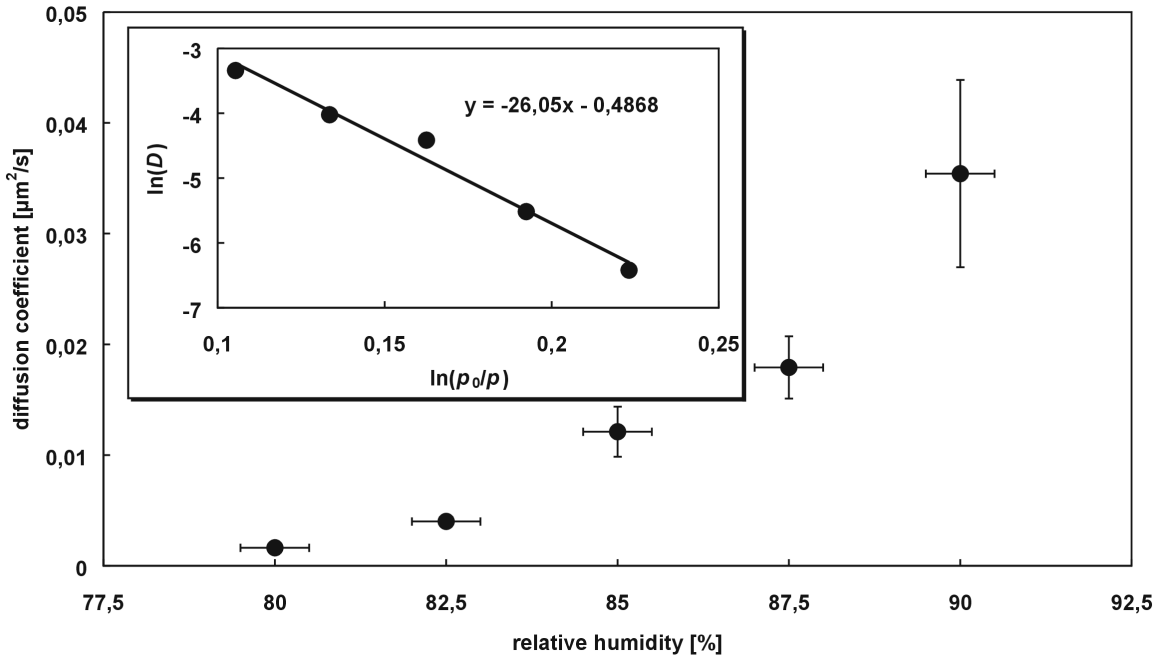

Figure 5.44: Diffusion coefficients in a chitosan-cushioned DMPC + 30 mol% cholesterol monolayer, lateral pressure 35 mN/m, fluorescence probe: NBD-PE, temperature 26 °C. The inset shows an axis transformation of the same data set.

The increase of the slope (26.1, Figure 5.44) compared to pure DMPC monolayers (13.4, Figure 5.35), is according with the observation, that a higher decay constant is found in DPPC [Rand, 1989] and eggPC [Mars, 1989] multibilayer stacks upon incorporation of cholesterol.

5.3.5 Variation of the substrate: agarose and glass

In the derivation of (5.3.23), a crucial assumption was that the nature of the substrate plays a minor role concerning the lateral diffusion properties in monolayers at different relative humidities. This assumption shall be examined in the following section. While a direct and independent proof of the above mentioned hypothesis is not feasible (monolayers always have to be supported by a substrate), it is possible to compare different substrates with respect to their influence on diffusion/humidity diagrams. Therefore, a DMPC monolayer was transferred onto a thin agarose cushion and analysed in terms of lateral diffusion with respect to changes in *RH* (Figure 5.45).

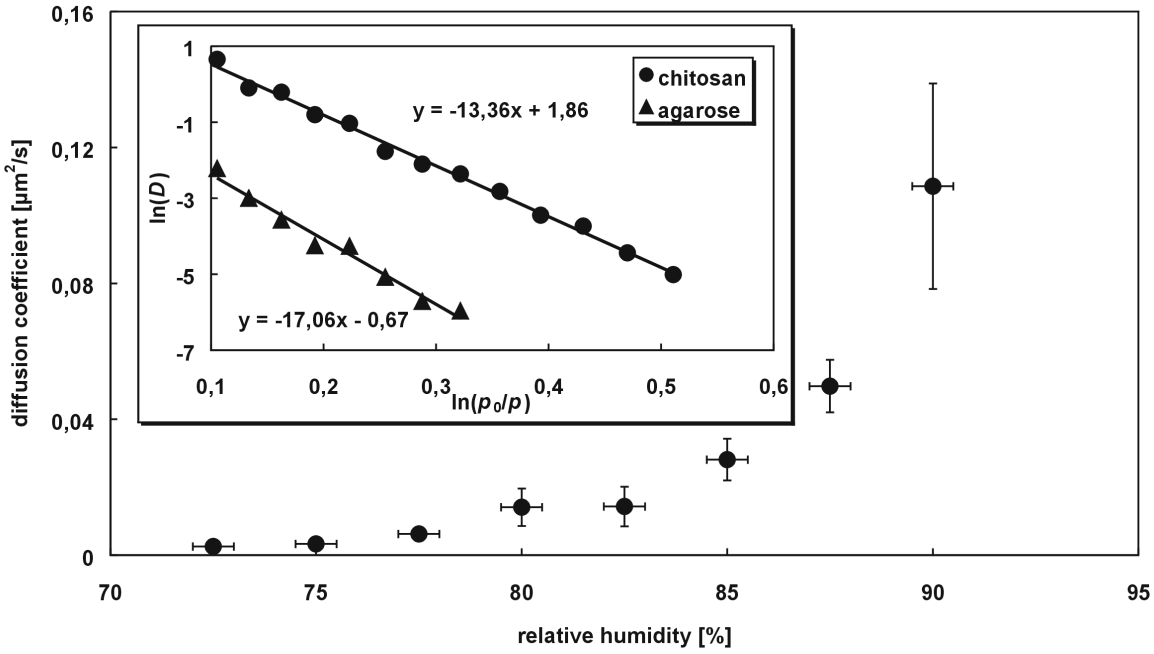

Figure 5.45: Diffusion coefficients in an agarose-cushioned DMPC monolayer, lateral pressure 35 mN/m, fluorescence probe: NBD-PE, temperature 26 °C. The inset shows an axis transformation of the same data set. Additionally, for comparison the data for a chitosan-supported monolayer prepared and analysed under the same conditions was added to the diagram shown in the inset.

A linear relationship in the usual axis transformed plot was found, like in all experiments performed on a chitosan cushion. Agarose possesses totally different molecular and packing properties compared to chitosan (see chapter 4). The generally reduced fluidity in case of agarose-cushioned DMPC monolayers may be due to either a substrate-mediated condensation, or the much higher surface roughness of agarose, compared to chitosan. In order to clarify this matter, temperature variations would have to be carried out.

The comparison depicted in Figure 5.45, strongly supports the hypothesis that the relationship expressed by (5.3.23) is independent from the nature of the actual substrate (as long as it is hydrophilic) and that (5.3.23) may therefore be assumed to be as generally applicable to local dynamics dependent on the state of hydration, as the universal validity of the exponential distance dependence of the hydration force itself.

In another set of experiments, polymer cushions were omitted completely and the lipid monolayer was transferred directly to anorganic surfaces. Mica would be especially well suited for the studies described in the present chapter due to its atomic flatness. However, using mica as a support for Langmuir-Blodgett monolayers, no sharp bleach-spots could be obtained, and diffusion coefficients were therefore prone to large errors. Instead, glass was used as a transparent, solid monolayer support.

The diffusion coefficients were remarkably lower as compared to water-swellable polymer supports. At a relative humidity of 90 %, in a DMPC matrix with the lateral pressure of 35

mN/m, using the fluorescence probe NBD-PC a value of $D = 4.9 \cdot 10^{-3}$ µm^2/s was found (at room temperature). As this value is already rather close to the resolution limit of the FRAP-setup, no systematic analysis of the response towards humidity changes could be carried out. However, it was shown that by a further increase of relative humidity to 100 % (by pouring MilliQ-water on top of the monolayer), the lateral self-diffusion could be increased remarkably. As can be seen in Figure 5.46, the monolayer was rather stable and had an almost totally homogeneous appearance, even though the hydrophobic tails of the lipid molecule were exposed directly to water.

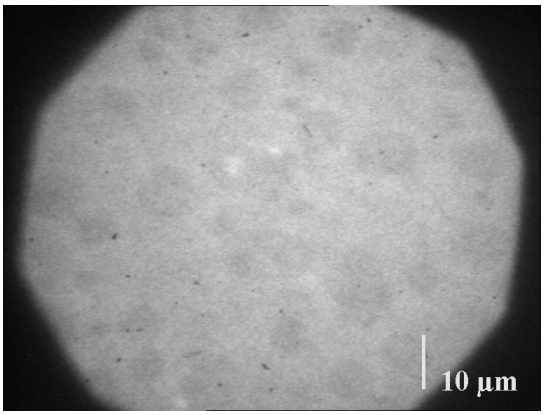

Figure 5.46: Fluorescence image of a DMPC monolayer (lateral pressure 35 mN/m, fluorescence probe NBD-PC, temperature 26 °C) on a glass surface, the lipid tails were facing towards a MilliQ-water bulk face.

The stability of supported lipid monolayers, immersed in a series of different liquids has been shown previously [Auch, 2000]. These authors also examined the lateral diffusion of monolayers. In the present case, a diffusion coefficient of $D = 0.17 \pm 0.008$ µm^2/s was found, which is almost two orders of magnitude higher, compared to the value found at *RH* = 90 %. In order to examine the influence of *RH* on lateral diffusion in glass-supported monolayers more systematically, therefore the humidity range of 90 % to 100 % would have to be explored. This, however, would necessitate a considerably more precise temperature and *RH* control, which would be possible by a much refined experimental setup only, which in the present work could not be performed.

5.3.6 Influence of non-aqueous solvents present in the surrounding gas phase

In order to round off the examinations described in the present chapter, which focus on the influence of hydration forces on the lateral dynamics of Langmuir-Blodgett films, it shall be examined, in as far non-aqueous gaseous solvents influence diffusion properties of solid-supported monolayers. It has been found for several non-aqueous solvents that

osmotic pressure/distance curves show essentially an exponential dependence (5.3.17), as in the case of water [McIn, 1989]. While a systematic variation of partial pressures of non-aqueous solvents could not be carried out in the present work, it could be shown qualitatively, that their presence in the gas phase could substantially elevate diffusion coefficients of monolayers (Figure 5.47).

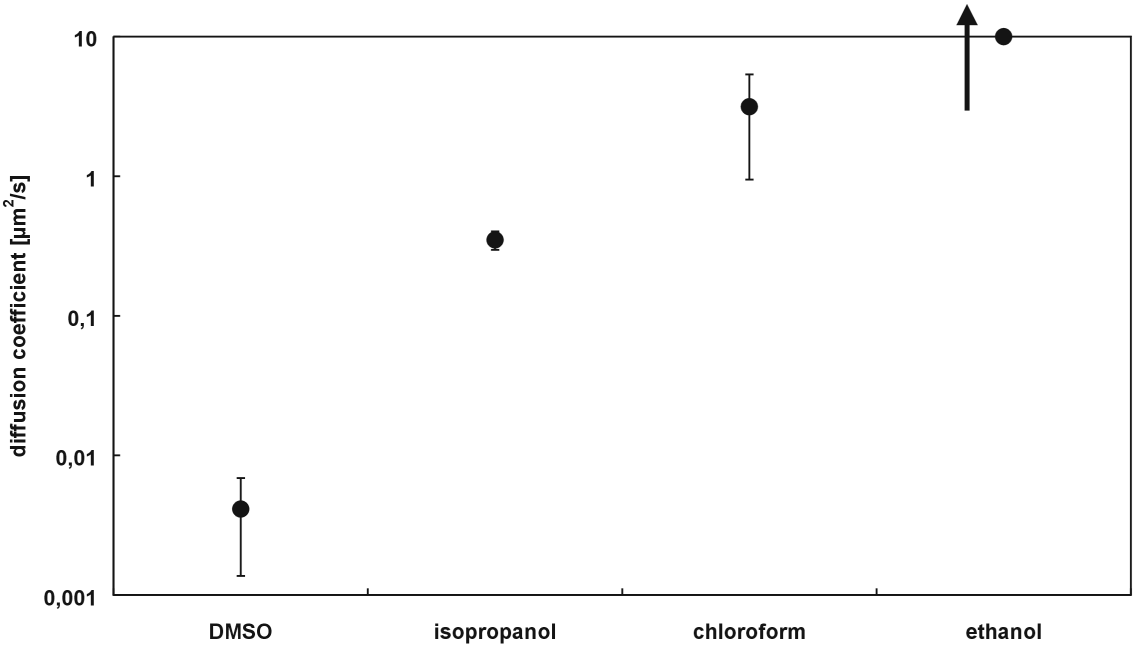

Figure 5.47: Diffusion coefficients of DMPC monolayers, lateral pressure 35 mN/m, supported by a chitosan film. The monolayer was exposed to the indicated saturated atmospheres. The diffusion coefficient for ethanol was found to be too high for being resolvable by the FRAP setup, as indicated by the arrow.

Ethanol, is known to bind to the lipid-water interface and to modify both headgroup and hydrophobic chain conformations (see [Ho, 1997] and references therein). Similar interactions can be assumed to occur in case of other solvents. Monolayers were exposed to solvent gases by placing a small, open container filled with the particular solvent into the sealed “humidity chamber”. The atmosphere was allowed to equilibrate for one hour and it was ensured that no condensation of solvent droplets on the sample surface occurred. The dependence of diffusion constants in DMPC monolayers on solvents present in the surrounding gas phase is not only influenced by lipid/solvent interactions, but also includes the vapour pressures of the solvents. Due to the difficulty to control the partial pressures of the latter, systematic studies could not be performed.

5.3.7 Conclusion and outlook

Supported lipid monolayers were analysed in terms of the lateral self-diffusion of lipid molecules as a function of relative humidity. Applying the Evans-Sackmann theory revealed that the reduced fluidity could not be explained by assuming no-slip boundaries and viscous dissipation in a thin water film between monolayer and support.

However, a universal response towards humidity changes was found for a variety of lipids in miscellaneous conditions and for two different substrates. Plotting the logarithm of the measured diffusion coefficients against $\ln(p_0/p)$, a quantity proportional to the applied osmotic pressure, essentially yielded a straight line in all cases. This was explained by assuming a reduction of activation energies for diffusion by hydration, i.e. the reduction of osmotic pressure. A simple model was derived, a crucial assumption of which is an exponential decay of the disjoining pressure with distance from the surface. From the model, decay constants of the hydration force in the monolayer/support system were calculated and found to be higher compared to the case of multibilayer stacks, which was explained by apparent over-simplifications of the model and the absence of inter-leaflet interactions in solid-supported monolayers. Particularly in case of phosphatidylethanolamine headgroups, these influence the swelling properties of multibilayer stacks and smaller decay constants are found compared to PC headgroups, which was not found to be paralleled by the present studies. Furthermore, no indications were found for humidity induced phase transitions in hydrogel-supported monolayers. This is also contrary to the case of multibilayer staples, where reducing the relative humidity exerts an effective lateral pressure leading to bilayer compression. The difference was explained by the high surface energy of the support, which prevents the monolayer from partial dewetting. Finally, it was qualitatively shown that fluidity enhancement in solid-supported lipid monolayers was not restricted to water – it was also found in case of non-aqueous solvents. This is in accordance with the fact that “hydration” forces are no peculiar feature of water (-structure effects) only – as was long believed and only recently shown to be erroneous [Isra, 1990], [Isra, 1992b].

Many biological processes, such as vesicle fusion and recognition processes involve dehydration/hydration cycles and it can be expected that the water activity significantly effects the kinetics of these processes in a manner outlined above.

Several important aspects could not be covered by the present study. It would be particularly interesting to examine a broader range of different supports in order to clarify whether the universal relation found in the case of chitosan and agarose, also holds for other supports. The influence of roughness effects could be another important aspect of

diffusion in supported monolayers. Two improvements of the experimental setup are desired. A much more precise temperature control should allow for a refined analysis especially in the high humidity regime, this should allow for the analysis of supports such as glass. Furthermore, the possibility to observe the monolayer directly (through a gas gap rather than through the support) would further widen the range of different (including non-transparent) substrates. Moreover, a determination of the hydration force itself, by measuring the membrane-substrate distance as a function of hydration would further allow for a more precise data interpretation. While such measurements are complicated by the swelling of a hydrogel support normal to the surface, an advantageous experimental configuration could be a substrate-supported "foam film" as proposed in Figure 5.48. The proximal monolayer would be transferred onto a hydrophobised substrate or chemically attached. In free standing foam films, a correlation between the thickness of the water film and monolayer mobility has been found in a number of works, [Lalc, 1994], [Lalc, 1995]. In that case, however, the thickness of the water layer was adjusted by the salt concentration, which regulates DLVO forces (see chapter 5.0.1).

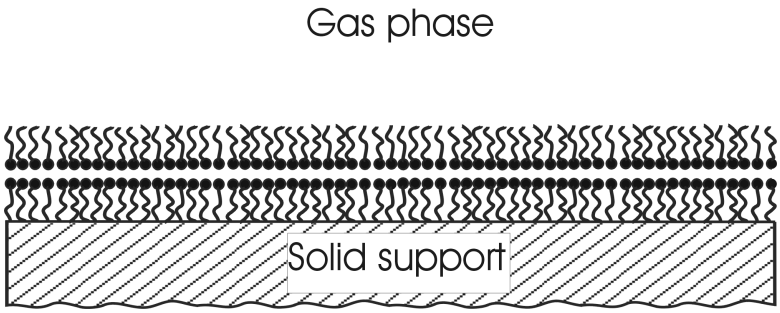

Figure 5.48: A solid-supported "foam film" as a possible experimental configuration for studying both lateral diffusion and the thickness of the interface between the two amphiphile leaflets.

The setup depicted in Figure 5.48, however, would allow for a refined study of lateral diffusion in foam films with water layers of molecular thickness, and thickness measurements in parallel.

A purpose of the present chapter was the study of hydration effects on properties of supported monolayers. The analysis of the lateral diffusion of monolayer molecules provides an indirect measure of the hydration level in the headgroup region of phospholipid monolayers. The direct measurement of hydration changes in the interfacial region of a supported lipid layer will be the purpose of the next chapter.

5.4 Effect of ambient humidities on the fluorescence of labelled lipid monolayers

As was pointed out in chapter 2, polymer-supported bilayer membranes provide promising systems for the incorporation of functional membrane proteins with large hydrophilic parts [Sack, 1996], [Sack, 2000], [Shen, 2000]. It is often assumed that membrane fluidity is an important parameter for the activity of reconstituted membrane proteins. However, the hydration state of the functionalised membrane may be of equal or even more importance [Ho, 1995], [Scar, 1996], [Ho, 1997], since structure and dynamics of proteins are to a large extent governed by interactions with water [Ho, 1992].

In addition to the function of lipid probes to stain bio- and model-membranes (chapter 5.1 and chapter 5.2) and to allow for the examination of membrane dynamics (chapter 5.3), fluorescence labelled lipids can be used to study the microenvironment of the particular label [Lako, 1983]. Following the general purpose of the present work, which is to study membrane/support interactions, this chapter will be concerned with direct measurements of the hydration state in the polar region of a supported lipid membrane. The extent of hydration is influenced by the nature of the actual headgroup region and by the kind of membrane support. While the hydration of multibilayer stacks has intensively been worked on for decades (see chapter 5.0.2), for more far-reaching model-membrane studies in terms of functionalised membranes, single solid-supported bilayers are favourable [Sack, 1996]. Bilayer membrane hydration has been shown to be a critical parameter determining the activity of membrane associated proteins [Scar, 1996]. Therefore, the successful assembly of solid-supported functionalised model membranes requires a detailed knowledge about the influence of the underlying support on membrane hydration. Lipid monolayers are particularly well suited for studying hydration changes in the membrane/support interface, since they allow for ready and fast changes of water activity by regulation of the relative humidity in the surrounding gas phase. Hydration changes in supported amphiphile monolayers have so far been examined indirectly, in terms of monolayer thickness changes as measured by the surface force apparatus [Chen, 1992] or by means of x-ray methods [Bolz, 2001] and in terms of the influence on monolayer dynamics (see chapter 5.3 and references therein) or on phase transition temperature changes [Chi, 1992b], [Chi, 1992b]. Infrared spectroscopy (IR) more directly monitors the presence of water in the headgroup region, since the phosphate and carbonyl vibrations of the fatty ester groups are sensitive to hydrogen bonding. The hydration of silane monolayers has been followed by IR methods [Le Gran, 1993], but IR spectroscopy and related techniques so far were mainly applied to study membranes in excess water [Hübn, 1998] or to examine the hydration of multibilayer stacks [Iono, 1996], [Sell, 1999]. Numerous other techniques have been used to study

membrane hydration (see chapter 5.0.2), but are difficult to apply to the case of supported lipid monolayers.

Most of the above-mentioned methodologies are either complicated, rather expensive or rare. Fluorescence methods, however, are widely spread in bio-sciences and often comparably cheap. Fluorescence probes have been applied to measure local hydration changes in water-swellable polymers as a response to a different relative humidity [Otsu, 1994], [Choi, 1999]. Furthermore, the environmental sensitivity of the fluorescence probe NBD, rather commonly being applied as a fluorescence label for phospholipid molecules [Chat, 1990], is known and well documented [Lin, 1991], [Forg, 1993], [Mukh, 1994], [Maze, 1996], [Al-Di, 1998], [Saha, 1998]. Therefore, it seems to be a natural strategy to use NBD-labelled lipid probes for analysing local hydration changes in the headgroup region of phospholipid membranes. The applicability of this strategy shall be examined in the following parts. Before proceeding with the experimental details, however, a short overview of environmental effects on fluorescence properties will be provided.

5.4.1 Environmental effects on fluorophores

The influences of a fluorophore's environment (which are generally referred to as solvent effects) on its fluorescence properties can be divided into general solvent effects and specific interactions between a fluorophore and the solvent or solutes [Lako, 1983]. The former are always present and reflect the influence of (I) the redistribution of electrons in the solvent as a response to a changed dipole moment of the fluorophore in the excited state, associated with a reactive electrical field and (II) the reorientation of solvent molecules around the excited state dipole, on the Stokes shift of the particular fluorophore. A simple model which describes these general environmental effects was provided by Lippert [Lipp, 1957] (Lippert-Mataga equation):

$$\overline{\upsilon_a} - \overline{\upsilon_f} = \frac{2}{hc}\left(\frac{\varepsilon - 1}{2\varepsilon + 1} - \frac{n^2 - 1}{2n^2 + 1}\right)\frac{(\mu^* - \mu)^2}{a^3} + const\,. \qquad \textbf{(5.4.1)}$$

$\overline{\upsilon_a}$ and $\overline{\upsilon_f}$ are the wave numbers of the absorption and emission maxima (in cm^{-1}), h is Planck's constant, c is the speed of light, ε and n are the dielectric constant and refractive index of the solvent (corresponding to low and high frequency polarizabilities), μ^* and μ are the dipole moments in the excited and in the ground state and a is the radius of the cavity in which the fluorophore resides (Onsager cavity radius). The first bracketed term on the right hand-side is called orientation polarizability. Higher order terms in (5.4.1) are

due to second-order effects such as contributions of the solvent-solvent interactions and induced dipole moments of the solvent molecules, to the reaction field of the fluorophore dipole. These higher order terms are generally neglected since their contributions are small [Lako, 1983]. The last term on the right hand can therefore be approximated by the Stokes shift S_0 of a molecule in the gas phase (isolated molecule) [Bern, 1998]. It is important to note that (5.4.1) was derived in the framework of the Onsager reaction field theory [Onsa, 1936], which assumes the fluorophore to be a point dipole held in the centre of a spherical cavity, in a homogeneous and continuous dielectric medium. Clearly, these conditions are not necessarily fulfilled in case of a fluorescence label located in the highly anisotropic environment of the headgroup region of an amphiphile membrane. This question will be addressed again further below. A second condition for the applicability of (5.4.1) is that the solvent reorientation is fast compared to the lifetime of the fluorophore. Due to a high solvent viscosity (such as in the polar region of lipid membranes, see below), however, it can be the case that solvent reorientation around the excited-state fluorophore is incomplete prior to emission. In that case, the Lippert equation does not apply quantitatively. However, this effect can be used to probe the microviscosity of the solvent's environment (see below). Third, as mentioned above, specific fluorophore/solvent interactions can lead to deviations from (5.4.1). Among these are hydrogen bonding, acid-base chemistry and the formation of charge transfer complexes. Specific effects are determined by the specific chemical properties of both fluorophore and solvent.

In general, fluorescence emission occurs from the zero vibrational level of the first excited electronic state of a molecule (Kasha's rule) [Birk, 1970]. Therefore, fluorescence decay rates and wavelength of maximum emission are independent of the excitation wavelength. This generalisation breaks down in case of polar fluorophores in motionally restricted media. If the solvent relaxation time is comparable or higher than the lifetime of an electronically excited state, excitation at the red edge of the absorption band preferentially excites fluorophores in a solvent relaxed environment. Since excitation at a wavelength shorter than the red edge of the absorption band leads to a broader excited state distribution due to insufficient solvent relaxation, emission occurs from higher energetic states compared to a completely relaxed environment. It is for this reason, that upon shifting the excitation wavelength to the red edge of the absorption band, the maximal emission intensity shows a red shift [Itoh, 1975]. This phenomenon is known as red edge excitation shift (REES) and has been used to analyse the microenvironment of lipid membrane probes [Chat, 1999a].

The applications of solvent sensitive fluorophores in bio-sciences are manifold [Lako, 1983]. In case of lipid membranes, these fluorophores can for example be used to localise

membrane bound fluorophores by probing the polarity of its environment [Wagg, 1970], to follow polarity changes as a response to altered system parameters [Bern, 1998], to examine the accessibility of a specific membrane location to water [Bade, 1978], [Chat, 1999b], to determine the onset of lamellar/non-bilayer transitions in liposomes [Elle, 1986], and rates of solvent reorientation in the vicinity of membrane-bound fluorophores [DeTo, 1976], [Chat, 1999a]. Dansyl and/or DPH-derivatives were used to probe hydration and order in lipid bilayers within the headgroup region and unpolar part of a bilayer upon incorporation of additional membrane components [Ho, 1995], [Ho, 1997], to determine solvent relaxation in bilayers [Stub, 1985] and to analyse hydration at the protein/lipid interface inside of a bilayer [Ho, 1992]. In the latter work, the intrinsic fluorescence of gramicidin due to tryptophan was used for determining hydration of the protein/lipid interface.

The fluorescence studies mentioned above are attributed throughout to membranes of liposomes, immersed in water or aqueous solutions. The aim of this chapter is to extend these studies to membrane/support interactions in general, and the influence of water activity on headgroup hydration in particular. After this rather general introduction, an overview concerning the specific properties of the NBD label shall be provided. Furthermore, the realisation of humidity/fluorescence intensity measurements, experiments to characterise the humidity sensitivity of NBD as well as model calculations, will be described.

5.4.2 Preliminary remarks

Photophysical properties of the fluorescence probe NBD

The chemical structure of NBD is shown in chapter 8.3. It is an electron donor-acceptor system with the nitrate-group as acceptor, and amine-group as donor. Figure 5.50 depicts a typical excitation and fluorescence emission spectrum of the NBD-PE label incorporated into a solid-supported DMPC monolayer (fluorescence spectroscopy of lipid monolayers was performed as described in chapter 3.2). Due to the small concentration of the label in the lipid monolayer (1 mol%), relatively large monochromator slit widths had to be used (the slit widths were corresponding to 7.2 nm optical bandwidth for the excitation and 14.4 nm for the emission pathway in all cases). All monolayer fluorescence spectra were measured using samples enclosed in a sealed quartz tube, which allowed a humidity adjustment, as described in chapter 3.5.

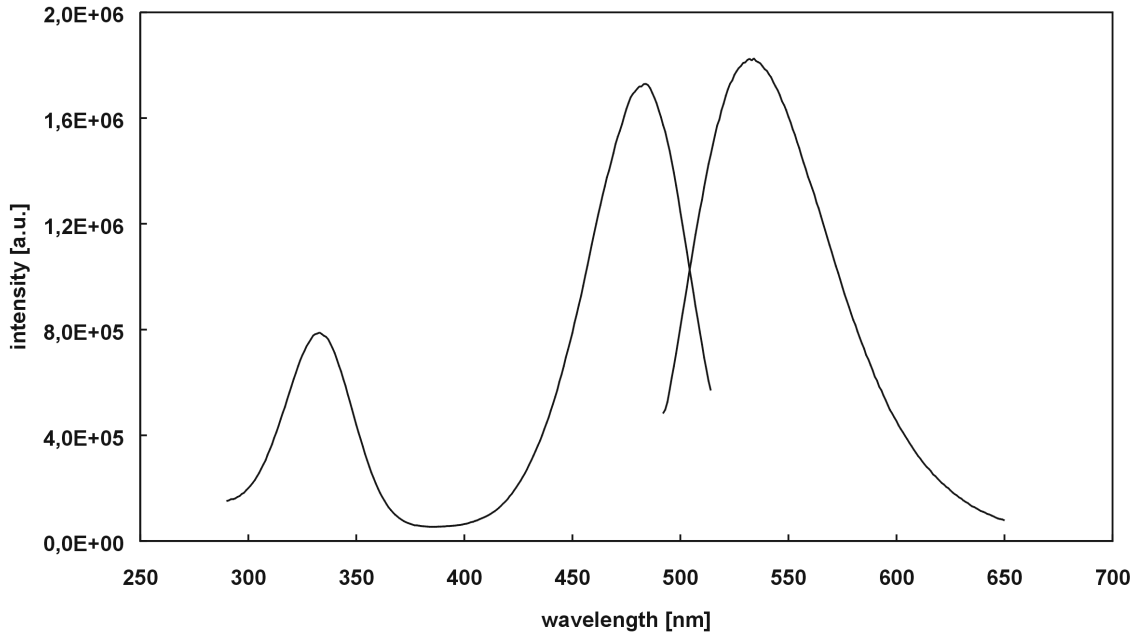

Figure 5.50: Typical fluorescence excitation (λ_{em} = 550 nm) and emission spectrum (λ_{ex} = 460 nm) of the fluorescence probe NBD-PE, embedded in a DMPC matrix on a chitosan polymer cushion, relative humidity: close to 0 %.

The excitation spectrum[3)] in the range between 300 and 500 nm shows two bands which correspond to a π,π^* transition (lower wavelength) and an intense charge transfer band.
Due to the intramolecular charge transfer (ICT) nature of the fluorescence, the emission band is broad and devoid of any fine structure [Forg, 1993]. The ICT is also responsible for the solvatochromic response of the fluorescence band: increasing solvent polarity leads to a bathochromic shift of the emission maximum [Saha, 1998], which is larger than the shift of the absorption band upon increasing solvent polarity. This can be explained by the higher polarity of the excited state: it has been shown that the dipole moment changes by approximately 3.9 D upon excitation [Mukh, 1994]. Additionally, the direction of the dipole moment is slightly changed [Papr, 1993].
NBD is highly fluorescent in low polarity solvents, but emits only weakly in water. Whereas the solvatochromism is dominated by solvent polarity [Mukh, 1994] (a general solvent effect), the non-radiative decay and hence the quantum yield is far more sensitive to the solvent's hydrogen bond donor strength [Lin, 1991] (which is a specific solvent effect). The presence of an intermolecular hydrogen bond between the solvent and fluorophore provides a vibrational accepting mode that can facilitate rapid internal conversion (thus a non-radiative decay) [Inou, 1982]. The label of the fluorescent phospholipid NBD-PE was shown to be located in the glycerol part of the headgroup

[3)] All fluorescence spectra in this chapter are displayed on a wavelength scale. While the wave number scale is linear in energy, the wavelength scale is usually more convenient [Lako, 1983].

region of unilamellar phosphatidylcholine vesicles [Maze, 1996], which was concluded from the local dielectric constant, ε ~27, monitored by the fluorescence label. The local dielectric constant, ε, is assumed to change in the membrane/water interface from the value of water ~80 to a value of ~2 in the hydrocarbon phase of the lipid [Sand, 1993].
NBD-PE was shown to exhibit a red edge excitation shift when being incorporated into unilamellar DPPC vesicles, both in the gel and in the fluid state. This was interpreted as increased water relaxation times, i.e. motional restriction in the headgroup region of the bilayers [Chat, 1999b].

Preliminary experiments

DMPC monolayers, which were stained with 1 mol% of NBD-PE, were deposited by Langmuir-Blodgett transfer onto thin chitosan films (with thicknesses in the range of 100 to 150 nm in the dry state). The chitosan films were supported by a thin glass plate, which could be mounted into the humidity chamber. After thoroughly cleaning the glass backside by means of an ethanol soaked tissue, the oil immersion objective was optically coupled to the glass plate and the sample was allowed to equilibrate thermally and mechanically for at least half an hour. Due to the fact that fluorescence intensities were determined quantitatively, it was important to minimise both photobleaching and mechanical relaxation of the setup (loss of focus). Illumination was performed by the 488 nm line of an argon ion laser (integrated into the FRAP setup, see chapter 3.1), the illumination spot had a diameter of 4.2 µm. All experiments described in this chapter were performed at room temperature. The relative humidity was then switched between ~4 and 90 % by means of the apparatus described in chapter 3.5, and the resultant fluorescence intensity was quantified with the help of a photomultiplier.
Figure 5.51 shows that the fluorescence intensity was by more than a factor of two higher at a relative humidity around 4 % (from hereon referred to as the “dry state”) compared to the value at a relative humidity RH = 90 %. Moreover, the intensity changes were completely reversible and no time lack between the change in RH and fluorescence intensity was found. On the contrary, the fluorescence intensity showed a much faster response towards humidity changes compared to the humidity sensor, which can be inferred from the faster completion of the total intensity jump compared to the signal from the commercial sensor (see Figure 5.51 B)). Moreover, the “fluorosensor” clearly resolves an intermediate step in the humidity changes, which could not be resolved by the commercial sensor. This step is due to the feedback loop of the humidity apparatus (see chapter 3.5).

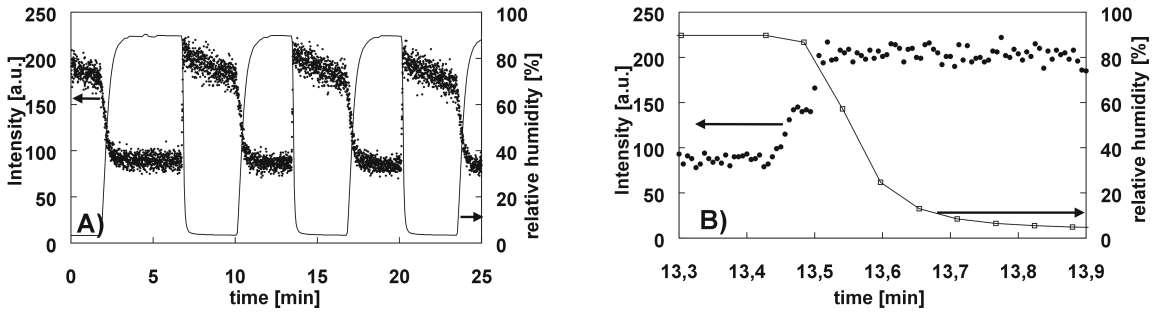

Figure 5.51: A) Reversibility of fluorescence intensity changes (left axis, dots) depending on changes in relative humidity (right axis, line), in lipid monolayers stained with a fluorescence label and supported by chitosan films. In order to allow for short counting times and hence high sampling rates, a relatively high illumination intensity was used. The fluorescence intensity loss at low humidities was due to irreversible bleaching inside of the illuminated spot, fast lateral diffusion at high humidities led to the observation of the same recovered fluorescence intensity. B) The same measurement as in A), with a stretched time axis. The response of the monolayer upon decreasing *RH* was faster compared to the commercial humidity sensor, as indicated (I) by the faster completion of the total step and (II) the high resolution of an intermediate step in *RH* (see text).

The gradual loss of fluorescence intensity in the dry state was due to photobleaching, which was a result of a moderately high illumination intensity. A high intensity was chosen in order to allow for high sampling rates. Due to an increased mobility of the lipid matrix at high humidities, bleached molecules in the illumination spot were exchanged by lateral diffusion, and hence reversibility was found with respect to intensity changes. In the case of precise intensity measurements (see below), however, the illumination intensity was minimised and the photon counting times appropriately increased, in order to avoid photobleaching. Photobleaching rates, as measured in completely immobile monolayers both in the dry and hydrated state, were found to be independent of relative humidity. Furthermore, upon varying the probe concentration in the monolayer matrix between 0.5 and 2 mol%, no significant influence of probe concentration on the fluorescence intensity ratios of dry samples and those kept at *RH* = 90 % was found.

Realisation of fluorescence intensity/humidity scans

Generally, in order to analyse fluorescence intensity/humidity relations, the stained film was illuminated by a laser beam and the corresponding fluorescence intensity was determined. Photobleaching was minimised by sufficiently reducing the beam intensity. Furthermore, the laser beam was switched off by a computer controlled shutter mechanism during the adjustment of a new *RH* value, which was completed in an interval of 100 s, (see chapter 3.5). After every 100 s the shutter opened automatically and photons were counted for 5 s. Emission photons were selected by means of the cut-off filter described in chapter 3.1. Intensity/humidity scans therefore consisted of (100 + 5) s intervals after which *RH* was increased by 10 % up to a value of 90 %. *RH* was not increased further due

to accuracy problems in the high humidity region, as explained in chapter 3.5. As reversibility was found, every scan was begun in the dry state. Each scan was repeated on at least three different positions on the same sample to allow for error estimation and averaging. The absence of significant bleaching was checked by illuminating the film in the dry state during a number of time intervals which covered at least the time needed for performing a complete humidity scan. After performing a scan, reversibility was confirmed by switching to the dry state again. Frequently, even at the lowest illumination intensities only a partial recovery of the initial intensity in the dry state after a complete humidity scan could be obtained. As this phenomenon was completely irreproducible, it was attributed to mechanical relaxation of the sample or the microscope setup (i.e. loss of focus). In these cases, appropriate data correction could be performed by assuming an additional linear intensity loss during the humidity scan due to defocussing. The total intensity loss due to this artefact is determined by the difference between the initial dry state fluorescence intensity and that one obtained after a complete humidity scan. While this procedure might not be completely correct quantitatively, no significant deviation from scans where the above-mentioned artefact was absent could be found. The correction procedure permits the comparison between different scans especially in the high humidity region. Fluorescence intensities thus obtained were normalised with respect to the dry state intensity, which according to chapter 3.5, is more accurate than normalising to the value obtained at the highest hydration level.

Model calculations

As mentioned above, the fluorescence properties of NBD are sensitive to the immediate probe environment. However, both the fluorescence emission and the absorption of point dipoles located at dielectric interfaces, depends on the optical properties of these interfaces as well as on the distance and orientation between dipole and interface [Luko, 1981].

For some of the experimental configurations described in this chapter model calculations could be performed. These calculations were done by M. Kreiter, ETH Zürich, following [Novo, 1996]. Very briefly, the radiation field of point dipoles was calculated, taking into account the interaction of the dipole with the reflection of its radiation field at a stratified layer system [Chan, 1978], [Hell, 1987]. In the case of fluorescence measurements in polymer-supported model membranes, this layer system was defined by two semi-infinite half spaces consisting of glass and air, which enclose a thin polymer film and the lipid membrane. Fresnel reflection and transmission coefficients were calculated by the transfer-matrix-algorithm [Azza, 1977]. The finite illumination and observation aperture of the actual setup was accounted for by restricting the maximum illumination and observation angles accordingly.

Influence of probe orientation

In order to exclude the artefactual possibility that the intensity change described above was dominated by changes in the fluorophore orientation upon hydration of the lipid layer, the NBD derivative NBD-X (see chapter 8.3) was dissolved in a chitosan solution, which was used to prepare a thin stained chitosan film on a glass substrate. In chapter 4.4, it was shown that chitosan is a water swellable polymer, the thickness increase amounts to 30 % upon changing *RH* from 0 % to 100 %. As can be seen in Figure 5.52, the fluorophore NBD in an isotropic microenvironment exhibits a significant, roughly linear fluorescence emission intensity reduction upon swelling of the polymer cushion, which can be used to probe changes in the local hydration state around the fluorophore.

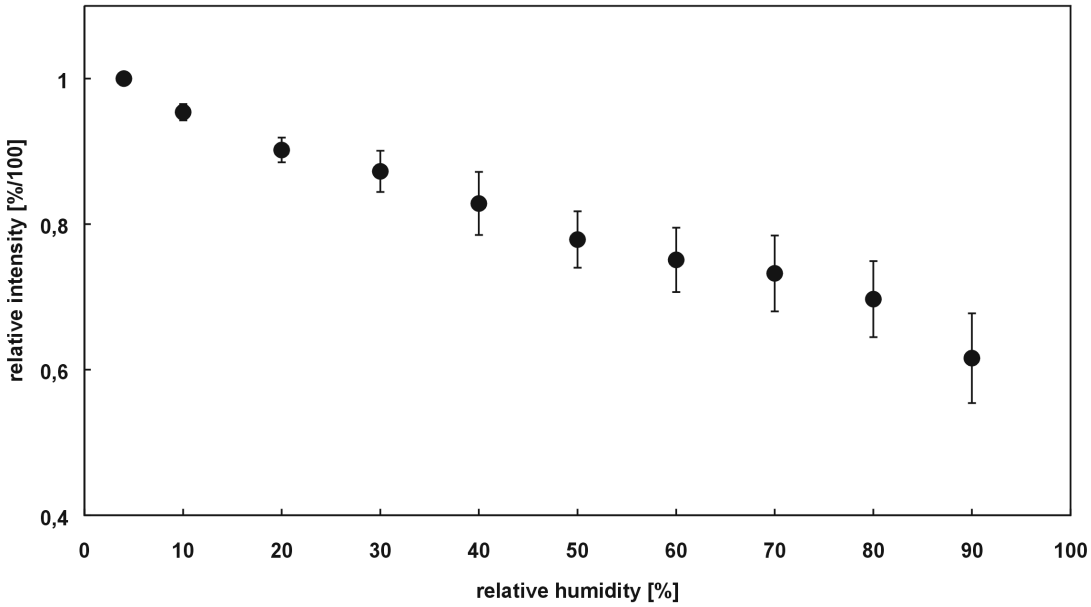

Figure 5.52: Relative fluorescence emission intensities of the fluorescence probe NBD-X, which was dispersed in a water-swellable chitosan matrix at a concentration of approximately 10^{-5} mol/g chitosan.

An approximately linear intensity/humidity relation was also found in case of rhodamin 6G dissolved in a gelatin matrix [Choi, 1999]. Model calculations revealed that the intensity reduction in case of the experiment described above cannot be explained by a change of the optical parameters of the layer system during swelling (i.e. a thickness increase and refractive index decrease of the polymer cushion, see chapter 4.4) [Krei, 2001]. Furthermore, it can be concluded, that the intensity variation of the membrane label NBD-PE in a substrate-supported monolayer (Figure 5.51), is not dominated by humidity induced changes in probe orientation.

In DPPC monolayers doped with a fluorescence labelled phospholipid, a perpendicular orientation of the transition dipole with respect to the plane of the membrane was found,

irrespective of the lateral pressure of the deposited monolayer [Holl, 2000]. In case of the NBD-label also, a perpendicular orientation of absorption and emission dipoles was observed [Smit, 1981]. Moreover, it was pointed out in chapter 5.3, that humidity induced phase transitions (which would be accompanied by a change of tilt angles of lipid tails and possibly influence probe orientation) in the systems studied in the present work are rather unlikely. Furthermore, it will be shown below, that the lateral pressure (which controls lipid tilt angles) of the transferred monolayer did not significantly effect humidity induced intensity changes. Taking these observations together, humidity induced variations in fluorescence intensity are rather unlikely to be influenced by changes in probe orientation.

5.4.3 Fluorescence intensity measurements in partially hydrated lipid monolayers

Clearly, the fluorescence intensity reduction is not linearly correlated with water concentration increase in the polymer film (Figure 5.52), since the water uptake of the latter is not linearly correlated with relative humidity (see chapter 4.4). There is no general theory available, which would connect fluorescence intensity with water activity; specific solvent effects depend on the chemical nature of solvent and solute [Otsu, 1994].
However, fluorescence intensity/hydration scans provide a simple comparative method for determining hydration changes. This will be the topic of the next section.
The humidity dependence of the fluorescence intensity of lipid monolayers, which were stained with NBD-PE, was analysed by varying the kind and conditions of the host lipid and the kind of support, in order to determine the influence of these parameters on the hydration state in the headgroup region. As a suitable reference system is missing, the hydration level cannot be assessed quantitatively, but the fluorescence measurements described in the following allow for the comparison of different experimental configurations.
Figure 5.53 shows a fluorescence intensity/humidity scan in monolayers with phosphoethanolamine (DLPE) and phosphatidylcholine (DMPC) headgroups, which were transferred to glass substrates. From the intensity decrease upon increasing *RH*, hydration in the headgroup region can be deduced. The hydration behaviour of both lipids in case of multibilayers was theoretically analysed and compared in [Damo, 1994]. In contrast to PC headgroups, PE lipid heads participate not only in hydrogen bonding with water molecules, but also form hydrogen bonds among each other. The difference is due to the fact that the ammonium group in PE is a hydrogen bond donor, which can bind to nonesterified oxygens of the phosphate group, whereas PC headgroups are only acceptors.

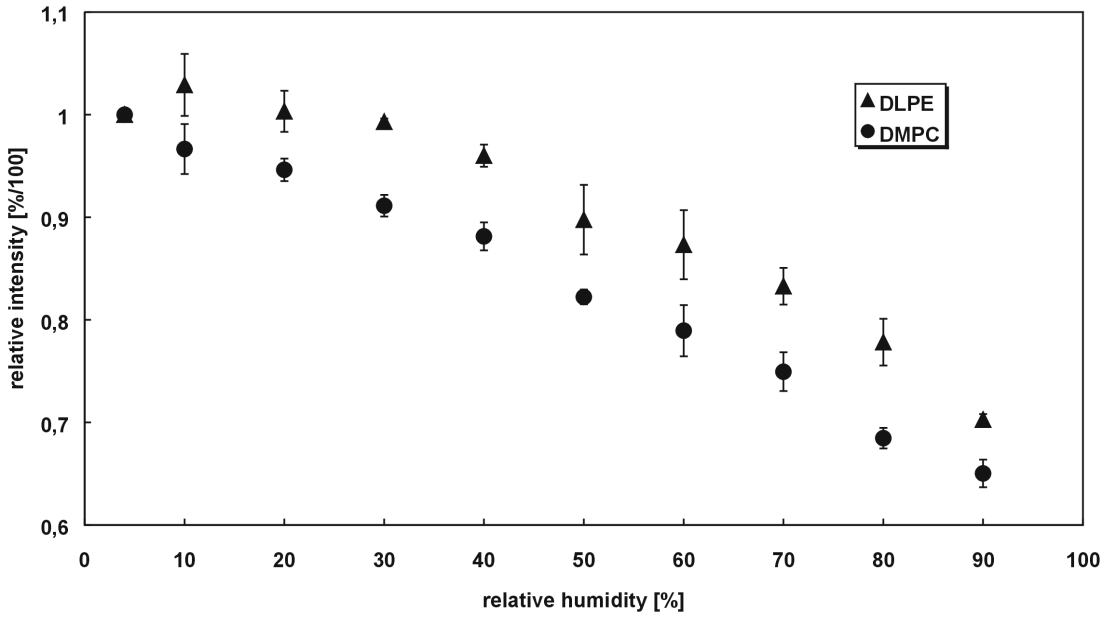

Figure 5.53: Relative fluorescence emission intensities of NBD-PE labelled DLPE and DMPC monolayers on a glass surface, lateral pressure: 35 mN/m. Normalisation in both cases was performed with respect to the value found at the lowest accessible relative humidity.

Therefore PC headgroups are solvated by a higher number of water molecules leading to a larger headgroup size in the fully hydrated state, compared to PE. From Figure 5.53, it can be deduced that the measured fluorescence intensity slightly rises upon increasing *RH* from 4 % to 10 %. According to Figure 5.61, a red shift of the emission maximum occurs upon hydration, due to a general solvent effect. It is reasonable to assume that at the lowest available value of *RH* = 4 %, the emission maximum of a DLPE monolayer is blue shifted with respect to DMPC, by a magnitude which places the maximum at a smaller wavelength than the cut-off wavelength of the emission filter (see Figure 5.61). A red shift upon hydration could then cause a rise of the detected fluorescence intensity, if the band shift over-compensates the intensity loss due to the specific solvent effect. Further hydration then causes a further red shift and intensity loss. Both effects reduce the observed fluorescence intensity. The blue shift of the DLPE emission band with respect to DMPC at *RH* = 4 % can be explained by a lower polarity as measured by the NBD-PE label. According to Figure 5.62, both polarity and emission band intensity are functions of the headgroup hydration. Therefore it can be concluded that DLPE monolayers on glass are less hydrated than DMPC in the whole humidity range which was examined. In order to clarify, whether the initial intensity rise observed for DLPE could be caused by a lower polarity in the environment of the NBD-PE label, a DMPC monolayer with an additional amount of cholesterol was prepared. Cholesterol content has been found to decrease the polarity in the headgroup region of bilayer membranes [Bern, 1998], as observed by a

strong blue shift of a polarity sensitive membrane label. An additional amount of cholesterol led to a significant increase of the fluorescence intensity upon moderately increasing the hydration level (Figure 5.54) which, along the lines of the argumentation provided above, is consistent with a decreased membrane polarity.

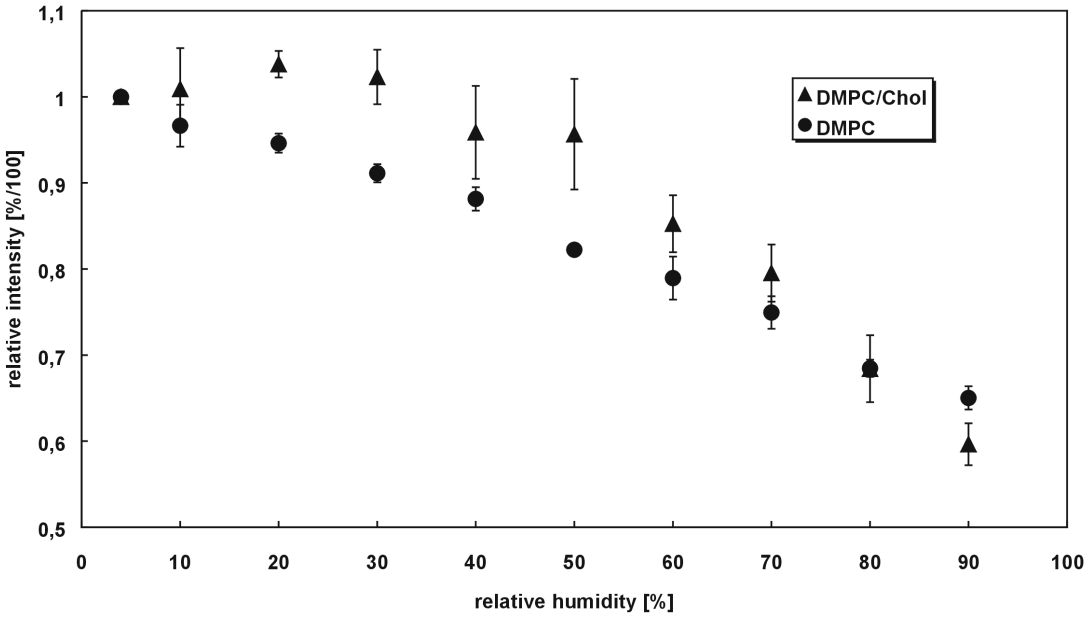

Figure 5.54: Relative fluorescence emission intensities of a NBD-PE labelled DMPC + 30 mol% cholesterol monolayer on a glass surface, lateral pressure: 35 mN/m. For the sake of comparison, the data for a pure DMPC monolayer have been added.

Furthermore, at high hydration levels, a lower fluorescence intensity was observed in membranes containing cholesterol, in comparison to pure DMPC monolayers (Figure 5.54). This can be explained by the additional specific solvent effect of water binding to the fluorophore. Cholesterol increases the spacing of the lipid heads, leading to a higher hydration in the headgroup region as has been found experimentally and by MD simulations (e.g. [Pase, 2000] and references therein). In the three-component system DMPC/cholesterol/NBD-PE demixing effects could be a problem. However cholesterol addition was found to *decrease* environmental heterogeneity, as measured by fluorescence properties of an additional label (see [Ho, 1992] and references therein). Taking into account the fact that humidity induced phase transitions were not observed (see chapter 5.3), humidity induced demixing effects are unlikely to contribute significantly to the measurement shown in Figure 5.54.

In order to evaluate the influence of different substrates on the hydration in the headgroup region, DMPC monolayers were transferred onto glass substrates covered by thin films of either chitosan or agarose. In Figure 5.55, the intensity/humidity scans for glass, agarose and chitosan supports are compared. In case of glass, the lowest intensity changes were

found upon hydration, which is in accordance with fluorescence spectroscopy measurements performed with monolayers transferred to SiO_2 surfaces (compare Figure 5.59 and Figure 5.60). Chitosan increases the hydration in the headgroup region with respect to glass, most probably due to a smaller interaction between the monolayer headgroups and the support.

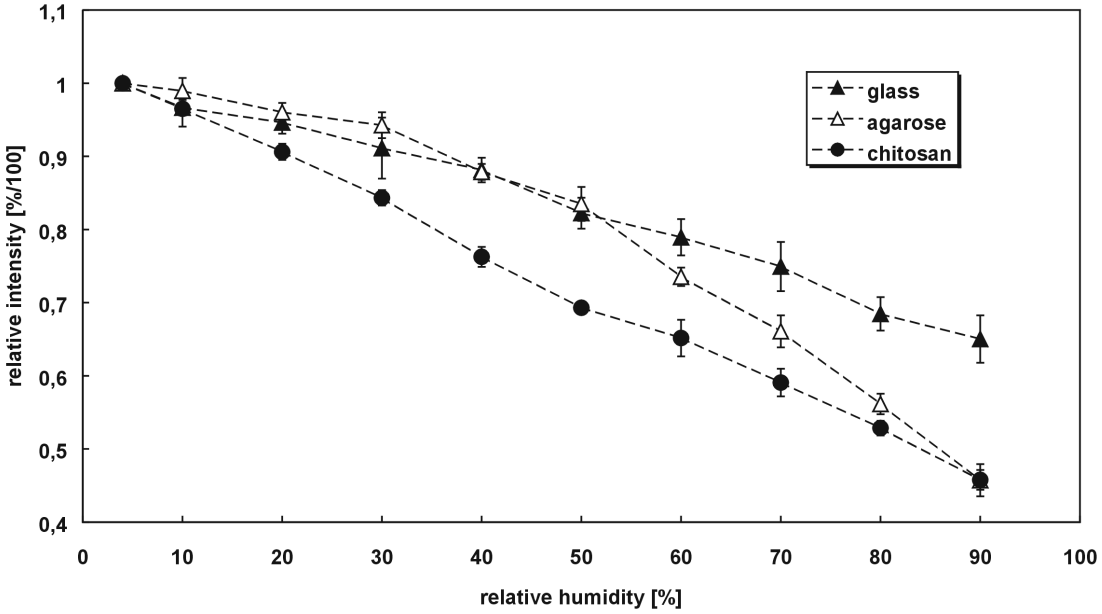

Figure 5.55: Comparison of the relative fluorescence emission intensities of NBD-PE labelled DMPC monolayers on glass, chitosan and agarose surfaces (lateral pressures in all cases 35 mN/m). The lines are a guide to the eye.

In the case of a water swellable polymer cushion as a membrane support, the optical properties of the layer system change in terms of thickness and refractive index of the polymer cushion. Therefore model calculations were performed in order to clarify the magnitude and direction of this effect on the fluorescence emission of fluorophores embedded in polymer-cushioned monolayer lipid membranes [Krei, 2001]. The optical parameters for a completely dried chitosan film and for a chitosan film in a water-saturated atmosphere were determined by ellipsometry, as described in chapter 4.4. The refractive index and thickness of the lipid monolayer was assumed to be independent of the relative humidity. Table 5.2 shows fluorescence intensities depending on the optical properties of chitosan in a dry and in a water-swollen state, normalised to the total intensity emitted by a dipole in vacuo. A slightly higher fluorescence intensity is predicted for the water swollen film. The fluorescence intensities shown in Table 5.2 were calculated by assuming an only radiative decay of excited states. With decreasing quantum efficiency, the difference of the fluorescence intensities of dry and water swollen state decreases [Krei, 2001].

relative humidity	n	d [nm]	intensity
0 %	1.579	198	0.2082
100 %	1.505	281	0.2263

Table 5.2: Fluorescence intensities of lipid monolayers supported by chitosan films in a dry and in a water-saturated atmosphere. For the calculations a perpendicular dipole orientation was assumed. Furthermore, all parameters of the layer system were kept constant, except from the refractive index and thickness of the polymer. The fluorescence intensities were normalised to the value of a point dipole in vacuo.

Since the quantum efficiency of NBD significantly decreases during hydration, it can be assumed that the difference of the fluorescence intensity in the dry and water swollen state in the present case was even smaller than predicted by the values shown in Table 5.2. Therefore, it can be concluded from these model calculations, that the fluorescence intensity difference between glass and chitosan-supported monolayers in the water-swollen state (see Figure 5.55) was not significantly influenced by the change of the optical parameters of the polymer cushion. The intensity difference is therefore due to a higher hydration in the headgroup region of a chitosan-supported monolayer, compared to a glass-supported lipid layer. It must be mentioned, however, that this difference was found for the humidity range below RH = 90 % and from the experiments described above, no predictions of the hydration state at water saturation can be made.

Clearly, the shape of the intensity/humidity scans in case of chitosan-supported monolayers, comparing fluorescence spectroscopy (Figure 5.62) and intensity measurements at a fixed wavelength (Figure 5.55) are different. This is partially due to the fact that the emission band shifts upon hydration, which alters the fluorescence intensity, measured at a fixed wavelength. Additionally, in case of fluorescence spectroscopy, due to the increased illumination intensity and the much longer illumination times, photobleaching cannot be avoided completely, as has been discussed above.

On an agarose support, an intermediate hydration behaviour was found (Figure 5.55). Whereas at low humidities the relative fluorescence intensity corresponded to the values found for glass, at higher RH the relative intensity became similar to a chitosan support. As was pointed out in chapter 4.4, swelling measurements by ellipsometry in case of agarose could not be performed, which makes it difficult to discuss the difference in the monolayer hydration. From the similar hydration at a high humidity, however, it can be inferred that the much smaller diffusion coefficients found for monolayers on agarose compared to chitosan (see chapter 5.3.5), cannot be attributed to a lower hydration (and therefore increased adhesion) of the headgroups to the support.

Besides the higher intensity decrease indicative of higher hydration in case of chitosan-supported monolayers compared to glass, the same trends of the intensity/humidity scans

in case of DLPE and DMPC that were observed on glass (see Figure 5.53, and Figure 5.54) were also found on chitosan (data not shown). This indicates that besides the reduced water content of the monolayer on glass and on chitosan found at every value of *RH*, the general hydration behaviour in the headgroup region is not altered by the underlying support.

In order to analyse the influence of monolayer density on the hydration in the headgroup region, DLPE monolayers were transferred at different lateral pressures onto chitosan supports. The fluorescence intensities measured at *RH* = 90 % and *RH* = 4 % were determined subsequently. However, no regular dependence of the intensity ratios at different *RH* with respect to lateral pressure could be found (data not shown). This indicates that the variation in headgroup hydration with different monolayer densities was smaller than the error in relative humidity, which is due to temperature differences.

As a further application of fluorescence intensity/hydration measurements, it was examined to what extent the chemical coupling of hydrophilic spacers to the polar heads of DSPE leads to a changed hydration behaviour in the headgroup region of lipid monolayers. For this purpose, an amphiphile molecule consisting of a short (45 monomer units) polyethylene glycol chain attached to the polar head of DSPE (DSPE-EO_{45}, see chapter 8.2.2) was used. Polyethylene glycol is a highly hydrophilic polymer, which swells upon increasing *RH*. The swelling behaviour of DSPE-EO_{45} was analysed in [Baek, 1995]. The hydration behaviour of pure DSPE-EO_{45}, labelled with NBD-PE and transferred at a lateral pressure of 42 mN/m was compared to pure NBD-PE labelled DSPE, and a mixture of DSPE and DSPE-EO_{45} of a molar ratio of 91/9 (Figure 5.56).

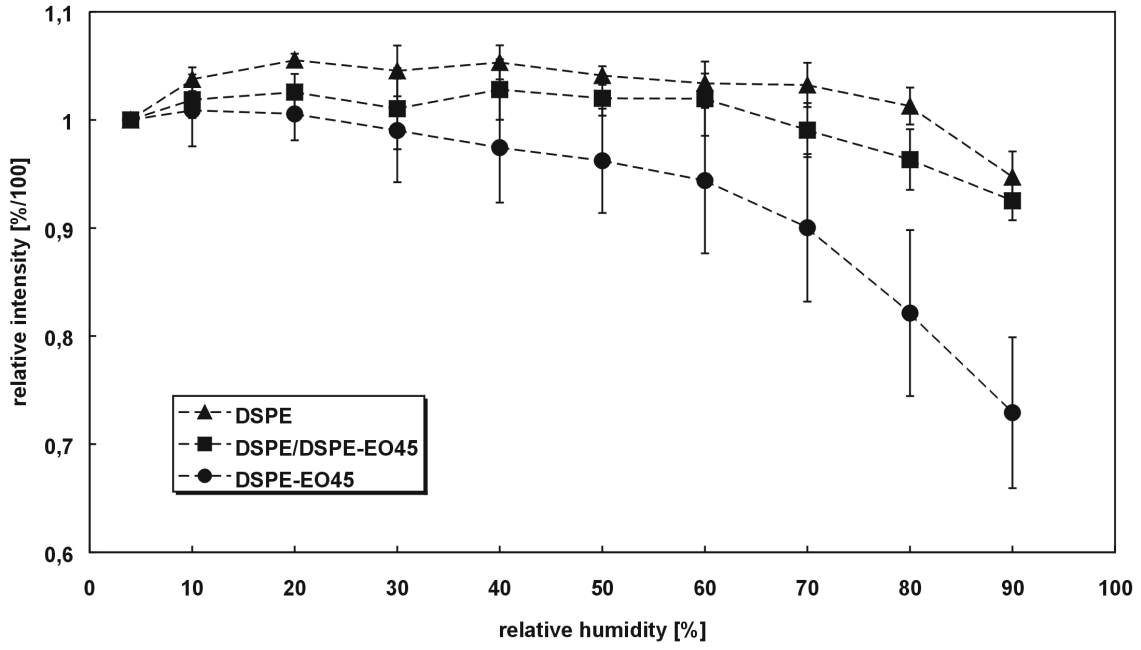

Figure 5.56: Comparison of the relative fluorescence emission intensities of NBD-PE labelled DSPE, DSPE-EO_{45} and a mixture of 91/9 mol/mol DSPE/DSPE-EO_{45} monolayers on a glass surface (in all cases lateral pressure 42 mN/m). The lines are guides to the eye.

A strong dependence of the fluorescence intensity changes on lipopolymer content was found. The strong variation of the normalised fluorescence intensities in case of pure DSPE-EO_{45} might be due to a phase separation or local inhomogeneities of the lipopolymer. Obviously, the presence of a short polyethylene glycol chain, attached to the polar head, increased the hydration in the polar headgroup region of the DSPE monolayer. A fraction of as low as 9 mol% of lipopolymer of the total lipid amount already led to a significant decrease of fluorescence intensity.

Since the thickness of the polymer cushion in the case of DSPE-EO_{45} is significantly smaller compared to the chitosan cushions mentioned above, a much smaller influence of the optical properties of the polymer cushion on the fluorescence emission intensity of labels incorporated into DSPE-EO_{45} monolayers can be expected. This was confirmed by model calculations, as shown in Table 5.3 [Krei, 2001].

relative humidity	n	d [nm]	intensity
0 %	1.469	2	0.2231
90 %	1.404	3.6	0.2229

Table 5.3: Fluorescence intensities of DSPE-EO_{45} monolayers in a dry and in a water saturated atmosphere. For the calculations a perpendicular dipole orientation was assumed. Furthermore, all parameters of the layer system were kept constant, except from refractive index and thickness of the polymer. The fluorescence intensities were normalised to the value of a point dipole in vacuo.

The optical parameters of DSPE-EO_{45} shown in Table 5.3 were obtained from [Baek, 1995]. Clearly, in the case of DSPE-EO_{45} monolayers the influence of the change of optical parameters of the polymer cushion upon hydration can be neglected.

The influence of the PEG chain on the hydration in the headgroup region is twofold. On the one hand, the polymer swells upon increasing *RH*, which leads to an increase in water concentration near the DSPE headgroup. Second, the polymer chain acts as a lateral spacer: at the same lateral pressure, pure DSPE monolayers possess a significantly smaller molecular area, compared to DSPE-EO_{45} monolayers [Baek, 1995], which could lead to a higher hydration, similar to the spacer effect of cholesterol (see above). However, the latter influence seemed to be relatively small, as no significant difference of the intensity/humidity scan of pure DSPE-EO_{45} monolayers was found between a lateral transfer pressure of 25 mN/m and 42 mN/m (data not shown).

Interestingly, a pure DSPE monolayer shows a rather different hydration behaviour compared to DLPE (see Figure 5.57). On the one hand, DSPE was in the liquid condensed state at the indicated transfer pressure (and at room temperature), while DLPE was transferred from the expanded state. However, as already mentioned, no indication for a

significant lateral pressure dependence for the hydration behaviour of DLPE monolayers was found.

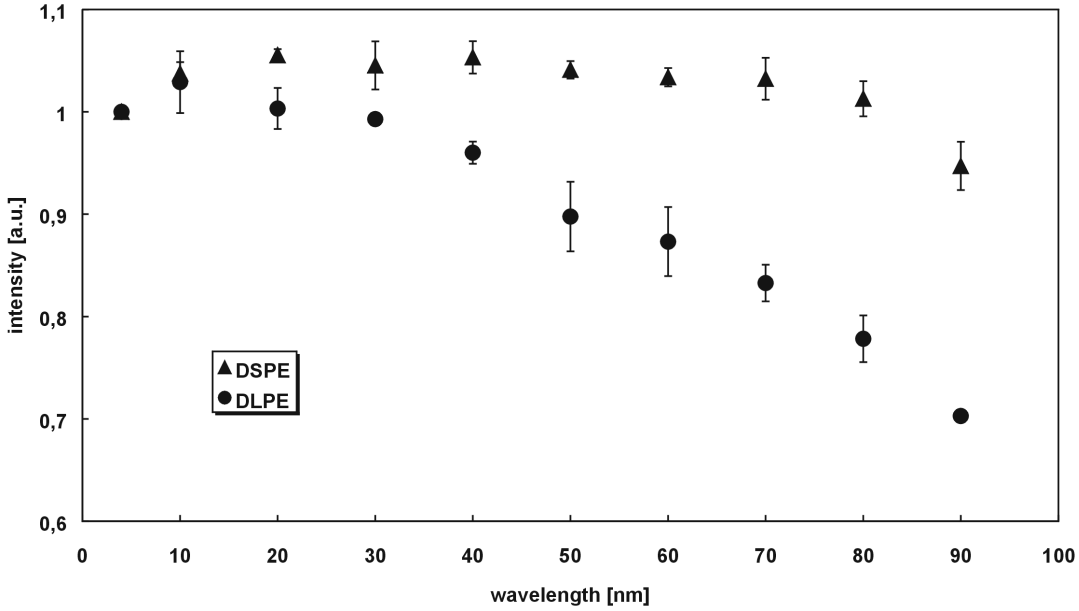

Figure 5.57: Comparison of the relative fluorescence emission intensities of NBD-PE labelled DSPE (lateral pressure 42 mN/m) and DLPE (lateral pressure 35 mN/m) monolayers on a glass surface.

From the pronounced initial rise of the fluorescence intensity of DSPE monolayers (Figure 5.57), it can be concluded that the fluorescence label is located in a more unpolar region compared to DLPE. As this observation cannot be explained by a different monolayer density, it could be the case that the label is situated at a different height (i.e. in a more polar region in case of the lipid host with shorter chains) of the membrane, with respect to the membrane normal. This could be due to the difference in alkyl chain length of the label and the host matrix.

5.4.4 Humidity dependence of fluorescence spectra

In the case of the fluorescence intensity/humidity scans discussed above, no information concerning the effect of hydration changes on the wavelength dependence of both absorption and emission of NBD was obtained. Such information can be acquired by fluorescence spectroscopy measurements, as will be described in the following.

Figure 5.58 shows fluorescence excitation spectra of NBD-PE in a DMPC monolayer transferred onto a chitosan film, at different humidities. The chitosan films were prepared on a silicon wafer, which was thermally coated with a SiO_2 layer of a thickness of 160 nm. The humid state corresponds to an atmosphere equilibrated with a saturated KNO_3 solution

(*RH* = 93 %, see chapter 3.5), whereas the dry atmosphere was established by placing NaOH pellets into the measurement chamber. Samples were equilibrated for at least two hours with the corresponding atmosphere. The emission intensities of the excitation spectra could not be drawn to scale since different scaling factors were used for data representation and the raw data were not available. However, normalisation with respect to the off-peak intensity around a wavelength of 390 nm (Figure 5.58) suggested, that the fluorescence intensities of the maxima of excitation spectra depended in a similar manner on relative humidity as the corresponding emission spectra (compare Figure 5.59). Moreover, the spectra changed in a reversible manner upon altering *RH* (see Figure 5.58). The short wavelength band in Figure 5.58 exhibited a slight bathochromic shift upon hydration, whereas the position of the charge transfer band seemed to be unaffected by a humidity change.

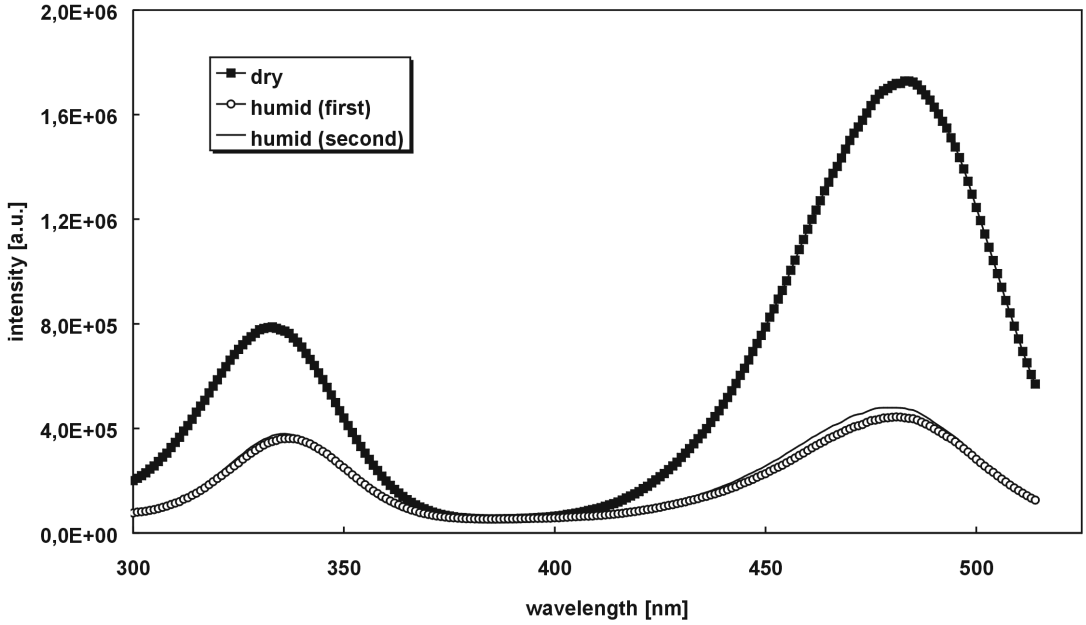

Figure 5.58: Fluorescence excitation spectra changes upon humidity changes of a DMPC monolayer, lateral pressure 35 mN/m on a chitosan polymer cushion, λ_{em} = 550 nm. Note: the intensities of the three different spectra are *not* to scale (see text).

An increase in solvent polarity has been found to induce bathochromic shifts of absorption spectra bands in case of NBD-derivatives in isotropic solvents, however, both bands exhibited similar shifts [Lin, 1991], [Saha, 1998]. While the absence of a wavelength shift of the charge transfer band in the present case could not be explained, the absence of a wavelength shift is favourable when comparing fluorescence intensities of samples in different atmospheres, which were excited in the long wavelength band. NBD possesses a short wavelength band around 225 nm, which is essentially insensitive to solvent

parameters [Forg, 1993]. In order to avoid pronounced photobleaching, however, all emission spectra were recorded while exciting the charge transfer band.

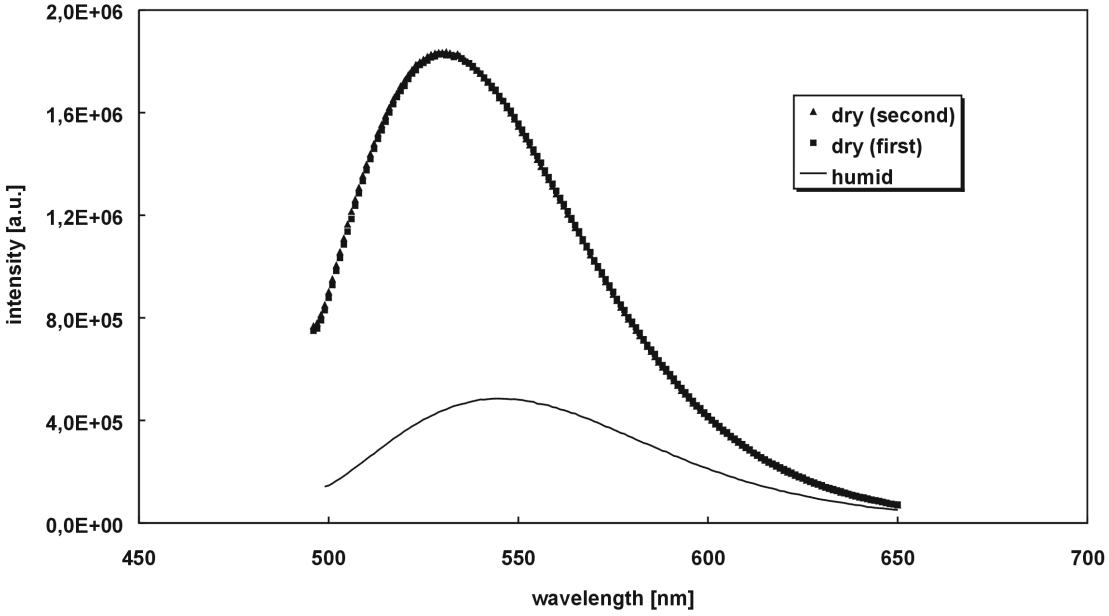

Figure 5.59: Changes in the emission spectra of a DMPC monolayer (lateral pressure 35 mN/m) on a chitosan film, λ_{ex} = 465 nm. Fluorescence intensities in all emission spectra correspond to the raw data and hence can be compared quantitatively (in contrast to excitation spectra).

It can be deduced from the emission spectrum of a NBD-PE stained DMPC monolayer on a chitosan cushion (Figure 5.59) that the maximum fluorescence intensity in the emission spectrum shows a larger bathochromic shift in comparison to the maxima of the excitation spectrum. A corresponding result was obtained in [Saha, 1998] when comparing absorption and fluorescence emission spectra of NBD-derivatives in isotropic solvents of different polarity. This difference is explained by a higher polarity of the excited state compared to the ground state [Saha, 1998]. Besides the wavelength shift, the fluorescence emission intensities exhibited a large reduction upon hydrating the monolayer/polymer system, which was completely reversible (Figure 5.59), similar to the excitation spectrum. The position of the fluorescence maximum in the hydrated state was found to be at 545.6 nm, which is slightly higher compared to the value found for NBD-PE incorporated into eggPC vesicles (540 nm, [Maze, 1996]). The difference might be due to different positions of the lipid label in the different host matrices. Dehydration of the monolayer led to a blue shift of the position of the emission maximum (545.6 nm and 531.1 nm according to Figure 5.59). According to the Lippert-Mataga equation (5.4.1), the solvent refractive index and dielectric constant determine the difference in the positions of absorption and emission maxima. As the position of the absorption maximum was poorly affected by the

monolayer water content (Figure 5.58), the Stokes shift difference due to solvent effects (left hand of (5.4.1)) is mainly influenced by the wavelength shift of the fluorescence emission maximum. Dehydration of the monolayer can be assumed to increase the refractive index in the headgroup region, which, according to (5.4.1), would lead to a decrease of the Stokes shift and hence to a blue shift of the emission maximum. Furthermore, it is reasonable to assume that dehydration decreases the dielectric constant of the headgroup region, which also causes a blue shift of the emission maximum. Both parameters of the orientation polarizability therefore cause a blue shift of the emission maximum upon dehydration, which is in accordance with the data presented in Figure 5.59. As the refractive index in the headgroup region is largely influenced by the presence of the polar lipid headgroups (values of n between 1.49 and 1.60 are found in case of complete hydration [Negr, 2000]), it can be assumed that n only slightly varies upon dehydration. Hence the wavelength shift observed in Figure 5.59 can be attributed mainly to a decrease of polarity upon dehydration. A decrease of polarity in the headgroup region (of vesicles immersed in water) upon dehydration in the headgroup region, has also been observed by others ([Bern, 1998], [Chat, 1999b] and references therein). In addition to chitosan supports, NBD-PE stained DMPC monolayers were transferred directly onto silicon wafers (thermally coated with a SiO_2-layer of a thickness of 160 nm). Reversible intensity changes were found upon changing RH (Figure 5.60), however, the relative intensity reduction upon hydration was much smaller compared to a chitosan-supported monolayer.

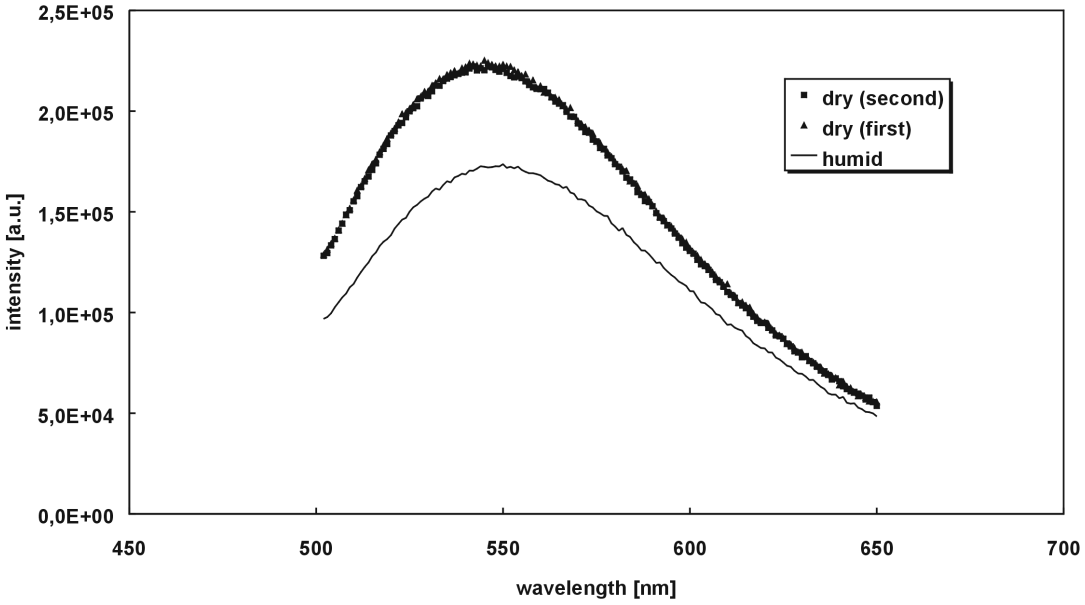

Figure 5.60: Changes in the emission spectra of a DMPC monolayer stained with NBD-PE (lateral pressure 35 mN/m) deposited onto a Si/SiO_2 substrate surface, λ_{ex} = 465 nm.

This observation can be explained by a reduced water uptake in the headgroup region, due to the interaction between headgroups and support [Yami, 1997]. In accordance with this conclusion is the emission maximum shift upon hydration found on SiO_2 (Figure 5.60), which is considerably smaller than on chitosan (Figure 5.59). The swelling of the polymer cushion (chapter 4.4) leads to a reduced binding site density and contributes additionally to the higher headgroup hydration. The comparison of the wavelength positions of the emission maxima in the dry state on both supports revealed a considerable red shift on a SiO_2-supported monolayer compared to chitosan, which is difficult to explain. It might be the case that this shift is an artefact caused by interference effects through reflections at the optical interfaces of the support. As the monolayer is located further away from the substrate in case of chitosan supports, this effect would be different in case of the latter. The same effect could possibly lead to fluorescence intensity changes upon changing *RH*, which are caused by a different membrane/support spacing only. However, the fluorescence intensity difference between dry and humid state (*RH* = 90 %) as obtained by fluorescence spectroscopy (see Figure 5.62) was found to be comparable to that one obtained by means of the measurements described in chapter 5.4.3 (see Figure 5.55). As in the latter case a significant distortion due to the changed optical parameters of the polymer cushion was ruled out, it is assumed that this contribution is small in the case of fluorescence spectroscopy measurements also.

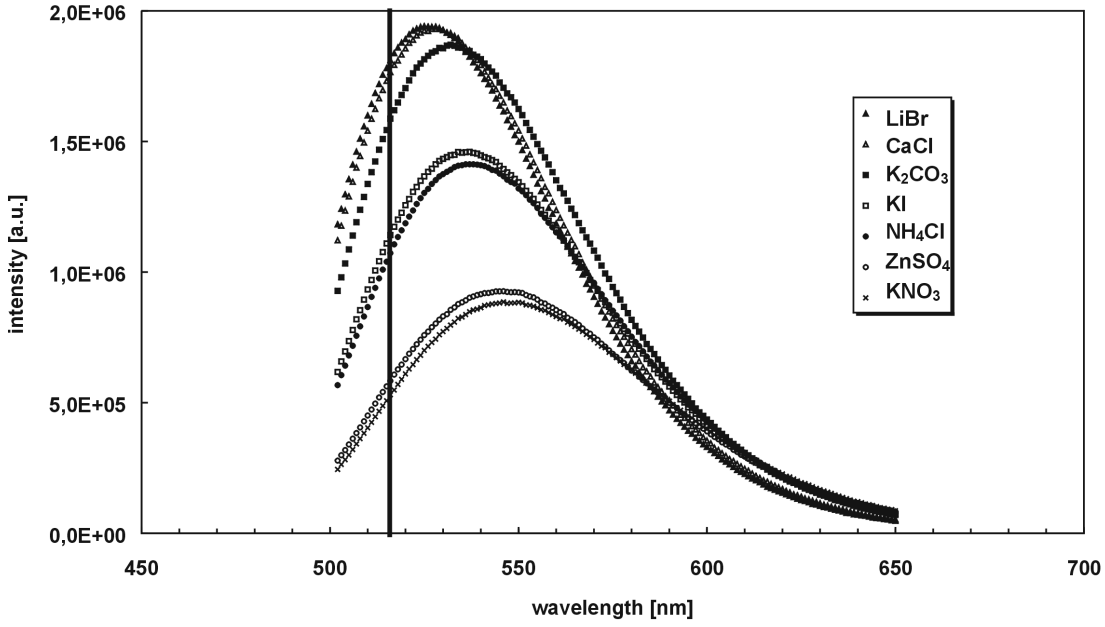

Figure 5.61: Fluorescence emission spectra of DMPC monolayers labelled with NBD-PE, transferred onto a chitosan film at a lateral pressure of 35 mN/m, λ_{ex} = 465 nm. The spectra were taken at different humidities, adjusted by saturated salt solutions, starting at the highest humidity. The salts specified in the panel are grouped corresponding to increasing *RH* from top to bottom (compare Figure 5.62). The bold vertical line indicates the cut-off wavelength of the emission filter used for humidity/fluorescence intensity scans.

The effect of *RH* on fluorescence emission spectra was further analysed by placing small open containers filled with saturated salt solutions into the measurement chamber (see chapter 3.2.2). Subsequent equilibration for at least 2 h allowed for the establishment of a defined relative humidity, depending on the kind of salt. The salts shown in the panel of Figure 5.61 correspond to increasing values of *RH* from the top to the bottom.
As depicted in Figure 5.61 and Figure 5.62, monotonous red shifts[4)] were obtained upon increasing *RH*. In parallel, the fluorescence intensity decreased continuously.

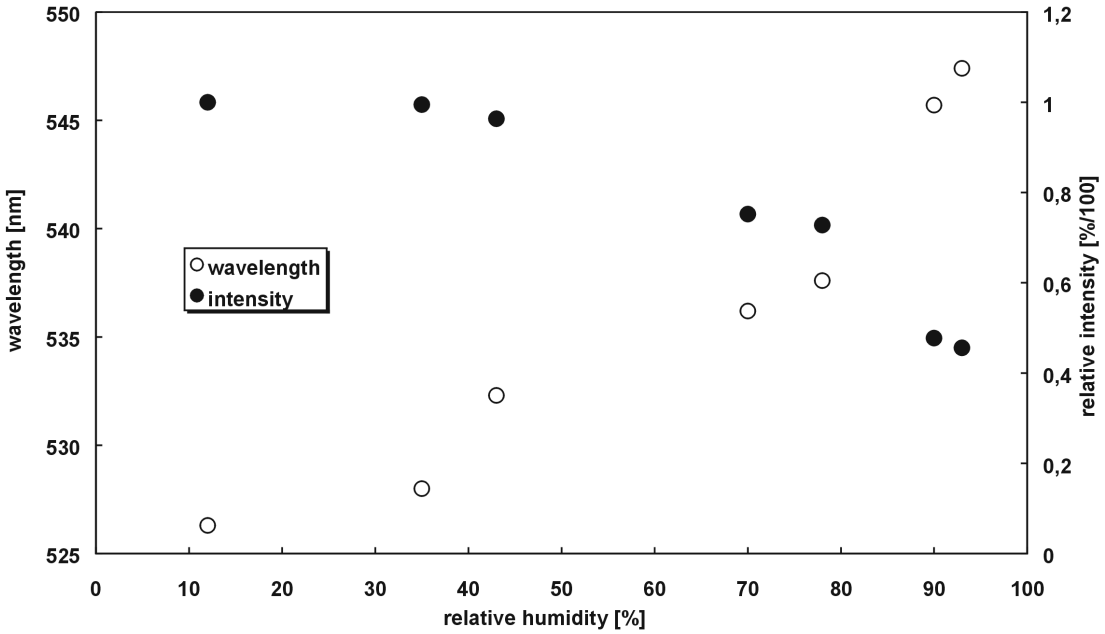

Figure 5.62: Wavelength shifts and normalised intensities at different relative humidities, from Figure 5.61. Intensities were normalised with respect to the value found at the lowest relative humidity.

As the measurements were performed starting at the highest relative humidity, photobleaching could possibly have caused an apparent levelling off of the intensity increase upon dehydration. As was pointed out above, the humidity dependence of the two parameters shown in Figure 5.62 is due to *different* physical effects. Whereas the wavelength shift of the fluorescence emission band is dominated by a general solvent effect (mainly an increase of polarity in the solvent cage of the fluorophore upon hydration), the reduction of fluorescence intensity upon hydration is due to a specific solvent effect: the binding of water to the fluorophore establishes a vibrational accepting mode which facilitates non-radiative decay. In principle, it is possible to prepare calibration curves (Lippert-plot) for the Stokes shift depending on the orientation

[4)] In principle, spectral shifts are most accurately determined by the "centre of gravity" of the spectra. However, since no significant deviations of the spectral shape was observed, red shifts in the present work were reported as shifts of the emission maximum [Itoh, 1975].

polarizability by using solvents with known high- and low-frequency polarizabilities (refractive index and dielectric constant) [Lako, 1983]. This has been performed in case of a NBD-derivative in [Mukh, 1994]. However, other authors did not find a regular dependence of the Stokes shift on the orientation polarizability in case of other NBD probes [Forg, 1993], [Saha, 1998]. Such a calibration curve could be used to quantify the dependence of the orientation polarizability (mainly influenced by the dielectric constant in the present case) on relative humidity by comparing the measured Stokes shifts (Figure 5.61) with those found in solvents.

Besides the difficulty to obtain a calibration plot, there are also conceptual problems in calculating absolute ε values in lipid membranes, by means of fluorescence probes using the Lippert-theory. As already mentioned, this theory assumes an isotropic fluorophore environment, a condition which is not fulfilled in the highly anisotropic headgroup region of a lipid membrane [Bern, 1998]. In this case, the dielectric constant is a tensor, but currently no theory exists which accounts for these anisotropy effects [Negr, 2000]. While therefore a quantification of membrane polarity is difficult, if not impossible, until refined theories are available, polarity changes upon modifying physical properties of membranes can be followed by fluorescence probes performing an internal comparison of the Stokes shift changes.

Besides membrane anisotropy, a second difficulty arises from the fact that the Lippert-Mataga equation is valid only if fluorescence is excited from a completely solvent relaxed state [Bern, 1998]. As was shown in [Chat, 1999b], NBD-PE incorporated into lipid vesicles exhibits a red edge excitation shift (REES), therefore solvent relaxation occurs on a time scale comparable or higher with respect to the excited state lifetime. In that case, the measured Stokes shift must be multiplied by a correction factor *f*:

$$f = 1 + \frac{\tau_r}{\tau_f} \qquad \textbf{(5.4.2)}$$

where τ_r and τ_f are the solvent relaxation time and fluorescence lifetime, respectively.

In order to examine the influence of *RH* on the magnitude of REES exhibited by NBD-PE in a solid-supported monolayer, emission spectra were recorded with varying excitation wavelengths. Figure 5.63 shows an example of the dependence of fluorescence emission spectra upon varying the excitation wavelength, in a relative humidity of 93 %, adjusted by a saturated KNO_3 solution. A pronounced red shift was observed upon increasing the excitation wavelength. In Figure 5.64, the red edge excitation shifts obtained from measurements in different humidities are shown. In DPPC vesicles in the fluid state, NBD-PE was found to exhibit a REES of 9 nm as was observed upon shifting the excitation

wavelength from 465 nm to 515 nm [Chat, 1999b]. According to Figure 5.64, in case of an atmosphere equilibrated with a saturated $ZnSO_4$ solution (*RH* = 90 %), an REES of 6.4 nm is found in the same excitation wavelength region.

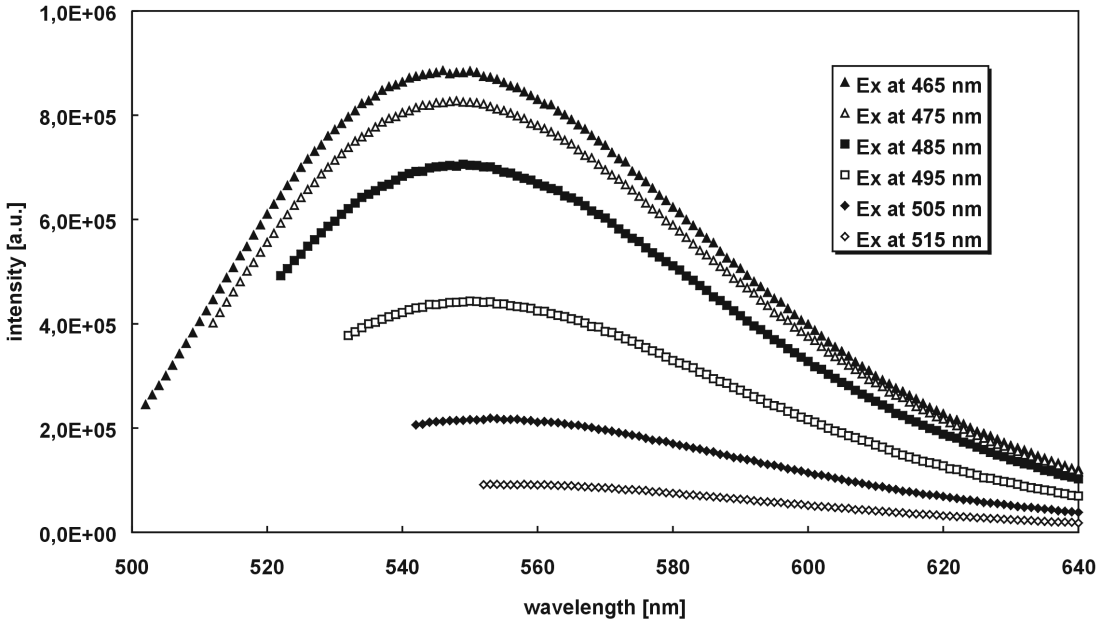

Figure 5.63: Typical REES observed in case of a DMPC monolayer, labelled with NBD-PE on a chitosan film. The relative humidity was adjusted by salt solutions, in the measurement shown in this figure KNO_3 was used. The intensities of the different spectra are not to scale.

However, in [Maze, 1996], an even lower value of 4 nm was found for an excitation wavelength sweep between 460 and 520 nm. The difference was attributed to different probe concentrations and slit widths, which could also be the reason for the intermediate value, found in the present case. Interestingly, the relative humidity had no remarkable influence on the slope of λ_{em}-λ_{ex}-plots (Figure 5.64). In case of SiO_2-supported monolayers also, no dependence of the red shift slopes on relative humidity was found (data not shown).

Apart from slow solvent reorientation (see above), spectral red shifts can be caused by binding site heterogeneity of the fluorophore, due to selective excitation of a particular subgroup of fluorophores, at a certain excitation wavelength [Lako, 1984]. As was pointed out in [Chat, 1993] (see also references therein), however, the label NBD-PE is located in a unique environment, absent of site heterogeneity. Therefore, the observed REES must be due to excited state heterogeneity caused by slow environmental relaxation with respect to the lifetime of the excited state. According to Figure 5.64, the contribution of slow solvent reorientation to the total Stokes shift is not seriously affected by an altered water content in

the membrane. As was shown in [Lako, 1984], from REES values measured at a particular set of excitation wavelengths, the solvent relaxation times may be obtained.

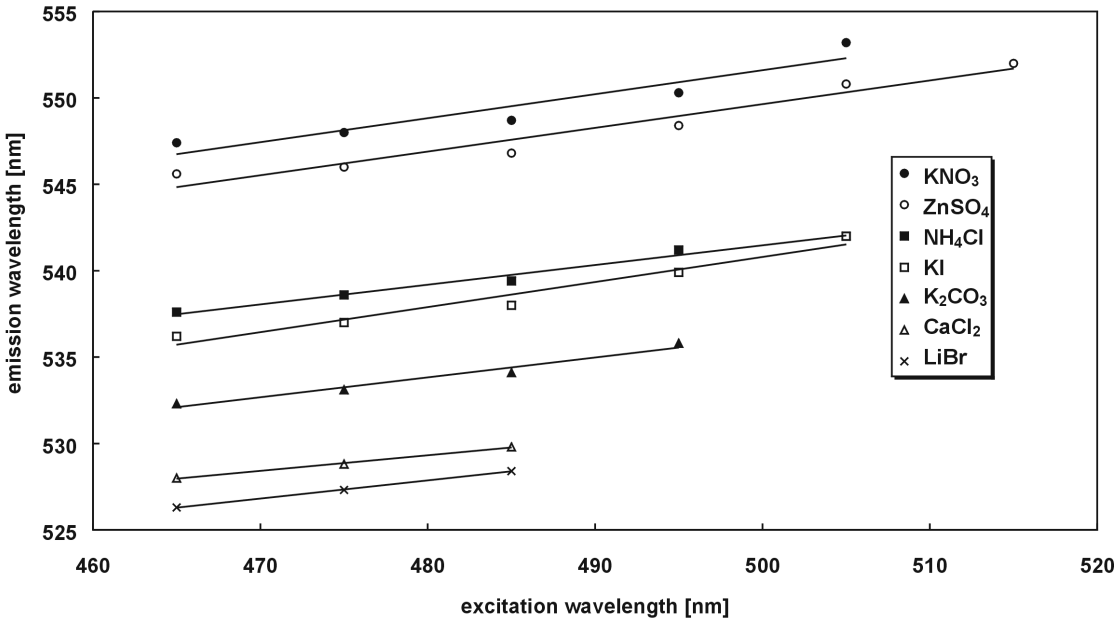

Figure 5.64: REES values for NBD-PE stained DMPC monolayers on a chitosan cushion at different ambient humidities.

The dynamics of water near lipid membrane surfaces was analysed in [Volk, 1994] by means of NMR techniques. An exponential dependence of several dynamic parameters on water content was found. However, it was pointed out that only a small fraction of water is slowed in molecular motion and is in rapid exchange with essentially unperturbed water [Volk, 1994]. Unperturbed water, however, according to [Chat, 1993], relaxes too fast for REES of the NBD-label to be observed. Hence the fact that a fluorescence probe situated in the headgroup region of a lipid membrane exhibits REES was attributed to a slowing down of environmental relaxation due to intermolecular interactions including the lipid headgroups [Chat, 1993]. These and other authors (see the references in [Chat, 1993]) found no influence of temperature or the phase state of the lipid on the magnitude of REES exhibited by NBD-PE. Additionally, the water content of the membrane did not significantly influence the red shift (Figure 5.64). A change in solvent relaxation times will, however, influence the magnitude of REES only if the solvent relaxation time is comparable to the fluorescence lifetime [Lako, 1984], [Milt, 1978]. It could therefore be the case that the solvent relaxation rate in the headgroup region, as probed by NBD-PE, is already too slow in the completely hydrated state, so that a further retardation by dehydration cannot be monitored by the particular label. Possibly, phosphorescent labels could therefore be better suited for probing low solvent relaxation rates [Milt, 1978] in partially dehydrated membranes.

It was shown above that fluorescence spectroscopy provides a tool for analysing several physical parameters depending on the hydration state of the headgroup region. However, NBD-PE stained monolayers are inclined to photobleaching, which necessitates reduced illumination intensities and reduced illumination time. Furthermore, the large illumination area of the spectrometer does not allow addressing monolayer domains in the μm region. Thirdly, the humidity control by means of salt solutions is rather time consuming, whereas the humidity controlling apparatus incorporated into the FRAP setup was difficult to couple to the fluorescence spectrometer. On the other hand, it can be inferred from Figure 5.61 that fluorescence intensity measurements at a single wavelength provide a useful method to analyse hydration changes in lipid monolayers. As was shown above, emission spectra are influenced by hydration changes both through intensity variations and spectral shifts. Intensity measurements therefore reflect both parameters and the intensity/humidity scans must be interpreted with regard to this fact.

5.4.5 Conclusion, discussion and outlook

For the first time, to the best of the author's knowledge, the environmental sensitivity of a fluorescence membrane label was used to monitor hydration changes in lipid membranes, as a function of water activity regulated by ambient humidity. It was shown, that both general and specific solvent effects could be determined by the membrane label NBD-PE which, upon incorporation into lipid membranes, participates selectively into the headgroup region of the particular membrane. The method was applied to the analysis of hydration changes in lipid monolayers on different substrates and of different compositions. Utilising fluorescence spectroscopy it was shown that dehydration of the membrane led to a decreased polarity in the headgroup region. In parallel, the decreased water concentration could be followed by an intensity decrease of the whole spectrum, which was attributed to a specific solvent effect. Both effects were shown to be considerably enhanced in a monolayer transferred onto a hydrophilic polymer cushion, as compared to monolayers deposited onto an SiO_2 support. This was explained by a smaller adhesion of the monolayer in the former case and the swelling behavior of the polymer cushion. Excitation at the red edge of the absorption spectrum revealed a red shift of the emission band, which is indicative of slow solvent relaxation in the environment of the fluorophore. However, no influence of *RH* on the extent of the red shift was found, indicating that already in the hydrated state solvent relaxation was much slower compared to the lifetime of the excited state. Using the dry state as an internal reference allowed comparing hydration changes in different samples. The problem of photobleaching while

using fluorescence spectroscopy was avoided by measuring only intensity changes at a fixed wavelength, at short observation times and reduced illumination intensity. In the case of fluorescence intensity measurements, photostability is obtained at the expense of spectral information, however, it was shown that from the intensity variation in the low-humidity region, reasonable estimations of polarity changes which were due to a different composition of the host matrix could be made. While the approach outlined in the present chapter provides a relatively simple and straightforward manner to follow hydration changes in supported *monolayers*, it should be mentioned that the same method cannot be applied to study the hydration of *multibilayer* stacks. The latter have extensively been used to examine the hydration of phospholipids (see chapter 5.0.2). The incorporation of fluorescence labels into such a layer, which usually consists of hundreds of bilayers, i.e. a system with many optical interfaces, leads to complex reflection and interference phenomena. Subsequent hydration results in a change in layer spacing, which alters interference effects and therefore obscures intensity changes due to local hydration effects. In fact it was shown in the present work, that in case of fluorescence labelled multibilayers the fluorescence intensity ratios as measured at high and low *RH* respectively, significantly depend on the width of the illumination and observation cone. The latter could be regulated by the numerical aperture of the observation objective. The same effect was absent, in case of single, fluorescence labelled lipid monolayers.

It is often assumed, that during LB-transfer a certain amount of water is transferred with the monolayer, which would influence phase transition temperatures [Chi, 1994], or smoothen the monolayer by filling cavities in the underlying substrate [Mikr, 1993]. The method outlined in this chapter provides a simple approach to clarify these apparent uncertainties (by complete drying and studying the intensity increase of incorporated, environmentally sensitive membrane probes).

As was shown above, the hydration state of the lipid membrane is significantly influenced by the underlying substrate on the one hand and water activity on the other hand. The approach developed in the present chapter might therefore contribute to the evaluation of suitable membrane supports for biosensor applications.

In this work, fluorescence methods could only be used in initial experiments to characterise the effects of hydration/dehydration in the headgroup region of supported lipid monolayers. However, the great variety of fluorescence methodologies (see e.g. [Lako, 1983]), the availability of numerous fluorescence molecules specially suited for probing different effects [Mole, 1996] and the large number of changeable system parameters leave an open field for research. Among these possibilities, only some shall be proposed in the following, to conclude the present chapter.

It was mentioned above that REES will be dependent on the solvent relaxation rate, k, only if $k \cong 1/\tau$, where τ is the lifetime of the fluorophore. If $k >> 1/\tau$, then no REES will be observed, if $k << 1/\tau$, then the REES will be independent of k [Itoh, 1975], [Lako, 1984]. In the latter case, which was observed in the present chapter, the choice of probes with a longer excited state lifetime, τ, could provide an access to estimate solvent relaxation rates. Thus possibly phosphorescence [Milt, 1978] labels attached to lipid molecules could be used with advantage to study the average magnitude and distribution of solvent relaxation rates as a function of membrane parameters, such as the hydration state or temperature. In addition to steady state fluorescence spectroscopy, fluorescence lifetime measurements or time resolved fluorescence spectroscopy [Stub, 1985] could be applied to analyse solvent relaxation and special solvent effects [Lin, 1991] in supported monolayers. The absence or presence of humidity induced phase transitions or changes in lipid tilt angle could be followed by determining the orientation of the fluorescence dipole with respect to the membrane normal. A number of different methods have been developed to determine the angle of both the absorption and emission dipole moments of a fluorophore with respect to the interface normal [Lieb, 1987], [Holl, 2000]. Finally, fluorescence depolarisation measurements could be applied to study the dynamics of the fluorescence probe, incorporated into the headgroup or the acyl-chain region of the monolayer [Chat, 1999a], which would further elucidate the effects of changed hydration, in substrate-supported lipid monolayers.

6 Characterisation of polymer-supported phospholipid bilayer membranes

The thin polysaccharide films, prepared and characterised as described in chapter 4, were used to cushion phospholipid monolayers as outlined in chapter 5. This experimental configuration was advantageous for a detailed physicochemical investigation of the properties of the membrane/support interface, which would have been too complicated in case of lipid *bilayers*. Clearly, the supported lipid bilayer, however, being surrounded by a water-rich environment at both surfaces, is the membrane state representing the target structure with respect to a suitable (model-) environment for membrane proteins. The present chapter therefore deals with properties of lipid bilayer membranes, deposited mainly onto agarose (chapter 6.1) and chitosan films (chapter 6.2). As pointed out in the previous chapters, the present work focuses on physisorbed membranes, which allows for the analysis of membrane/support interactions in a more straightforward manner, as compared to partially chemically tethered membranes. Since a chemical fixation is absent, the stability of the substrate-supported membrane is determined by the spreading parameter, S, which is calculated from the interfacial energies, γ, of the surfaces indexed in (6.0.1).

$$S = \gamma_{polymer,water} - (\gamma_{polymer,lipid} + \gamma_{lipid,lipid} + \gamma_{lipid,water}) \qquad \textbf{(6.0.1)}$$

The spreading power, S, has to be positive in case of a stable membrane. Since $\gamma_{polymer,water}$ in case of a highly hydrated polymer cushion is on the same order as $\gamma_{water,water}$, which is zero, the spreading power is expected to be small or even negative [Kühn, 1994]. On the other hand, the stability of monolayers on a hydrated polymer support is much higher compared to bilayers, since in that case

$$S = \gamma_{polymer,vapour} - (\gamma_{polymer,lipid} + \gamma_{lipid,vapour}) \qquad \textbf{(6.0.2)}$$

and $\gamma_{polymer,vapour}$ is of the same order as $\gamma_{water,vapour}$. Therefore the spreading power is positive. While the polymer-cushioned lipid monolayers, prepared and analysed as described in chapter 5 were homogeneous and stable under all conditions, the deposition of a second monolayer is a critical step, which – according to (6.0.1) – may be followed by membrane decomposition. Even in case of a positive spreading coefficient, the membrane/substrate interaction may be considerably reduced by a disjoining pressure due

to undulations, i.e. thermally driven collective out-of-plane movements of the bilayer membrane [Helf, 1978], [Sack, 1997],

$$P_{und} = \frac{3}{4}\frac{kT}{K_c d^3} \qquad \textbf{(6.0.3)}$$

where P_{und} is the disjoining pressure due to undulations, k is Boltzmann's constant, T is the temperature, K_c is the bending modulus of the bilayer and d the membrane/substrate distance.
In the following, fluorescence microscopy is applied to study bilayer membrane quality and successful preparations were further characterised.

6.1 Lipid bilayer membranes supported by agarose cushions

As outlined in chapter 4, agarose was used extensively to cushion lipid bilayers, which were prepared by the thinning of a lipid solution, which was painted across a small aperture. It was first found by Hongyo et al. [Hong, 1987] that freely suspended bilayer lipid membranes (classical BLMs, [Muel, 1962], [Howa, 1968], [Gold, 1970]) can be stabilised by supporting them with the help of a soft and hydrated agarose cushion. Interestingly, these agarose-supported BLM-like membranes (i.e. lipid membranes coupled to a solvent-enriched lipid reservoir formed in an aperture, see chapter 2) possess electrical properties, which are comparable to those found for free standing BLMs [Hong, 1987], [Lu, 1996], [Uto, 1994], [Zieg, 1998], [Novo, 1997]. It was shown in [Ide, 1999] that agarose-cushioned lipid bilayers allow for the analysis of single ion channels, incorporated into the membrane. In case of other polymer-supported bilayer systems, however, often electrical properties were found which remarkably differ from free-standing BLMs, ([Lind, 1996], [Sinn, 1999], [Cass, 1999], [Jenk, 2000]) which are regarded as a reference in terms of an electrically "perfect" membrane. The following chapter is meant to contribute to the understanding of these discrepancies. Therefore, in the next part, these black-lipid-membrane-like agarose-cushioned bilayers will – as preliminary experiments – be analysed with respect to homogeneity, stability and lateral fluidity. Afterwards, bilayer lipid membranes prepared by LB-methods, which lead to better-defined membranes, will be prepared and examined and the two approaches will be compared.

6.1.1 Preliminary experiments

A variety of setups for agarose-cushioned lipid bilayers were used in the past. These include an agarose filled hole, drilled into a PMMA sheet [Hong, 1987], the use of a teflon or polypropylene foil with a small circular aperture to separate an agarose film compartment from an aqueous compartment [Uto, 1994], [Novo, 1997], [Ide, 1999] or two agarose sheets separated by a thin teflon film with a small opening [Cost, 1998], [Cost, 1999].

Probably the simplest setup was introduced in [Lu, 1996]. It basically consists of a teflon tube, which is filled with a hot agarose/buffer solution. Upon cooling, agarose forms a gel (see chapter 8.1.2 for details). Afterwards, the tube can be cut into convenient pieces by means of a sharp knife. The preparation of a polymer-supported BLM is preceded by the formation of a lipid reservoir, which is simply accomplished by dipping the agarose-filled tube into a lipid solution, followed by brief drying. The tube is then ready to use and BLMs can be produced by established techniques [Gold, 1970].

In the present work, initial experiments were carried out with the help of a similar setup, which is depicted in Figure 6.1.

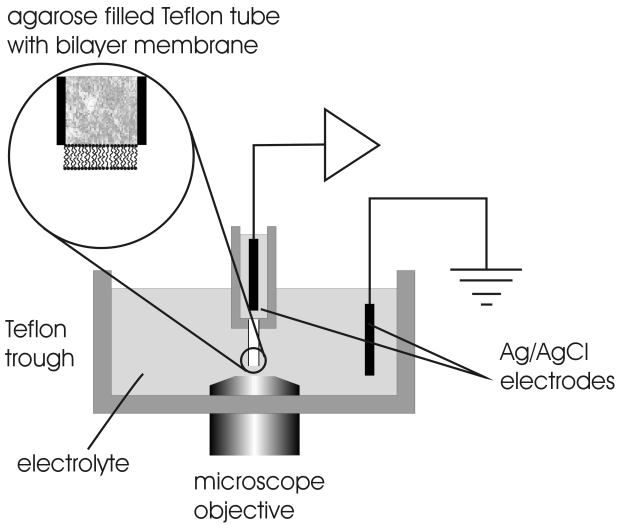

Figure 6.1: Schematic picture of the setup, which was used for initial experiments on polymer-supported bilayer lipid membranes (BLMs). The bilayer membrane is shown schematically, in reality the bilayer rims are connected to a solvent enriched lipid reservoir.

By means of this experimental configuration, fluorescence microscopy could be applied to analyse the bilayer. It could be shown, by staining the lipid solution with the fluorescence probe DiI, that polymer-supported BLMs were homogeneous, at the resolution of the classical fluorescence microscope (Figure 6.2). The formation (thinning) of the bilayer from a lipid solution deposited onto the tip of the agarose filled Teflon tube was monitored

by applying TTL (square-wave)-pulses to the membrane. Thinning was indicated by the broadening of capacitive spikes [Zieg, 1998]. FRAP experiments indicated, that the bilayer was in a fluid state and that the fluidity was barely reduced by the presence of the polymer cushion: a diffusion coefficient D = 4.7 $\mu m^2/s$ and a complete fluorescence recovery was found. It must be noted, however, that BLMs, which are prepared from a hydrocarbon solution, still contain a considerable amount of solvent.

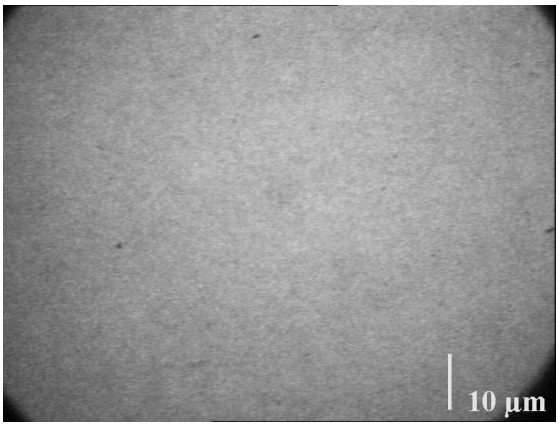

Figure 6.2: Fluorescence image of an agarose-supported BLM (lipid: asolectin), prepared in an agarose filled teflon tube. For details of the setup see Figure 6.1.

Therefore, a quantitative comparison with FRAP experiments which were carried out with solvent free bilayer membranes (e.g. [Vaz, 1985]) is not possible.

While BLMs have favourable electrical properties, a gross disadvantage is their small lifetime, which is usually in the range of minutes to some hours [Gold, 1970]. The low lifetime is assumed to be a result of the surface tension between water and membrane [Flor, 1993], which tends to minimise the area of the film and therefore increases the probability of hole formation. Another reason for the instability of free-standing BLMs is their sensitivity against mechanical distortions. On the other hand, a polymer support should reduce surface tension on one side of the membrane and should additionally suppress pressure gradients due to mechanical distortions.

It was observed in the present work that while the presence of an agarose cushion significantly enhanced the stability of the polymer-supported membrane against mechanical distortion with respect to a freely suspended BLM, the long-term stability was not improved at all. Additionally it was observed that the breakdown of the thinned bilayer did not proceed in a stepwise fragmentation, but in a more or less instant dewetting, as indicated by the fact, that the fluorescence intensity on the agarose cushion was lost almost completely, upon film rupture. The low bilayer lifetime and the fact that an almost instant, nearly complete dewetting accompanied membrane rupture is in contrast to films which were prepared by a LB/LS deposition onto other polysaccharides like dextran [Elen, 1996]

and cellulose [Hill, 1999]. In those cases, membrane lifetime in terms of a homogeneous fluorescence picture was in the range of weeks [Elen, 1996].
The goal of the next part of the present work therefore is the evaluation of the possibility, to deposit bilayer membranes onto agarose cushions by LB/LS transfer, as described in chapter 3.10.3. Subsequently, the membranes were analysed and possible routes for a stabilisation on agarose cushions were evaluated.

6.1.2 Bilayer lipid membranes on agarose cushions, deposited by LB/LS transfer

The possibility to deposit two phospholipid monolayer membranes subsequently, by LB/LS-transfer to yield a stable polymer-supported bilayer membrane, was demonstrated by examining the lateral pressure on the LB-trough upon deposition of the second monolayer (Figure 6.3).

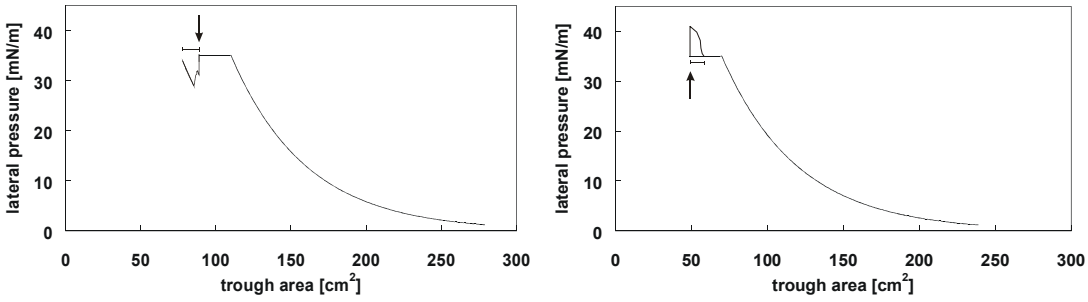

Figure 6.3: Left: trough-area/pressure isotherm of a successful transfer of a second phospholipid monolayer onto a pre-deposited polymer-cushioned LB-film. The successful transfer expressed itself by a decrease of the trough area after transfer. Right: trough-area/pressure isotherm of a non-successful transfer of a second phospholipid monolayer onto a pre-deposited polymer-cushioned LB-film. The coming off of lipid material is shown by an increase of trough area after the LS-transfer (indicated by the arrow).

In Figure 6.3, trough-area/pressure isotherms are shown, which indicate the compression of the bilayer to the target pressure, the reduction of trough area due to deposition of a monolayer at a constant transfer pressure of 35 mN/m and the area changes upon performing an LS-transfer (at a trough area indicated by the arrow). A successful deposition of a second monolayer was indicated by a decrease of the trough area (Figure 6.3, left), while an unsuccessful transfer was indicated by an area increase (Figure 6.3, right), due to the removal of lipid from the substrate. Generally, successful LS-transfers onto polymer-cushioned lipid monolayers could only be performed by drying the substrate after deposition of the first monolayer in a stream of dry nitrogen gas. Omitting this drying procedure led to a floating off of the bilayer from the substrate. In [Lind, 1996], it was pointed out that a drying period of 30 – 45 min after the first monolayer transfer was

essential. Another group even reported the failure of LS-transfer onto a lipid monolayer, supported by a polyethylenimine layer [Wong, 1999a]. Obviously, as indicated by (6.0.1) and (6.0.2), the LS-transfer to yield a supported bilayer is a critical step and the proximal monolayer (i.e. the monolayer facing to the polymer film) must be in a sufficiently adsorped state in order to allow for a successful deposition of the distal monolayer. A successful transfer of both bilayer leaflets could also be followed by fluorescence microscopy. The left part of Figure 6.4 shows a homogeneous lipid bilayer prepared from the natural lipid mixture asolectin [Zieg, 1998], directly after the transfer. However, during storage over night at 25 °C, the deposited membrane decomposed and membrane buds and single vesicles, still adhering to the agarose surface were observed. They appear in the right part of Figure 6.4 as bright spots, with the rims showing an increased fluorescence, stemming from a higher amount of dyes due to the curvature of the membranes.

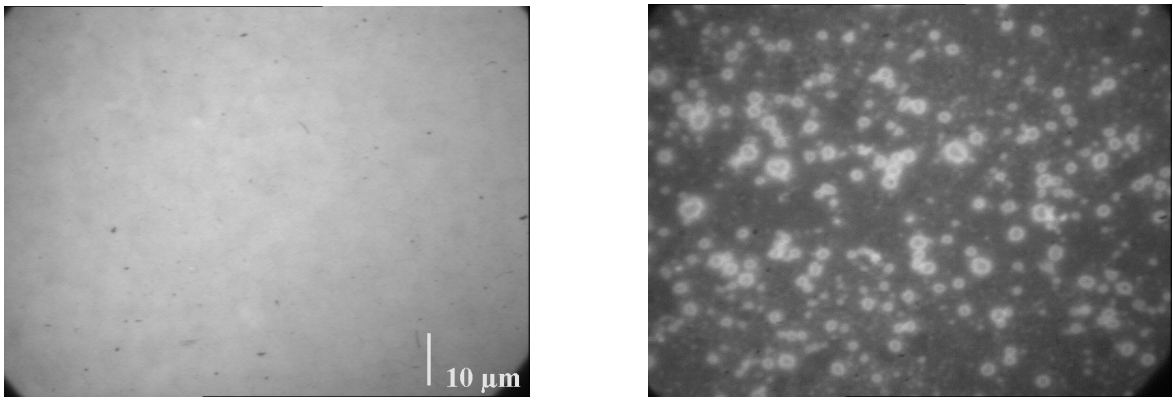

Figure 6.4: Fluorescence images of asolectin bilayer membranes on agarose prepared by LB/LS transfer (lateral pressure 35 mN/m, deposition temperature 25 °C), fluorescence dye: DiI. Left picture: directly after preparation, right picture: after storage over night at 25 °C.

The membrane decomposition was probably due to high amplitude undulations (see (6.0.3)) of the membrane which led to membrane budding, membrane rupture and to the formation of vesicles [Sack, 1997], [Elen, 1996].

Asolectin is a complex, naturally occurring mixture of several different lipids. In order to analyse lipid/polymer interactions more specifically, pure synthetic lipids were used.

While asolectin bilayers initially appeared to be perfectly homogeneous under the view of the classical fluorescence microscope (Figure 6.4, left), DMPC bilayers were always slightly structured (Figure 6.5, left), which indicates a partial fragmentation of the membrane. However, lipid bilayers consisting of the same compositions, deposited onto glass supports, always were found to show a perfectly homogeneous fluorescence and this condition did not change with time. The increased lateral structuring of agarose-supported bilayers is also in contrast to agarose-supported monolayers. This may be explained by a

small spreading coefficient of the supported bilayer (6.0.2), in combination with a laterally inhomogeneous substrate [Kühn, 1994].

Rather often, in addition to the structuring shown in the left part of Figure 6.5, an additional pattern was found which consisted of parallel bars, oriented perpendicular to the direction along which the substrate was pulled out of the subphase while performing the LB-transfer (Figure 6.5, right part). A similar pattern was found in [Spra, 1994a], in case of monolayers transferred at a lateral pressure slightly below the main phase transition of the monolayer. A substrate mediated condensation was assumed to cause a physisorption instability during withdrawing the sample from the subphase, leading to an alternating deposition of lipid in a more condensed and in a more expanded state. A similar process is likely to cause the morphology observed in the present case, since LB-transfer of a DMPC monolayer at a lower temperature (15 °C), which corresponds to a value below the main phase transition temperature (at the particular lateral pressure of 35 mN/m) did not lead to stripes.

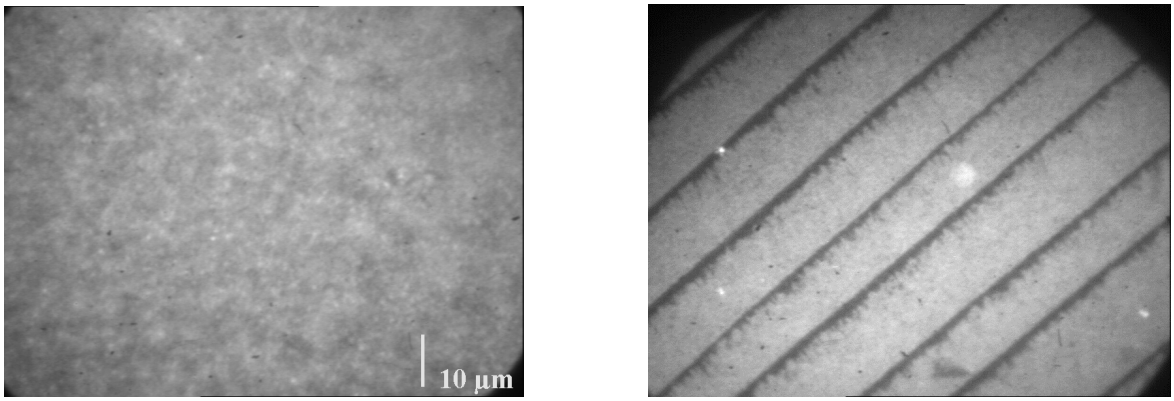

Figure 6.5: Fluorescence images of a DMPC bilayer membrane prepared by LB/LS transfer (lateral pressure 35 mN/m, deposition temperature 25 °C), fluorescence dye DiI, directly after transfer. Both structures were found on the same substrate, the bars seen in the right picture have an orientation orthogonal to the drawing direction during LB-transfer.

The deposition of a second monolayer onto the proximal, structured monolayer could then cause the formation of a discontinuous bilayer in terms of bilayer bars, separated by small, non-fluorescent stripes of the bear substrate surface. Such a partial dewetting process could be explained by the fact that a bilayer membrane possesses an optimum lateral pressure [Pink, 1983], leading to a resistance towards lateral stretching [Crem, 1999]. The same stretching resistance could be a driving force for the dewetting or decomposition of a bilayer, which was prepared from a monolayer with low lateral pressure, due to the physisorption instability mentioned above.

During storage, a surprising rearrangement of the membrane took place. Both in the regions shown in the left and in the right part of Figure 6.5, the development of large bright spots was observed. Two examples are shown in Figure 6.6. From this figure, the

following facts can be stated: the almost circular spots developed after LB/LS transfer.

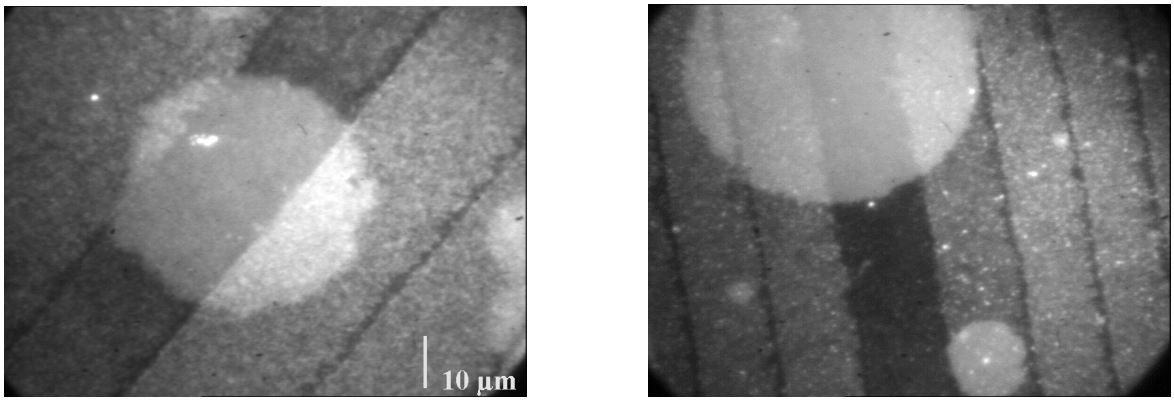

Figure 6.6: Fluorescence images demonstrating a structural rearrangement of a DMPC bilayer, with a patterning shown in Figure 6.5.

Accompanying the development of a spot was the loss of fluorescence in a bar. The spots seemed to grow by incorporating molecules from the bar. Lipid molecules forming a single bar appeared to be laterally connected, while different bars were not connected. The latter is indicated by the fact that always only the bar including the centre of a spot lost its fluorescence intensity.

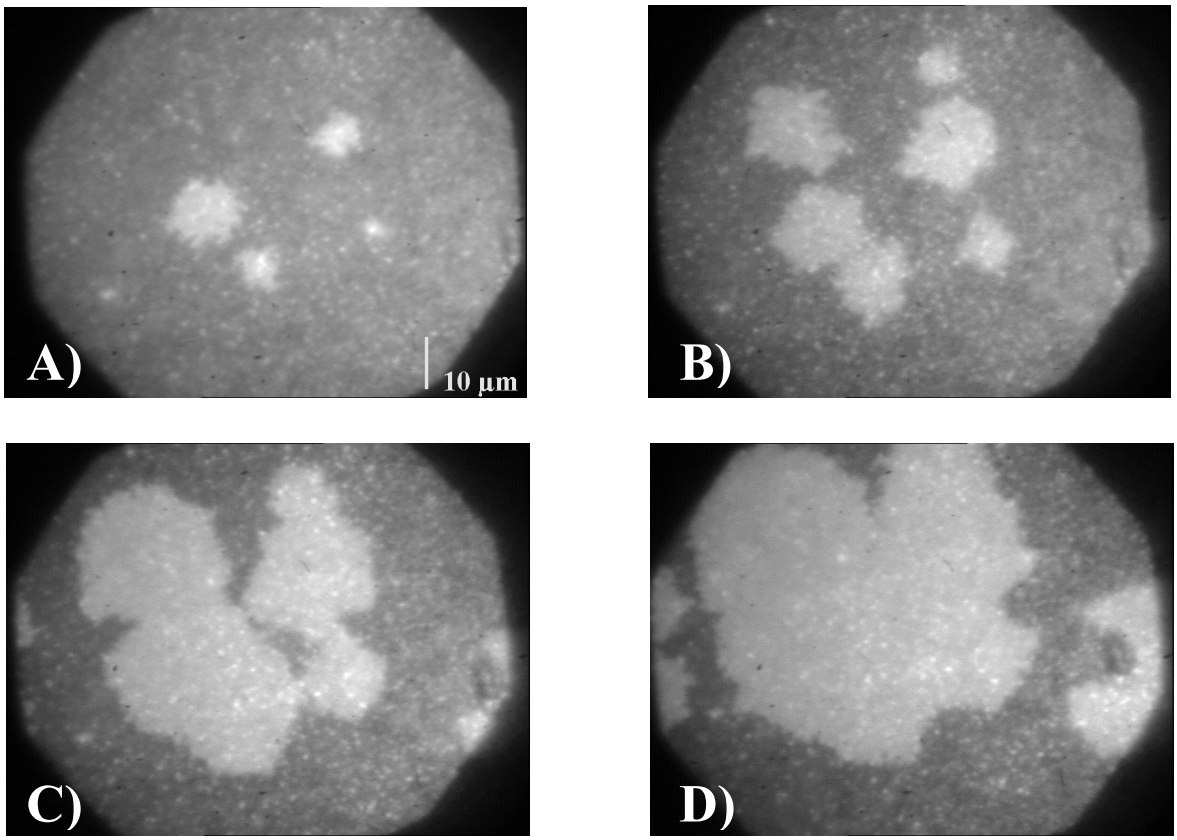

Figure 6.7: Time sequence of a structural transition found in DMPC bilayer membranes on agarose, B): 30 min after picture A), C): 90 min after A), D): 150 min after A).

The spots had a more homogeneous appearance than bars, however, heterogeneous fluorescence stemming from a bar was still visible, after a spot had grown up to a diameter increasing the width of a single bar. In fact, fluorescence of a spot seemed to be added to that of a bar, yielding an increased fluorescence intensity in locations where both patterns can still be observed.

The growth kinetics of the structural rearrangement were analysed in regions which did not show the bar-like pattern. An example of such a growth process is shown in Figure 6.7. The transition from Figure 6.7 A) to D) took place in 150 min. After storage over night, the new feature covered large areas of the substrate (in some cases hundreds of micrometers in diameter).

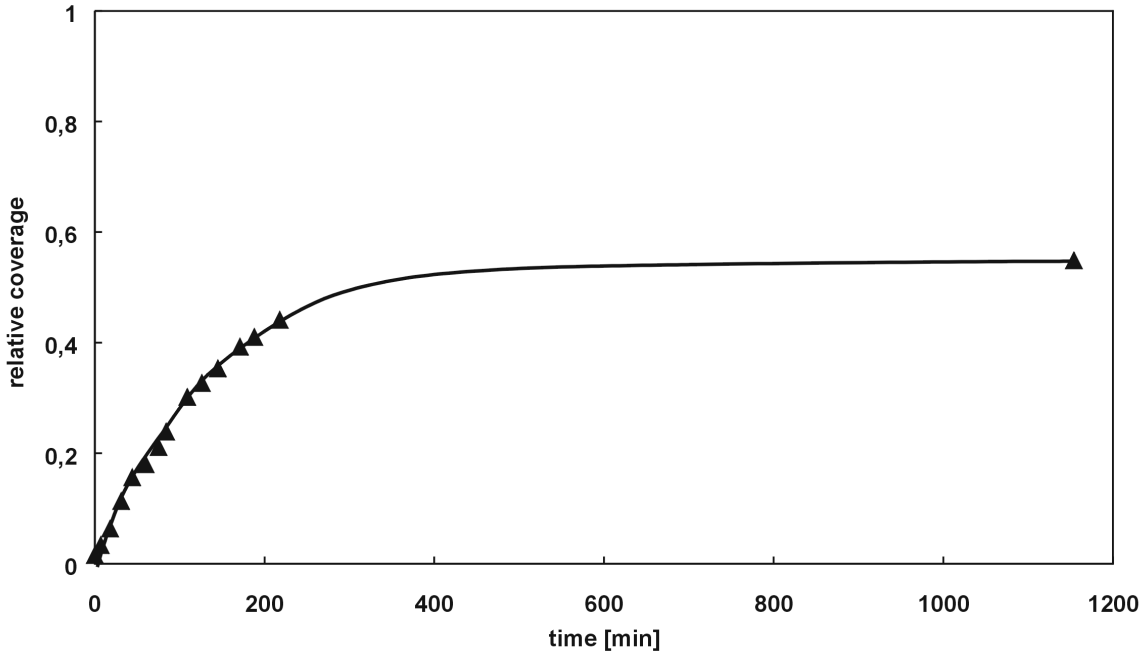

Figure 6.8: Kinetics of the structural transition demonstrated in Figure 6.7, at a temperature of 25 °C.

The spreading kinetics were analysed in more detail by converting the fluorescence pictures to binary pictures by thresholding (with the help of an image processing software), and determining the relative coverage area. Such an investigation was carried out for two different temperatures (25 °C and 40 °C). At the lower temperature, the transition was observed (see Figure 6.8).

The increased homogeneity of the fluorescence images in the later stages of the transition process could additionally be demonstrated by a considerable decrease of the width of the image histogram.

At the temperature of 40 °C, however, the situation was remarkably different. No structural transitions as shown above were observed. Instead, the initially grainy structure right after

transfer became more heterogeneous, large vesicles formed, which eventually left the surface (see Figure 6.9).

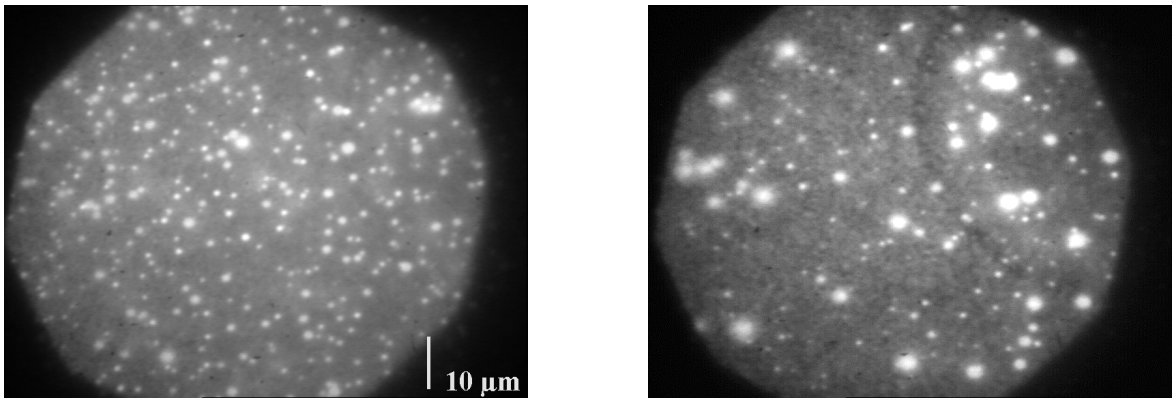

Figure 6.9: Fluorescence images of DMPC bilayer membranes, deposited by LB/LS-transfer at a lateral pressure of 35 mN/m and a deposition temperature of 25 °C, observed at a temperature of 40 °C. Left picture: directly after heating up to 40 °C, right picture: the same location on the sample, 2.5 h later. Note: the total number of bright spots was reduced while the remaining spots partially grew with time.

In order to clarify, whether the supporting surface had an influence on the possibility to observe the structural transitions mentioned above, an LB/LS deposition onto a gold-supported agarose cushion was carried out. In case the above transition could be regarded as a floating of the bilayer from the polymer cushion onto the underlying support, through a defect in the former, then on gold the fluorescence would be quenched considerably [Kuhn, 1970], [Ende, 2000]. Should on the other hand the transition have taken place on top of the polymer cushion, then there should be no disturbance of the fluorescence pattern by the gold support. In case of a gold-supported agarose cushion, exactly the same pattern as in the right part of Figure 6.5 was found (data not shown). However, a structural transition as shown in Figure 6.6 could not be detected.

The only reasonable explanation for the transitions in the fluorescence pictures as observed at 25 °C, is a spreading of a lipid bilayer directly on the glass surface, through local defects in the polymer cushion. The hypothetical result of such a transformation is shown schematically in Figure 6.10. This assumption is supported by a) the higher homogeneity of the layer after the transition, b) the fact that the initial structure could still be seen „through“ a homogeneous spot, this indicates that either structure is located at a different height, c) that no spots were observed on gold-supported agarose cushions, d) the observation that FRAP experiments yielded lower diffusion coefficients and reduced recoveries for the more heterogeneous structure (D = 0.29 ± 0.052 µm^2/s, R = 98 ± 1.4 % in the homogeneous case and D = 0.067 ± 0.126 µm^2/s, R = 52 ± 4.8 % in the more heterogeneous regions). Both latter values indicate a fragmented bilayer for the heterogeneous structure. Therefore the diffusion coefficient in that case can only be

regarded as an apparent one (note that the evaluation of *D*-values is based on the assumption of a completely circular diffusion geometry and a homogeneous, infinite diffusion reservoir).

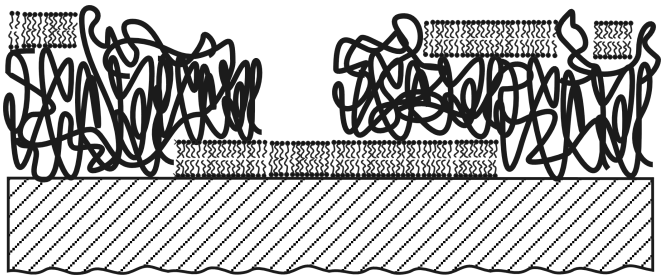

Figure 6.10: Hypothetical schematic representation of the membrane patches observed by fluorescence microscopy, as shown in Figure 6.6 and Figure 6.7. A homogeneous membrane patch is formed by bilayer spreading on the glass support through local defects in the polymer cushion. The bilayer on top of the agarose cushion is inhomogeneous, the hydrophobic rims of membrane defects are possibly stabilised by hydrophobic parts of the polymer strands.

As indicated above, no bilayer spreading onto the glass surface was observed at 40 °C. Undulation forces are strongly temperature dependent (compare (6.0.3)), therefore the membrane decomposition is likely to be faster than spreading onto the glass support.

6.1.3 Concepts to stabilise bilayer lipid membranes on an underlying support

The results mentioned above showed that bilayer lipid membranes on agarose cushions were unstable, which explains the low lifetime of agarose-cushioned BLMs (chapter 5.1.1). The following chapter will therefore introduce concepts to increase the bilayer/substrate interaction. On the one hand such a stabilisation could be performed by chemically coupling the monolayer to the substrate. On the other hand, at least a fraction of the membrane lipid molecules should be in a merely physisorbed state, in order not to suppress membrane fluidity too drastically, which is favourable for the functioning of membrane proteins. Therefore, the next part will deal with increasing the physisorption of bilayer membranes prepared by LB/LS-transfer. The relevant interactions have been introduced in chapter 5.0.1. They are namely: the DLVO forces (van der Waals and electrostatic), hydration forces and undulation forces, among others. The concepts to stabilise bilayers used in the present work are: a decreased deposition temperature, addition of cholesterol, the use of charged lipids and embedding of the bilayer between two polymer cushions.

Decreased deposition temperature

An LB/LS deposition at a decreased temperature of 15 °C, which is below the main phase transition of an unperturbed DMPC bilayer (23.8 °C), slightly increased initial bilayer quality (compare the left parts of Figure 6.5 and Figure 6.11). The hydration force and membrane undulations are repulsive forces, which decrease with temperature, since they are due to thermally excited collective or individual out-of-plane motions of membrane lipids.

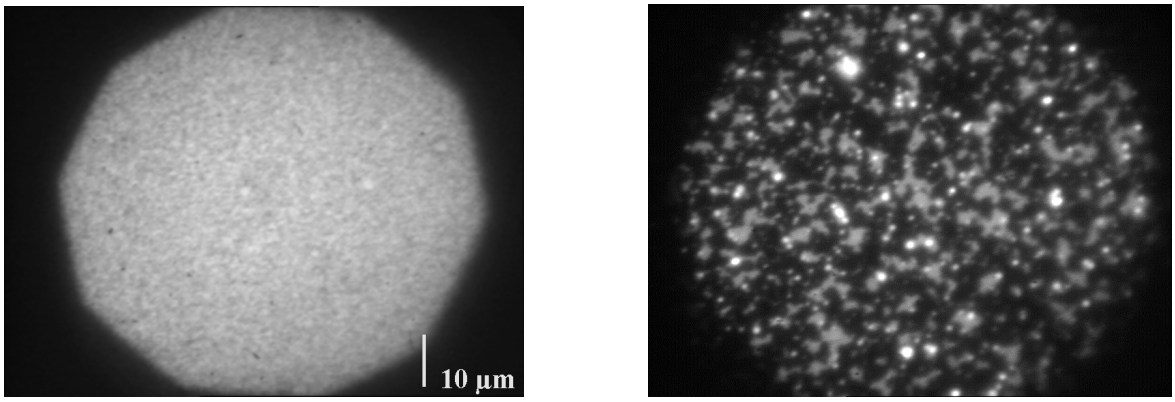

Figure 6.11: DMPC bilayer on agarose, deposited by LB/LS transfer at a lateral pressure of 35 mN/m and a deposition temperature of 15 °C. Left picture: directly after deposition, right picture: after storage over night at 25 °C.

However, bilayers deposited at a reduced temperature also decomposed at a storage above the main phase transition temperature of the bilayer. As shown in the right part of Figure 6.11, after storage over night at 25 °C, vesicles still adhering to the agarose surface, planar membrane fragments and dewetted areas could be observed.

Addition of cholesterol

One way to decrease the disjoining pressure contribution due to undulations is to reduce temperature. This, however, is unfavourable because lateral fluidity could be reduced by phase transitions in the bilayer, due to a decreased temperature. A second approach is the addition of cholesterol. Its influence on the elastic properties of bilayers is well known [Sack, 1997] and in fact it has been found [Kühn, 1994] that homogeneous bilayers on planar dextran cushions could only be obtained, if the membrane contained a considerable amount of cholesterol. The latter observation was explained in [Kühn, 1996a] by a), a reduction of undulations, and b), by an interaction of the polar OH-group of the cholesterol molecule with the underlying polysaccharide surface. Cholesterol additionally compresses the membrane considerably, which is favourable for the electrical tightness of the bilayer [Grit, 1998]. However, in the case of agarose-cushioned lipid bilayers, the addition of cholesterol to DMPC membranes did not improve bilayer quality. Instead, directly after

deposition at a temperature of 15 °C, large vesicles were observed on the surface and in the surrounding medium beneath the supporting surface (Figure 6.12). However, the comparison of Figure 6.12 with Figure 6.11 reveals, that the non-dewetted areas in the case of cholesterol containing bilayers are much more homogeneous compared to bilayers without cholesterol.

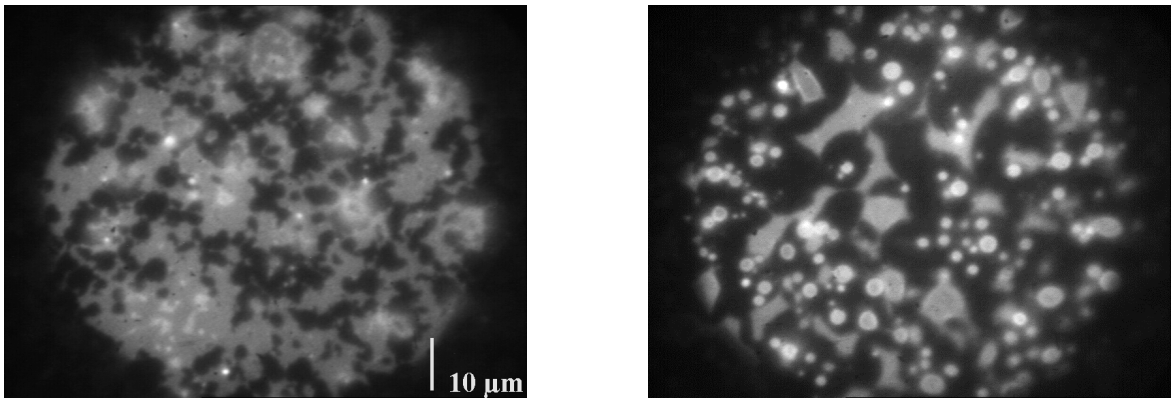

Figure 6.12: Fluorescence images of DMPC (30 mol% cholesterol) bilayer preparations on agarose cushions. Deposition temperature and observation temperature in both pictures: 15 °C. Left picture: directly after transfer, right picture: 10 min after transfer (different location on the same sample as compared to the left picture).

In the case of bilayers containing cholesterol, however, vesicle budding and fission was observed already at the deposition temperature of 15 °C. This can be explained by the influence of cholesterol on the phase transition temperature of the bilayer. At 15 °C, a DMPC bilayer is in the liquid condensed state, while for a cholesterol content above 30 mol%, no transition to the liquid condensed state is found [Alme, 1992]. Another reason for an increased dewetting tendency upon addition of cholesterol is the comparably high roughness of the polymer cushion (see chapter 4.2). While a bilayer with a low bending modulus could embed itself into a rough surface structure, this becomes more difficult for a bilayer with an increased bending modulus (as in the case of cholesterol-containing bilayers). The result would be a decreased contact area and hence, a decreased sticking of the membrane to the support.

Embedding of the bilayer between two polymer cushions

Another strategy for membrane stabilisation is to prepare a bilayer in a sandwich configuration, which has successfully been accomplished by [Cost, 1998], [Cost, 1999] with a painted type of bilayer membrane. In the present work, sandwiched bilayers were prepared by LB-transfer of monolayers onto two agarose substrates while taking care that the polymer cushions did not dry (by storage in a high humidity atmosphere). Both substrates were then pressed against each other to form a bilayer embedded between two sheets of agarose.

Large areas with a completely homogeneous appearance were found. However, as can be seen in Figure 6.13, there were also parts, which could refer to a collapsed bilayer. The membrane was found to be fluid and did not change appearance during storing over several hours at 25 °C.

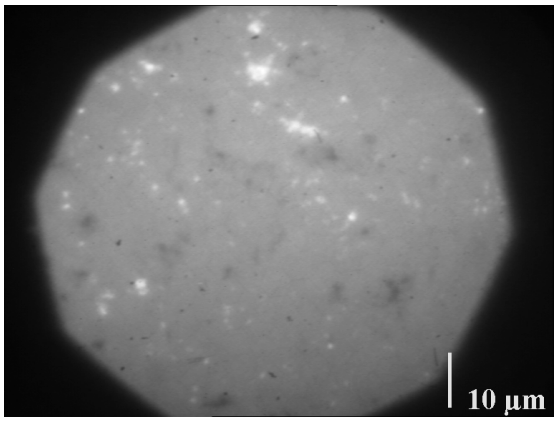

Figure 6.13: DMPC bilayer membrane, obtained by deposition of monolayers onto two different polymer cushions and pressing both monolayers against each other in an atmosphere with increased humidity.

The membrane stabilisation in a sandwich configuration is due to the strong damping of membrane undulations caused by the polymer cushions on both sides of the membrane.

Electrostatic coupling

Besides the reduction of repulsive membrane/substrate interactions, as described above, the attractive interactions may be increased by increasing the electrostatic forces.

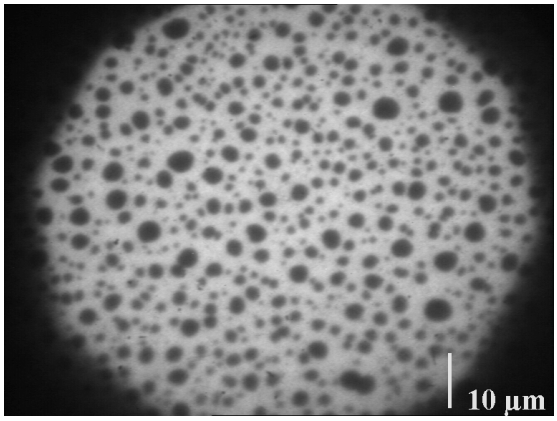

Figure 6.14: DMPC bilayer membrane on agarose, stained with 10 mol% of the fluorescence probe DiI (positively charged).

The fluorescence probe DiI, which was used for all fluorescence experiments with agarose-supported membranes, is positively charged. Agarose on the other hand, is slightly negatively charged, due to partial coupling of OH-groups to sulfate residues [Izum, 1973].

The fact that the deposition of NBD-PE stained bilayers (NBD-PE is negatively charged) was not possible [Diet, 1999], already hints to an electrostatic coupling of bilayer and support in the case of a positively charged fluorescence probe. In an initial experiment to examine this possibility, a membrane stained with 10 % DiI was transferred onto agarose. The result is shown in Figure 6.14. On the one hand, circular non-fluorescent spots were found, which appear to be a result of a phase separation and fluorescence self-quenching. The dark spots then would be probe-enriched areas. On the other hand, the remaining, possibly probe diminished areas were much more homogeneous, compared to the membrane shown in Figure 6.5.

In order to avoid quenching processes due to high probe concentrations, a purely positively charged bilayer membrane was deposited, consisting of the synthetic lipid DHDAB. The possibility of this lipid to form bilayers even when the pure lipid is used, is well documented (e.g. [Okah, 1981]). Figure 6.15 shows an example of a DHDAB bilayer, transferred onto agarose. The bilayer appeared totally homogeneous right after deposition and did not change appearance during storage over night at 45 °C, which is above the main phase transition of DHDAB bilayers in the fully hydrated state (28 °C, [Okah, 1981]). FRAP experiments indicated a considerably reduced fluidity – expressed by a small diffusion coefficient D and a small relative recovery R ($D = 0.12 \pm 0.017$ μm^2/s, $R = 66 \pm 11.7$ % at 45 °C), which may be compared to DMPC bilayers on glass supports ($D = 3$ μm^2/s and $R \sim 100$ %, at a temperature of 45 °C [Merk, 1989]).

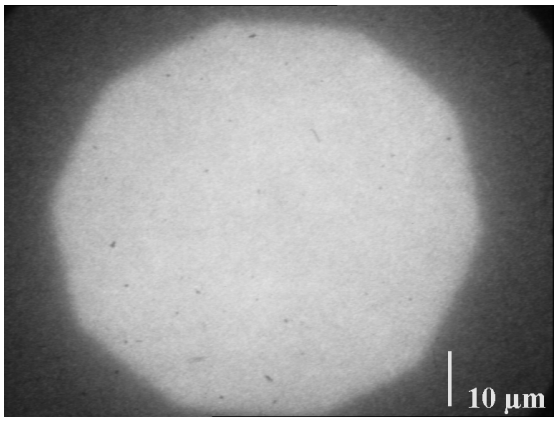

Figure 6.15: Fluorescence image of a DHDAB bilayer membrane, deposited at a lateral pressure of 35 mN/m and a deposition temperature of 15 °C. The homogeneous picture did not change appearance, even during prolonged heating at 45 °C.

The addition of cholesterol (which is a favourable membrane component, as has been mentioned above) to DHDAB, however, led to a considerable distortion of bilayer homogeneity, as shown in Figure 6.16 for two different cholesterol contents.

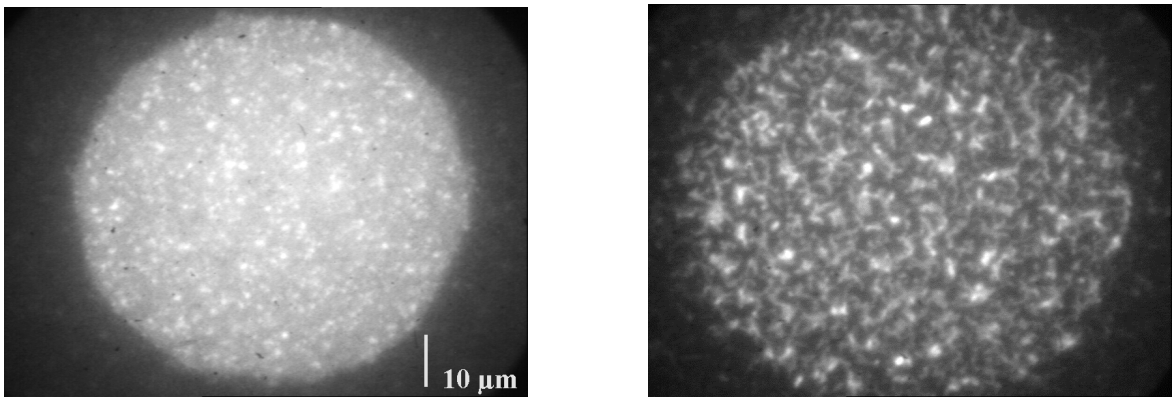

Figure 6.16: DHDAB bilayer membranes with an additional amount of cholesterol. Left picture: 5 mol%, right picture: 20 mol%.

In this case, no vesicles were observed to leave the surface. The increased inhomogeneity therefore was likely due to a demixing problem.

6.1.4 Interaction of the agarose surface with multilamellar giant liposomes

In order to analyse the interaction between bilayer phospholipid membranes and agarose further, giant multilamellar liposomes were prepared as described in chapter 3.10.5 and added to the aqueous phase into which an agarose film was immersed. With the results of the preceding chapters in mind, a strong adhesion of liposomes to the agarose surface could not be expected.

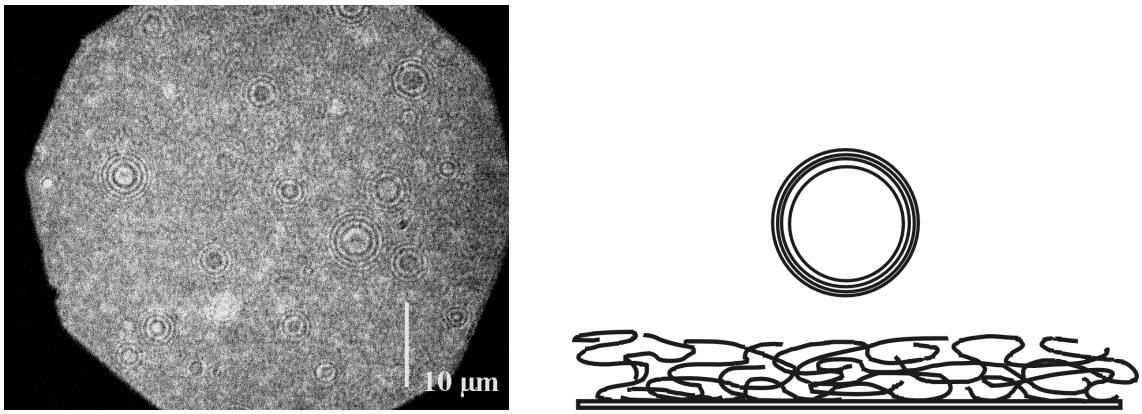

Figure 6.17: RICM image of DMPC vesicles hovering over an agarose surface (left), schematic drawing of a giant, multilamellar vesicle, hovering over the polymer surface.

Indeed it was found by reflection interference contrast microscopy (see chapter 3.3) that liposomes were hovering over the agarose surface (Figure 6.17, right part). Fast changes in height and position were found, due to thermally activated movements of liposomes [Rädl, 1992]. Height fluctuations were observed by changes in the interference fringes shown in

Figure 6.17. The thermal energy seemed to be high enough to compensate for any attractive force between polymer and bilayer membrane, because in no case an adhesion of giant liposomes to an agarose surface was observed.

6.1.5 Vesicle fusion experiments on agarose

In order to test the hypothesis stated in chapter 6.1.2 (lipid bilayers of neutral phospholipids are unstable and can float – through small defects in the polymer cushion – onto the glass support) vesicle fusion experiments were carried out.

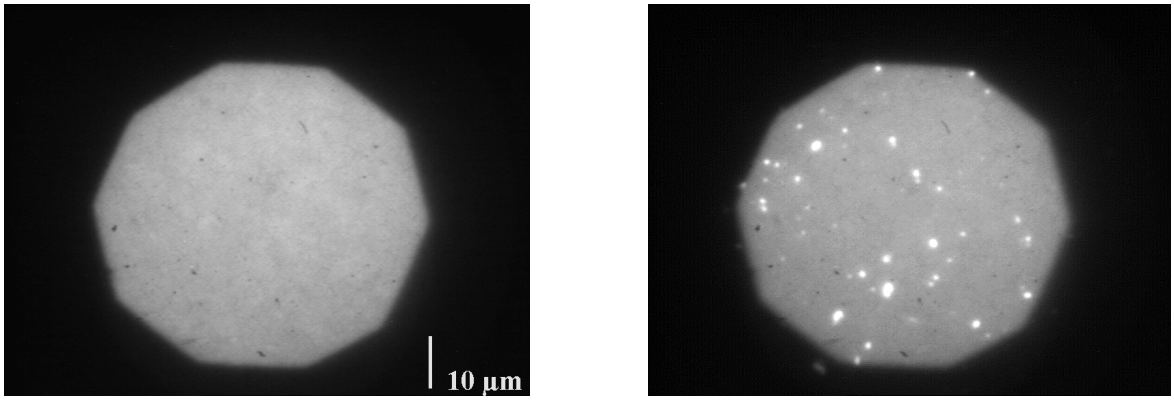

Figure 6.18: Fluorescence images of a vesicle fusion experiment of DMPC-SUVs on agarose, the substrate was exposed to a vesicle dispersion at 30 °C over night. Left part: dominating, completely homogeneous appearance of the sample, right part: at some locations brightly shining circular spots were found.

Vesicle fusion was performed with small unilamellar vesicles (SUVs) consisting of DMPC, at a temperature of 30 °C, over night. Afterwards, the vesicle dispersion was removed and the sample was rinsed with MilliQ-water (while avoiding any contact of the substrate with air). The result was a completely homogeneous fluorescence image on almost all positions of the substrate. Only seldom, circular spots were found (see Figure 6.18). The bright spots observed in the right part of Figure 6.18 are most likely vesicles, which were formed by the fusion of SUVs. They possibly still adhere to the agarose surface, due to an incomplete rinsing procedure. In order to test the lateral fluidity, FRAP experiments were carried out. As depicted in Figure 6.19, the fluorescence recovery after photobleaching was rather low (approximately 10 %). Additionally, an unusually high fluorescence intensity was found. However, when bleaching in the same area for a second time, fluorescence recovery was much higher. The fitting parameters D and R (D = 0.57 ± 0.116 µm^2/s and R = 85 ± 5.3 %) were comparable to those found in chapter 6.1.2, for the case of the homogeneous part of a sample, which had undergone the structural transition, mentioned in chapter 6.1.2.

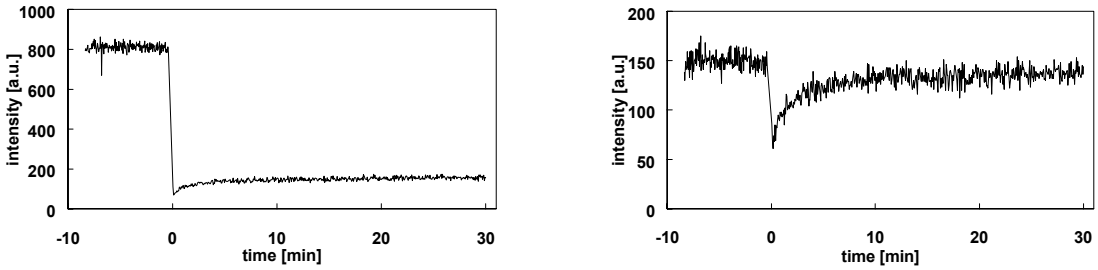

Figure 6.19: FRAP experiments performed with an agarose substrate, which had been exposed to a vesicle dispersion (see Figure 6.18). Left: initial bleaching, right: second bleaching at the same location as in the left part after recovery.

Moreover, the same spot could be bleached several times and an almost complete fluorescence recovery was observed in every case. The latter can hardly be explained by assuming adsorbed vesicles, which are partially located inside, and outside the bleachspot. If this would be the case, fluorescence intensity would decrease stepwise, after each bleaching experiment.

Instead, the latter observation is likely due to a laterally homogeneous bilayer resting directly on top of the supporting glass surface. The presence of a laterally connected bilayer resting on top of the polymer cushion can be assumed to be rather unlikely, since such a bilayer was shown to be unstable, as shown above. The additional fluorescence intensity, which could irreversibly be bleached, is most likely due to vesicles adhering to the agarose surface, which did not fuse to yield a laterally connected bilayer.

6.1.6 Spreading of lipid bilayer membranes from a lipid reservoir on agarose

Another expressive experiment concerning the analysis of membrane/support interactions are spreading experiments from a lipid reservoir [Rädl, 1995a], [Niss, 1999]. In the present work, the advancement of bilayers on agarose cushions was never observed (zwitterionic lipids were used in all cases). Moreover, after washing away the completely hydrated lipid reservoir, below its original position homogeneous spots of the same appearance as shown in Figure 6.7 were found. This again supports the finding, that a), bilayer membranes of uncharged phospholipids were not sufficiently stabilised by the agarose support and b), bilayers could float onto the supporting glass surface, through defects inside of the polymer cushion.

6.2 Lipid bilayer membranes supported by chitosan films

In the preceding chapter it was shown that physisorbed bilayer lipid membranes on agarose cushions were unstable, if the bilayer was made up of zwitterionic lipids. While bilayers on agarose cushions could be stabilised by a number of different approaches (chapter 6.1.3), chitosan is known to be able to coat the surfaces of liposomes consisting of zwitterionic lipids [Henr, 1994], [Henr, 1996], [Take, 1996], [Henr, 1997]. Additionally, it was shown in chapter 4.2 that by spin-coating, relatively smooth chitosan films could be prepared, with thicknesses over a wide range. Therefore the aim of the next part is the evaluation of the possibility, to prepare lipid bilayers on thin chitosan films by LB/LS-transfer. Furthermore, the bilayer/chitosan-interaction will be further analysed. Successful bilayer preparations were characterised in terms of homogeneity, lateral fluidity and electrical properties.

6.2.1 Homogeneity of bilayers

The quality of bilayer membranes was analysed by fluorescence microscopy. Two different probes were used to stain the membranes, at a concentration of 1 mol%. DiI is a positively charged amphiphilic probe, while NBD-PE is a negatively charged, labelled phospholipid.

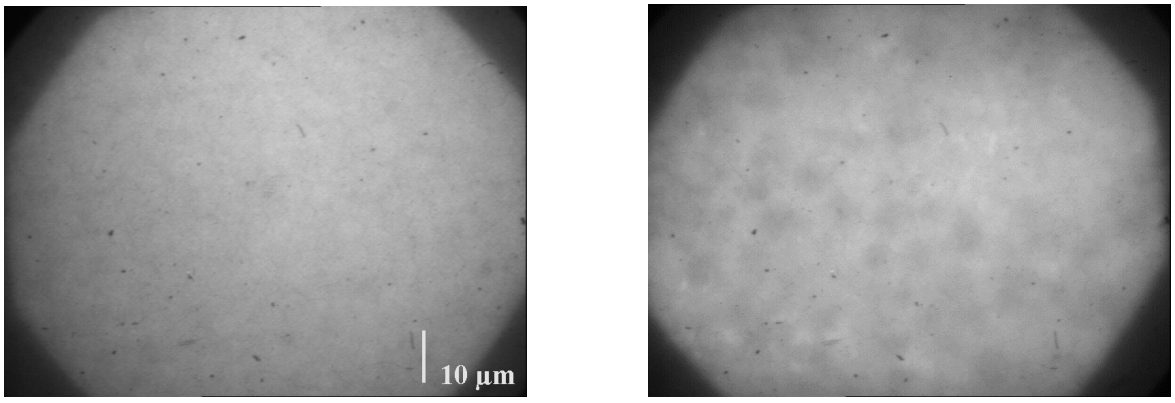

Figure 6.29: Fluorescence micrographs of DMPC bilayers, prepared by LB/LS transfer at a lateral pressure of 35 mN/m, deposition temperature: 15 °C. Left picture: fluorescence probe NBD-PE, right picture: fluorescence probe DiI. Pictures were taken at room temperature.

As can be seen in Figure 6.29, staining with DiI led to a slightly reduced bilayer homogeneity compared to membranes labelled with NBD-PE. This may be due to the fact that both DiI and the chitosan surface are positively charged (see chapter 8) which reduces attractive membrane/substrate interactions.

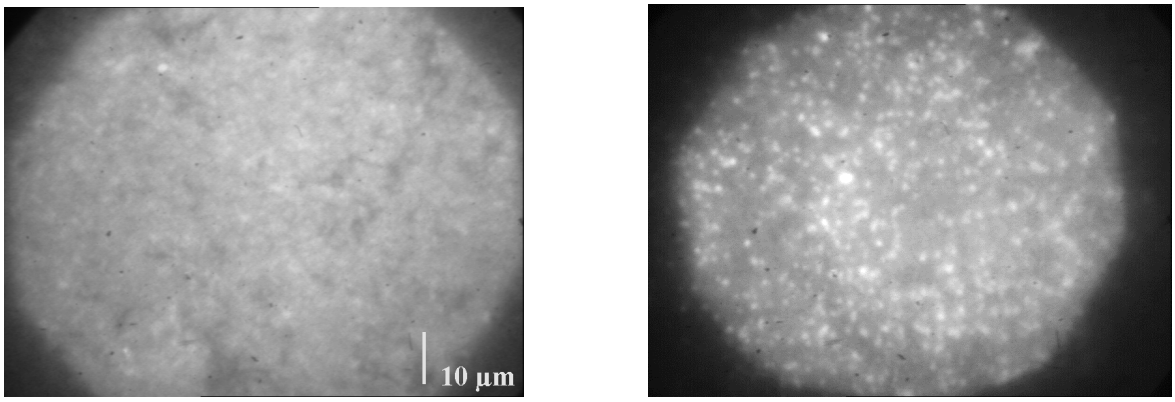

Figure 6.30: The same DMPC bilayers as shown in Figure 6.29, after storage over night at a temperature of 40 °C. Left picture: fluorescence probe NBD-PE, right picture: fluorescence probe DiI.

Homogeneous fluorescence micrographs of bilayers on chitosan did not change appearance after storage over night at room temperature (25 °C) (data not shown). Storage over night at 40 °C, however, led to a decomposition of the supported membrane, to be seen in Figure 6.30. The comparison of the left and right part of Figure 6.30 demonstrates again a higher stability of NBD-PE stained DMPC bilayer membranes compared to those labelled with DiI. Lipid bilayers supported by chitosan were stable over several hours (and probably much longer) which is in contrast to membranes supported by agarose. The higher fixation might be due to the positive surface charge of chitosan (see chapter 8). Bilayers with choline headgroups, on the other hand, have got a slightly negative electrostatic potential across the membrane/water interface, which is due to an overcompensation of the lipid potential by a water potential, caused by the ordering of water molecules near the bilayer surface [Marr, 1996]. An additional electrostatic attraction arises by the use of the negatively charged membrane probe NBD-PE. This interaction leads to a higher stability of membranes compared to those where uncharged fluorescence probes were used, as described in chapter 5.1. However, it has been shown that chitosan forms a stable coating layer even on zwitterionic lipid vesicles (e.g. [Henr, 1994]). This behaviour of chitosan is remarkably different from uncharged, water-soluble polymers. Poly(ethyleneglycol) (PEG) for example does not bind to the surface of phosphatidylcholine membranes and the exclusion from the membrane surface leads to a dehydration of liposomes, often accompanied by phase separations [Leht, 1995]. While PEG acts as a liposome fusogen, chitosan coated liposomes (“chitosomes”) are stable and the polymer coating does not desorb during washing by centrifugation [Henr, 1994].

Moreover, it will be shown below that chitosan strongly interacts with multilamellar giant liposomes consisting of zwitterionic lipids. Hence it can be concluded that even membranes made up of zwitterionic lipids are stabilised on chitosan cushions, by an electrostatic interaction.

Moreover, as in the case of agarose-cushioned membranes, a considerable influence of deposition temperature (25 °C compared to 15 °C) on initial bilayer quality was found (see Figure 6.31). This was the case even though the lipid layer was still in the fluid state at the lower temperature, due to an additional cholesterol content (at a cholesterol content higher than 30 mol%, no transition to a solid phase is found for DMPC/cholesterol mixtures [Alme, 1992]).

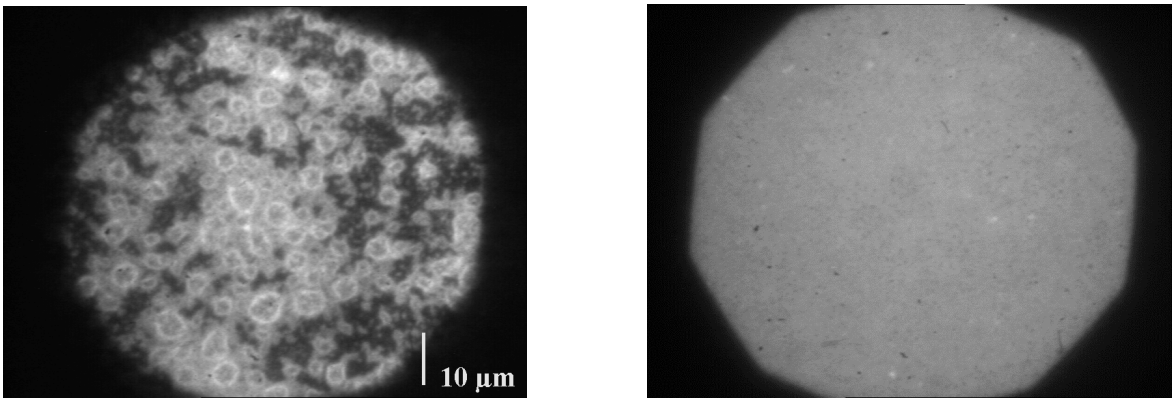

Figure 6.31: Fluorescence micrographs of DMPC (30 mol% cholesterol) membranes obtained by LB/LS transfer at a lateral pressure of 35 mN/m and a deposition temperature of 25 °C (left picture) and 15 °C (right picture), fluorescence probe NBD-PE.

As has been mentioned above (see (6.0.3)), membrane undulations lead to a disjoining pressure, which separates the membrane from a support. As undulations are thermally excited, temperature reduction leads to a stabilisation of the supported membrane. The latter is crucial especially during the Langmuir-Schäfer transfer, as strong flow in the subphase can cause bilayer rupture. Therefore, in every case of the following experiments, the LB/LS transfer was carried out at 15 °C.

The long-term stability of chitosan-cushioned membranes at increased temperatures could be increased considerably, by the addition of cholesterol. No decrease of membrane homogeneity was observed for DMPC membranes, containing 30 mol% of cholesterol, during storage over night at 35 °C. The stabilisation of supported membranes by cholesterol is due to the suppression of membrane undulations, as described in chapter 6.1.

Homogeneous membranes could be prepared on polymer cushions, which had been prepared by the three different methods presented in chapter 4 (physisorption of a monomolecular layer, spin-coating and dip-coating or solution casting, respectively). However, relatively thick polymer cushions, prepared by dip-coating or solution-casting often developed cracks during drying steps. Bilayer membranes prepared by LB/LS transfer were not able to span these cracks (see Figure 6.32).

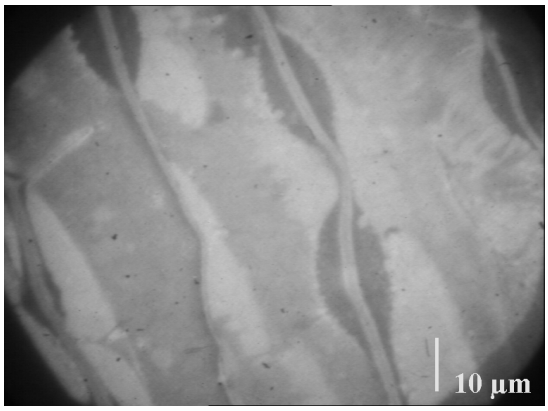

Figure 6.32: Fluorescence micrograph of a DMPC bilayer membrane on a thick, dip-coated chitosan film. The heterogeneous surface structure of the polymer due to cracks is imprinted into the bilayer.

All of the chitosan cushions used in the following were prepared by spin-coating, which led to homogeneous membranes (Figure 6.29 left and Figure 6.31 right) and was relatively time-saving, compared to molecularly thin, physisorbed chitosan films.
Both for chitosan-cushioned bilayer membranes stained with NBD-PE and DiI, lateral fluidity as detected by FRAP was observed. Due to the lower membrane quality in case of DiI, those membranes were not further analysed. FRAP measurements with NBD-PE labelled membranes will be presented in the following.

6.2.2 Lateral diffusion behaviour in chitosan-supported lipid bilayer membranes

As has been mentioned already several times, the lateral fluidity of bilayers is important for the function of model membrane systems. In addition to quasi-neutral phospholipids like cholines, sterols are an important part of the biomembrane [Genn, 1989]. Therefore, the influence of a varying amount of cholesterol on the diffusion behaviour was examined. The temperature behaviour of lateral diffusion can reveal details about the membrane/substrate interactions. In particular, an influence on phase transition temperatures can be studied [Chi, 1992a]. Therefore, also a temperature dependent analysis was carried out.
Figure 6.33 shows the temperature dependence of lateral diffusion coefficients in lipid bilayers on chitosan and on glass in an Arrhenius-plot. From the comparison, the following conclusions may be drawn. The magnitude of the lateral fluidity was not significantly increased by the presence of a hydrated polymer cushion, compared to a glass support. This behaviour is quite different, compared to the case of monolayers, self-diffusing at a reduced relative humidity, which corresponds to a reduced water activity. In that case (as was shown in chapter 5.3), chitosan led to a large enhancement of lateral diffusion. Due to

the different hydration pressures encountered in supported lipid bilayer membranes immersed in water on the one hand, and supported monolayers subject to a relative humidity below 100 % on the other hand, the measurements may not be compared.

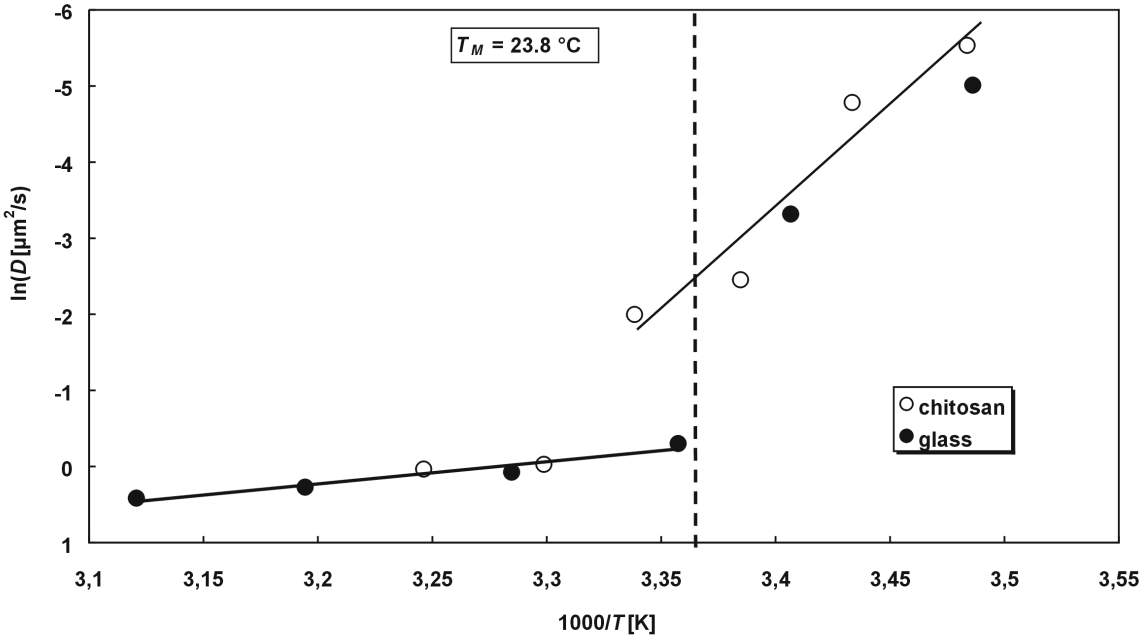

Figure 6.33: Comparison of the temperature dependent lateral diffusion behaviour of DMPC bilayer membranes labelled with NBD-PE, supported by glass and chitosan. In the case of glass, the phase transition as seen by lateral diffusion occurs around the phase transition temperature found in non-perturbed DMPC bilayers (broken line). However, in the case of chitosan, the phase transition occurs at a higher temperature. Each data point represents the average of three to five single measurements.

Furthermore, while the diffusion coefficients on chitosan and glass-supported membranes were generally similar in magnitude, in the temperature region of the main phase transition of an unperturbed DMPC membrane, differences were found (see Figure 6.33, dashed line). The main phase transition of unperturbed DMPC bilayers occurs at 23.8 °C [Mars, 1990]. In the glass-supported bilayer, this first order transition is indicated by a jump of the diffusion coefficients in an interval of 20.4 °C to 24 °C. This is in accordance with [Merk, 1989], where a phase transition was observed around 20 °C (by FRAP experiments), in case of a glass-supported DMPC bilayer. A transition temperature close to the value for unperturbed bilayers was found in [Tamm, 1985], again for a glass-supported DMPC membrane.

In case of chitosan, however, the jump of *D* occurred in the interval 26.4 to 30.0 °C, which indicates an increased phase transition temperature, due to the presence of chitosan. Such an increase could be due to a slight dehydration of the membrane surface, with respect to an unperturbed bilayer. The increase of the phase transition temperature would then be a result of a closer packing of lipid headgroups in the proximal leaflet, caused by headgroup

dehydration. Such dehydration could be due to the attractive chitosan/lipid interaction mentioned above. A similar effect can be observed in case of DMPC bilayers supported by poly(acrylamide) films [Kühn, 1994], [Pink, 1995], although not explicitly stated by the authors. The assumption of a slight, chitosan-induced dehydration of the membrane surface is contrary to the hydration measurements, which were presented in chapter 5.4. In that case, it was observed that chitosan-supported lipid monolayers show an increased hydration in the headgroup region, compared to glass-supported monolayers. Again, as has been mentioned above, the monolayer experiments were carried out at different hydration pressures compared to bilayers immersed in water, and the monolayer and bilayer measurements therefore cannot be compared to each other.

In another series of experiments, chitosan-cushioned DMPC bilayers were prepared with varying cholesterol contents and analysed with respect to the temperature dependent lateral fluidity (Figure 6.34). For every lipid composition, homogeneous fluorescence micrographs were obtained. Figure 6.34 indicates that for membranes in the fluid state, e.g. at a temperature around 35 °C, the diffusion coefficients were reduced with increasing cholesterol content. The latter may be compared with diffusion measurements in multibilayer stacks composed of DMPC/cholesterol mixtures [Alme, 1992]. In that work, at a temperature of 35 °C, the diffusion coefficient was found not to vary upon addition of cholesterol up to about 10 mol%.

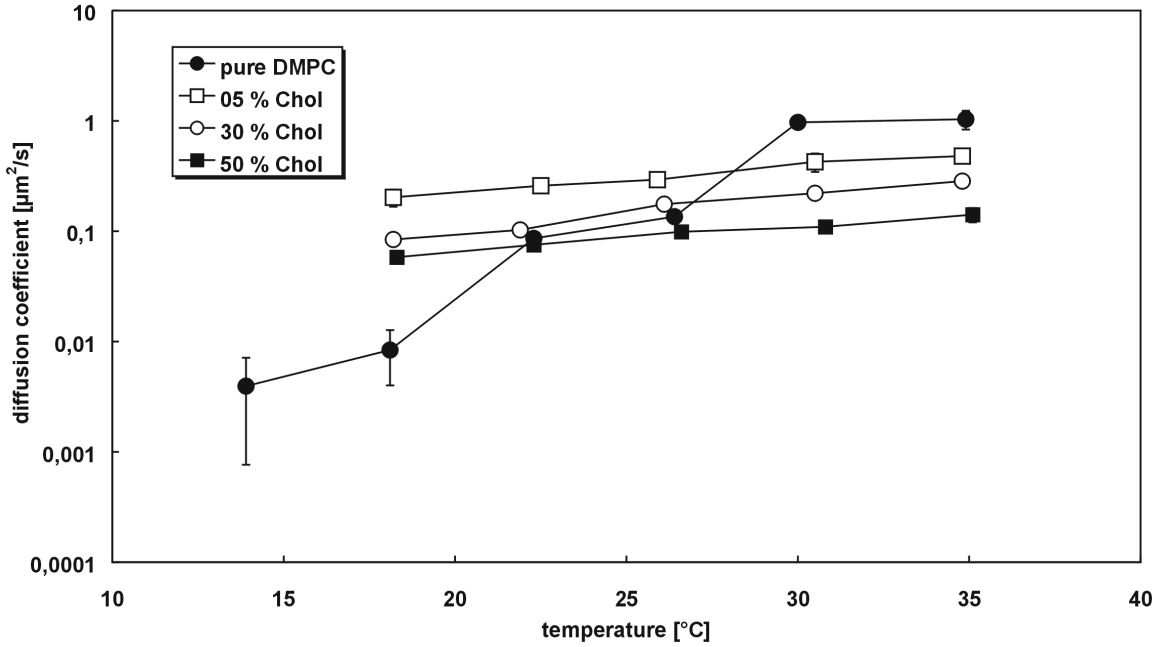

Figure 6.34: Temperature dependent lateral diffusion behaviour of chitosan-supported DMPC bilayer membranes with varying cholesterol contents. Membranes were prepared by LB/LS transfer at a lateral pressure of 35 mN/m.

At this temperature and composition, a transition occurs from a homogeneous liquid disordered (L_d) to a coexistence region of L_d and L_o (liquid ordered) phase. Between 10 and 30 mol% a decrease of *D* was observed while further increasing the cholesterol content and between 30 and 50 mol% a rise was observed. This rise is due to an increased lateral spacing of lipid groups in a homogeneous L_o phase [Alme, 1992]. Clearly, these findings differ from the measurements presented in Figure 6.34. Additionally, the diffusion coefficients found in [Alme, 1992] are significantly higher than those depicted in Figure 6.34, at the same temperature. These differences between multibilayer stacks and chitosan-supported single bilayers can most probably be explained by a direct friction of the membrane with the underlying support. In [Kühn, 1996a], an increased adhesion of membranes containing cholesterol to polysaccharide supports was attributed to interactions of the OH-groups of cholesterol and the polysaccharide. The same effect probably leads to a continuous reduction of lateral fluidity, with increasing cholesterol content, in chitosan-supported bilayers.

Furthermore, at a temperature around 18 °C, the fluidity increased upon adding 5 mol% cholesterol, and decreased again upon further increasing the cholesterol content to 30 and 50 mol% (Figure 6.34). The initial increase can be explained by the phase diagram of the DMPC/cholesterol mixture [Alme, 1992]. Around 5 mol% cholesterol, at 18 °C, a transition from a solid state to a coexistence region with an additional L_o phase is encountered, accompanied by an increase of lateral fluidity. The reduction of diffusion coefficients at this temperature upon further increasing the cholesterol content can be explained by additional friction, as mentioned above.

The fluorescence recovery values generally showed little temperature dependence except in case of the pure DMPC bilayer (data not shown). For pure DMPC, passing through the main phase transition temperature is accompanied by domain formation, hence the relative recovery drops with decreasing temperature. In principle, the fluorescence recovery may provide useful information about membrane domains [Vaz, 1989], [Alme, 1993], [Salo, 1998]. However, domain formation in single supported lipid bilayers depends in a very complex way on membrane/substrate interactions [Pink, 1995], therefore this topic was not further analysed.

6.2.3 Interaction of the chitosan surface with multilamellar giant liposomes

As mentioned in chapter 6.1, reflection interference contrast microscopy provides a tool for studying membrane/substrate interactions. In case of agarose the negligible substrate/liposome interaction underlined the low stability of bilayer membranes deposited

onto agarose cushions. According to the observations described above, a higher interaction of chitosan with liposome surfaces is expected. Giant multilamellar liposomes consisting of DMPC were prepared under the same conditions used in chapter 5.1 and added to the aqueous phase above a chitosan film on a glass substrate. Indeed, in case of chitosan an adsorption of liposomes was found. The liposomes after the initial contact flattened fast and finally ruptured. As in all cases multilamellar liposomes were used, the remaining lamellae could still be observed in the interferogram. Figure 6.35 shows two adsorption spots of giant liposomes on a chitosan surface.

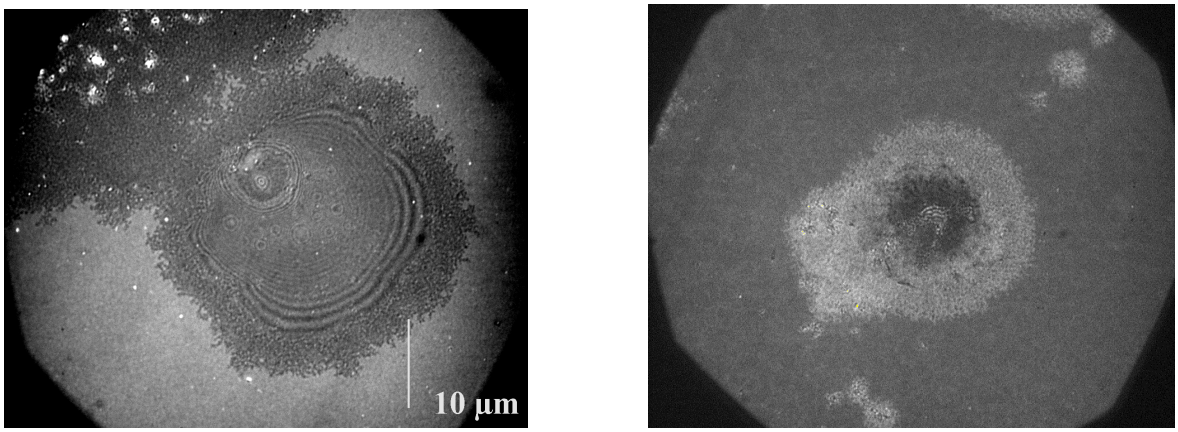

Figure 6.35: RICM image of giant multilamellar liposomes, partially spread on a chitosan surface at room temperature. Surrounding medium: saccharide solution as described in chapter 3.10.5.

Figure 6.35 clearly demonstrates that the contrast between lipid covered and uncovered surface varied on the substrate. This is easily explained by the fact that the film thickness of the chitosan film was variable. While the mean thickness of the chitosan film used in Figure 6.35 was approximately 300 nm, a thickness change of only 45 nm can maximally reverse the intensity difference between membrane-covered and free chitosan area, as can be seen in Figure 6.36 A). This relative intensity difference was calculated according to $(I_{free}\text{-}I_{cov})/I_{free}$, where I_{free} is the total reflected intensity in case of a free chitosan surface and I_{cov} is the intensity reflected by a membrane-covered chitosan surface. The graphs in Figure 6.36 were calculated by means of the software Winspall (written by J. Worm, MPIP). From Figure 6.36 A), it follows that in order to image a chitosan-supported bilayer membrane, an optimal thickness of the chitosan film is an important prerequisite. In addition to the contrast between covered and uncovered area, the contrast between maxima and minima in the interferograms of the remaining lamellae of the giant liposome varies with chitosan film thickness, as shown in Figure 6.36 B). The contrast was calculated according to $(I_{max}\text{-}I_{min})/(I_{max}+I_{min})$.

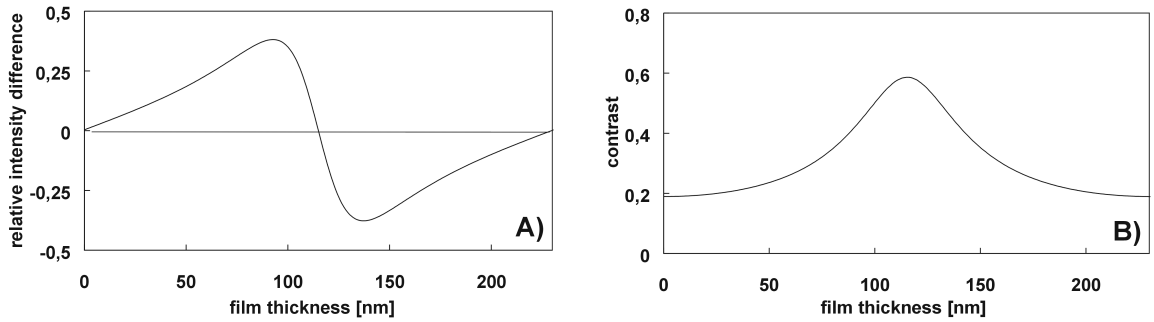

Figure 6.36: Relative intensity difference (left) and contrast variation (right) of reflection interferograms of a lipid bilayer membrane on chitosan for a varying film thicknesses. For a definition of the quantities see text.

From Figure 6.36 B), it follows that in order to determine the topography of giant liposomes or biological cells on a chitosan surface by means of RICM, an optimal chitosan film thickness is favourable. This film thickness can be adjusted by means of spin-coating, as described in chapter 4.

From Figure 6.35 it can be deduced that the polymer/liposome interaction is much stronger in case of chitosan as compared to agarose films, which explains the higher stability of planar chitosan-supported bilayer membranes. Bilayer spreading on planar surfaces can take place in different modes. These modes are namely bilayer sliding, the advancing of a single bilayer by a tank-tread motion and thirdly the rolling of double-bilayers (see [Niss, 1999] for details).

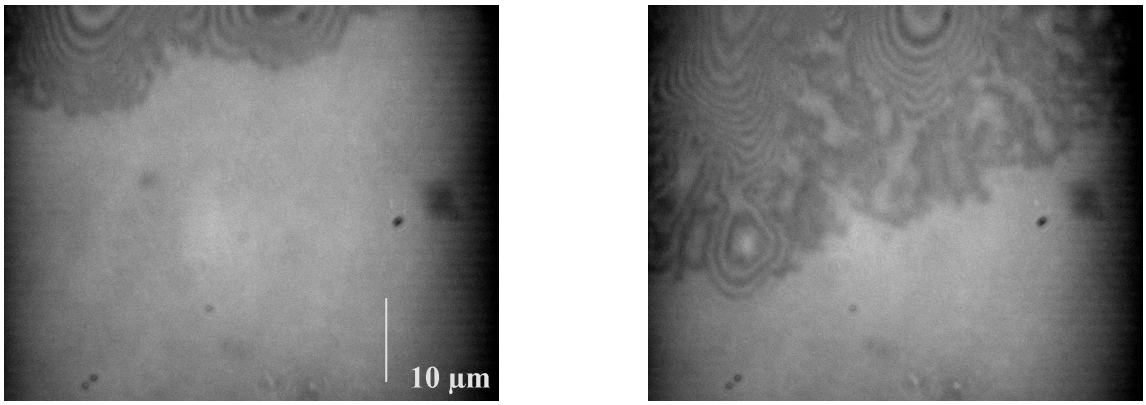

Figure 6.37: RICM image of the spreading of a patch of giant multilamellar liposomes. The right picture was taken 100 s later than the left picture.

From Figure 6.37, it is obvious that the spreading process on chitosan can involve a double bilayer rolling process. Strong intensity variations and interference fringes directly at the spreading front indicated a non-planar surface profile of the spreading membrane. The height variations were in the range of the wavelength of the illuminating light, which can only be explained by the fact that spreading did not occur by the advancement of a single bilayer membrane, but by a flattening and rolling out of vesicles. Such a spreading process

on chitosan was much faster, than the advancement of single bilayers, the kinetics of which will be analysed in chapter 6.2.4 (compare Figure 6.37 and Figure 6.41).
The adsorption behaviour on chitosan may be compared to the situation on glass, as shown in the left part of the next figure.

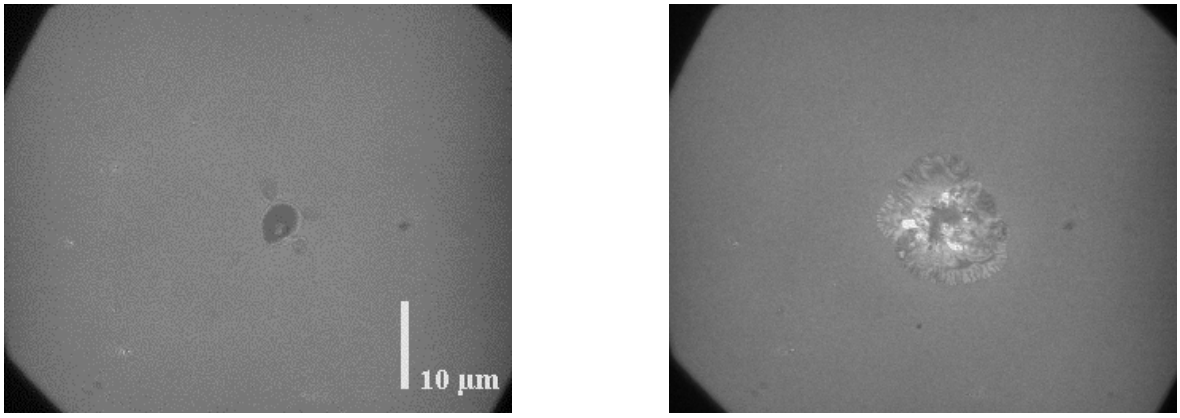

Figure 6.38: RICM image of a giant liposome adhering to a glass surface (left). Right: the same vesicle as in left picture after addition of salt.

Upon initially contacting the glass surface, the contact zone of the adhering liposome grows, until the adhesion energy is balanced by membrane tension [Rädl, 1995b]. As glass surfaces are negatively charged [Rädl, 1992], adhesion of DMPC liposomes on glass is dominated by the van der Waals interaction, which is not high enough to lead to the rupture of the giant liposome.

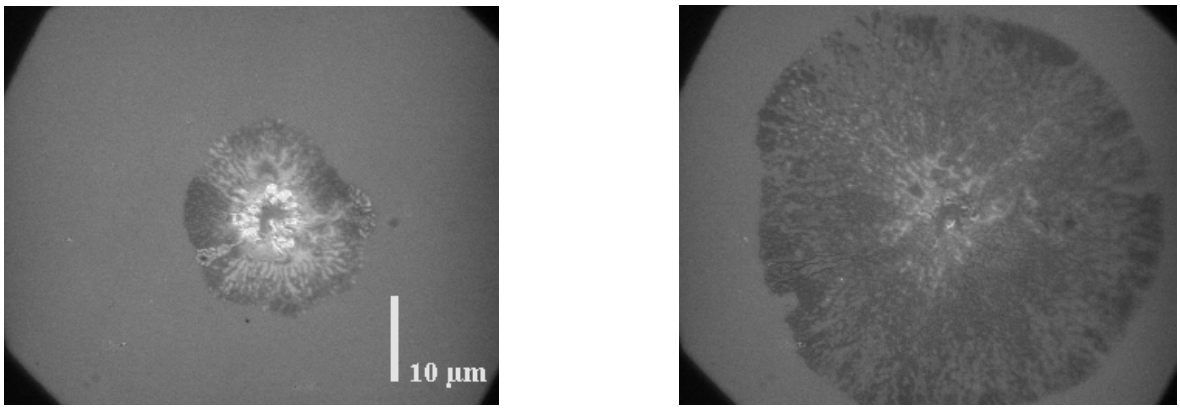

Figure 6.39: RICM image of the spreading of lipid bilayers on a glass surface. Left picture: 1.5 s after vesicle rupture (Figure 6.38), right picture: 25 s after vesicle rupture.

Rupturing of the adhering liposome and subsequent spreading, however, could be forced by the exertion of an osmotic shock. This was accomplished by adding salt to the surrounding medium. The spreading of such a ruptured liposome is demonstrated in the left part of Figure 6.38. After rupture, the lipid material spread continuously to form a circular spot on the glass surface (see Figure 6.39). No interference fringes were observed after

vesicle rupture (Figure 6.39), therefore it can be inferred that the spreading on glass occurred by bilayer sliding [Rädl, 1995a]. The inhomogeneity of the membrane spot in Figure 6.39 is probably due to multilayers, which fused subsequently into a single, glass-supported bilayer.
The spreading kinetics of lipid bilayers on glass were analysed in detail in [Rädl, 1995a]. The spreading of lipid membranes by bilayer sliding on chitosan, however, will be the subject of the next chapter.

6.2.4 Spreading of lipid bilayer membranes from a lipid reservoir on chitosan

In order to further analyse the nature of the interaction between a bilayer lipid membrane and chitosan films, spreading experiments from a lipid reservoir on a chitosan film were carried out. The effect of single bilayer spreading on planar surfaces was first observed by Rädler et al. [Rädl, 1995a].

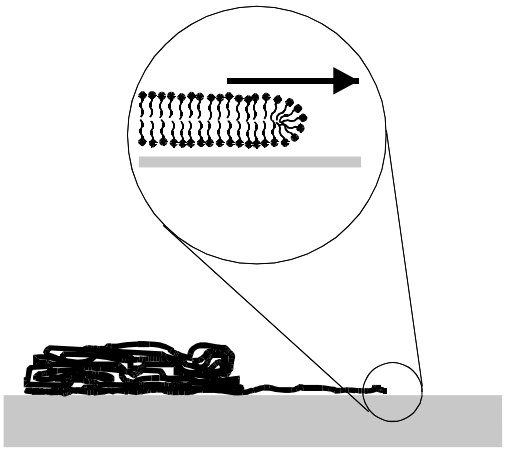

Figure 6.40: Bilayer spreading from a lipid reservoir, deposited onto a hydrophilic substrate from a solution. The substrate is immersed in water or a buffer solution afterwards.

In that work a lipid reservoir was deposited from a solution onto inorganic surfaces (like glass or MgF_2), followed by thorough drying and subsequent hydration with water or buffer solution. The result was an advancement of single bilayers from the lipid reservoir, as shown schematically in Figure 6.40. Later [Niss, 1999] it was found that such bilayer spreading is also possible on extremely thin, soft and hydrated polymer cushions, like dextran and cellulose. Both polymers were assumed not to specifically interact with lipid membranes. Therefore, the energy gain by bilayer spreading was attributed to the van-der-Waals interaction between membrane and the underlying (glass-) substrate. It was argued above, that the interaction between chitosan and zwitterionic membranes can be assumed to be attractive. This assumption was further proved by examining bilayer spreading on

chitosan films with a wet thickness of approximately 300 nm. In that case, the van der Waals attraction between membrane and underlying glass substrate can be neglected because van der Waals attractions between planar surfaces decay to the second power[5)] of the separation distance [Isra, 1992a].

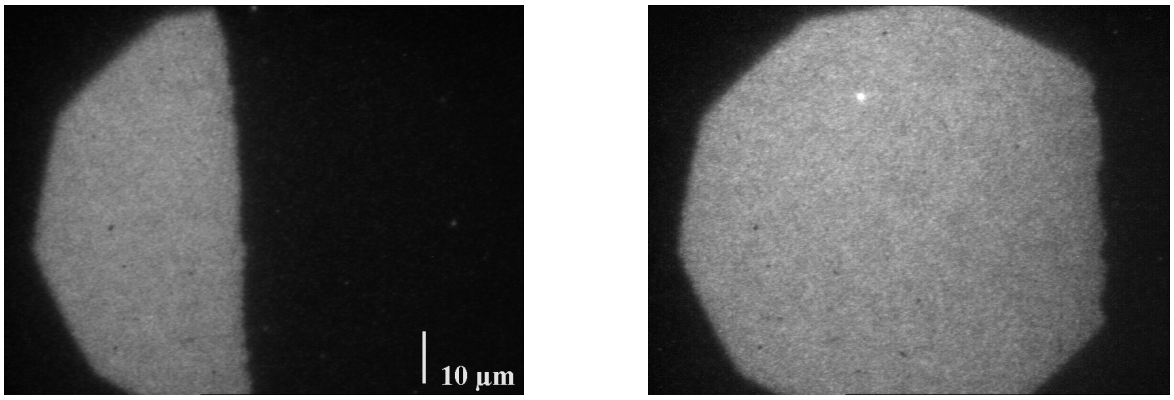

Figure 6.41: Fluorescence images of a spreading experiment on a chitosan surface. An eggPC lipid reservoir was deposited onto the polymer film and the substrate was immersed into MilliQ water. The right picture was taken 34 min after the left one.

Hence it is interesting to analyse, whether bilayer sliding on moderately thin chitosan films occurs. Bilayer spreading in terms of sliding is considered to be important for practical applications of solid-supported bilayer lipid membranes, since it leads to self-healing properties of such systems [Rädl, 1995a]. According to Figure 6.41, the spreading of a single bilayer from a lipid reservoir on chitosan was possible, which means that bilayers on chitosan possess self-healing properties. During the edge displacement of the bilayer, a considerable roughening of the spreading front was observed (see Figure 6.42). The contour line of the spreading monolayer was extracted from the fluorescence images as described in chapter 5.2. Such a roughening was also found in case of spreading on glass surfaces and was attributed to line pinning, induced by the substrate roughness [Rädl, 1995a]. It must be noted that this edge roughening is in contrast to monolayer spreading on the same substrates, where no significant line roughening was observed. On the contrary, as described in chapter 5.2, initially rough monolayer edges smoothed during spreading to yield an essentially straight spreading front. The difference with respect to bilayer spreading can be explained by the much higher spreading power of lipid monolayers (compare (6.01) and (6.02), which diminishes the spreading-edge pinning on the chitosan surface. In order to further analyse the kinetics of bilayer spreading, the time dependency of the edge displacement was examined.

[5)] This distance dependence is valid only for small separation distances of a few nm, since at larger separations the decay is even faster, due to the effect of retardation.

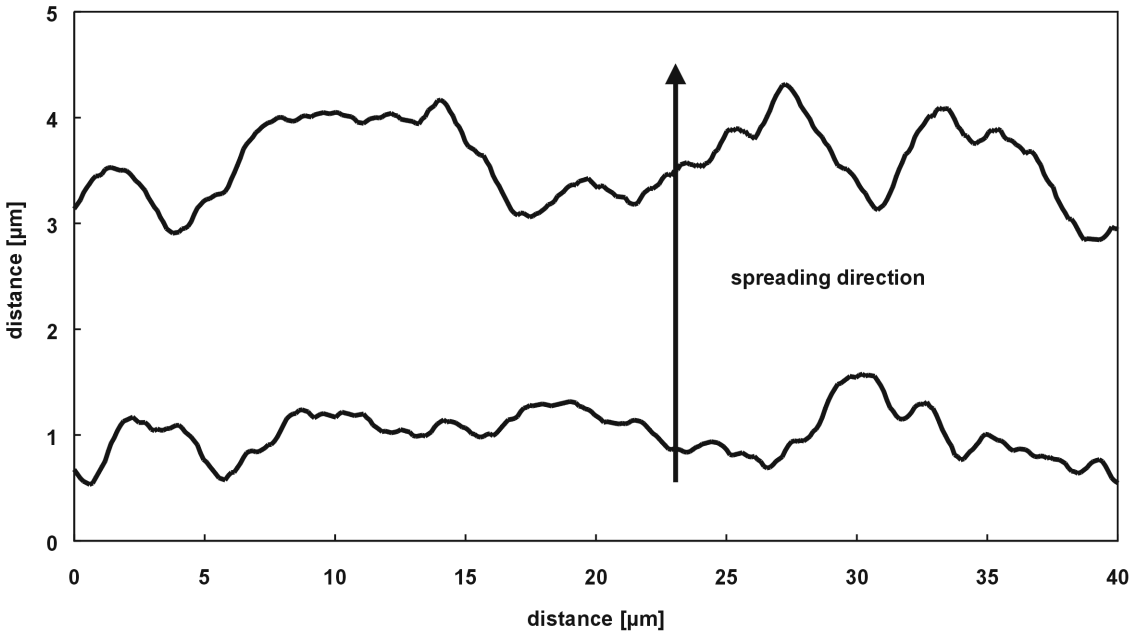

Figure 6.42: Comparison of the spreading front of a lipid bilayer membrane spreading from a lipid reservoir deposited onto a chitosan film (corresponding to Figure 6.41).

The length of the spreading monolayer was taken as the distance of the monolayer edge from the lipid reservoir (see Figure 6.40).

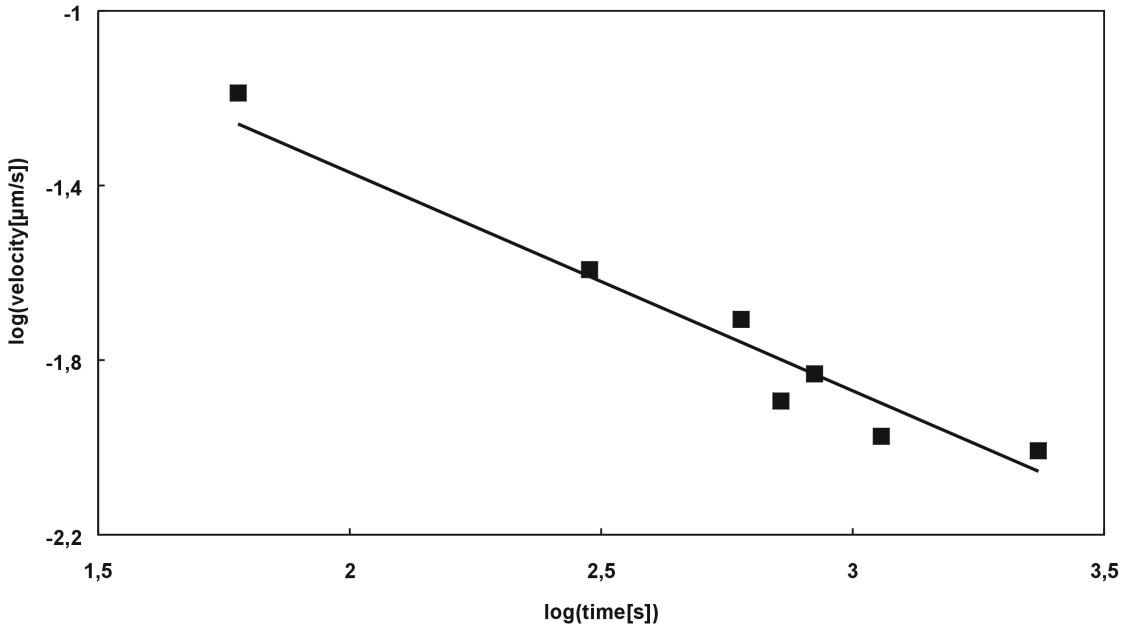

Figure 6.43: Double logarithmic plot of the spreading velocity against measurement time, for an eggPC bilayer spreading on chitosan from a lipid reservoir, bold line: one-parameter fit with a fixed slope of -0.5.

As explained in detail in chapter 5.2, bilayer spreading can be described by means of the following equation [Rädl, 1995a],

$$v(t) = \sqrt{\frac{W_A}{2\zeta}} \frac{1}{\sqrt{t}} = \sqrt{\frac{\beta}{t}} \qquad \textbf{(6.2.1)}$$

where W_A is the energy per unit area gained by spreading, ζ is a viscous drag coefficient and β is a kinetic spreading coefficient [Rädl, 1995a]. Hence plotting of log(v) against log(t) should yield a straight line with a slope of –0.5. From Figure 6.43 it can be deduced that a linear fit with a slope of –0.5 successfully describes the spreading behaviour on chitosan. From the interpolation to log(t) = 0, the kinetic spreading coefficient was determined to be $\beta = 1.8 \cdot 10^{-13}$ μm^2/s. This value is about two orders of magnitude smaller compared to the spreading of a DMPC bilayer on glass and one order of magnitude smaller compared to DMPC bilayers spreading on cellulose or dextran films [Niss, 1999]. The smaller value could be explained by a higher friction due to dehydration of the membrane/substrate gap in case of chitosan-supported membranes (see above). Additionally, the driving force for spreading might be smaller, since an energy gain by the van der Waals interaction between membrane and glass substrate is absent in this case. In principle, the contribution of the latter to the velocity of bilayer spreading could be analysed by preparing films in the range of a few nm and varying the film thickness. An advantage of chitosan films is the possibility to prepare films with a wide range of different film thicknesses quite readily. Therefore, the influence of film thickness on the kinetic spreading coefficient was analysed. However, the scattering of the data was too high and prevented a detailed analysis. For each film thickness only one or two spreading experiments were carried out. A larger number of experiments for each film thickness would thus be necessary.

6.2.5 Vesicle fusion experiments on chitosan

Besides Langmuir-Blodgett methods, the fusion of small vesicles to hydrophilic surfaces is a convenient way to prepare supported lipid bilayers. While it was shown above that bilayer membranes on chitosan were stable, giant liposomes adhered, flattened and ruptured and bilayer membranes spread from a lipid reservoir, the fusion of small vesicles to yield a laterally connected bilayer was not possible. This was revealed by the fact that FRAP indicated only a very small, partial fluorescence recovery, pointing to a considerable amount of adsorbed, non-spread vesicles (see Figure 6.44).

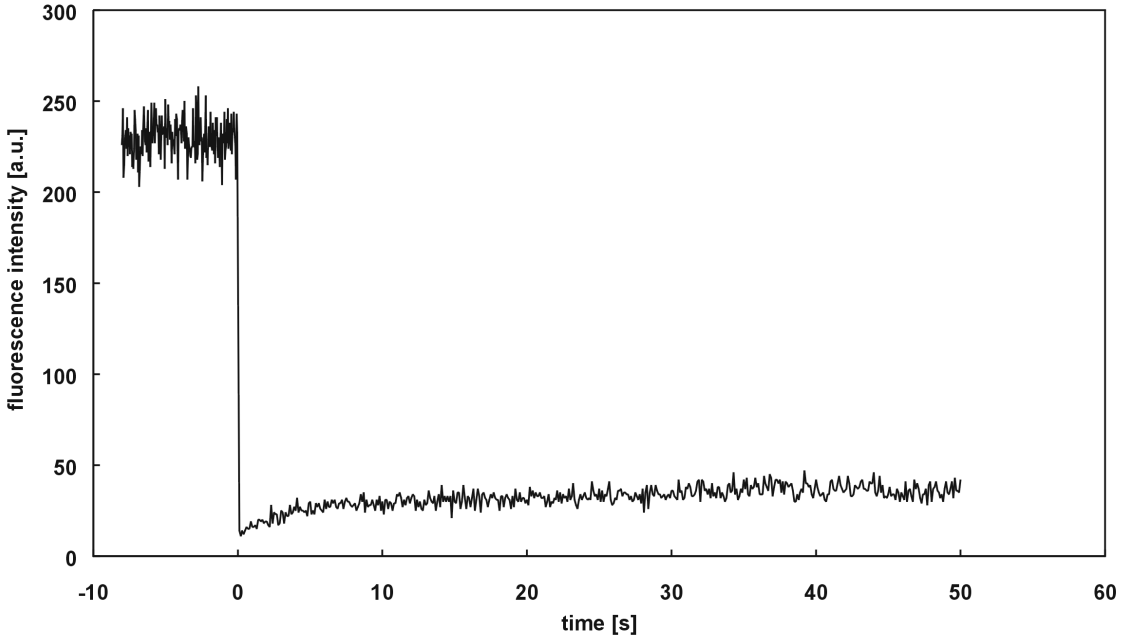

Figure 6.44: FRAP diagram of a chitosan film, which was exposed to an eggPC SUV-dispersion for half an hour at 30 °C. Measurement temperature: *RT*.

This was further underlined by the fact that the observed fluorescence intensity before bleaching as measured by a photomultiplier was always higher in the case of samples, which were prepared by vesicle fusion, as compared to the case, where LB/LS transfer was used to prepare the bilayer. The fluorescence intensity after bleaching did not reach an intensity that was usually observed for bilayers prepared by LB/LS transfer (with the same concentration of the fluorescence probe and comparable illumination conditions. This indicates that the partial fluorescence recovery cannot be explained by the existence of a laterally connected planar bilayer membrane with adsorped vesicles on top or below this membrane. Instead, the recovery seemed to stem from lipid aggregates, which were partially located inside and outside of the laser bleach spot. Such lipid aggregates could for example be liposomes, which were formed by the fusion of SUVs to form larger liposomes. The fact that SUVs adhere to the chitosan surface but do not rupture and yield a laterally connected, chitosan-supported bilayer so far is unexplained. However, this observation is equivalent to the case of ultrathin dextran films, in which case the fusion of small unilamellar vesicles seems to be impossible also [Hill, 2000].

6.2.6 Electrical properties of the bilayer lipid membrane/chitosan system

Impedance spectroscopy measurements (see chapter 3.6) with gold electrodes covered by thin chitosan films revealed a spectrum with a single time constant (Figure 6.45).

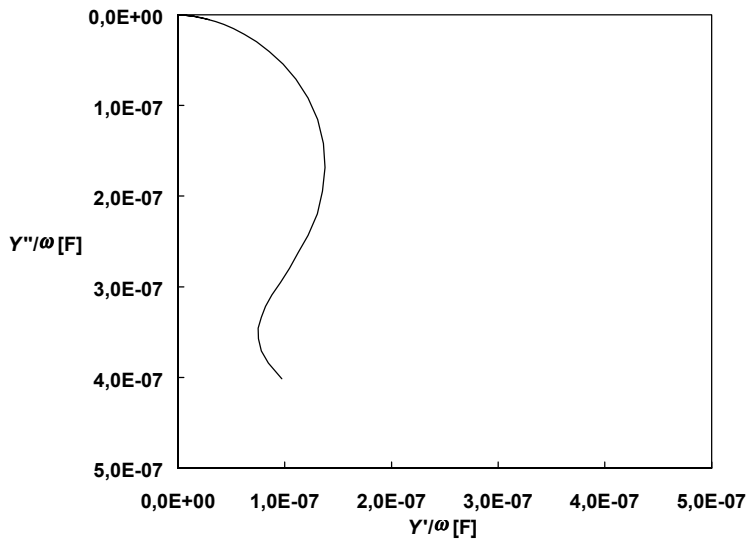

Figure 6.45: Complex admittance over ω plot for a chitosan film on a gold electrode. Dry thickness of the polymer film: approximately 15 nm, electrode area: 0.0354 cm^2.

Chitosan is only a weak polyelectrolyte, hence its influence on double layer properties through intrinsic charge and Donnan potential [Berg, 1991] should be small. Therefore the capacitance observed in Figure 6.45 can be ascribed to the double layer capacitance on a gold surface. In fact, for the spectrum shown in Figure 6.45, a normalised capacitance of 10 µF/cm^2 was found, which is in the usual range found for bare gold electrodes (fresh gold has a capacitance of approximately 30 µF/cm^2, which is reduced quickly by ageing processes) [Lind, 1996]. The spectrum was fitted by a series connection of capacitor (double layer capacitance) and resistor (solution and connection resistances). The resistance was found to be 135 Ω·cm^2, indicating a high conductivity of the polymer cushion itself.

Several lipids were tested in the present work for their ability to form bilayers with high insulating properties on polymer cushions. These include the most commonly used cholines (e.g. [Mill, 1990], [Plan, 1993], [Flor, 1993], [Naum, 1995b], [Ling, 1997] [Naum, 1999]) like DMPC and eggPC, and mixtures of cholines with cholesterol [Grit, 1998]. The popularity of cholines most probably stems from its high headgroup hydration and the zwitterionic character. While the former is favourable for bilayer preparation by vesicle fusion (lower hydrated phosphatidylethanolamins, for example, lead to multilamellar structures [Egaw, 1999]) and a decoupling from the underlying support by a thin water layer, the latter is regarded to be favourable for the incorporation of functional membrane proteins. The lower hydration of lipids with a PE headgroup, however, could possibly lead to a stronger adsorption to the underlying substrate [Soll, 1996] – associated with a lower tendency for pore formation. Additionally, the amino-reactive anchor lipid described in chapter 8.2.1 was used for partial covalent bonding of the proximal lipid layer.

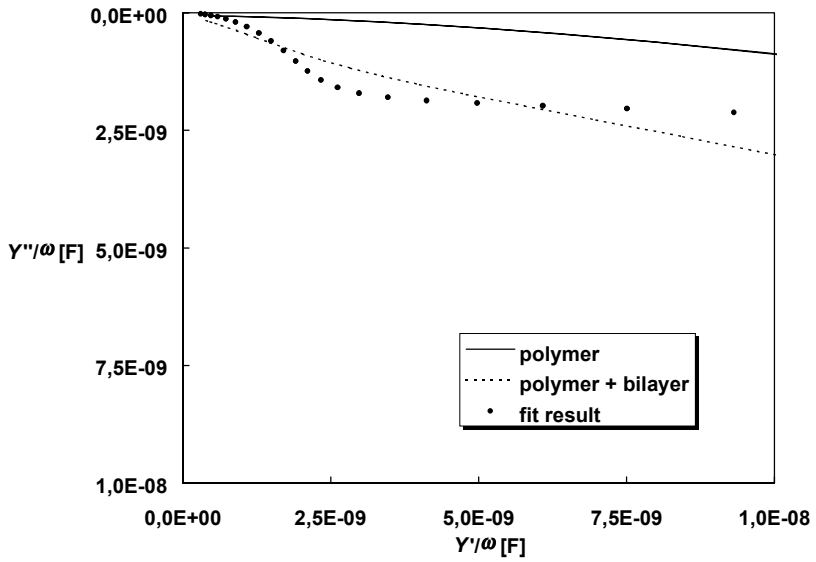

Figure 6.46: Impedance spectroscopy of a chitosan polymer cushion, DMPG bilayer (prepared by LB/LS transfer and a fit of the polymer-cushioned bilayer: complex admittance/ω plots. Electrode area: $3.296 \cdot 10^{-3}$ cm^2. Dry thickness of the polymer film: approximately 15 nm.

However, in almost all cases, the bilayer membrane could hardly be detected by impedance spectroscopy. This is most likely due to a high number of pores, which lead to a leaky membrane. The most successful measurements were carried out using bilayers composed of DMPG (Figure 6.46). It was already shown by others [Grit, 1998], [Lind, 1996], [Jenk, 2000] that an additional coupling of bilayer and substrate by Coulomb interactions is favourable for increased insulating properties. The negatively charged DMPG headgroup is assumed to be attracted by positively charged NH_3^+- groups of the partially protonated chitosan. The impedance data presented in Figure 6.46 were fitted by an equivalent circuit consisting of a resistance in series with a capacitance and an additional RC element. The latter accounts for the bilayer lipid membrane resistance and capacitance. The fit yielded a bilayer capacitance of 1.39 µF/cm^2 and a bilayer resistance of 1.1 kΩ·cm^2. The capacitance is not far exceeding the values, which are ascribed to a "perfect" lipid bilayer. These values have been measured on BLMs to be approximately 0.45 µF/cm^2 [Howa, 1968]. The resistance, however, is several orders of magnitude lower compared to those values found for BLMs (several hundreds of MΩ·cm^2 [Howa, 1968]).

The small resistance is disadvantageous for the use of chitosan-supported bilayer membranes as electrical insulators, which would be a prerequisite for the analysis of functional membrane proteins by single channel measurements or impedance spectroscopy. Low insulating properties of polymer-supported lipid membranes have been reported by several authors (e.g. [Lind, 1996], [Cass, 1999], [Sinn, 1999]). A satisfying explanation, however, is still missing.

As has been pointed out in chapter 6.2.5, vesicle fusion experiments on chitosan cushions did not yield a laterally connected bilayer. Instead, an adsorption of vesicles was observed. The same was revealed by electrical measurements. Figure 6.47 shows a sequence of impedance spectroscopy data readings, which were obtained during a vesicle fusion experiment on a chitosan cushion. The measured capacitance (as indicated by the radius of the semicircle in Figure 6.47) decreased with time, indicating a partial coverage of the polymer surface by a small capacitance lipid bilayer. However, even after exposure of the chitosan-covered gold electrode to the vesicle dispersion for 24 h, small resistances (in the range of 10 $k\Omega \cdot cm^2$) and high capacitancies (in the range of 15 $\mu F/cm^2$) were found. Both values indicate a high area fraction of membrane defects, probably due to the adsorption of vesicles which did not spread to yield a laterally connected bilayer, as indicated by FRAP experiments also.

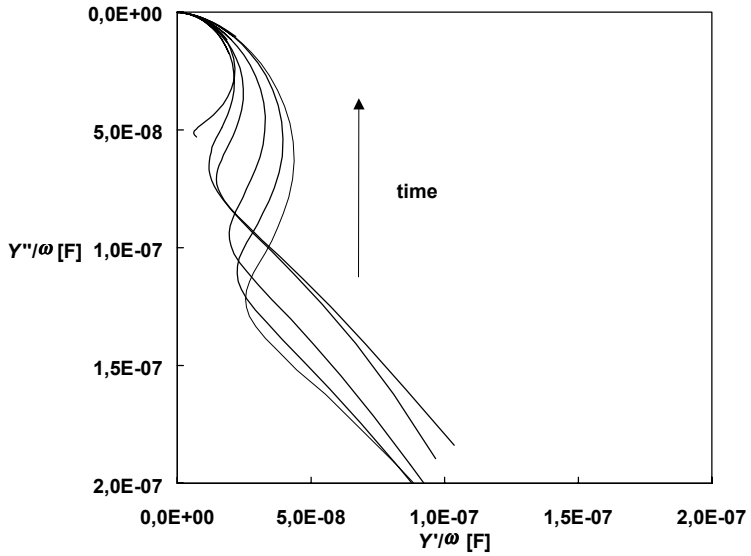

Figure 6.47: Vesicle fusion experiment on a chitosan polymer cushion: complex admittance over ω plot. A vesicle dispersion (DMPC) was added at a temperature of 30 °C. Time between first and last spectrum: 12 h. Dry thickness of polymer film: approximately 15 nm.

6.3 Conclusion, discussion and outlook

Lipid bilayer membranes prepared by Langmuir-Blodgett methods on agarose cushions were shown to be unstable, if they were made up of zwitterionic lipids. The bilayer instability was indicated by a) membrane decomposition as observed by fluorescence microscopy upon storage, b) missing adhesion of giant multilamellar liposomes to the agarose surface as measured by RICM, and c) the impossibility of bilayer spreading from a lipid reservoir on the agarose surface. On the other hand, routes to stabilise bilayer lipid membranes on agarose cushions were worked out. These were namely firstly the use of a

decreased deposition temperature, secondly the incorporation of cholesterol into the bilayer, thirdly the embedding of the lipid membrane between two polymer cushions in a sandwich geometry and fourthly the use of positively charged lipids, to increase electrostatic interactions between membrane and polymer support.

Despite the low stability of bilayer membranes consisting of zwitterionic lipids, extremely high insulating properties of agarose-cushioned lipid membranes were found, which were prepared by the thinning of a lipid solution in an aperture. On the other hand, it was shown that while these BLMs were stable against mechanical vibrations, their long-term stability was not increased compared to freely suspended black lipid membranes.

Bilayer lipid membranes cushioned by thin chitosan films were shown to possess a major stability compared to agarose-cushioned membranes. The sufficient stability was shown by a) the observation of homogeneous bilayer membranes as found by fluorescence microscopy, b) a strong attraction of zwitterionic, giant unilamellar liposomes leading to vesicle rupture and c) the fact that single bilayer sliding on chitosan surfaces from a lipid reservoir deposited onto the polymer cushion was observed.

Chitosan-supported lipid membranes in general, and agarose-cushioned bilayer membranes stabilised along the concepts outlined above provide easy to prepare model membrane systems. They allow for studying the bilayer itself and for the incorporation and examination of membrane proteins. An example of the latter will be provided in the next chapter. Fundamental biological processes may be mimicked with the help of these supported model membrane systems. Advantages of the polymer cushions described in the present work are their simple preparation and controllable film thicknesses, which for example provides an access to polymer-cushioned membranes also for biological laboratories, where facilities allowing for extensive chemical synthesis are missing. By the presence of a soft and hydrated polymer cushion, it is probable that integral membrane proteins may be incorporated into these model membrane systems in a functionally active way. A possible application could for example be the modelling of exocytosis events, i.e. the fusion of vesicles into the plasma membrane, which would in the present case be mimicked by a polymer-supported model membrane. Such investigations could for example further clarify the role of SNAREs and SNARE regulators [Söll, 1993] controlling fusion events [Gers, 1999]. SNAREs can successfully be incorporated into artificial liposomes, as has been shown in [Webe, 1998]. The polymer-supported, planar bilayers described in the present work, however, allow for the application of surface sensitive techniques, such as total internal fluorescence microscopy and others (see chapter 4). An important question, which could be answered by such an approach is, how many SNARE molecules are involved in the process of exocytosis, for example by the use of single molecule fluorescence techniques.

A disadvantage of the supported model membranes described in the present and other works is, however, that the insulating properties are generally poor. An intrinsic problem of solid-supported lipid membranes is likely to be the distortion of the self-assembly feature of the bilayer membrane. It was shown above that the insulating properties of supported lipid membranes may be low, even though these membranes possess a self healing ability, i.e. large defects can heal by lateral spreading of the bilayer. Bilayer spreading, however, only leads to a healing of large defects. Obstacles to bilayer spreading, however, induced by the surface roughness of the bilayer support, are assumed to be circumflown by the spreading bilayer [Rädl, 1995a], leading to bilayer pores. The possibility for such pores to be formed during spreading depends on the ratio of the pore energy (being influenced by the energy of hydrophobic membrane rims) and the energy gained by spreading. Hence spreading in cases where membranes are bound by strong adhesion (which is favourable for stabilising a planar bilayer on a support) will enhance pore formation during spreading and decrease the membrane's insulating properties.

One solution to this problem is the use of extremely smooth substrates, such as the recently developed cellulose Langmuir-Blodgett films [Scha, 1993], [Hill, 1999]. As was pointed out in chapter 2, however, the aim of substrate-supported bilayer model membrane systems is to provide a suitable environment for integral membrane proteins with large peripheral parts. It is clear that membranes resting on extremely smooth substrates are not well suited for such a purpose, because no space is left for voluminous protein heads.

It was shown in [Moel, 1986] that classical black lipid membranes could be stabilised considerably by coating with polysaccharides bearing hydrophobic anchor groups, after the membrane had been formed. A solution to the common problem of insufficiently insulating supported model membranes could therefore be a top-down concept in terms of the bilayer: to deposit an intact bilayer onto a stabilising support. An access to such an approach was, for example, developed in [Schm, 2000], where giant unilamellar liposomes were guided onto small holes in a silicon device by means of an electric field gradient (electrophoretic trap). The authors showed that this device allows for the analysis of single channel proteins, since so called "giga-seals" were obtained. The membrane, however, suffers from small lifetime and surface sensitive techniques cannot be applied. Another interesting variation of the above proposed top-down concept is the formation of a black lipid membrane on a thin polymer film or at the tip of a pipette immersed into an aqeous solution and pressing the BLM against an agarose cushion [Ide, 1999]. The agarose cushion consisted of a thin film deposited on a glass slide, hence this configuration allowed for fluorescence microscopy and electrical measurements in parallel. Low membrane stability, however, was observed in that case also.

It is likely that a combination of the above-mentioned concepts could yield substrate-supported bilayer membranes with improved properties. Such a configuration could consist of a device providing an aperture, this aperture would be faced on one side with a substrate with a thin chitosan film on top. The higher stability of chitosan-cushioned membranes, as was shown above, could lead to improved membrane lifetimes.

Another advantageous model membrane configuration could be similar to polymer filled teflon tubes (see Figure 6.1). However, chitosan is not suitable for filling tubes, since the polymer shrinks considerably during gelling, i.e. during raising the pH of the acetic acid solutions of chitosan. On the other hand, it is possible to spin fibers from chitosan, by spinning the chitosan solution into an alkali solution [East, 1993]. Coating of such a fiber with a hydrophobic shell and cutting the fiber in order to leave a free chitosan surface at the tip of the fiber would then probably lead to suitable bilayer membrane cushions as easy to handle as agarose filled teflon tubes but with improved membrane stability.

Often overlooked in model membrane research is the fact that physisorbed bilayer membranes confined to a certain area are subject to lipid loss [Fang, 1997], when the surrounding aqueous phase is exchanged continuously [Helm, 1989], [Helm, 1991], as for example in a flow cell. This phenomenon will lead to a fast reduction of the insulating properties of the membrane [Lind, 1996]. Future device configurations suitable to long-term applications have to take this effect into account either by adding lipid to the aqeous solution which keeps the lipid concentration above the CMC (critical micell concentration) or by using membranes with an excess area[6)].

[6)] Another solution to this problem is a complete tethering of the monolayer facing the electrode, which, however, is unfavourable for protein functioning. Partial tethering, however, does not solve this problem, since physisorbed lipids can still be dissolved in the electrolyte solution.

7 Incorporation and examination of membrane proteins in supported bilayer lipid membranes

It was shown in the previous chapter that chitosan-cushioned lipid membranes possess a sufficient stability and lateral fluidity. According to chapter 2, the last step towards a functionalised model membrane is the incorporation of trans-membrane proteins, which add functionality to the membrane. The present chapter presents first steps towards functionalised model membranes on field-effect transistors, which, however, have more the character of an outlook. In the first part, as a proof of principle, the proton pump cytochrome c oxidase [Naum, 1999] will be incorporated into a chitosan-cushioned bilayer lipid membrane. In the second part, the proton pumps nitrate reductase [Borc, 1999], [Kirs, 1999], [Zaum, 2000] and H^+-ATPase (CF_0F_1 ATPase from chloroplasts) [June, 1987], [Kaga, 1999], [Naum, 1995b] will be used to bio-functionalyse the surface of an ion sensitive field-effect transistor gate (electrolyte-oxide ion sensitive field-effect transistors, EOSFETs), by the formation of a protein-containing bilayer lipid membrane.

7.1 Incorporation of membrane proteins: addition of cytochrome c oxidase (COX) to chitosan-supported lipid membranes

In the following section, cytochrome c oxidase from bovine heart labelled with the fluorescence probe FITC [Mara, 1998] (see chapter 8.4) was used to detect protein incorporation into a pre-formed chitosan-supported bilayer lipid membrane.

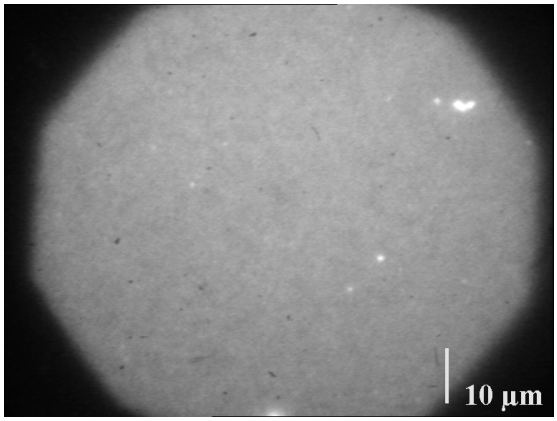

Figure 7.1: Fluorescence image of an eggPC bilayer on chitosan, which contained the integral membrane protein COX, labelled with a fluorescence probe (the bilayer itself was not labelled in that case). Previously to protein incorporation, the bilayer was deposited using 35 mN/m as lateral pressure and 15 °C as deposition temperature. Detergent dilution was performed at room temperature.

Protein incorporation was performed by the method of detergent dilution, as described in chapter 3.10.6. An almost completely homogeneous appearance of the protein-lipid membrane was obtained, as indicated by Figure 7.1. Hence, there was no domain formation resolvable by the optical microscope.

The protein itself was partially mobile at room temperature, as indicated by FRAP measurements (Figure 7.2).

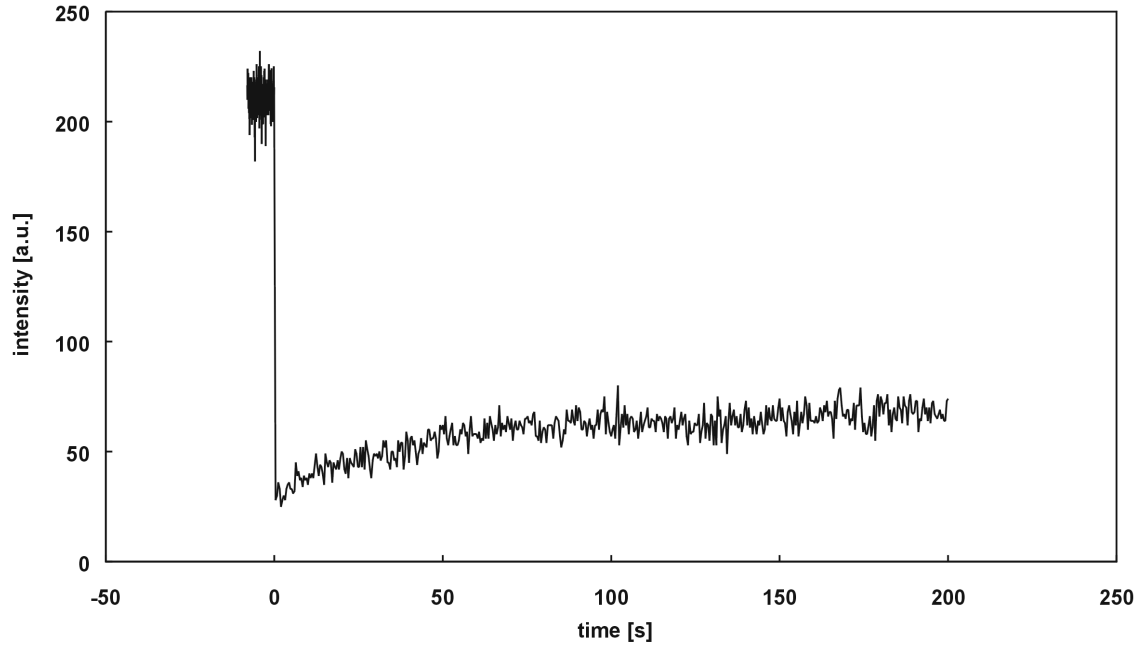

Figure 7.2: Diagram of a FRAP measurement, performed by bleaching fluorescence probes chemically attached to the integral membrane protein COX, incorporated into an eggPC bilayer membrane supported by a chitosan cushion, temperature: 25 °C.

Diffusion coefficients, however, were highly variable: D = 0.08 ± 0.093 μm^2/s at room temperature. Recovery values were found to be 26 ± 6.1 %. The high variability of D, as well as the low recovery values could be a result of a domain or cluster formation, not resolvable by the fluorescence microscope. Assuming the applicability of the Saffman-Delbrück equation (see chapter 5.3.1), according to (7.1.1), the radius R (not to be confused with a relative recovery) of the membrane protein may be estimated from diffusion measurements.

$$R = \frac{\eta h}{\eta_w}\left(\exp\left(\frac{4\pi h D}{kT}\right)+\gamma\right)^{-1} \qquad \textbf{(7.1.1)}$$

(7.1.1) results from solving (5.3.5) for R (see chapter 5.3.1 for details). Inserting suitable values for the membrane viscosity, η [Merk, 1989], water viscosity, η_w, membrane

thickness, h, Boltzmann constant, k, temperature, T, and the Euler constant, γ, the calculated radius of the protein turned out to be much too high to be reasonable [Tsuk, 1995]. Hence a considerable friction of the protein at the membrane/support interface had to be assumed [Evan, 1988], [Kühn, 1994]. In natural cells the diffusion of membrane proteins is slowed down also, by the presence of cytoskeletal constraints. This has been shown by detaching the membrane from the cytoskeleton by the exertion of hypoosmotic stress [Thom, 1992].

It can be deduced from the experiment described above that large trans-membrane proteins can be incorporated into pre-formed, chitosan-cushioned bilayer lipid membranes in a laterally mobile and therefore possibly functionally active form. It was shown in chapter 6.2.6 that chitosan-cushioned membranes prepared by Langmuir-Blodgett trough methods possess poor electrical properties. This does not necessarily pose a problem for an analysis of protein activity by means of EOSFETs, since the transistor gate monitors the local concentration of protons at the gate surface. Hence even in case of leaky membranes, trans-membrane proton pumps, which are pumping into the gate direction will increase the local proton concentration at the gate surface, provided the polymer cushion which separates the membrane from the gate is sufficiently thin. As was shown in chapter 6.2.5, vesicle fusion was not possible on chitosan cushions. However, the EOSFETs available at the time the experiments described in the present work were carried out, did not allow for a Langmuir-Blodgett transfer of lipid membranes. Backside contacted EOSFET-chips were developed by S. Ingebrandt, MPI-P Mainz [Inge, 2001], but were available only too late to be used in the present work. Hence, as a further proof of principle, bilayer lipid membranes were deposited directly onto the oxidic gate of EOSFETs by vesicle fusion. Proteins could be incorporated into such EOSFET-supported bilayer lipid membranes by using vesicles, containing reconstituted proteins such as nitrate-reductase, or H^+-ATPase. The activity of these functionalised model membranes was then analysed qualitatively. It is possible that the presence of solid oxide substrates reduces the protein activity. On the other hand, the experiments outlined above can be regarded as first steps towards the setup depicted in Figure 7.3.

7.2 Analysis of protein functionality by means of ion sensitive field-effect transistors

The possibility to monitor the functional activity of transmembrane proteins by means of field-effect transistors is a fascinating way to merge biological and electronic components (Figure 7.3). While FETs are currently widely explored for their use as planar transducers

for electrical signals of single biological cells, artificial networks of biological cells and tissue slices [Berg, 1970], [Berg, 1976], [From, 1991], [Offe, 1995], [Offe, 1997], [Sprö, 1997b] only seldom have they been used for studying functionalised model membrane systems [Otte, 1992], [Otte, 1993]. To the best of the author's knowledge, the only transmembrane protein, which was successfully incorporated into a FET-supported model membrane so far, is the transport protein lactose permease. It cotransports lactose and H^+ ions through the erythrocyte membrane in a stoichiometric ratio of 1:1 [Otte, 1992].

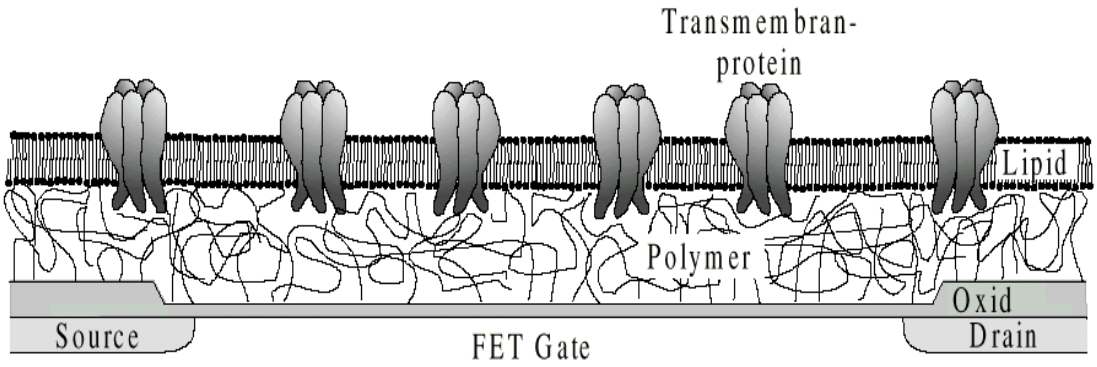

Figure 7.3: Schematic setup for the measurement of trans-membrane protein activities by means of field-effect transistors. It is favourable for protein functioning, to decouple the membrane from an oxide support.

Principally, FETs can be used in two different modes for the measurement of transport through a cell membrane or a model membrane. The first one is purely electrical in nature. It is basically the measurement of changes in transmembrane potential, occurring as a result of changes in the concentration of ions in one or both of the compartments, which are separated by the membrane. This can for example be the result of a passive transport by channel proteins, or an active transport by ion pumps. The detection of transmembrane potential changes due to channel activity, however, needs either a rather high signal or an extremely minimised signal to noise ratio of the electrical setup [Inge, 2001].

The second effect is partially chemical in nature: ion sensitive field-effect transistors (ISFETs) bind certain ions specifically (see chapter 3.7). Thereby, the surface potential of the ISFET changes, which is monitored by alterations in the source-drain current. The latter effect, the signal magnitude of which is at least two orders of magnitude higher compared to the former one [Inge, 2001], was used in the present work.

7.2.1 Self-healing and lateral fluidity of membranes deposited onto FETs

A first step in building up a functionalised model membrane system on the gate surface of a field-effect transistor is the characterisation of properties of the model membrane itself. The self-healing of membranes is an advantageous condition for their long-term stability.
In [Krau, 2000], so called extended gate electrodes (EGEs) were developed which allow for an analysis of membrane signals by means of commercially available field-effect transistors. The EGEs consisted of glass wafers onto which thin photolithographically patterned gold films were deposited.

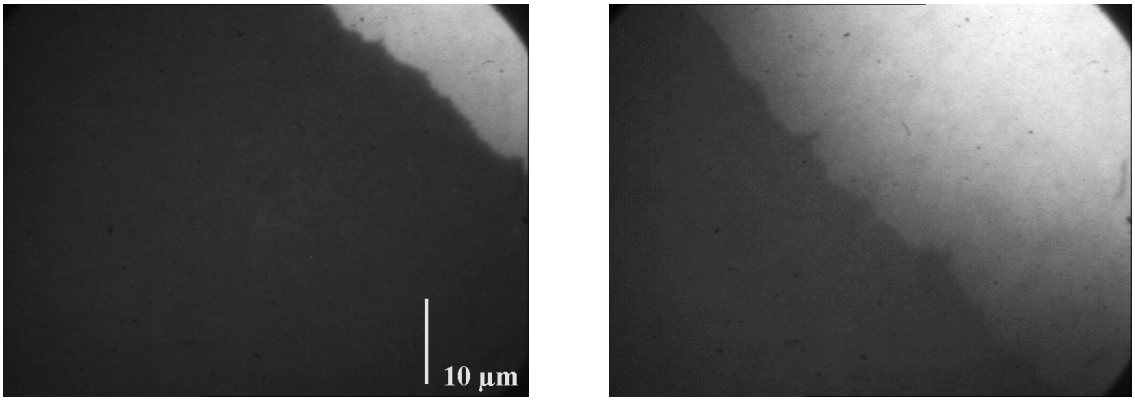

Figure 7.4: Fluorescence images of a spreading sequence of a lipid bilayer, spreading from an eggPC reservoir which had been deposited onto the FET surface and re-swollen in MilliQ water. Time difference between the two pictures: 7 min. Spreading was analysed at room temperature.

These were isolated by the deposition of additional layers [Krau, 2000]. Small holes (of a depth of approximately 0.5 µm) in the insulating layers defined the electrode area. The top layer of the isolated areas of EGEs (and the gate area of EOSFETs) consisted of a SiO_2 film (thickness 100 nm), which allowed for bilayer sliding from a lipid reservoir deposited onto the SiO_2 surface, as shown in Figure 7.4. Hence bilayer membranes on EOSFET gates and on the isolating surface of EGEs possess self-healing properties.
Bilayer lipid membranes spanning the wells above the gold film of an EGE would represent suitable model membrane systems, since large integral membrane proteins could be incorporated due to the freely suspended bilayer. Such a method for forming model membranes on devices was proposed in [Rädl, 1993a]. However, experiments with EGEs revealed, that the spreading bilayer did not span the hole on top of the EGE surface, as depicted in Figure 7.5. Black areas at the location of the EGE indicated either a ruptured bilayer, or a partial adsorption of the membrane. In the latter case, the reduced fluorescence intensity would be the result of fluorescence quenching by gold.

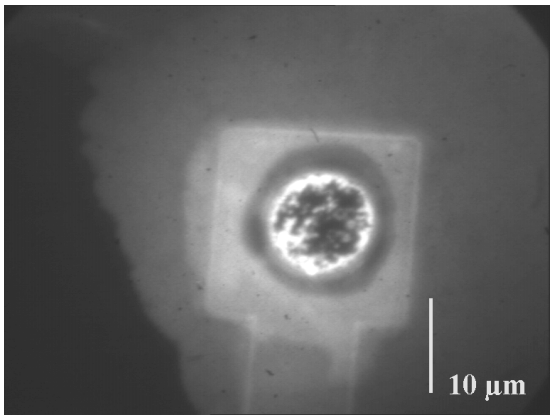

Figure 7.5: Fluorescence image of a spreading bilayer. The impossibility to span the hole in the SiO_2 surface on top of the EGE is expressed by the heterogeneous membrane structure in the EGE area. The black areas at the area of the EGE either stem from a ruptured membrane or from a partially adsorped membrane on the gold support.

The impossibility to use the spreading effect of lipid bilayer membranes on surfaces to span bilayers over holes in the µm range has been observed by others also [Grit, 1997]. Hence considerably smaller electrode holes would be required in order to prepare a freely suspended membrane by bilayer spreading.

Vesicle fusion experiments on EOSFET surfaces, however, indicated that fluid, homogeneous membranes resulted, with an almost complete fluorescence recovery, and diffusion coefficients in the range which were obtained for glass-supported membranes. Hence lipid bilayer membranes on ion sensitive EOSFETs are interesting systems to study membrane functionalisation. Functionalised membranes were prepared by the fusion of vesicles containing integral membrane proteins onto the surface of EOSFETs.

7.2.2 Functional activity of nitrate reductase

The dissimilatory, membrane-bound nitrate reductase, isolated from the bacterium "Pseudomonas stutzeri" [Blüm, 1991] and reconstituted into vesicles consisting of POPE/DMPC (1:1) was kindly provided by P. Steinrücke, Institute of Molecular Biotechnology, Jena, Germany. The above mentioned enzyme converts nitrate to nitrite in a mediated redox reaction (see Figure 7.6). It has been shown that the natural redox mediator ubiquinol can be replaced by artificial ones like benzylviologen [Kirs, 1999]. Nitrate reductase from "Pseudomonas stutzeri" is assumed to transport two protons per converted nitrate molecule through the bilayer membrane (see Figure 7.6) into the interior of the bacterium. The nitrate conversion of the enzyme described above has been used as a basis for a number of nitrate biosensors (e.g. [Borc, 1999] and references therein).

Liposomes containing nitrate reductase were extruded as described in chapter 3.10.4 and fused onto the gate surface of n-channel EOSFETs [Inge, 2001]. Fusion times were generally one hour or longer. An electrolyte solution (110 mM K_2SO_4) was used, buffered by 20 mM Hepes at a pH of 7.5, which corresponds to the maximum activity of nitrate reductase [Borc, 1999].

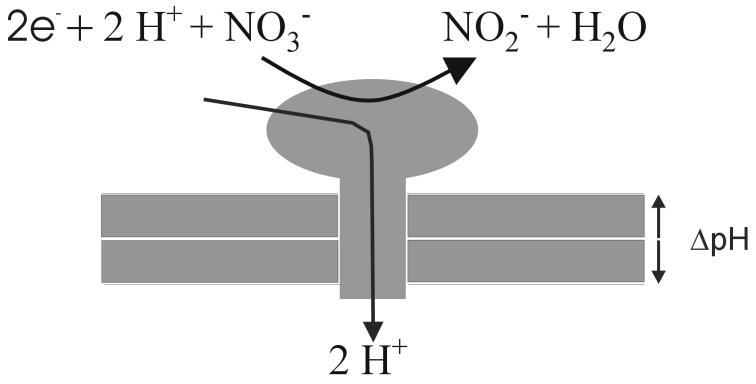

Figure 7.6: Schematic representation of membrane-bound nitrate reductase. The enzyme catalyses the reduction of nitrate to nitrite and is assumed to transport two protons per converted nitrate molecule through the bilayer membrane, thereby producing a pH gradient.

Figure 7.7 shows the source-gate voltage of a nitrate reductase containing membrane – covering an EOSFET array – as a function of time. The source-gate voltage depends on the proton concentration at the gate surface, according to the so-called site-binding model (see [Sprö, 1997a], [Yate, 1974] and chapter 3.7 for details). In case of a n-channel EOSFET, an increase in proton concentration will yield an increase in source-gate voltage [Inge, 2001]. According to Figure 7.7, the addition[7)] of the redox mediator benzylviologen (which was enzymatically reduced by Diaphorase/NADH, see chapter 8.4), which is necessary as an electron donor for the reduction of nitrate, led to an increase in the source-gate voltage. On the other hand, the addition of nitrate solution prior to the addition of the redox mediator did not lead to a measurable signal response. This can be explained by assuming a local increase in proton concentration in the membrane/gate gap. The slight relaxation of the signal after the initial rise could have arisen from a diffusion potential due to transient concentration gradients after addition of the mediator solution. As a reference experiment, both nitrate and redox mediator were added to a membrane-covered EOSFET array, while the protein was omitted.

[7)] In every case, the addition of a certain compound in the present chapter refers to the addition of 10 µl of solutions of the concentrations described in chapter 8.4.

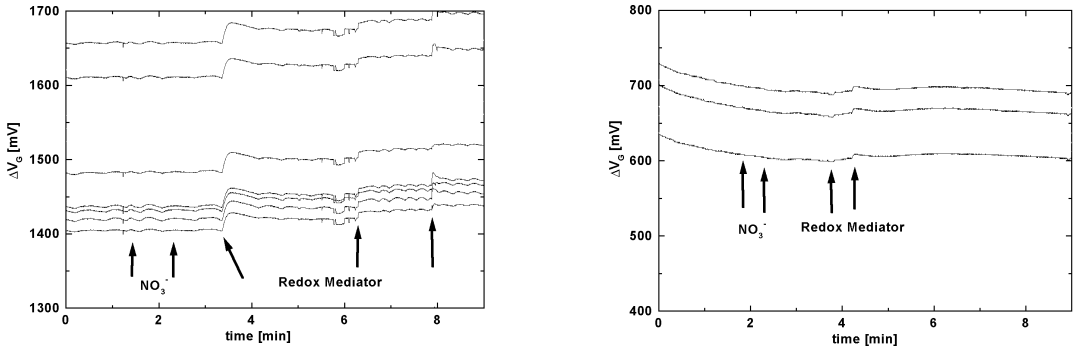

Figure 7.7: Left picture: EOSFET activity measurements of nitrate reductase incorporated into a DMPC/DOPC planar supported bilayer obtained from vesicle fusion of protein-containing vesicles. Right picture: as a reference experiment, the addition of nitrate and redox mediator to an EOSFET system without membrane (and protein) was analysed.

The addition of the mediator resulted in a slight, transient rise of the source-gate voltage, which again could possibly be ascribed to a diffusion potential (Figure 7.7, right part). The much larger step of the source-gate voltage in case of a protein containing membrane, is a strong support for the hypothesis that nitrate reductase can be incorporated into EOSFET-supported bilayer lipid membranes in a functionally active form. Protons are accumulated in the membrane/gate gap by an active proton transport process by the proton pump nitrate reductase. The signal shape and the dependence on system parameters, however, have to be clarified in future experiments.

7.2.3 Functional activity of H^+-ATPase

As a second example for the functionalisation of EOSFET-supported lipid membranes the proton pump H^+-ATPase was used. The natural function of the membrane bound H^+-ATPase is the synthesis of ATP from ADP, which is energetically coupled to a relaxation of a proton concentration gradient across the membranes of e.g. mitochondria and chloroplasts. Provided an excess of ATP is present, this process can be reversed, i.e. protons can be pumped against a trans-membrane gradient by converting ATP to ADP [Kaga, 1999]. H^+-ATPase has been used successfully in a number of biosensor applications (e.g. [Naum, 1995b]). In the present case, H^+-ATPase containing bilayer membranes on EOSFET surfaces were prepared by fusing protein-containing eggPC vesicles to the gate surface. H^+-ATPase reconstituted into eggPC vesicles was a kind donation of P. Gräber, Freiburg. Vesicle fusion was performed in a pH = 7.4 buffer, described in chapter 8.4. Figure 7.8 demonstrates the EOSFET response upon addition of ATP solution. An initial strong and steep rise of the source-gate voltage was followed by a decay to a value below the original one. Furthermore, a reference experiment was carried out using the same

configuration as described above, however, with the specific H^+-ATPase inhibitor venturicidin [Naum, 2001] present in the buffer solution. A step towards a lower source-gate voltage was observed upon addition of ATP solution (the pH of which was adjusted to 7.4). However, the initial signal rise, was absent in this case (Figure 7.8, right part). The initial rise could be explained by an increased proton concentration at the gate surface, due to proton pumping of H^+-ATPase. This process is inhibited in case of venturicidin present in the buffer solution. The subsequent drop of the source-gate voltage is a passive effect induced by the ATP solution, which could be an altered ionic strength in general or a changed sodium concentration in particular. According to [Inge, 2001], the EOSFET is sensitive not only to the proton concentration, but also to the sodium and potassium concentration of the buffer. The initial signal rise in case of H^+-ATPase present in the bilayer membrane could be explained by the fact that the increase in proton concentration at the membrane/gate gap is due to an active proton transport. The latter could be faster than a passive alteration of the membrane/gate gap medium, which occurs upon addition of ATP solution due to diffusion through small defects in the membrane.

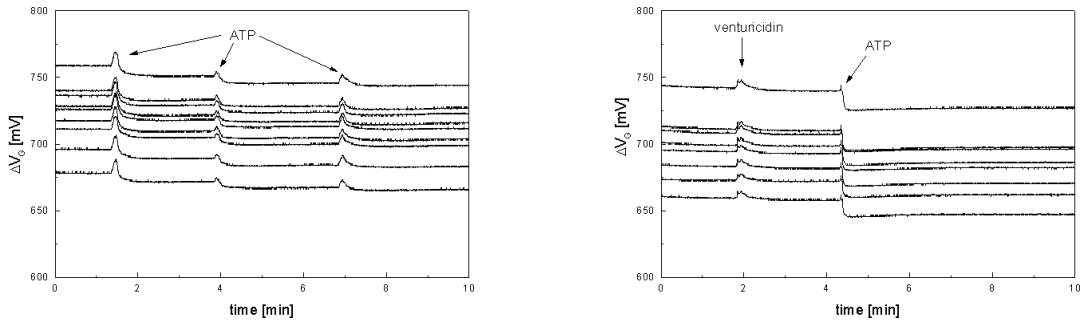

Figure 7.8: EOSFET activity measurements of H^+-ATPase, incorporated into a planar supported eggPC bilayer obtained from vesicle fusion of protein-containing vesicles. Left: no inhibitor was added, right: inhibitor-containing system.

As a further reference experiment, eggPC vesicles were fused to the gate of an EOSFET array. Neither the addition of venturicidin nor ATP solution led to the signal rise observed in the left part of Figure 7.8, underlining the hypothesis that this initial rise could stem from an active proton transport by H^+-ATPase. On the other hand, the drop of the source-gate voltage upon addition of ATP as observed in Figure 7.8 was found in that case also.

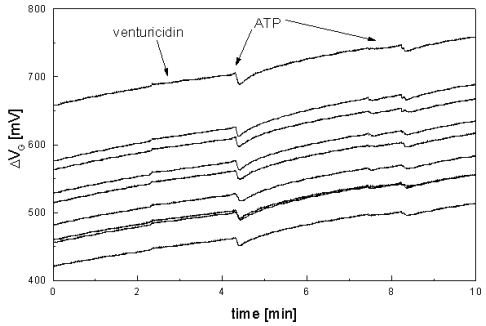

Figure 7.9: Reference experiment: eggPC bilayer on an EOSFET surface, without H^+-ATPase present. The baseline drift is due to a transistor instability [Sprö, 1997a].

7.3 Conclusion and outlook

Clearly, the experiments described in the present chapter were only qualitative and highly preliminary in nature at the current stage of research. They were mostly designed to provide an outlook for future applications of the systems described. However, reference experiments as outlined above underline the hypothesis that membrane functionalisation of EOSFET-supported bilayer lipid membranes in case of nitrate reductase and H^+-ATPase was achieved.

It must be noted that several conditions, used for the detection of the functional activity of trans-membrane proteins described above, were highly unfavourable and can well be optimised in future experiments. Firstly, the influence of the non-biological SiO_2 surface of the field-effect transistor gate is likely to affect protein properties in an unfavourable way. In fact the bio-functionalisation of an EOSFET-supported lipid membrane with cytochrome c oxidase failed, i.e. no protein activity could be detected. This might by due to protein denaturation through interaction with the gate surface. Secondly, it is known that the application of a positive potential pulse to H^+-ATPase leads to increased activities [June, 1987]. Thirdly, the setup could be much improved by building a flow cell for fluid exchange.

Finally, the backside-contacted EOSFET-array chips developed by S. Ingebrandt, MPIP Mainz [Inge, 2001], which allow for Langmuir-Blodgett transfer of model membranes, offer a promising route for studying functionalised model membrane systems in more detail. This approach might possibly open a way for studying membrane/substrate interactions on a "higher level", i.e. to analyse the influence of substrate properties on protein functionality. Such an investigation would include both the effect of the direct substrate/protein interaction on the protein activity and the indirect influence of the membrane support on protein functionality by the membrane/support interaction.

8 Materials

In the following, the compounds that were used to build up model membrane systems will be described and – where necessary – some background information concerning the physicochemical behaviour of these compounds will be provided.

8.1 Bilayer support

8.1.1 Substrates

In most cases, microscopic coverglasses served as supporting substrates (Mettler Glas, Rettberg, Göttingen, width 2.6 cm, length 3.2 cm, thickness between 130 and 160 µm, roughness 3.0 Å in a region of 1 µm²). Alternatively, silicon wafers (IMM, Mainz, thickness 600 µm) were cut into convenient pieces (usually 1 cm times 3 cm). The wafers were either thermally oxidised (160 nm SiO_2, roughness 1.8 Å in a region of 1 µm²) to avoid quenching in fluorescence experiments or covered by a natural oxide layer (about 1.5 nm thick, roughness 1.5 Å in a region of 1 µm²).

8.1.2 Polymers

The polymers agarose and chitosan were used as spacer between substrates and membranes. Both polymers possess the ability to form water insoluble, but water swellable hydrogels. These have no covalent crosslinks are therefore physically crosslinked in the insoluble state. Additionally, a lipopolymer was applied, which, however, will be described in chapter 8.2.2.

Agarose

Agarose is the main component of agar, which is a mixture of two different polymers. Agarose is a linear polysaccharide, consisting of a disaccharide repeating unit. Additionally, agar contains 30 % of agaropectin, a linear molecule with a complicated structure. Agar is – besides carrageenans and alginates – the most familiar polysaccharide from the class of marine polysaccharides. It is derived from certain genera of the Rhodophyceae group of Red Sea weeds [Clar, 1987]. The function of agarose *in vivo* is to provide retention by structuring the interstitial fluid regions of marine plant organisms. The molecular weight of agarose is about 10^5 g/mol. It shows a thermoreversible gelation

which occurs when a hot solution is cooled below ~ 40 °C, at concentrations in excess of 0.1 mass%. The gel melting point is much higher (~ 90 °C) than the gel forming temperature. The molecular origin of cross-linking in agarose gel networks is currently not well understood. Mechanisms considered to be responsible for gel formation include the formation of double helix junction zones or junction zones arising from anisotropic microcrystalline domains dispersed in an isotropic supporting phase (see [Clar, 1987] and references therein).

Figure 8.1 shows the predominant chemical structure of the disaccharide repeating unit consisting of a β-D-galactose and a 3,6-anhydro-α-L-galactose residue.

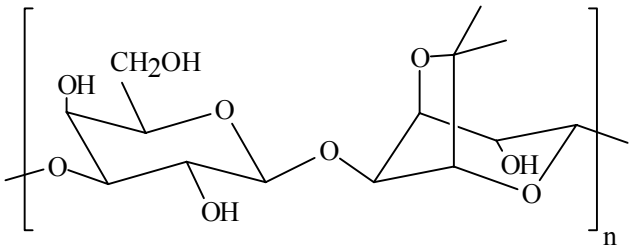

Figure 8.1: Chemical structure of the repetition unit of agarose, left unit: β-D-galactose, right unit: 3,6-anhydro-α-L-galactose.

The galactose units are partially ether- and esterified by the formation of O-methyl groups, sulfate groups and pyruvic acid residues, which render the agarose molecule slightly negatively charged. Agarose applied in the present work was obtained from Fluka, and used without purification.

Chitosan

As an alternative to agarose, chitosan, another polysaccharide, was used. Chitosan (poly(glucoseamine)) is a linear molecule (~ 10^6 g/mol) and has a monosaccharide repeating unit. It is derived from chitin by deacetylisation. Chitin is the second most abundant polysaccharide on earth (after cellulose) and is the main structural unit of the exoskeletons of insects and crustacea. Chitosan is built up by β-1,4-glucoside linkages and is therefore structurally similar to cellulose, the only difference being the amino group instead of a hydroxyl group in the C-2 position.

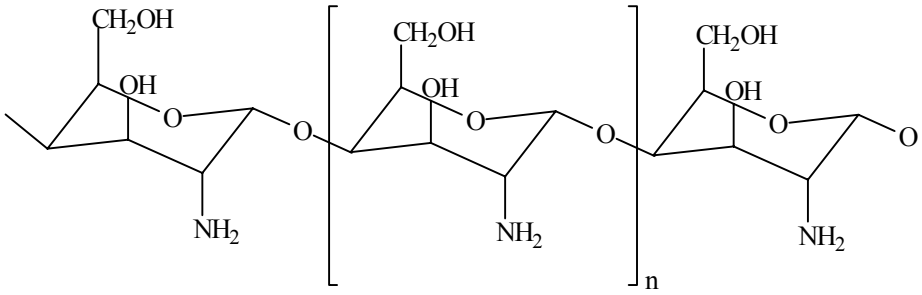

Figure 8.2: Chemical structure of the repetition unit (glucoseamine) of chitosan.

Chitosan is soluble in weak acids like diluted acetic acid. The pK_a value of the glucoseamine segments is in the range 6.3 – 7 [Clae, 1992], which leads to a slight protonation in case the polymer is immersed in MilliQ water (pH = 5.5). Upon rehydration of a dry chitosan film in neutral or alkali solutions, a hydrogel forms [Blai, 1987], [Mats, 1999], [Khal, 1999], which can be regarded as an entanglement network. While usually chitosan films are neutralised by means of strong alkali solutions, this procedure was not followed in the present work due to the edging effect of alkali on SiO_2 surfaces. Instead, neutralisation of the polymer film was performed using a borate buffer (pH = 9.22, Merck, Darmstadt). Dissolution of chitosan was performed in 1 vol% acetic acid solution, by stirring over night. Usually, chitosan concentrations used for preparing films were 1 mass%. Insoluble components were removed by centrifuging and filtering. Chitosan was obtained from Fluka and used without purification.

8.2 Lipids

In the present work, in most cases phospholipid molecules (apart from DHDAB) were used for the preparation of mono- and bilayer membranes. In the following subsection, lipids with relatively small headgroups will be described. Afterwards, phospholipid molecules with hydrophilic polymer chains attached to the lipid headgroup will be presented. All lipids were used as obtained without purification.

8.2.1 Lipids with small headgroups

DMPC

DMPC (1,2-Dimyristoyl-*sn*-glycero-3-phosphatidylcholine, M_w = 677.95 g/mol, Avanti Polar Lipids, Alabaster, USA) has two identical, fully saturated hydrocarbon chains.

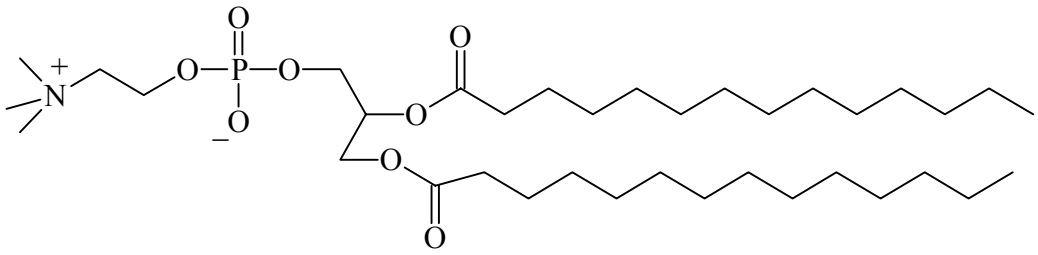

Figure 8.3: Chemical structure of DMPC (1,2-Dimyristoyl-*sn*-glycero-3-phosphatidylcholine).

The main transition of DMPC bilayers occurs at 23.8 °C [Mars, 1990]. The following diagram shows the temperature dependence of DMPC-isotherms on a Langmuir trough.

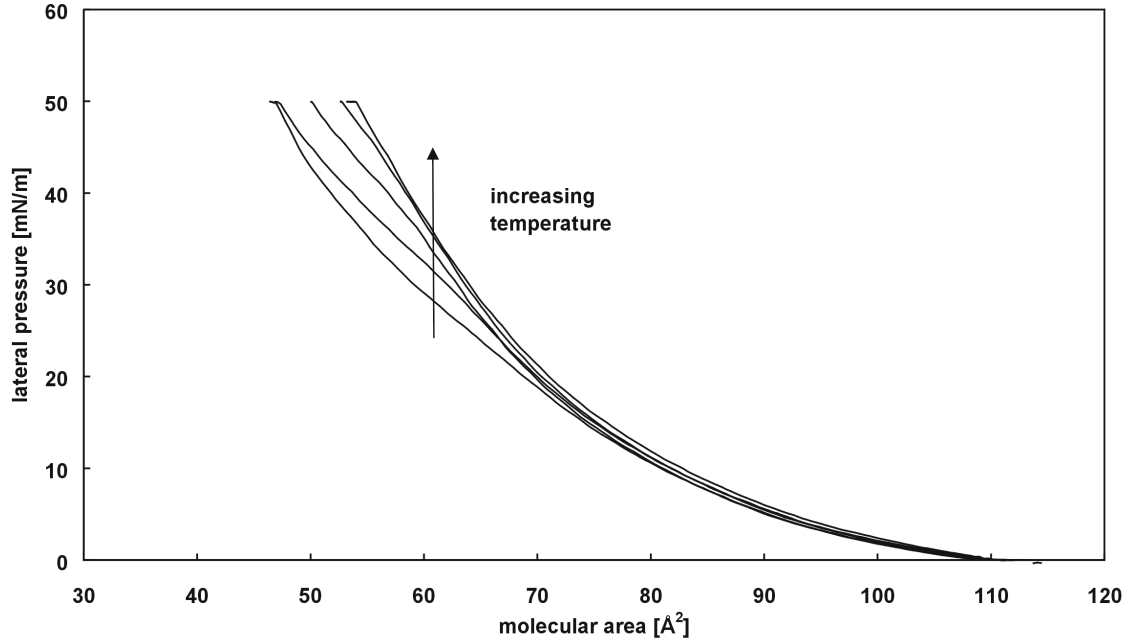

Figure 8.4: DMPC isotherms obtained with a Langmuir film balance, at different temperatures. The temperature was varied between 10 °C and 30 °C at steps of 5 °C.

The isotherms show the pressure-dependent main transition of lipid monolayers. The coexistance region, however, becomes more narrow at higher temperatures, indicating that the temperatures used for the isotherm recordings shown in Figure 8.4 approach the critical temperature of the main phase transition for DMPC monolayers. At the critical temperature, the area difference due to the phase transition from the expanded to the condensed state approaches zero [Albr, 1978].

DLPE

DLPE (1,2-Dilauroyl-*sn*-glycero-3-phosphoethanolamine, M_w = 579.75 g/mol, Avanti Polar Lipids, Alabaster, USA) is a symmetric, fully saturated phospholipid with an ethanolamine headgroup.

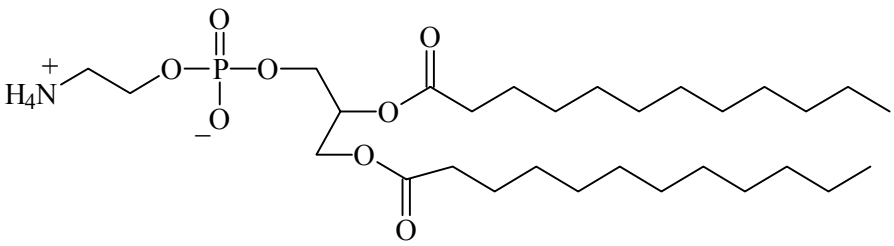

Figure 8.5: Chemical structure of DLPE (1,2-Dilauroyl-*sn*-glycero-3-phosphoethanolamine).

The main transitions of a DLPE bilayer occurs at 29 °C [Mars, 1990]. The following diagram shows the temperature dependence of the main transition in DLPE monolayers as observed in pressure/area isotherms on a Langmuir film balance.

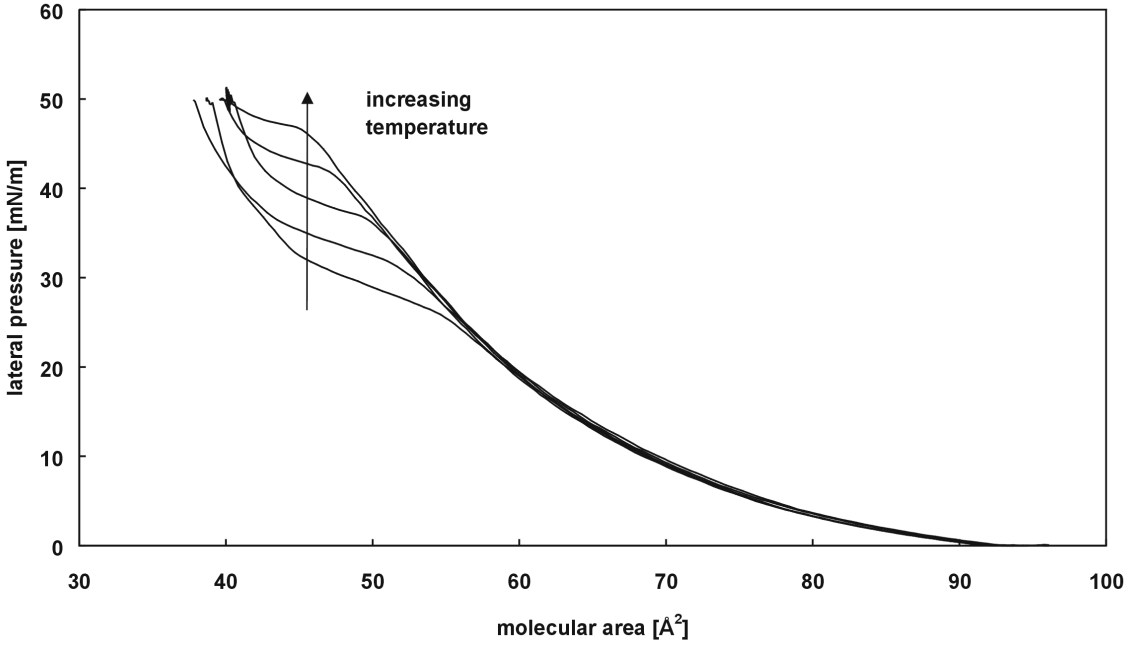

Figure 8.6: DLPE isotherms obtained with a Langmuir film balance, at different temperatures. The temperature was varied between 10 °C and 30 °C at steps of 5 °C.

Obviously, also in the case of DLPE a narrowing of the coexistence region (with respect to the molecular area) with increasing temperature is observed, indicating the approach to the critical temperature, which, however, seems to be higher compared to DMPC monolayers.

DPhyPC

DPhyPC (1,2-Diphytanoyl-*sn*-glycero-3-phosphatidylcholine, M_w = 846.27 g/mol, Avanti Polar Lipids, Alabaster, USA) possesses two identical phytanoyl residues. Due to these relatively bulky chains, the chain region occupies a higher area compared to the headgroup

region. The lipid bilayer does not show any phase transition between –120 °C and 120 °C [Lind, 1979].

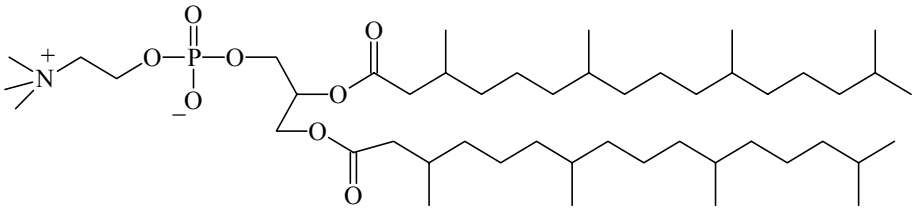

Figure 8.7: Chemical structure of DPhyPC (1,2-Diphytanoyl-*sn*-glycero-3-phosphatidylcholine).

No phase transitions were found on the Langmuir film balance also. Figure 8.8 shows isotherms of DPhyPC monolayers, which indicate the existence of a liquid expanded phase throughout the pressures and temperatures applied in the present work.

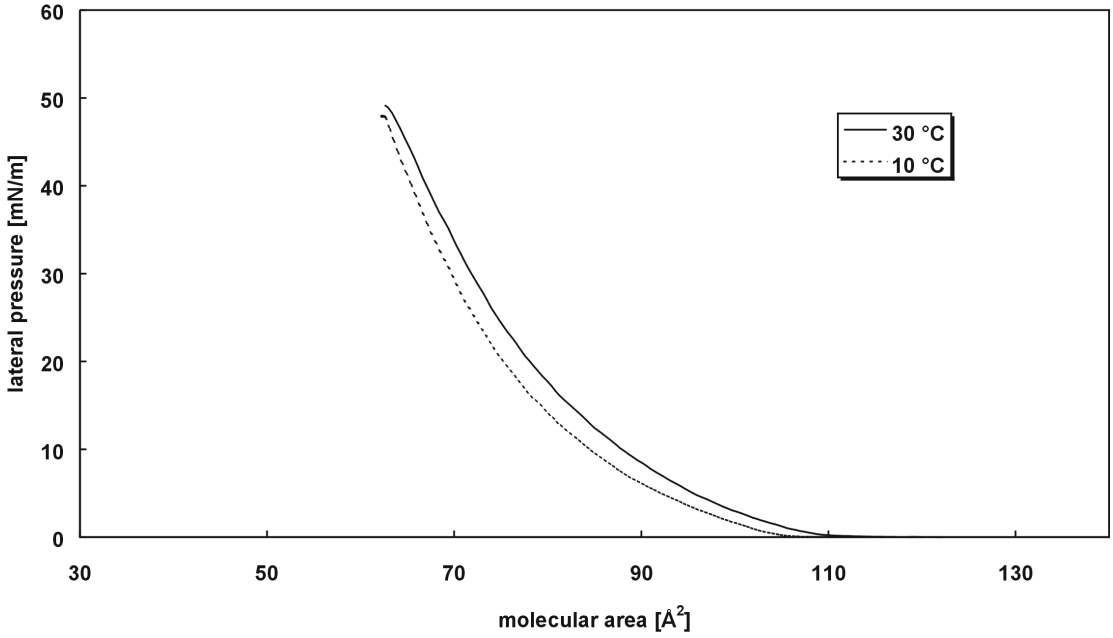

Figure 8.8: DPhyPC isotherms obtained with a Langmuir film balance, at different temperatures.

DSPC and DSPE

Furthermore, the lipids DSPC (1,2-Distearoyl-*sn*-glycero-3-phosphatidylcholine, M_w = 790.15 g/mol, Avanti Polar Lipids, Alabaster, USA) and DSPE (1,2-Distearoyl-*sn*-glycero-3-phosphoethanolamine, M_w = 748.07 g/mol, Avanti Polar Lipids, Alabaster, USA) were used, which are - at the temperatures and lateral pressures used in the present work - in the liquid condensed phase-state (in case of bilayers: gel state).

DHDAB

DHDAB (Dihexadecyldimethylammoniumbromid, M_w = 574.85 g/mol, Fluka) is a synthetic lipid. It was used in the present work to build up bilayer membranes. Bilayers from DHDAB possess a main phase transition at 28 °C [Okah, 1981].

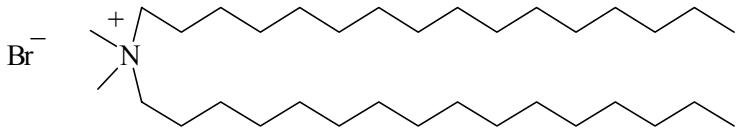

Figure 8.9: Chemical structure of Dihexadecyldimethylammoniumbromid.

EggPC and Asolectin

Besides the synthetic lipids described above, the natural lipid mixtures eggPC (average M_w = 760.6 g/mol, Avanti Polar Lipids, Alabaster, USA) and Asolectin (Fluka) were used. EggPC is derived from hen's eggs, and consists to 95 % of a phosphatidylcholine mixture of saturated and unsaturated lipids. A minor component is sphingomyelin. EggPC bilayer membranes do not show a gel phase.

Asolectin is derived from soybeans. It consists to about equal amounts of cholines, cephalines and phosphatidylinositol.

Reactive lipids

In addition to the lipid molecules above, which were used to prepare physisorbed mono- and bilayer membranes on planar supports, a reactive fatty acid was synthesised in cooperation with S. Schiller, MPIP, Mainz (see Figure 8.10).

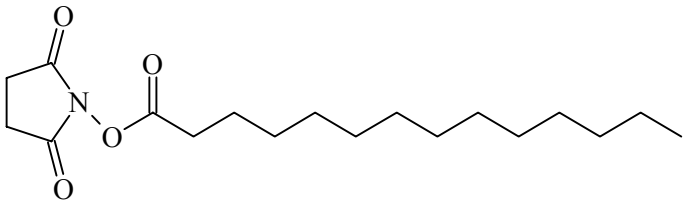

Figure 8.10: Chemical structure of N-succinimidomyristidic ester.

The amino-reactive active ester (M_w = 325.44 g/mol) was synthesised according to a receipt to be found in [Beye, 1996a].

Cholesterol

Cholesterol (3β-Hydroxy-5-cholesten, M_w = 386 g/mol, Avanti Polar Lipids, Alabaster, USA) is an important component of plant and animal membranes. Although the molecule

has an amphiphilic character (see Figure 8.11), cholesterol does not form bilayer membranes.

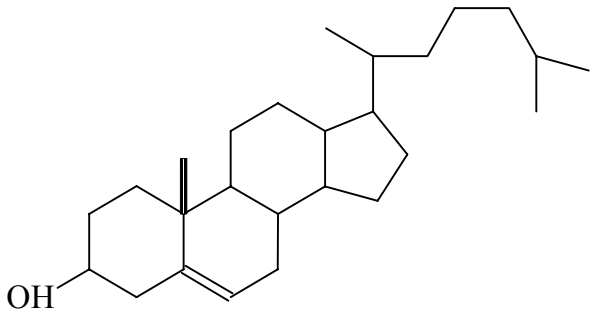

Figure 8.11: Chemical structure of cholesterol (3β-Hydroxy-5-cholesten).

Cholesterol causes an increase in density of membranes when incorporated into phospholipid bilayers. It occupies free volume and decreases the elastic properties of bilayer membranes.

8.2.2 Lipopolymers

As an alternative to the lipid molecules with relatively small headgroups mentioned above, lipopolymers were used. These consisted of DSPE, to which a short poly(ethyleneoxide) chain is attached (see next figure).

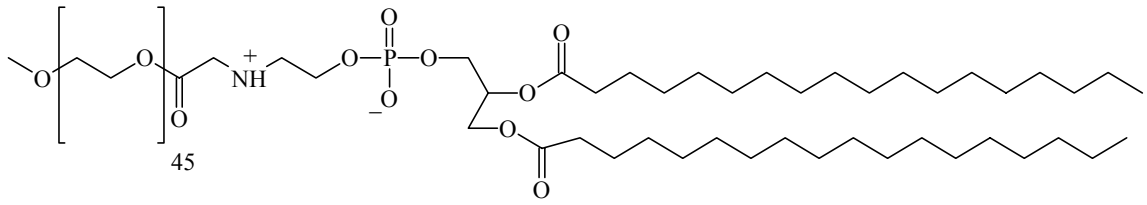

Figure 8.12: Chemical structure of DSPE-EO_{45}.

In most cases, a lipopolymer with 45 ethylene oxide units was used (1,2-Distearoyl-*sn*-glycero-3-phosphoethanolamine-N-[methoxy(polyethylene glycol)-2000], M_w = 2787.49 g/mol, Avanti Polar Lipids, Alabaster, USA). This lipopolymer was characterised as a component of Langmuir monolayers [Baek, 1995], [Maje, 1997], [Maje, 1998], [Maje, 2000] and used as a polymer support for bilayer membranes (e.g. [Sinn, 1998]).

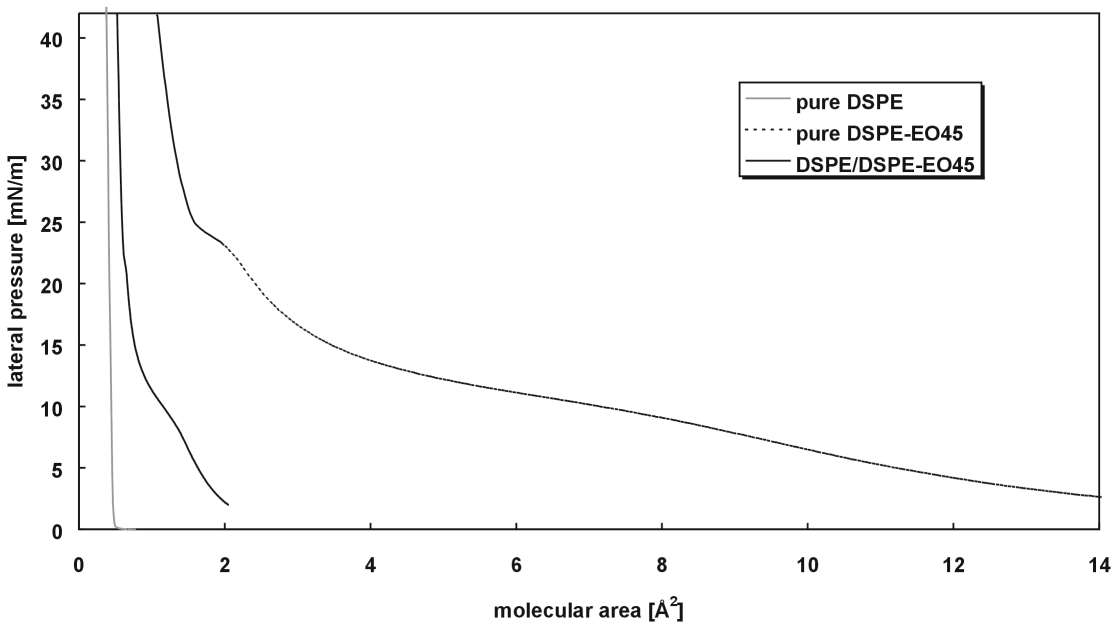

Figure 8.13: Isotherms obtained on a Langmuir film balance for DSPE, DSPE-EO_{45} and a mixture of both components of a molar ratio of 91/9, at 25 °C.

Figure 8.13 shows pressure/area isotherms for the pure lipopolymer, pure DSPE and a mixture of both components of a molar ratio of 91/9. At high molecular areas, the lateral pressure is dominated by the polymer attached to the lipid headgroup, whereas at small molecular areas the lateral pressure is largely influenced by the lipid molecules. The pure lipopolymer shows two phase transitions, the low-pressure transition corresponds to a pancake to mushroom transition, the high-pressure transition is a mushroom to brush transition [Baek, 1995].

8.3 Fluorescence dyes

In most cases in the present work, nitrobenzoxadiazole derivatives (NBD) were used. The amino- and thiol-reactive NBD-Cl (4-chloro-7-nitrobenz-2-oxa-1,3-diazole) was first synthesised in 1968 [Ghos, 1968] and has since then been widely used to label proteins, lipids and other biological compounds (for an overview over studies with NBD-labelled phospholipids see [Chat, 1990]). In the present work, head- and chain-labelled phospholipids (NBD-PE and NBD-PC, respectively), labelled cholesterol NBD-Chol and a further hydrophilic NBD derivative (NBD-X) were applied (see Figure 8.14). All probes (except from NBD-PC which was obtained from Avanti Polar Lipids, Alabaster, USA) were obtained from Molecular Probes, Leiden, Netherlands.

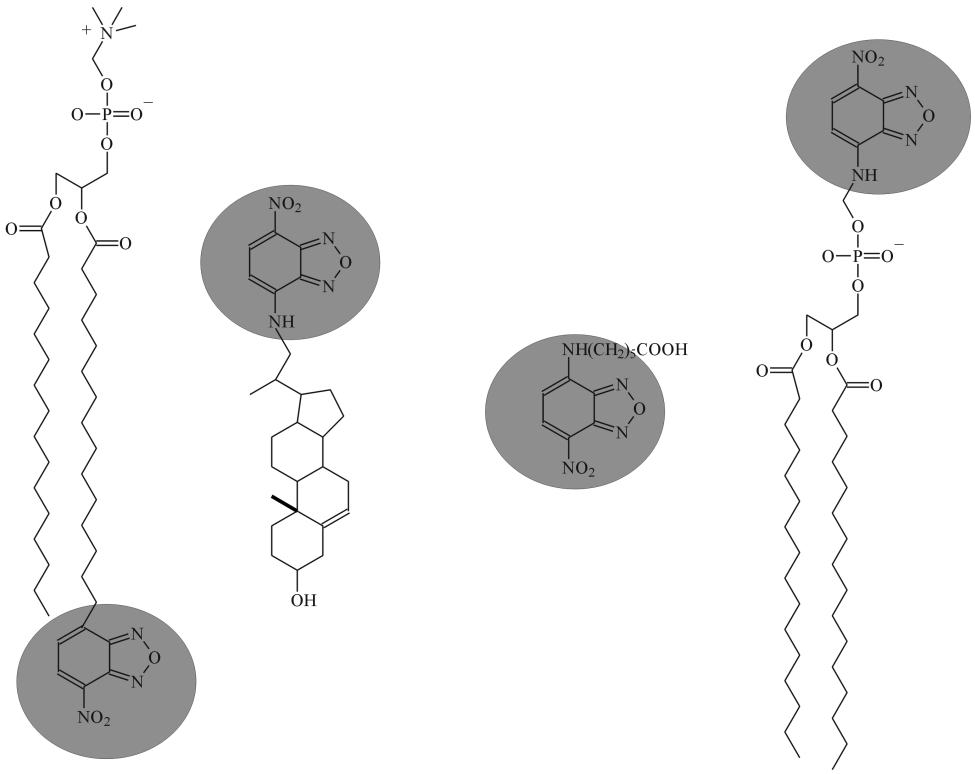

Figure 8.14: NBD derivatives used in the present work. From left to right: NBD-PC (M_w = 869.08 g/mol), NBD-cholesterol (M_w = 494.63 g/mol), NBD-X (M_w = 294.27 g/mol) and NBD-PE (M_w =956.25 g/mol).

Furthermore, the amphiphilic membrane probe DiI (Figure 8.15, Molecular Probes, Leiden, Netherlands) was used. Dialkylcarbocyanine probes belong to the most strongly absorbing dyes known, but have an only moderate fluorescence quantum yield. They are used in several different areas of research. An advantage compared to NBD is the higher photostability, which makes the probe more useful for fluorescence microscopy studies. However, despite the higher photostability DiI is still amenable to FRAP experiments [Mole, 1996]. The probe has been largely used for the staining of living cells where – once it has been applied – the probe is distributed laterally and the whole cell is stained (see [Mole, 1996] and references therein).

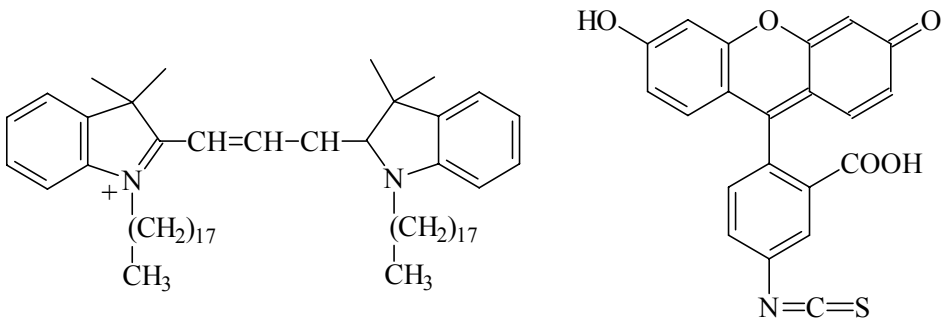

Figure 8.15: Chemical structures of DiI (M_w = 993.88) and FITC (M_w = 389.38 g/mol).

Finally, COX molecules labelled with the amino-reactive fluorescein derivative FITC were obtained from A. Aagaard, Göteborg. FITC is the most commonly used dye for protein labelling. The advantages of using FITC include its relatively high absorptivity, excellent fluorescence quantum yield, good water solubility and the fact that the excitation maximum closely matches the 488 nm line of argon ion laser, which allows for confocal microscopy, FRAP and other applications. There are, however, disadvantages of this particular probe, including the pH-dependent emission properties and a relatively high rate of photobleaching. In all cases of fluorescence labelling of lipid membranes, dye molecules were added to the lipid stock solution at a concentration of 1 mol% (with respect to the host lipid).

8.4 Proteins

Reconstituted H^+-ATPase was obtained from P. Gräber, Freiburg. Solubilised fluorescence labelled cytrochrome c oxidase was a gift from A. Aagaard, Göteborg, Sweden. Reconstituted nitrate reductase was kindly donated by P. Steinrücke, Jena. Additionally, the H^+-ATPase inhibitor venturicidin was obtained from P. Gräber, Freiburg (as a stock solution in ethanol).

The following solutions were used in case of protein studies:

H^+-ATPase buffer (pH = 7.4):

component	concentration [mol/l]
Tricin	0.01
Na_2HPO_4	0.01
$MgSO_4$	0.002
KCl	0.1

In some cases the buffer contained venturicidin, at a concentration of 220 µmol/l.

ATP solution (pH = 7.4):

component	concentration [mol/l]
ATP	0.1

COX buffer (pH = 7.4):

component	concentration [mol/l]
Hepes	0.04
KCl	0.1

Nitrate reductase buffer (pH = 7.5):

component	concentration [mol/l]
Hepes	0.02
KSO_4	0.11
NADH	0.01
Diaphorase	0.001
Benzylviologen[8)]	0.01

Nitrate solution (pH = 7.5)

component	concentration [mol/l]
$NaNO_3$	0.1

In every case the adjustment of pH was performed by adding diluted KOH solution and determining pH by a pH electrode (pH 526 WTM Weilheim, Germany).

[8)] The presence of this compound was optional

9 Abbreviations

$\overline{\upsilon}$	wave number
k	inverse of Debye screening length ($1/l$)
μ	chemical potential
	dipole moment
Θ	contact angle
l	Debye screening length
	jump length
	wavelength
r	density
Π	disjoining pressure
Ω	droplet volume
	Ohm
Δ	ellipsometric parameter Delta
Ψ	ellipsometric parameter Psi
	electrical potential
	surface potential
χ	Flory-Huggins parameter
ν	frequency
	protrusion potential
	molar volume
g	interfacial energy
	surface tension
	Euler constant
β	kinetic spreading coefficient
π	lateral pressure
∇	Nabla operator
ε	dielectric permittivity
τ	relaxation time
	density parameter
ω	angular frequency
	spinning velocity
s	surface charge
	lateral dimension of protrusions
η	viscosity
ζ	viscous drag coefficient
ϕ	volume fraction
ε_0	dielectric permittivity of the vacuum ($\varepsilon_0 = 8.854 \cdot 10^{-12}\ C^2J^{-1}m^{-1}$)
λ_w	decay constant of hydration pressure
µm	micrometer
δ	phase shift
Φ	internal reflection angle
τ_D	characteristic diffusion time
A	area
a	free area
	molecular area
	Onsager cavity radius

Å	angstroems
a.u.	arbitrary units
a_0	diameter of a polysaccharide monomer unit
ADP	adenosine diphosphate
AFM	atomic force microscopy
ATP	adenosine triphosphate
ATR	attenuated total internal reflection
a_w	water activity
BLM	black lipid membrane (or bilayer lipid membrane)
b_s	interfacial friction coefficient
c	concentration
	velocity of light
C	curvature
	probability distribution
CMC	critical micelle concentration
COX	cytochrome c oxidase
D	diffusion coefficient
D	Debye
DHDAB	Dihexadecyldimethylammonium bromide
DiI	1,1'-Dioctadecyl-3,3,3',3'-tetramethylindocarbocyanine perchlorate
DLPE	1,2-Dilauroyl-*sn*-glycero-3-phosphoethanolamine
DLVO	Debye-Landauer-Verwey-Overbeck
DMPC	1,2-Dimyristoyl-*sn*-glycero-3-phosphatidylcholine
DPH	1,6-Diphenyl-1,3,5-hexatriene
DPhyPC	1,2-Diphytanoyl-*sn*-glycero-3-phosphatidylcholine
DPhyPE	1,2-Diphytanoyl-*sn*-glycero-3-phosphoethanolamine
DPPC	1,2-Dipalmitoyl-*sn*-glycero-3-phosphatidylcholine
DSPC	1,2-Distearoyl-*sn*-glycero-3-phosphatidylcholine
DSPE	1,2-Distearoyl-*sn*-glycero-3-phosphoethanolamine
DSPE-EO_{45}	DSPE with 45 ethyleneoxy-units attached to the lipid headgroup
e	electronic charge ($e = -1.602 \cdot 10^{-19}$C)
	minimum height of spreading films
E_a	activation energy
EGE	extended-gate electrode
eggPC	mixture of phosphatidylcholines obtained from eggs
EOSFET	electrolyte oxide semiconductor field-effect transistor
F	Farad
f	force per unit length
	friction coefficient
F	fluorescence intensity
	force
FET	field-effect transistor
FITC	fluorescein isothiocyanate
FRAP	fluorescence recovery after photobleaching
FTIR	Fourier transform infrared spectroscopy
g	acceleration constant ($g \approx 9.8$ m/s²)
	surface contour of an object
G	Gibbs free energy
H	Hamaker constant
h	hours
	Planck's constant ($h = 6.626 \cdot 10^{-34}$ Js)

	membrane thickness
	height
H^+-ATPase	proton pump catalysing ATP hydrolysis
I	light intensity
	electrical current
ICT	intramolecular charge transfer
INA	illumination numerical aperture
ISFET	ion sensitive field-effect transistor
ITO	indium tin oxide
I_x	modified Bessel function of order *x*
J	Joule
k	Boltzmann constant ($k = 1.381 \cdot 10^{-23}$ JK^{-1})
	relaxation rate
	wave vector
K	Kelvin
K	partition coefficient
	contrast
	equilibrium constant
K_c	bending modulus
l	liters
	length
L	distance between monomer units
LB	Langmuir-Blodgett transfer
L_d	liquid disordered
L_o	liquid ordered
LS	Langmuir-Schäfer transfer
m	meter
M	molecular weight
mass%	percentage weight by weight
MD	molecular dynamics simulations
min	minutes
mol%	percentage mol/mol
MOSFET	metal oxide semiconductor field-effect transistor
N	Newton
n	number of sites per unit area
	particle density
	refractive index
NA	numerical aperture
NBD	7-Nitrobenzofurazan
nm	nanometers
NSOM	near field scanning optical microscopy
OSM	osmotic stress method
p	pressure
	partial pressure
p_0	partial pressure at saturation
PC	phosphatidylcholine
Pe	Peclet number
PE	phosphatidylethanolamine
PEG	polyethylene glycole
pH	negative logarithm of proton concentration
pK_s	negative logarithm of acid dissociation constant

PMMA	polymethylmethacrylate
POPE	1-Oleyl-2-palmitoyl-*sn*-glycero-3-phosphoethanolamine
r	radius
	relative permeability
	reflection coefficient of a single interface
R	radius
	relative recovery
	reflection coefficient of a multilayer system
REES	red edge excitation shift
RH	relative humidity
RICM	reflection interference contrast microscopy
RMS	root mean square
RT	room temperature
s	seconds
S	spreading coefficient (spreading power)
SNARE	soluble *N*-ethylmaleimide-sensitive fusion protein attachement protein receptor
SPS	surface plasmon resonance spectroscopy
STM	scanning tunnelling microscopy
SUV	small unilamellar vesicles
t	time
T	temperature
TIRF	total internal reflection fluorescence
T_M	main phase transition temperature of lipids
U	voltage
UV	ultraviolet light
v	velocity
V	Volt
V	volume
vdW	van der Waals
W	energy per unit area
w	interaction energy
	radius of bleach spot
x	lateral distance
	mole fraction
Y	admittance
z	charge number of an ion
	protrusion length
	vertical distance
Z	impedance

10 Table of Figures

Figure 2.1: Schematic representation of a biomembrane according to the fluid mosaic model. Picture taken from [Chir, 1997]. 4
Figure 2.2: Lipid model membrane systems. a) Lipid monolayer at the gas/liquid interface on the Langmuir film balance. b) Lipid Langmuir-Blodgett film resting on a solid support, at the solid/gas interface. c) Solid-supported lipid bilayer membrane at the solid/liquid interface or separated from the support by an ultrathin water film. d) Spherical liposome separating two liquid compartments. e) Black lipid membrane (BLM) spanning an aperture usually in a teflon cup. The bilayer in the latter case is coupled to the hydrophobic teflon via a solvent enriched lipid reservoir. f) Soap film, a thin water phase is enclosed between two amphiphile monolayers. 5
Figure 2.3: Basic structure of phospholipids. Common examples for the substituent X are the alcohols ethanolamine and choline. Both kinds of phospholipids are zwitterionic at a neutral pH. The substituents R_1 and R_2 are the hydrophobic tails of fatty acids (see text)..... 6
Figure 2.4: Hierarchy of structural complexity (capital letters), and fabrication steps (numbers) of functionalised polymer-supported model membranes. 7
Figure 3.1: Basic principle of the FRAP method. A) Fluorescence labelled lipid molecules are added in a low concentration to a lipid membrane. The membrane is illuminated in a circular region and a fluorescence intensity $F(i)$ is observed. Switching to a high illumination intensity during a short time interval leads to complete or partial bleaching of the fluorescence labels (fluorescence intensity $F(t = 0)$. Provided the membrane is laterally fluid, bleached membrane labels are replaced by unbleached labels leading to a fluorescence recovery. B) Time dependence of the fluorescence recovery $F(t)$ after photobleaching. The recovery curve $F(t)$ is a function of the lateral diffusion coefficient D and the relative recovery R..... 12
Figure 3.2: Laser intensity (measured by means of a photomultiplier tube) as a function of pockels cell voltage. 15
Figure 3.3: Laser intensity as a function of observation time (the measurement was started directly after switching-on the laser). 16
Figure 3.4: Message box of the shutter panel in the FRAP data acquisition and setup control program. 17
Figure 3.5: Humidity chamber for microscopic observation and FRAP measurements on supported lipid monolayers. The chamber walls were temperature-controlled by a water circle. The temperature and humidity sensor was thermally isolated from the chamber walls by a Teflon capsule. Prior to gluing the objective to the sample backside (microscopic coverglass), lipid on the backside of the coverglass was thoroughly wiped off with isopropanol. 19
Figure 3.6: Left: photograph of the humidity chamber depicted in Figure 3.5, mounted on the microscope stage. Lateral position adjustments were performed by micrometer screws moving the microscope stage. Focus control was performed by moving the objective in the z-direction. Right: photograph of the humidity and temperature sensor. 19
Figure 3.7: Fluorescence micrographs of a supported lipid monolayer mounted into the humidity chamber. Illumination by laser light (prior to bleaching, left) and the mercury burner (after bleaching, right) insured a homogenous, circular illumination by the laser without severe reflections. 20
Figure 3.8: Measurement chamber used for fluorescence spectroscopy with substrate-supported lipid monolayers. The chamber consisted of a quartz cuvette, which was sealed by an airtight lid. The relative humidity was adjusted by means of a saturated salt solution. 21
Figure 3.9: Principle and experimental realisation of a reflection interference contrast microscope. 22
Figure 3.10: Schematic depiction of the home built aperture stop. Lamp housing and microscope (grey parts) were separated and two quartz lenses and an iris diaphragm aperture stop inserted. 25
Figure 3.11: Influence of the aperture stop opening (Figure 3.10) on the contrast of interferograms of a glass bead (radius 73 µm) on a microscopic coverglass in air. Left: aperture stop completely opened. Right: INA reduced to 0.15. 26
Figure 3.12: Glass bead hovering over a microscopic coverglass in MilliQ water. Left: RICM image. Right: Line profile drawn from the centre of the sphere. The bold line corresponds to a fit of (3.15) to the data. 27
Figure 3.13: Spreading of a single bilayer from a lipid reservoir deposited onto a microscopic coverglass. The latter was covered by a layer of 45 nm MgF_2 for contrast enhancement and an additional layer of 5 nm SiO_2. The right picture was taken several minutes after the left one. 27
Figure 3.14: Reflection and refraction of light at an interface of two media with refractive indices n_1 and n_2. 28
Figure 3.15: Schematic setup for a null-ellipsometer with external reflection. 30

Figure 3.16: Configuration used for MAIRE-measurements of film thicknesses as a function of relative humidity. 31
Figure 3.17: Velocity of humidity changes detected in the measurement chamber shown in Figure 3.5, chapter 3.1.3. 34
Figure 3.18: Complex frequency reduced admittance plot for a resistor connected in series with a RC element consisting of a resistor and capacitor in parallel. 36
Figure 3.19: Schematic depiction of an n-channel FET. The gate oxide is contacted by an electrolyte solution. The gate-source voltage leads to a conducting n-channel, through which a current may flow due to the drain-source voltage. The drain current depends on the gate oxide surface charges, which are influenced by pH. 37
Figure 3.20: Photo of an EOSFET array chip mounted onto a DIL ceramic carrier. The chip contacts were sealed by a silicon funnel surrounded by a glass ring, which served as a container for the electrolyte bath. 38
Figure 3.21: Schematic setup of an atomic force microscope. 39
Figure 3.22: Langmuir-Blodgett trough with a single moveable barrier. The trough possesses a well to allow for substrate immersion during or prior to vertical monolayer transfer. 41
Figure 3.23: Schematic representation of a typical isotherm for a monolayer at the air/water interface. 42
Figure 3.24: Langmuir-Blodgett transfer of an amphiphile monolayer onto A) a hydrophilic substrate by an upstroke and B) onto a hydrophobic substrate by a downstroke. 43
Figure 3.25: Langmuir-Schäfer transfer to obtain a substrate-supported bilayer. A monolayer-covered substrate is horizontally pressed through a monolayer at the air/water interface. 43
Figure 4.1: Thickness of agarose films as measured by an α-stepper. The films were prepared by dip-coating from a hot solution. Thicknesses were measured after gelation and drying the film at ambient conditions. 50
Figure 4.2: Thickness of chitosan films prepared by spin-coating as measured by ellipsometry. Both spinning speed and concentration of the chitosan solution was varied. The lines result from a simultaneous fit of (4.2) to the whole data set. 51
Figure 4.3: AFM topogram (tapping mode) of agarose in a dry (left) and water swollen (right) state (the right picture was taken while imaging under water). 53
Figure 4.4: Tapping mode AFM pictures of chitosan in a dry (left, before neutralising) and water swollen (right, after neutralising) state. 53
Figure 4.5: Tapping mode AFM topography images of spin-coated chitosan films. Left: film after neutralising the polymer, imaged in the dry state (in air). Right: chitosan film immersed and imaged in MilliQ water without neutralising prior to addition of MilliQ water. Due to the imaging artefacts in the right picture, the image was not converted into a surface profile plot. 54
Figure 4.6: Psi (1a) and 2a)) and delta (1b) and 2b)) curves of a chitosan film in a dry (1a) and 1b)) and in a water swollen state (2a) and 2b)). 56
Figure 4.7: Relative humidity variation experiments on a chitosan film. The initial film thickness was 198nm. The bold line is a fit of the Flory-Huggins equation with the Flory-Huggins interaction parameter of 1.05. 57
Figure 4.8: Logarithm of disjoining pressure and swelling ratios of chitosan films, as determined from relative humidities and film thicknesses shown in Figure 4.7. An alternative data representation in terms of plotting ln(Π) against the distance *L* between monomer units (see text) is shown in the inset. 58
Figure 4.9: Measured and calculated refractive indices as determined by ellipsometry, in parallel to the film thicknesses shown in Figure 4.7. 60
Figure 4.10: Immobilisation of a photo-reactive benzophenone derivative, used to chemically attach chitosan films to oxide surfaces. 61
Figure 5.1: Energy per area versus distance profiles of surface interactions for the four-layer system glass, water, lipid and air. For the simulation the parameter were as follows: non-retarded Hamaker constant $5 \cdot 10^{-21}$ J [Frey, 1995], Y_{glass} = 70 mV, Y_{lipid} (zwitterionic) = 0.5 mV, Y_{lipid} (zwitterionic + small amount of negatively charged lipid) = 5mV, l = 900 nm (pure water), $\Pi_0 = 3.16 \cdot 10^9$ N/m^2, λ_w = 2.2 Å (see [Iono, 1996] and chapter 5.3). 68
Figure 5.2: Left: interference fringes of water droplets, freshly condensed on a DMPC monolayer (lateral pressure 35 mN/m,) on a glass surface, right: schematic drawing of the configuration observed in the left image. 74
Figure 5.3: Fluorescence pictures of DMPC monolayers (lateral pressure 35 mN/m, fluorescence probe NBD-PC) on a glass surface. Left picture: structure of the monolayer upon condensation of water droplets, right picture: recovery of a homogeneous structure after 17 min of storage at a relative humidity near condensation. 76

Figure 5.4: Left: RICM image of water droplets on a DMPC monolayer on a chitosan film (lateral pressure 35 mN/m) and an additional fluorescence probe (NBD-PC), right: schematic drawing of the configuration observed in the left image. 77
Figure 5.5: Fluorescence images: observation of the flow of monolayer defects on a DMPC monolayer (lateral pressure 35 mN/m, fluorescence probe NBD-PC) on chitosan. The monolayer was detached from the surface and was subject to convection, as can be seen by the movement of heterogeneities (for the sake of a simple assignment, the same defect has been numbered in each image). The pictures were taken at a time interval of approximately 5 s. 78
Figure 5.6: Fluorescence images showing A) the structure of a lipid monolayer (DMPC, lateral pressure 35 mN/m, fluorescence probe NBD-PC) which had been subject to a condensation of water droplets, and which had been dried rapidly afterwards, B) – D) the same location on the same monolayer as in A), after switching to a high (near condensation) humidity. The time interval between each picture was approximately 1 minute. 79
Figure 5.7: RICM image of water droplets on a DMPC monolayer supported by a chitosan cushion (lateral pressure 35 mN/m, fluorescence probe NBD-PE). 80
Figure 5.8: Fluorescence image: water droplets on a DMPC monolayer (lateral pressure 35 mN/m, fluorescence probe NBD-PE) resting on chitosan. The right picture was taken approximately five seconds after the left picture. Note: a) defects did not change position but could fuse to yield bigger ones, b) the fluorescence intensity of areas between the droplets is increased in the right picture compared to the left one (both pictures were taken at exactly the same conditions), c) water covered regions showed a faint fluorescence. 81
Figure 5.9: Water droplets on a DLPE monolayer on chitosan (left: fluorescence, right: RICM), fluorescence probe NBD-PE. Note: the bright spots in the left picture are regions where droplets have dried previously. 82
Figure 5.13: Height profile of the water film near a substrate prior (a), and after (b) spreading lipid solution on the trough subphase *before* compression of the monolayer film. Due to a local collapse of the water film at the leading edge and possibly a substrate induced dehydration of lipid headgroups, the initial three phase line retracts upon spreading lipid solution, indicated by a height difference Δz. During the retraction, lipid is deposited at a higher lateral pressure compared to the uncompressed monolayer. The retraction of the initial wetting front during spreading is assumed to being grossly reduced, if not diminished, due to the presence of a hydrated polymer cushion. 88
Figure 5.14: DMPC monolayer on a chitosan film, lateral pressure 50 mN/m, relative humidity 90 %, left picture: beginning of the spreading experiment, right picture: 9 min later. Note: the broadening of the spreading front during the spreading process was negligibly small. 90
Figure 5.15: Intensity profiles of the monolayer edge (along a line orthogonal to the edge) during spreading. Note: the width of the edge prior to spreading is comparable to the resolution of the optical microscope. The intensity profiles have been shifted arbitrarily with respect to the length axis. Profiles were examined directly after deposition (0 µm), and after spreading over distances of 50 µm and 65 µm. 91
Figure 5.16: DMPC monolayer on a chitosan film, lateral pressure 20 mN/m, relative humidity 90 %, left picture: prior to increasing humidity, right picture: 50 min later. In the case of the right picture, the sample had been shifted in order to compensate for the movement of the spreading front (approximately 40 µm). 92
Figure 5.17: Development of the spreading front of a lipid monolayer spreading from a Langmuir-Blodgett film (see Figure 5.16). The spreading fronts have been turned by 90° with respect to Figure 5.16. Note: a) the two lines have been shifted arbitrarily towards each other in the y-direction, b) x- and y-axis are scaled differently. 92
Figure 5.18: Spreading front displacement of a DMPC monolayer on chitosan, lateral pressure 20 mN/m, relative humidity 90 %. The slope of a linear fit yielded a velocity of 0.88 µm/min, corresponding to 0.015 µm/s. 93
Figure 5.19: Spreading of a lipid monolayer initially confined to a fraction of the whole substrate area. Molecules in the "bulk" film have the same transition probabilities in each direction. Boundary particles, however, have a higher tendency $q > p$ to jump into the direction of the film, due to long-range attractive forces on the particle exerted by the monolayer. s_0: initial length of the monolayer film, $s(t)$: total length of the film at time, t, $x(t)$: spreading distance at time, t. The polymer supporting the lipid monolayer has been omitted for clarity. 94
Figure 5.20: Comparison of the spreading velocities of DMPC monolayers transferred at different lateral pressures at two different relative humidities. Closed circles: 85 %, open circles: 90 %. The lines are guides to the eyes. Inset: pressure/area isotherm of DMPC at 25 °C, the dots refer to the transfer pressures. 98
Figure 5.21: DMPC monolayer on a Chitosan film, lateral pressure 50 mN/m. The picture was taken at RH = 50 %, after 2 min exposure to a humidity near condensation (> 98 %). 99

Figure 5.22: Line profile indicating the intensity distribution along the horizontal axis of Figure 5.21. Note: the picture was taken without background subtraction, hence the non-zero intensities in the right tail of the curve. 100
Figure 5.23: Monolayer edge of DSPC on Chitosan, lateral transfer pressure 40 mN/m. 101
Figure 5.24: Spreading from a lipid reservoir deposited from a chloroform solution onto a chitosan film, left picture: 5 min after increasing *RH*, right picture: 25 min later. 103
Figure 5.25: Spreading front displacement obtained by spreading from a multilayer reservoir deposited onto a chitosan cushion at a relative humidity of 90 %. 104
Figure 5.26: Possible experimental configuration for correlating monolayer spreading with the water content of the lipid/lipid interface, i.e. the thickness of the water layer *d*. Spreading is due to the advancement of the upper monolayer, while the lower one is fixed on the substrate. 106
Figure 5.33: Reversibility of changes of the diffusion coefficient (dots) upon switching between different ambient humidities (line), in a DMPC monolayer on chitosan, lateral pressure 35 mN/m, fluorescence probe NBD-PE. 112
Figure 5.34: Temperature dependence of diffusion coefficients on chitosan-cushioned monolayers, lateral pressure 35 mN/m, fluorescence probe NBD-PE, at a relative humidity of 80 %. 113
Figure 5.35: Diffusion coefficients of a chitosan-cushioned DMPC monolayer, lateral pressure 35 mN/m, fluorescence probe: NBD-PE, temperature 26 °C. The inset shows an axis transformation of the same data set, the natural logarithm of *D* is plotted against the natural logarithm of $p_0/p = 100/RH$. 114
Figure 5.36: A) Relation between the measured diffusion coefficient in a substrate-supported monolayer membrane and the corresponding friction coefficient b_s, calculated by means of (5.3.7), i.e. the Evans-Sackmann theory. B) Relation between measured diffusion constant and lubrication layer thicknesses calculated from the friction coefficients in A), according to $b_s = \hbar/d$ (see text). 116
Figure 5.37: Lattice model for humidity dependent activated diffusion in a substrate-supported lipid monolayer. Grey line: depth of potential wells (E_h) in the completely dry state. Black line: depth of the potential wells ($E_a(RH)$) at the relative humidity *RH*. 117
Figure 5.38: Diffusion coefficients in a chitosan-cushioned DMPC monolayer, lateral pressure 35 mN/m, fluorescence probe: NBD-PC, temperature: 30 °C. The inset shows an axis transformation of the same data set. 121
Figure 5.39: Diffusion coefficients in a chitosan-cushioned DMPC monolayer, lateral pressure 35 mN/m, fluorescence probe: NBD-Chol, temperature 26 °C. The inset shows an axis transformation of the same data set. 122
Figure 5.40: Diffusion coefficients in a chitosan-cushioned DPhyPC monolayer, lateral pressure 35 mN/m, fluorescence probe: NBD-PE, temperature 26 °C. The inset shows an axis transformation of the same data set. 123
Figure 5.41: Double logarithmic plots of diffusion constants measured in DMPC monolayers on chitosan, transferred at the lateral pressures of 10, 35 and 50 mN/m, fluorescence probe NBD-PE, temperature 26 °C. 123
Figure 5.42: Diffusion coefficients in a chitosan-cushioned DLPE monolayer, lateral pressure 35 mN/m, fluorescence probe: NBD-PE, temperature 26 °C. The inset shows an axis transformation of the same data set. 126
Figure 5.43: Diffusion coefficients in a chitosan-cushioned DLPE monolayer, lateral pressure 35 mN/m, fluorescence probe: NBD-PE, temperature 30 °C. The inset shows an axis transformation of the same data set. 127
Figure 5.44: Diffusion coefficients in a chitosan-cushioned DMPC + 30 mol% cholesterol monolayer, lateral pressure 35 mN/m, fluorescence probe: NBD-PE, temperature 26 °C. The inset shows an axis transformation of the same data set. 128
Figure 5.45: Diffusion coefficients in an agarose-cushioned DMPC monolayer, lateral pressure 35 mN/m, fluorescence probe: NBD-PE, temperature 26 °C. The inset shows an axis transformation of the same data set. Additionally, for comparison the data for a chitosan-supported monolayer prepared and analysed under the same conditions was added to the diagram shown in the inset. 129
Figure 5.46: Fluorescence image of a DMPC monolayer (lateral pressure 35 mN/m, fluorescence probe NBD-PC) on a glass surface, the lipid tails were facing towards a MilliQ-water bulk face. 130
Figure 5.47: Diffusion coefficients of DMPC monolayers, lateral pressure 35 mN/m, supported by a chitosan film. The monolayer was exposed to the indicated saturated atmospheres. The diffusion coefficient for ethanol was found to be too high for being resolvable by the FRAP setup, as indicated by the arrow. 131
Figure 5.48: A solid-supported "foam film" as a possible experimental configuration for studying both lateral diffusion and the thickness of the interface between the two amphiphile leaflets. 133
Figure 5.50: Typical fluorescence excitation (λ_{em} = 550 nm) and emission spectrum (λ_{ex} = 460 nm) of the fluorescence probe NBD-PE, embedded in a DMPC matrix on a chitosan polymer cushion, relative humidity: close to 0 %. 138

Figure 5.51: A) Reversibility of fluorescence intensity changes (left axis, dots) depending on changes in relative humidity (right axis, line), in lipid monolayers stained with a fluorescence label and supported by chitosan films. In order to allow for low counting times and hence high sampling rates, a relatively high illumination intensity was used. The fluorescence intensity loss at low humidities was due to irreversible bleaching inside of the illuminated spot, fast lateral diffusion at high humidities led to the observation of the same recovered fluorescence intensity. B) The same measurement as in A), with a stretched time axis. The response of the monolayer upon decreasing *RH* was faster compared to the commercial humidity sensor, as indicated (I) by the faster completion of the total step and (II) the high resolution of an intermediate step in *RH* (see text). 140
Figure 5.52: Relative fluorescence emission intensities of the fluorescence probe NBD-X, which was dispersed in a water swellable chitosan matrix at a concentration of approximately 10^{-5} mol/g chitosan... 142
Figure 5.53: Relative fluorescence emission intensities of NBD-PE labelled DLPE and DMPC monolayers on a glass surface, lateral pressure: 35 mN/m. Normalisation in both cases was performed with respect to the value found at the lowest accessible relative humidity. 144
Figure 5.54: Relative fluorescence emission intensities of a NBD-PE labelled DMPC + 30 mol% cholesterol monolayer on a glass surface, lateral pressure: 35 mN/m. For the sake of comparison, the data for a pure DMPC monolayer have been added. 145
Figure 5.55: Comparison of the relative fluorescence emission intensities of NBD-PE labelled DMPC monolayers on glass, chitosan and agarose surfaces (lateral pressures in all cases 35 mN/m). Lines are a guide to the eye. 146
Figure 5.56: Comparison of the relative fluorescence emission intensities of NBD-PE labelled DSPE, DSPE-EO_{45} and a mixture of 91/9 mol/mol DSPE/DSPE-EO_{45} monolayers on a glass surface (in all cases lateral pressure 42 mN/m). The lines are guides to the eye. 148
Figure 5.57: Comparison of the relative fluorescence emission intensities of NBD-PE labelled DSPE (lateral pressure 42 mN/m) and DLPE (lateral pressure 35 mN/m) monolayers on a glass surface. 150
Figure 5.58: Fluorescence excitation spectra changes upon humidity changes of a DMPC monolayer, lateral pressure 35 mN/m on a chitosan polymer cushion, λ_{em} = 550 nm. Note: the intensities of the three different spectra are *not* to scale (see text). 151
Figure 5.59: Changes in the emission spectra of a DMPC monolayer (lateral pressure 35 mN/m) on a chitosan film, λ_{ex} = 465 nm. Fluorescence intensities in all emission spectra correspond to the raw data and hence can be compared quantitatively (in contrast to excitation spectra). 152
Figure 5.60: Changes in the emission spectra of a DMPC monolayer stained with NBD-PE (lateral pressure 35 mN/m) deposited onto a Si/SiO_2 substrate surface, λ_{ex} = 465 nm. 153
Figure 5.61: Fluorescence emission spectra of DMPC monolayers labelled with NBD-PE, transferred onto a chitosan film at a lateral pressure of 35 mN/m, λ_{ex} = 465 nm. The spectra were taken at different humidities, adjusted by saturated salt solutions, starting at the highest humidity. The salts specified in the panel are grouped corresponding to increasing *RH* from top to bottom (compare Figure 5.62). The bold vertical line indicates the cut-off wavelength of the emission filter used for humidity/fluorescence intensity scans. 154
Figure 5.62: Wavelength shifts and normalised intensities at different relative humidities, from Figure 5.61. Intensities were normalised with respect to the value found at the lowest relative humidity. 155
Figure 5.63: Typical REES observed in case of a DMPC monolayer, labelled with NBD-PE on a chitosan film. The relative humidity was adjusted by salt solutions, in the measurement shown in this figure KNO_3 was used. The intensities of the different spectra are not to scale. 157
Figure 5.64: REES values for NBD-PE stained DMPC monolayers on a chitosan cushion at different ambient humidities. 158
Figure 6.1: Schematic picture of the setup, which was used for initial experiments on polymer-supported bilayer lipid membranes (BLMs). The bilayer membrane is shown schematically, in reality the bilayer rims are connected to a solvent enriched lipid reservoir. 165
Figure 6.2: Fluorescence image of an agarose-supported BLM (lipid: asolectin), prepared in an agarose filled teflon tube. For details of the setup see Figure 6.1. 166
Figure 6.3: Left: trough-area/pressure isotherm of a successful transfer of a second phospho-lipid monolayer onto a predeposited polymer-cushioned LB-film. The successful transfer expressed itself by a decrease of the trough area after transfer. Right: trough-area/pressure isotherm of a non-successful transfer of a second phospholipid monolayer onto a predeposited polymer-cushioned LB-film. The coming off of lipid material is shown by an increase of trough area after transfer. 167
Figure 6.4: Fluorescence images of asolectin bilayer membranes on agarose prepared by LB/LS transfer (lateral pressure 35 mN/m, deposition temperature 25 °C), fluorescence dye: DiI. Left picture: directly after preparation, right picture: after storage over night at 25 °C. 168

Figure 6.5: Fluorescence images of a DMPC bilayer membrane prepared by LB/LS transfer (lateral pressure 35 mN/m, deposition temperature 25 °C), fluorescence dye DiI, directly after transfer. Both structures were found on the same substrate, the bars seen in the right picture have an orientation orthogonal to the drawing direction during LB-transfer....169
Figure 6.6: Fluorescence images demonstrating a structural rearrangement of a DMPC bilayer, with a patterning shown in Figure 6.5....170
Figure 6.7: Time sequence of a structural transition found in DMPC bilayer membranes on agarose, B): 30 min after picture A), C): 90 min after A), D): 150 min after A). 170
Figure 6.8: Kinetics of the structural transition demonstrated in Figure 6.7, for two different temperatures.171
Figure 6.9: Fluorescence images of DMPC bilayer membranes, deposited by LB/LS-transfer at a lateral pressure of 35 mN/m and a deposition temperature of 25 °C, observed at a temperature of 40 °C. Left picture: directly after heating up to 40 °C, right picture: the same location on the sample, 2.5 h later. Note: the total number of bright spots was reduced while the remaining spots partially grew with time. ... .172
Figure 6.10: Hypothetical schematic representation of the membrane patches observed by fluorescence microscopy, as shown in Figure 6.6 and Figure 6.7. A homogeneous membrane patch is formed by bilayer spreading on the glass support through local defects in the polymer cushion. The bilayer on top of the agarose cushion is inhomogeneous, the hydrophobic rims of membrane defects are possibly stabilised by hydrophobic parts of the polymer strands. 173
Figure 6.11: DMPC bilayer on agarose, deposited by LB/LS transfer at a lateral pressure of 35 mN/m and a deposition temperature of 15 °C. Left picture: directly after deposition, right picture: after storage over night at 25 °C. 174
Figure 6.12: Fluorescence images of DMPC (30 mol% cholesterol) bilayer preparations on agarose cushions. Deposition temperature and observation temperature in both pictures: 15 °C. Left picture: directly after transfer, right picture: 10 min after transfer (different location on the same sample as compared to the left picture). 175
Figure 6.13: DMPC bilayer membrane, obtained by deposition of monolayers onto two different polymer cushions and pressing both monolayers against each other in an atmosphere with increased humidity. 176
Figure 6.14: DMPC bilayer membrane on agarose, stained with 10 mol% of the fluorescence probe DiI (positively charged)....176
Figure 6.15: Fluorescence image of a DHDAB bilayer membrane, deposited at a lateral pressure of 35 mN/m and a deposition temperature of 15 °C. The homogeneous picture did not change appearance, even during prolonged heating at 45 °C. 177
Figure 6.16: DHDAB bilayer membranes with an additional amount of cholesterol. Left picture: 5 mol%, right picture: 20 mol%. 178
Figure 6.17: RICM image of DMPC vesicles hovering over an agarose surface (left), schematic drawing of a giant, multilamellar vesicle, hovering over the polymer surface....178
Figure 6.18: Fluorescence images of a vesicle fusion experiment of DMPC-SUVs on agarose, the substrate was exposed to a vesicle dispersion at 30 °C over night. Left part: dominating, completely homogeneous appearance of the sample, right part: at some locations brightly shining circular spots were found.....179
Figure 6.19: FRAP experiments performed with an agarose substrate, which had been exposed to a vesicle dispersion (see Figure 6.18). Left: initial bleaching, right: second bleaching at the same location as in the left part after recovery. 180
Figure 6.29: Fluorescence micrographs of DMPC bilayers, prepared by LB/LS transfer at a lateral pressure of 35 mN/m, deposition temperature: 15 °C. Left picture: fluorescence probe NBD-PE, right picture: fluorescence probe DiI. Pictures were taken at room temperature. 181
Figure 6.30: The same DMPC bilayers as shown in Figure 6.29, after storage over night at a temperature of 40 °C. Left picture: fluorescence probe NBD-PE, right picture: fluorescence probe DiI. 182
Figure 6.31: Fluorescence micrographs of DMPC (30 mol% cholesterol) membranes obtained by LB/LS transfer at a lateral pressure of 35 mN/m and a deposition temperature of 25 °C (left picture) and 15 °C (right picture), fluorescence probe NBD-PE. 183
Figure 6.32: Fluorescence micrograph of a DMPC bilayer membrane on a thick, dip-coated chitosan film. The heterogeneous surface structure of the polymer due to cracks is imprinted into the bilayer. 184
Figure 6.33: Comparison of the temperature dependent lateral diffusion behaviour of DMPC bilayer membranes labelled with NBD-PE, supported by glass and chitosan. In the case of glass, the phase transition as seen by lateral diffusion occurs around the phase transition temperature found in non-perturbed DMPC bilayers (broken line). However, in the case of chitosan, the phase transition occurs at a higher temperature. Each data point represents the average of three to five single measurements. 185
Figure 6.34: Temperature dependent lateral diffusion behaviour of chitosan-supported DMPC bilayer membranes with varying cholesterol contents. Membranes were prepared by LB/LS transfer at a lateral pressure of 35 mN/m. 186

Figure 6.35: RICM image of giant multilamellar liposomes, partially spread on a chitosan surface at room temperature. Surrounding medium: saccharide solution as described in chapter 3.10.5. 188
Figure 6.36: Relative intensity difference (left) and contrast variation (right) of reflection interferograms of a lipid bilayer membrane on chitosan for a varying film thicknesses. For a definition of the quantities see text. 189
Figure 6.37: RICM image of the spreading of a patch of giant multilamellar liposomes. The right picture was taken 100 s later than the left picture. 189
Figure 6.38: RICM image of a giant liposome adhering to a glass surface (left). Right: the same vesicle as in left picture after addition of salt. 190
Figure 6.39: RICM image of the spreading of lipid bilayers on a glass surface. Left picture: 1.5 s after vesicle rupture (Figure 6.38), right picture: 25 s after vesicle rupture. 190
Figure 6.40: Bilayer spreading from a lipid reservoir, deposited onto a hydrophilic substrate from a solution. The substrate is immersed in water or a buffer solution afterwards. 191
Figure 6.41: Fluorescence images of a spreading experiment on a chitosan surface. An eggPC lipid reservoir was deposited onto the polymer film and the substrate was immersed into MilliQ water. The right picture was taken 34 min after the left one. 192
Figure 6.42: Comparison of the spreading front of a lipid bilayer membrane spreading from a lipid reservoir deposited onto a chitosan film (corresponding to Figure 6.41). 193
Figure 6.43: Double logarithmic plot of the spreading velocity against measurement time, for an eggPC bilayer spreading on chitosan from a lipid reservoir, bold line: fit with a fixed slope of -0.5. 193
Figure 6.44: FRAP diagram of a chitosan film, which was exposed to an eggPC SUV-dispersion for half an hour at 30 °C. Measurement temperature: *RT*. 195
Figure 6.45: Complex admittance over ω plot for a chitosan film on a gold electrode. Dry thickness of the polymer film: approximately 15 nm, electrode area: 0.0354 cm^2. 196
Figure 6.46: Impedance spectroscopy of a chitosan polymer cushion, DMPG bilayer (prepared by LB/LS transfer and a fit of the polymer-cushioned bilayer: complex admittance/ω plots. Electrode area: $3.296 \cdot 10^{-3}$ cm^2. Dry thickness of the polymer film: approximately 15 nm. 197
Figure 6.47: Vesicle fusion experiment on a chitosan polymer cushion: complex admittance over ω plot. A vesicle dispersion (DMPC) was added at a temperature of 30 °C. Time between first and last spectrum: 12 h. Dry thickness of polymer film: approximately 15 nm. 198
Figure 7.1: Fluorescence image of an eggPC bilayer on chitosan, which contained the integral membrane protein COX, labelled with a fluorescence probe (the bilayer itself was not labelled in that case). Previously to protein incorporation, the bilayer was deposited using 35 mN/m as lateral pressure and 15 °C as deposition temperature. Detergent dilution was performed at room temperature. 203
Figure 7.2: Diagram of a FRAP measurement, performed by bleaching fluorescence probes chemically attached to the integral membrane protein COX, incorporated into an eggPC bilayer membrane supported by a chitosan cushion. Temperature: 25 °C. 204
Figure 7.3: Schematic setup for the measurement of trans-membrane protein activities by means of field-effect transistors. It is favourable for protein functioning, to decouple the membrane from an oxide support. 206
Figure 7.4: Fluorescence images of a spreading sequence of a lipid bilayer, spreading from an eggPC reservoir which had been deposited onto the FET surface and re-swollen in MilliQ water. Time difference between the two pictures: 7 min. Spreading was analysed at room temperature. 207
Figure 7.5: Fluorescence image of a spreading bilayer. The impossibility to span the hole in the SiO_2 surface on top of the EGE is expressed by the heterogeneous membrane structure in the EGE area. The black areas at the area of the EGE either stem from a ruptured membrane or from a partially adsorbed membrane on the gold support. 208
Figure 7.6: Schematic representation of membrane-bound nitrate reductase. The enzyme catalyses the reduction of nitrate to nitrite and is assumed to transport two protons per converted nitrate molecule through the bilayer membrane, thereby producing a pH gradient. 209
Figure 7.7: Left picture: EOSFET activity measurements of nitrate reductase incorporated into a DMPC/DOPC planar supported bilayer obtained from vesicle fusion of protein-containing vesicles. Right picture: as a reference experiment, the addition of nitrate and redox mediator to an EOSFET system without membrane (and protein) was analysed. 210
Figure 7.8: EOSFET activity measurements of H^+-ATPase, incorporated into an eggPC planar supported bilayer obtained from vesicle fusion of protein-containing vesicles. Left: no inhibitor was added, right: inhibitor-containing system. 211
Figure 7.9: Reference experiment: eggPC bilayer on an EOSFET surface, without H^+-ATPase present. The baseline drift is due to a transistor instability [Sprö, 1997a]. 212
Figure 8.1: Chemical structure of the repetition unit of agarose, left unit: β-D-galactose, right unit: 3,6-anhydro-α-L-galactose. 214

Figure 8.2: Chemical structure of the repetition unit (glucoseamine) of chitosan. 215
Figure 8.3: Chemical structure of DMPC (1,2-Dimyristoyl-*sn*-glycero-3-phosphatidylcholine). 216
Figure 8.4: DMPC isotherms obtained with a Langmuir film balance, at different temperatures. The temperature was varied between 10 °C and 30 °C at steps of 5 °C. 216
Figure 8.5: Chemical structure of DLPE (1,2-Dilauroyl-*sn*-glycero-3-phosphoethanolamine). 217
Figure 8.6: DLPE isotherms obtained with a Langmuir film balance, at different temperatures. The temperature was varied between 10 °C and 30 °C at steps of 5 °C. 217
Figure 8.7: Chemical structure of DPhyPC (1,2-Diphytanoyl-*sn*-glycero-3-phosphatidylcholine). 218
Figure 8.8: DPhyPC isotherms obtained with a Langmuir film balance, at different temperatures. 218
Figure 8.9: Chemical structure of dihexadecyldimethylammoniumbromid. 219
Figure 8.10: Chemical structure of N-succinimidomyristidic ester. 219
Figure 8.11: Chemical structure of cholesterol (3β-Hydroxy-5-cholesten). 220
Figure 8.12: Chemical structure of DSPE-PEG 2000. 220
Figure 8.13: Isotherms obtained on a Langmuir film balance for DSPE, DSPE-PEG 2000 and a mixture of both components of a molar ratio of 91/9, at 25 °C. 221
Figure 8.14: NBD derivatives used in the present work. From left to right: NBD-PC (M_w = 869.08 g/mol), NBD-cholesterol (M_w = 494.63 g/mol), NBD-X (M_w = 294.27 g/mol) and NBD-PE (M_w =956.25 g/mol). 222
Figure 8.15: Chemical structures of DiI (M_w = 993.88) and FITC (M_w = 389.38 g/mol). 222

11 Literature

[Abra] Abraham D.B., Collet P., Coninck J.D. and Dunlop F. "Langevin Dynamics of Spreading and Wetting". *Physical Review Letters* **65**, 195 - 198 (1990).

[Adam] Adamson A.W. (1990) *Physical Chemistry of Surfaces,* Wiley, New York, Chichester, Brisbane, Toronto, Singapore.

[Albe] Alberts B., Bray D., Lewis J., Raff M., Roberts K. and Watson J.D. (1994) *Molecular Biology of the Cell,* Garland Publications, New York.

[Albr] Albrecht O., Gruler H. and Sackmann E. "Polymorphism of Phospholipid Monolayers". *Journal de Physique* **39**, 301 - 313 (1978).

[Al-Di] Al-Dirbashi O., Kuroda N. and Nakashima K. "Characterisation of the Fluorescence Properties of 4-Fluoro-7-nitrobenzo-2-oxa-1,3-diazole Derivatives of some Primary and Secondary Sympathomimetic Amines". *Analytica Chimica Acta* **365**, 169 - 176 (1998).

[Alme] Almeida P.F.F. and Vaz W.L.C. (Eds.) (1995) *Lateral Diffusion in Membranes,* Elsevier, Amsterdam.

[Alme] Almeida P.F.F., Vaz W.L.C. and Thompson T.E. "Lateral Diffusion in the Liquid Phases of Dimyristoylphosphatidylcholine/Cholesterol Lipid Bilayers: A Free Volume Analysis". *Biochemistry* **31**, 6739 - 6741 (1992).

[Alme] Almeida P.F.F., Vaz W.L.C. and Thompson T.E. "Percolation and Diffusion in three-Component Lipid Bilayers: Effect of Cholesterol on an Equimolar Mixture of two Phosphatidylcholines". *Biophysical Journal* **64**, 399 - 412 (1993).

[Arig] Ariga K. and Okahata Y. "Hydration Behaviour of Phospholipid Langmuir-Blodgett (LB) Films Deposited on a Quartz-Crystal Microbalance Depending on Temperatures in Water". *Langmuir* **10**, 2272 - 2276 (1994).

[Arya] Arya A., Krull U.J., Thompson M. and Wong H.E. "Langmuir-Blodgett Deposition of Lipid Films on Hydrogel as a Basis for Biosensor Development". *Analytica Chimica Acta* **173**, 331 - 336 (1985).

[Auch] Auch M., Fischer B. and Möhwald H. "Lateral Lipid Diffusion in Phospholipid Monolayers Coupled to Polyelectrolyte Films". *Colloids and Surfaces A: Physicochemical and Engineering Aspects* **164**, 39 - 45 (2000).

[Axel] Axelrod D., Koppel D.E., Schlessinger J., Elson E. and Webb W. W. "Mobility Measurement by Analysis of Fluorescence Photobleaching Recovery Kinetics". *Biophysical Journal* **16**, 1055 - 1069 (1976).

[Azza] Azzam R.M.A. and Bashara N.M. (1977) *Ellipsometry and Polarized Light,* , Amsterdam, New York, Oxford.

[Bade] Badea M.G., De Toma R.P. and Brand L. "Nanosecond Relaxation Processes in Liposomes". *Biophysical Journal* **24**, 197 - 212 (1978).

[Baek] Baekmark T.R., Elender G., Lasic D.D. and Sackmann E. "Conformational Transitions of Mixed Monolayers of Phospholipids and Poly(ethylene oxide) Lipopolymers and Interaction Forces with Solid Surfaces". *Langmuir* **11**, 3975 - 3987 (1995).

[Balc] Balcom B.J. and Petersen N.O. "Lateral Diffusion in Model Membranes is Independent of the Size of the Hydrophobic Region of Molecules". *Biophysical Journal* **65**, 630 - 637 (1993).

[Bang] Bangham D. and Saweris S. *Transactions of the Faraday Society* **33**, 554 (1938).

[Baum] Baumgart T., Kreiter M., Lauer H., Naumann R., Jung G., Jonczyk A., Offenhäusser A. and Knoll W. "Fusion of Small Unilamellar Vesicles onto Laterally Mixed Self-Assembled Monolayers of Thiolipopeptides". *submitted* (2001).

[Bech] Bechinger B. and Seelig J. "Conformational Changes of the Phosphatidylcholine Headgroup due to Membrane Dehydration: A ^{2}H-NMR Study". *Chemistry and Physics of Lipids* **58**, 1 - 5 (1991).

[Bere] Bereiter-Hahn J., Fox C.H. and Thorell B. "Quantitative Reflection Contrast Microscopy of Living Cells". *Journal of Cell Biology* **82**, 767 - 779 (1979).

[Berg] Bergveld P. "Development of an Ion-Sensitive Solid State-State Device for Neurophysiological Measurements". *IEEE Transactions of Biomedical Engineering* **BME-17**, 70 - 71 (1970).

[Berg] Bergveld P. "A Critical Evaluation of Direct Electrical Protein Detection Methods". *Biosensors & Bioelectronics* **6**, 55 - 72 (1991).

[Berg] Bergveld P., Wiersmal J. and Meertens H. "Extracellular Potential Recordings by Means of a Field Effect Transistor without Gate Metal, Called OSFET". *IEEE Transactions of Biomedical Engineering* **23**, 136 - 144 (1976).

[Berm] Berman A.D., Cameron S.D. and Israelachvili J.N. "Mobility of Surfactants in and between Adsorbed Monolayers". *Journal of Physical Chemistry B* **101**, 5692 - 5697 (1997).

[Bern] Bernik D.L. and Negri R.M. "Local Polarity at the Polar Head Level of Lipid Vesicles Using Dansyl Fluorescent Probes". *Journal of Colloid and Interface Science* **203**, 97 (1998).

[Beye] Beyer D. (1996a), "Polymere Oberflächen: Darstellung und Untersuchung der Wechselwirkung mit Plasmaproteinen und Modellmembranen", Johannes Gutenberg Universität, Mainz.

[Beye] Beyer D., Elender G., Knoll W., Kühner M., Maus S., Ringsdorf H. and Sackmann E. "Influence of Anchor Lipids on the Homogeneity and Mobility of Lipid Bilayers on Thin Polymer Films". *Angewandte Chemie: International Edition in English* **35**, 1682 - 1685 (1996b).

[Bies] Biesalski M. (1999), "Terminal an Festkörperoberflächen gebundene Polyelektrolytbürsten: Synthese und Quellungsverhalten", *PhD thesis,* Johannes Gutenberg Universität, Mainz.

[Bies] Biesalski M. and Rühe J. "Swelling of a Polyelectrolyte Brush in Humid Air". *Langmuir* **16**, 1943 - 1950 (2000).

[Bind] Binder H. "Infrared Dichroism Investigations on the Acyl Chain Ordering in Lamellar Structures". *Vibrational Spectroscopy* **21**, 151 - 163 (1999).

[Bind] Binder H., Gutberlet T., Anikin A. and Klose G. "Hydration of the Dienic Lipid Dioctadecadienoylphosphatidylcholine in the Lamellar Phase - An Infrared Linear Dichroism and X-Ray Study on Headgroup Orientation, Water Ordering, and Bilayer Dimensions". *Biophysical Journal* **74**, 1908 - 1923 (1998).

[Binn] Binnig G., Quate C.F. and Gerber C. "Atomic Force Microscopy". *Physical Review Letters* **56**, 930 (1986).

[Birc] Birch W.R., Knewtson M.A., Garoff S., Suter R.M. and Satija S. "Structure of Precursing Thin Films of an Anionic Surfactant on a Silicon Oxide/Silicon Surface". *Langmuir* **11**, 48 - 56 (1995).

[Birk] Birks J.B. (1970) *Photophysics of Aromatic Molecules,* Wiley-Interscience, London.

[Blai] Blair H.S., Huthrie J., Law T.-K. and Turkington P. "Chitosan and Modified Chitosan Membranes I. Preparation and Characterisation". *Journal of Applied Polymer Science* **33**, 641 - 656 (1987).

[Blak] Blake T.D., Decamps C., De Connink J., de Ruijter M. and Voue M. "The Dynamics of Spreading at the Microscopic Scale". *Colloids and Surfaces A: Physicochemical and Engineering Aspects* **154**, 5 - 11 (1999).

[Blüm] Blümle S. and Zumft W.G. "Respiratory Nitrate Reductase from Denitrifying Pseudomonas Stutzeri, Purification, Properties and Target of Proteolysis". *Biochimica et Biophysica Acta* **1057**, 102 - 108 (1991).

[Bolz] Bolze J., Baumgart T., Takahasi M., Mizuki J., Offenhaeusser A. and Knoll W. "Structural Characterization of Langmuir-Blodgett Lipid Monolayers Under Controlled Humidity: an X-ray Reflectivity and Grazing Incidence X-ray Diffraction Study". *in preparation* (2001).

[Borc] Borcherding H., Leikefeld S., Frey C., Diekmann S. and Steinrücke P. "Enzymatic Microtiter Plate-Based Nitrate Detection in Environmental and Medical Analysis". *Analytical Biochemistry* **282**, 1 - 9 (1999).

[Borg] Borgas M.S. and Grotberg J.B. "Monolayer Flow on a Thin Film". *Journal of Fluid Mechanics* **193**, 151 - 170 (1988).

[Born] Bornside D.E., Macosko C.W. and Scriven L.E. "Spin-Coating: One-Dimensional Model". *Journal of Applied Physics* **66**, 5185 - 5193 (1989).

[Bria] Brian A.A. and McConnell H.M. *Proceedings of the National Academy of Science, USA* **81**, 6159 - 6163 (1984).

[Burl] Burlatsky S.F., Oshanin G., Cazabat A.-M. and Moreau M. "Microscopic Model of Upward Creep of an Ultrathin Wetting Film". *Physical Review Letters* **76**, 86 - 89 (1996a).

[Burl] Burlatsky S.F., Oshanin G., Cazabat A.-M., Moreau M. and Reinhardt W.P. "Spreading of a Thin Wetting Film: Microscopic Approach". *Physical Review E* **54**, 3832 - 3845 (1996b).

[Cass] Cassier T., Sinner A., Offenhäusser A. and Möhwald H. "Homogeneity, Electrical Resistivity and Lateral Diffusion of Lipid Bilayers coupled to Polyelectrolyte Multilayers". *Colloids and Surfaces B: Biointerfaces* **15**, 215 - 225 (1999).

[Caza] Cazabat A.M., De Coninck J., Hoorelbeke S., Valignat M.P. and Villette S. "Influence of Substrate Heterogeneities on the Spreading of a Drop". *Physical Review E* **49**, 4149 - 4153 (1994).

[Chan] Chance R.R., Prock A. and Silbey R. (1978) In *Advances in Chemical Physics*(Ed, Prigogine I., R. S. R.) Wiley, New York.

[Chat] Chattopadhyay A. "Chemistry and Biology of N-(7-nitrobenz-2-oxa-1,3-diazol-4-yl)-labeled Lipids: Fluorescent Probes of Biological and Model Membranes". *Chemistry and Physics of Lipids* **53**, 1 - 15 (1990).

[Chat] Chattopadhyay A. and Mukherjee S. "Fluorophore Environments in Membrane-Bound Probes: A Red Edge Excitation Shift". *Biochemistry* **32**, 3804 - 3811 (1993).

[Chat] Chattopadhyay A. and Mukherjee S. "Depth-Dependent Solvent Relaxation in Membranes: Wavelength-Selective Fluorescence as a Membrane Dipstick". *Langmuir* **15**, 2142 - 2148 (1999a).

[Chat] Chattopadhyay A. and Mukherjee S. "Red Edge Excitation Shift of a Deeply Embedded Membrane Probe: Implications in Water Penetration in the Bilayer". *Journal of Physical Chemistry B* **103**, 8180 - 8185 (1999b).

[Chen] Chen T., Kumar G., Harris M.T., Smith P.J. and Payne G.F. "Enzymatic Grafting of Hexyloxyphenol onto Chitosan to Alter Surface and Rheological Properties". *Biotechnology and Bioengineering* **70**, 564 - 573 (2000).

[Chen] Chen Y.-L. and Israelachvili J. "Effects of Ambient Conditions on Adsorbed Surfactant and Polymer Monolayers". *Journal of Physical Chemistry* **96**, 7752 - 7760 (1992).

[Chen] Chen Y.L.E., Gee M.L., Holm C.A., Israelachvili J.N. and McGuiggan P.M. "Effects of Humidity on the Structure and Adhesion of Amphiphilic Monolayers on Mica". *Journal Physical Chemistry* **93**, 7057 - 7059 (1989).

[Chi] Chi L.F., Anders M., Fuchs H., Johnston R.R. and Ringsdorf H. "Domain Structures in Langmuir-Blodgett Films Investigated by Atomic Force Microscopy". *Science* **259**, 213 - 216 (1993).

[Chi] Chi L.F., Fuchs H., Johnston R.R. and Ringsdorf H. "Investigation of Phase-Separated Langmuir-Blodgett Films by Atomic Force Microscopy". *Thin Solid Films* **242**, 151 - 156 (1994).

[Chi] Chi L.F., Johnston R.R. and Ringsdorf H. "Mobile Supported Monolayers of Ionic Amphiphiles: Variation of Domain Morphology via Preadsorbed Polyelectrolytes". *Langmuir* **8**, 1360 - 1365 (1992a).

[Chi] Chi L.F., Johnston R.R., Ringsdorf H., Kimizuka N. and Kunitake T. "Polymeric Gegenions induced Variability and Mobility of Amphiphilic Supramolecular Structures on Solid Substrates". *Thin Solid Films* **210**, 111 - 113 (1992b).

[Chir] Chiras DD. (1997) *Human Biology,* Jones & Bartlett Pub.

[Chit] Chittur K.K. "FTIR/ATR for Protein Adsorption to Biomaterial Surfaces. Biomaterials". *Biomaterials* **19**, 357 - 369 (1998a).

[Chit] Chittur K.K. "Surface Techniques to Examine the Biomaterial-Host Interface: An Introduction to the Papers". *Biomaterials* **19**, 301 - 305 (1998b).

[Choi] Choi M.M.F. and Ling Tse O. "Humidity-Sensitive Optode Membrane Based on a Fluorescent Dye Immobilised in Gelatin Film". *Analytica Chimica Acta* **378**, 127 - 134 (1999).

[Chun] Chung H.S. "On the Macedo-Litovitz Hybrid Equation for Liquid Viscosity.". *Journal of Chemical Physics* **44**, 1362 - 1364 (1966).

[Clae] Claesson P.M. and Ninham B.W. "pH-Dependent Interactions between Adsorbed Chitosan Layers". *Langmuir* **8** (1992).

[Clar] Clark A. (1970) *The Theory of Adsorption and Catalysis,* Academic Press, New York, London.

[Clar] Clark A.H. and Ross-Murphy S.B. "Structural and Mechanical Properties of Biopolymer Gels". *Advances in Polymer Science* **83**, 57 - 192 (1987).

[Cleg] Clegg R.M. and Vaz W. L.C. (1985) In *Progress in Protein Lipid Interactions*(Ed, Pont, W. D.) .

[Cohe] Cohen M.H. and Turnbull D. "Molecular Transport in Liquids and Glasses". *Journal of Chemical Physics* **31**, 1164 - 1169 (1959).

[Coni] Coninck J.D., Dunlop F. and Menu F. "Spreading of a Solid-on-Solid Drop". *Physical Review E* **47**, 1820 - 1823 (1993).

[Corn] Cornell B.A., Braach-Maksvytis V.L.B., King L.G., Osman P.D.J., Raguse B., Wieczorek L. and Pace R.J. "A Biosensor that Uses Ion-Channel Switches". *Nature* **387**, 580 - 583 (1997).

[Cost] Costello R.F., Evans S.W., Evans S.D., Peterson I.R. and Heptinstall J. "Detection of Complement Activity by using a Polysaccharide-Protected Membrane". *Enzyme and Microbial Technology* **26**, 301 - 303 (2000).

[Cost] Costello R.F., Peterson I.R., Heptinstall J., Byrne N.G. and Miller L.S. "A Robust Gel-Bilayer Channel Biosensor". *Advanced Materials for Optics and Electronics* **8**, 47 - 52 (1998).

[Cost] Costello R.F., Peterson I.R., Heptinstall J. and Walton D.J. "Improved Gel-Protected Bilayers". *Biosensors & Bioelectronics* **14**, 265 - 271 (1999).

[Crem] Cremer P.S. and Boxer S.G. "Formation and Spreading of Lipid Bilayers on Planar Glass Supports". *Journal of Physical Chemistry B* **103**, 2554 - 2559 (1999).

[Curt] Curtis A.S.G. "The Mechanism of Adhesion of Cells to Glass, a Study by Interference Reflection Microscopy". *Journal of Cell Biology* **20**, 199 (1964).

[Damo] Damodaran D.V. and Merz K.M. "A Comparison of DMPC- and DLPE-Based Lipid Bilayers". *Biophysical Journal* **66**, 1076 - 1087 (1994).

[De Co] De Coninck J., Fraysse N., Valignat M.P. and Cazabat A.M. "A Microscopic Simulation of the Spreading of Layered Droplets". *Langmuir* **9**, 1906 - 1909 (1993).

[de Gen] de Gennes P.G. "Wetting: Statics and Dynamics". *Reviews of Modern Physics* **57**, 827 - 863 (1985).

[de Ge] de Gennes P.G. "Deposition of Langmuir-Blodgett Layers". *Colloid & Polymer Science* **264**, 463 - 465 (1986).

[DeTo] De Toma R.P., Easter J.H. and Brand L. "Dynamic Interactions of Fluorescence Probes with the Solvent Environment". *Journal of the American Chemical Society* **98**, 5000 - 5007 (1976).

[Derj] Derjaguin B. and Obukhov E. *Acta Physicochim. URSS* **5**, 1 (1936).

[Derj] Derjaguin B.V., Churaev N.V. and Muller V.M. (1987) *Surface Forces,* Plenum Publishing Corporation, New York, London.

[Derj] Derjaguin B.V. and Landau. *Acta Physicochim. URSS* **14**, 633 - 662 (1941).

Dietrich C. (1999) .

[Diet] Dietrich C. and Tampe R. "Charge Determinatin of Membrane Molecules in Polymer-Supported Lipid Layers". *Biochimica et Biophysica Acta* **1238**, 183 - 191 (1995).

[Duhe] Duhem P. (1954) *The Aim and Structure of Physical Theory,* Princeton, University Press, Princeton, New Jersey.

[East] East G.C. and Qin Y. "Wet Spinning of Chitosan and the Acetylation of Chitosan Fibers". *Journal of Applied Polymer Science* **50**, 1773 - 1779 (1993).

[Egaw] Egawa H. and Furusawa K. "Liposome Adhesion on Mica Surface Studied by Atomic Force Microscope". *Langmuir* **15**, 1660 - 1666 (1999).

[Elen] Elender G., Kühner M. and Sackmann E. "Functionalisation of Si/SiO2 and Glass Surfaces with Ultrathin Dextran Films and Deposition of Lipid Bilayers". *Biosensors & Bioelectronics* **11**, 565 - 577 (1996).

[Elen] Elender G. and Sackmann E. "Wetting and Dewetting of Si/SiO_2-Wafers by Free and Lipid-Monolayer Covered Aqueous Solutions Under Controlled Humidity". *Journale de Physique II France* **4**, 455 - 479 (1994).

[Elia] Elias H.G. (1990) *Makromoleküle,* Hüthig & Wepf Verlag, Basel, Heidelberg, New York.

[Elle] Ellens H., Bentz J. and Szoka F. C. "Destabilization of Phosphoethanolamine Liposomes at the Hexagonal Phase Transition Temperature". *Biochemistry* **25**, 285 - 294 (1986).

[Elwo] Elworthy P.H. "The Adsorption of Water Vapour by Lecithin and Lysolecithin, and the Hydration of Lysolecithin Micelles.". *Chem. Soc. J.*, 5305 - 5389 (1961).

[Ende] Enderlein J. "A Theoretical Investigation of Single-Molecule Fluorescence Detection on Thin Metallic Layers". *Biophysical Journal* **78**, 2151 - 2158 (2000).

[Evan] Evans E. and Sackmann E. "Translational and rotational drag coefficients for a disk moving in a liquid membrane associated with a rigid substrate". *Journal of Fluid Mechanics* **194**, 553 - 561 (1988).

[Fang] Fang Y. and Yang J. "The Growth of Bilayer Defects and the Induction of Interdigitated Domains in the Lipid-Loss of Supported Phospholipid Bilayers". *Biochimica et Biophysica Acta* **1324**, 309 - 319 (1997).

[Finn] Finney J.L. "Hydration Processes in Biological and Macromolecular Systems". *Faraday Discussions* **103**, 1 - 18 (1996).

[Fisc] Fischer A. and Sackmann E. "Electron-Microscopy and Diffraction Study of Phospholipid Monolayers Transferred from Water to Solid Substrates". *Journale de Physique France* **45**, 517 - 527 (1984).

[Flor] Florin E.-L. and Gaub E. "Painted Supported Lipid Membranes". *Biophysical Journal* **375 - 383** (1993).

[Flor] Flory P.J. (1953) *Principles of Polymer Chemistry,* Cornell University Press, Ithaca, New York.

[Forg] Forgues-Fery S., Fayet J.-P. and Lopez A. "Drastic changes in the fluorescence properties of NBD probes with the polarity of the medium: involvement of a TICT

state?". *Journal of Photochemistry and Photobiology A: Chemistry* **70**, 229 - 243 (1993).

[Fray] Fraysse N., Valignat M.P., Cazabat A.M., Heslot F. and Levinsson P. "The Spreading of Layered Microdroplets". *Journal of Colloid and Interface Science* **158**, 27 - 32 (1993).

[Frey] Frey W. and Sackmann E. "Solitary Waves in Asymmetric Soap Films". *Langmuir* **8**, 3150 - 3154 (1992).

[Frey] Frey W. and Sackmann E. "Dynamic Stabilization of Asymmetric Soap Films". *Journal of Colloid and Interface Science* **174**, 378 - 391 (1995).

[From] Fromherz P., Kiessling V., Kottig V. and Zeck G. "Membrane Transistor with Giant Lipid Vesicle Touching a Silicon Chip". *Applied Physics A* **69**, 571 - 576 (1999).

[From] Fromherz P., Offenhäusser A., Vetter T. and Weis J. "A Neuron-Silicon Junction: a Retzius Cell of the Leech on an Insulated-Gate Field-Effect Transistor". *Science* **252**, 1290 - 1293 (1991).

[From] Fromme P., Dahse I. and Gräber P. *Zeitschrift für Naturforschung* **47c**, 239 (1992).

[Gall] Galla H.J., Hartmann W., Theilen U. and Sackmann E. "On Two-Dimensional Passive Random Walk in Lipid Bilayers and Fluid Pathways in Biomembranes". *Journal of Membrane Biology* **48**, 215 - 236 (1979).

[Gall] Galle J. and Volke F. "Computer Simulation of the Temperature- and Hydration-Dependent Lateral Diffusion of Phosphatidylcholine in Lipid Bilayers". *Biophysical Chemistry* **54**, 109 - 117 (1995).

[Gave] Gaver D. P. and Grotberg J. B. "The Dynamics of a Localized Surfactant on a Thin Film". *Journal of Fluid Mechanics* **213**, 127 - 148 (1990).

[Genn] Gennis R.B. (1989) *Biomembranes: Molecular Structure and Function,* Springer, New York, Berlin, Heidelberg.

[Gers] Gerst J.E. "SNAREs and SNARE Regulators in Membrane Fusion and Exocytosis". *Cellular and Molecular Life Sciences* **55**, 707 - 734 (1999).

[Ghos] Ghosh P.B. and Whitehouse M.W. *Biochemical Journal* **108**, 155 - 156 (1968).

[Ging] Gingell D. and Todd I. "Interference Reflection Microscopy: A Quantitative Theory for Image Interpretation and its Application to Cell-Substrate Separation Measurements". *Biophysical Journal* **26**, 507 - 526 (1979).

[Gold] Goldup A., Ohki S. and Danielli J.F. "Black Lipid Films". *Recent Progress in Surface Science* **3**, 193 - 256 (1970).

[Gouy] Gouy G. *Annalen der Physik* **7**, 129 (1917).

[Grah] Grahame D.C. *Chemical Reviews* **41**, 441 (1947).

[Grit] Gritsch S. (1997), "Impedanzspektroskopie an festkörpergestützten Lipidmembranen auf Indium-Zinn-Oxid-Elektroden - Mögliche Anwendungen zum Nachweis von

Membrankanälen und in der Biosensorik", *PhD Thesis,* Technische Universität München, München.

[Grit] Gritsch S., Nollert P., Jähnig F. and Sackmann E. "Impedance Spectroscopy of Porin and Gramicidin Pores Reconstituted into Supported Lipid Bilayers on Indium-Tin-Oxide Electrodes". *Langmuir* **14**, 3118 - 3125 (1998).

[Györ] Györvary E., Wetzer B., Sleytr U.B., Sinner A., Offenhäusser A. and Knoll W. "Lateral Diffusion of Lipids in Silane-, Dextran-, and S-Layer-Supported Mono- and Bilayers". *Langmuir* **15**, 1337 - 1347 (1999).

[Habi] Habicht J., Schmidt M., Rühe J. and Johannsmann D. "Swelling of Thick Polymer Brushes Investigated with Ellipsometry". *Langmuir* **15**, 2460 (1999).

[Hama] Hamaker H.C. *Physica* **4**, 1058 (1937).

[Hard] Hardy W. *Philosophical Magazine* **38**, 49 (1919).

[Mole] Haugland R.P. (1996) *Handbook of Fluorescence Molecules,* Molecular Probes, Inc., Eugene, OR.

[Haus] Hausch M., Beyer D., Knoll W. and Zentel R. "Ultrathin Polymer Films on Gold Supports: LB-Transfer versus Self Assembly". *Langmuir* **14**, 7213 - 7216 (1998).

[He] He S. and Ketterson J.B. "Steady Transfer of a Monolayer between two Langmuir Troughs via the Marangoni Effect". *Philosophical Magazine B* **77**, 831 - 847 (1998).

[Heib] Heibel C., Maus S., Knoll W. and Rühe J. "Polymer Supported Biomembrane Models". *Organic Thin Films* **695**, 104 - 118 (1998).

[Helf] Helfrich W. "Steric Interaction of Fluid Membranes in Multilayer Systems". *Zeitschrift für Naturforschung* **33a**, 305 - 315 (1978).

[Hell] Hellen E.H. and Axelrod D. "Fluorescence Emission at Dielectric and Metal-Film Interfaces". *Journal of the Optical Society of America B* **4**, 337 - 350 (1987).

[Helm] Helm C.A., Israelachvili J.N. and McGuiggan P.M. "Molecular Mechanism and Forces Involved in the Adhesion and Fusion of Amphiphilic Bilayers". *Science* **246**, 919 - 922 (1989).

[Helm] Helm C.A., Israelachvili J.N. and McGuiggan P.M. "Role of Hydrophobic Forces in Bilayer Adhesion and Fusion". *Biochemistry* **31**, 1794 - 1805 (1991).

[Henr] Henriksen I., Green K. L., Smart J. D., Smistad G. and Karlsen J. "Bioadhesion of Hydrated Chitosans: an in vitro and in vivo Study". *International Journal of Pharmaceutics* **145**, 231 - 240 (1996).

[Henr] Henriksen I., Smistad G. and Karlsen J. "Interactions between Liposomes and Chitosan". *International Journal of Pharmaceutics* **101**, 227 - 236 (1994).

[Henr] Henriksen I., Vagen S.R., Sande S.A., Smistad G. and Karlsen G. "Interactions between Liposomes and Chitosan II: Effect of selected Parameters on Aggregation and Leakage". *International Journal of Pharmaceutics* **146**, 193 - 204 (1997).

[Hesl] Heslot F., Cazabat A.M. and Levinson P. "Dynamics of Wetting of Tiny Drops: Ellipsometric Study of the Late Stages of Spreading". *Physical Review Letters* **62**, 1286 - 1289 (1988).

[Hesl] Heslot F., Fraysse N. and Cazabat A.M. "Molecular Layering in the Spreading of Wetting Liquid Droplets". *Nature* **338**, 640 - 642 (1989).

[Hian] Hianik T., Dlugopolsky J., Gyeppessova M., Sivak B., Tien H.T. and Ottova-Leitmannova A. "Stabilization of Bilayer Lipid Membranes on Solid Supports by Trehalose". *Bioelectrochemistry and Bioenergetics* **39**, 299 - 302 (1996).

[Hick] Hickson R.G.L. and Polson A. "Some Physical Characterisation of the Agarose Molecule". *Biochimica et Biophysica Acta* **165**, 43 - 58 (1968).

[Hill] Hill R.M. "Superspreading". *Current Opinion in Colloid & Interface Science* **3**, 247 - 254 (1998).

[Hill] Hillebrandt H. "personal communication". (2000).

[Hill] Hillebrandt H., Wiegand G., Tanaka M. and Sackmann E. "High Electric Resistance Polymer/Lipid Composite Films on Indium-Tin-Oxide Electrodes". *Langmuir* **15**, 8451 - 8459 (1999).

[Hirs] Hirsa A., Korenowski G.M., Logory L.M. and Judd C.D. "Determination of Surface Viscosities by Surfactant Concentration and Velocity Field Measurements for an Insoluble Monolayer". *Langmuir* **13**, 3813 - 3822 (1997).

[Ho] Ho C., Slater S.J. and Stubbs C.D. "Hydration and Order in Lipid Bilayers". *Biochemistry* **34**, 6188 - 6195 (1995).

[Ho] Ho C. and Stubbs C.D. "Hydration at the Membrane Protein-Lipid Interface". *Biophysical Journal* **63**, 897 - 902 (1992).

[Ho] Ho C. and Stubbs C.D. "Effect of n-Alkanols on Lipid Bilayer Hydration". *Biochemistry* **36**, 10630 - 10637 (1997).

[Holl] Hollars C.W. and Dunn R.C. "Probing Single Molecule Orientations in Model Lipid Membranes with Near-Field Scanning Optical Microscopy". *Journal of Chemical Physics* **112**, 7822 - 7830 (2000).

[Hong] Hongyo K., Joseph J., Huber R.J. and Janata J. "Experimental Observation of Chemically Modulated Admittance of Supported Phospholipid Membranes". *Langmuir* **3**, 827 - 830 (1987).

[Howa] Howard R.E. and Burton R.M. "Thin Lipid Membranes with Aqueous Interfaces: Apparatus Design and Methods of Study". *The Journal of the American Oil Chemists Society* **45**, 202 - 229 (1968).

[Hübn] Hübner W. and Blume A. "Interactions at the Lipid-Water Interface". *Chemistry and Physics of Lipids* **96**, 99 - 123 (1998).

[Hugh] Hughes B.D., Pailthorpe B.A. and White L.R. "The Translational and Rotational Drag on a Cylinder Moving in a Membrane". *Journal of Fluid Mechanics* **110**, 349 - 372 (1981).

[Hwan] Hwang J., Tamm L.K., Böhm C., Ramalingam T.S., Betzig E. and Edidin M. "Nanoscale Complexity of Phospholipid Monolayers Investigated by Near-Field Scanning Optical Microscopy". *Science* **270**, 610 - 614 (1995).

[Ide] Ide T. and Yanagida T. "An Artificial Lipid Bilayer Formed on an Agarose-Coated Glass for Simulaneous Electrical and Optical Measurement of Single Ion Channels". *Biochemical and Biophysical Research Communications* **265**, 595 - 599 (1999).

[Inge] Ingebrandt S. (2001), "Characterisation of the Cell-Transistor Coupling", *PhD Thesis,* Johann-Gutenberg Universität Mainz, Mainz.

[Inou] Inoue H., Hida M., Nakashima N. and Yoshihara K. "Picosencond Fluorescence Lifetimes of Anthraquinone Derivates. Radiationless Deactivation via Intra- and Intermolecular Hydrogen Bonds". *Journal of Chemical Physics* **86**, 3184 - 3188 (1982).

[Iono] Ionov R. and Angelova A. "Swelling of Bilayer Lipid Membranes". *Thin Solid Films* **284 - 285**, 809 - 812 (1996).

[Isra] Israelachvili J. "Solvation Forces and Liquid Structure as Probed by Direct Force Measurements". *Acc. Chem. Res* **20**, 415 - 421 (1987).

[Isra] Israelachvili J. and Wennerström. "Role of Hydration and Water Structure in Biological and Colloidal Interactions". *Nature* **379**, 219 - 225 (1996).

[Isra] Israelachvili J.N. (1992a) *Intermolecular and Surface Forces,* Academic Press, London, san Diego, New York, Boston, Sydney, Tokyo, Toronto.

[Isra] Israelachvili J.N. and Wennerstroem H. "Hydration or Steric Forces between Amphiphilic Surfaces". *Langmuir* **6**, 873 - 876 (1990).

[Isra] Israelachvili J.N. and Wennerstroem H. "Entropic Forces between Amphiphilic Surfaces in Liquids". *Journal of Physical Chemistry* **96**, 520 - 531 (1992b).

[Itoh] Itoh K. and Azumi T. "Shift of the Emission Band upon Excitation at the long Wavelength Absorption Edge. II. Importance of the Solute-Solvent Interaction and the Solvent Reorientation Relaxation Process". *Journal of Chemical Physics* **62**, 3431 - 3438 (1975).

[Ivan] Ivanov G.R., Petkova J.I., Okabe Y., Aoki D., Takano H., Kawate H. and Fujihira M. "Scanning Probe Microscopy Studies of Aggregation in Langmuir-Blodgett Films". *Supramolecular Science* **4**, 549 - 557 (1997).

[Izum] Izumi K. "Structural Analysis of Agar-Type Polysaccharides by NMR Spectroscopy". *Biochimica et Biophysica Acta* **320**, 311 - 317 (1973).

[Jend] Jendrasiak G.L. "The Hydration of Phospholipids and its Biological Significance". *Nutritional Biochemistry* **7**, 599 - 609 (1996).

[Jenk] Jenkins A.T.A., Hu J., Wang Y.Z., Schiller S., Foerch R. and Knoll W. "Pulsed Plasma Deposited Maleic Anhydride Thin Films as Supports for Lipid Bilayers". *Langmuir* **16**, 6381 - 6384 (2000).

[Jens] Jensen O. E. "Insoluble Surfactant Spreading on a Thin Viscous Film: Shock Evolution and Film Rupture". *Journal of Fluid Mechanics* **240**, 259 - 288 (1992).

[Joan] Joanny J.F. *C. R. Acad. Sci.* **299II**, 279 (1984).

[June] Junesch U. and Gräber P. "Influence of the Redox State and the Activation of the Chloroplast ATP Synthase on Proton-Transport-Coupled ATP Synthesis/Hydrolysis". *Biochimica et Biophysica Acta* **983**, 275 - 288 (1987).

[Kaga] Kagawa Y. "Biophysical Studies on ATP Synthase". *Advanced Biophysics* **36**, 1 - 25 (1999).

[Kalb] Kalb E., Frey S. and Tamm L.K. "Formation of Supported Planar Bilayers by Fusion of Vesicles to Supported Phospholipid Monolayers". *Biochimica et Biophysica Acta* **1103**, 307 - 316 (1992).

[Kamb] Kamphampati D.K. and Knoll W. "Surface-Plasmon Optical Techniques". *Current Opinion in Colloid & Interface Science* **4**, 273 - 280 (1999).

[Khal] Khalid M.N., Ho L., Agnely F., Grossiord J.L. and Couarraze G. "Swelling Properties and Mechanical Characterization of a semi-Interpenetrating Chitosan/Polyethylene Oxide Network. Comparison with a Chitosan Reference Gel". *S. T. P. Pharma Sciences* **9**, 359 - 364 (1999).

[Kirs] Kirstein D., Kirstein L., Scheller F., Borcherding H., Ronnenberg J., Diekmann S. and Steinrücke P. "Amperometric Nitrate Biosensors on the Basis of Pseudomonas Stutzeri Nitrate Reductase". *Journal of Electroanalytical Chemistry* **474**, 43 - 51 (1999).

[Knol] Knoll W., Frank C.W., Heibel C., Naumann R., Offenhäusser A., Rühe J., Schmidt E.K., Shen W.W. and Sinner A. "Functional Tethered Lipid Bilayers". *Journal of Molecular Biotechnology* **74**, 137 - 158 (2000).

[Krau] Krause M. (2000), "Untersuchungen zur Zell-Transistor Kopplung mittels der Voltage-Clamp Technik", *PhD Thesis,* Johannes Gutenberg Universität, Mainz.

[Krei] Kreiter M. "unpublished results". (2001).

[Kuhn] Kuhn H. "Classical Aspects Energy Transfer in Molecular Systems". *Journal of Chemical Physics* **53**, 101 - 108 (1970).

[Kühn] Kühner M. (1996a), "Präparation und Charakterisierung von Polysaccharid-Monofilmen, Lipid-Doppelschichten und Polysaccharid-Lipid-Verbundfilmen auf Festkörperoberflächen", Technische Universität München,

[Kühn] Kühner M., Rampe R. and Sackmann E. "Lipid Mono- and Bilayer Supported on Polymer Films: Composite Polymer-Lipid Films on Solid Substrates". *Biophysical Journal* **67**, 217 - 226 (1994).

[Kühn] Kühner M. and Sackmann E. "Ultrathin Hydrated Dextran Films Grafted on Glass: Preparation and Characterization of Structural, Viscous, and Elastic Properties by Quantitative Microinterferometry". *Langmuir* **12**, 4866 - 4876 (1996b).

[Lako] Lakowicz J.R. (1983) *Principles of Fluorescence Spectroscopy,* Plenum Press, New York, London.

[Lako] Lakowicz J.R. and Keating-Nakamoto S. "Red Edge Excitation of Fluorescence and Dynamics Properties of Proteins and Membranes". *Biochemistry* **23**, 3013 - 3021 (1984).

[Lalc] Lalchev Z., Todorov R., Ishida H. and Nakazawa H. "Lateral Mobility of Phospholipid Molecules in thin Liquid Films". *European Biophysics Journal* **23**, 433 - 438 (1995).

[Lalc] Lalchev Z.I., Wilde P.J. and Clark D.C. "Surface Diffusion in Phospholipid Foam Films". *Journal of Colloid and Interface Science* **167**, 80 - 86 (1994).

[Land] Landau D. and Levich B.G. *Acta Physiochim, URSS* **17**, 42 - 54 (1942).

[Lang] Langmuir I. *Journal of Chemical Physics* **6**, 873 - 896 (1936).

[Lawr] Lawrence C.J. "The Mechanics of Spin-Coating of Polymer Films". *Physics of Fluids* **31**, 2786 - 2795 (1988).

[Le Gran] Le Grange J.D., Markham J.L. and Kurkjian C.R. "Effects on Surface Hydration on the Deposition of Silane Monolayers on Silica". *Langmuir* **9**, 1749 - 1753 (1993).

[Lehn] Lehninger A.L. (1983) *Biochemie,* Verlag Chemie, Weinheim, Deerfield Beach, Florida, Basel.

[Leht] Lehtonen J.Y.A. and Kinnunen P.K.J. "Poly(ethylene glycol)-Induced and Temperature-Dependent Phase Separation in Fluid Binary Phospholipid Membranes". *Biophysical Journal* **68**, 525 - 535 (1995).

[Leik] Leikin S., Parsegian A. and Rau D.C. "Hydration Forces". *Annual Reviews in Physical Chemistry* **44**, 369 - 395 (1993a).

[Leik] Leikin S., Rau D.C. and Parsegian V.A. *Biophysical Journal* **64**, A270 (1993b).

[Lieb] Lieberherr M., Fattinger Ch. and Lukosz W. "Optical-Environment-Dependent Effects on the Fluorescence of Submonomolecular Dye Layers on Interfaces". *Surface Science* **189/190**, 954 - 959 (1987).

[Lifs] Lifshitz E.M. *Eksp. Teor. Fiz.* **29**, 94 (1955).

[Lin] Lin S. and Struve W.S. "Time Resolved Fluorescence of Nitrobenzoxadiazole-Aminohexanoic Acid: Effect of Intermolecular Hydrogen-Bonding on non-Radiative Decay". *Photochemistry and Photobiology* **54**, 361 - 365 (1991).

[Lind] Lindholm-Sethson B. "Electrochemistry at Ultrathin Organic Films at Planar Gold Electrodes". *Langmuir* **12**, 3305 - 3314 (1996).

[Lind] Lindsey H., Peterson N. and Chan S. "Physicochemical Characterization of 1,2-Diphytanoyl-sn-glycero-3-phosphatidylcholine in Model Membrane Systems". *Biochimica et Biophysica Acta* **555**, 147 - 167 (1979).

[Ling] Lingler S. (1998), "Entwicklung und Charakterisierung von festkörpergestützten Modellmembranen zur Rekonstitution von Valinomycin und F0F1-ATPase", *PhD thesis,* Johannes Gutenberg Universität, Mainz.

[Ling] Lingler S., Rubinstein I., Knoll W. and Offenhäusser A. "Fusion of Small Unilamellar Lipid Vesicles to Alkanethiol and Thiolipid Self-Assembled Monolayers on Gold". *Langmuir* **13**, 7085 - 7091 (1997).

[Lipp] Lippert von E. "Spektroskopische Bestimmung des Dipolmomentes aromatischer Verbindungen im ersten angeregten Singulettzustand". *Zeitschrift für Elektrochemie* **61**, 962 - 975 (1957).

[Lope] Lopez J., Miller C.A. and Ruckenstein E. "Spreading Kinetics of Liquid Drops on Solids". *Journal of Colloid and Interface Science* **56**, 460 - 468 (1976).

[Lu] Lu X., Ottova A.L. and Tien H.T. "Biophysical Aspects of Agar-Gel Supported Bilayer Lipid Membranes: a new Method of Forming and Studying Planar Bilayer Lipid Membranes". *Bioelectrochemistry and Bioenergetics* **39**, 285 - 289 (1996).

[Luch] Lucht R. and Bahr C. "Surface Plasmon Resoncance Study of the Spreading of a Liquid-Crystal Smectic-A Droplet on a Gold Substrate". *Physical Review Letters* **85**, 4080 - 4083 (2000).

[Luko] Lukosz W. "Light Emission by Multipole Sources in Thin Layers. I. Radiation Patterns of Electric and Magnetic Dipoles". *Journal of the Optical Society of America* **71**, 744 - 754 (1981).

[MacD] MacDonald J.R. (1987) *Impedance Spectroscopy - Emphasizing Solid Materials and Systems,* Wiley, New York.

[MacD] MacDonald R.C., MacDonald R.I., Menco B.P.M., Takeshita K., Subbarano N.K. and Hu L. "Small-Volume Extrusion Apparatus for Preparation of Large Unilamellar Vesicles". *Biochimica et Biophysica Acta* **1061**, 297 - 303 (1991).

[Maje] Majewski J., Kuhl T.L., Gerstenberg M.C., Israelachvili J.N. and Smith G.S. "Structure of Phospholipid Monolayers Containing Poly(ethylene glycol) Lipids at the Air-Water Interface". *Journal of Physical Chemistry B* **101**, 3122 - 3129 (1997).

[Maje] Majewski J., Kuhl T.L., Kjaer K., Gerstenberg M.C., Als-Nielsen J., Israelachvili J.N. and Smith G.S. "X-Ray Synchrotron Study of Packing and Protrusions of Polymer-Lipid Monolayers at the Air-Water Interface". *Journal of the American Chemical Society* **120**, 1469 - 1473 (1998).

[Maje] Majewski J., Kuhl T.L., Wong J.Y. and Smith G.S. "X-Ray and Neutron Surface Scattering for Studying Lipid/Polymer Assemblies at the Air-Liquid and Solid-Liquid Interface". *Journal of Molecular Biotechnology* **74**, 207 - 232 (2000).

[Mara] Marantz Y., Nachliel E., Aagaard A., Brzezinski P. and Gutman M. "The Proton Collecting Function of the Inner Surface of Cytochrome c Oxidase from Rhodobacter Sphaeroides". *Proceedings of the National Academy of Sciences of the United States of America* **95**, 8590 - 8595 (1998).

[Marc] Marcelja S. and Radic N. *Chemical Physics Letters* **42**, 129 (1976).

[Marr] Marrink S.-J., Berkowitz M. and Berendsen H.J.C. "Molecular Dynamics Simulation of a Membrane/Water Interface: The Ordering of Water and Its Relation to the Hydration Force". *Langmuir* **9**, 3122 - 3131 (1993).

[Marr] Marrink S.-J., Tieleman D.P., van Bueren A.R. and Berendsen H.J.C. "Membranes and Water: an Interesting Relationsship". *Faraday Discussions* **103**, 191 - 201 (1996).

[Mars] Marsh D. "Water Adsorption Isotherms and Hydration Forces for Lysolipids and Diacyl Phospholipids". *Biophysical Journal* **55**, 1093 - 1100 (1989).

[Mars] Marsh D. (1990) *CRC Handbook of Lipid Bilayers,* CRC Press, Boca Raton, Ann Arbor, Boston.

[Math] Mathe G., Albersdörfer A., Neumaier K.R. and Sackmann E. "Disjoining Pressure and Swelling Dynamics of Thin Adsorbed Polymer Films under Controlled Hydration Conditions". *Langmuir* **15**, 8726 - 8735 (1999).

[Mats] Matsuyama H., Shirishi H. and Kitamura Y. "Effect of Membrane Preparation Conditions on Solute Permeability in Chitosan Membrane". *Journal of Applied Polymer Science* **73**, 2715 - 2725 (1999).

[Maze] Mazeres S., Schram V., Tocanne J.-F. and Lopez A. "7-Nitrobenz-2-oxa-1,3-diazole-4-yl-Labeled Phospholipids in Lipid Membranes: Differences in Fluorescence Behavior". *Biophysical Journal* **71**, 327 - 335 (1996).

[McCo] McConnell H. "Structures and Transitions in Lipid Monolayers at the Air-Water Interface". *Annual Review of Physical Chemistry* **42**, 171 - 195 (1991).

[McCo] McCown J.T., Evans E., Diehl S. and Wiles H.C. "Degree of Hydration and Lateral Diffusion in Phoshpolipid Multibilayers". *Biochemistry* **20**, 3134 - 3138 (1981).

[McIn] McIntosh T.J., Magid A.D. and Simon S.A. "Range of the Solvation Pressure between Lipid Membranes: Dependence on the Packing Density of Solvent Molecules". *Biochemistry* **28**, 7904 - 7912 (1989).

[Merk] Merkel R., Sackmann E. and Evans E. "Molecular Friction and Epitactic Coupling between Monolayers and Supported Bilayers". *Journale de Physique France* **50**, 1535 - 1555 (1989).

[Meyv] Meyvis T.K.L., De Smedt S.C., Van Oostveldt P. and Demeester J. "Fluorescence Recovery After Photobleaching: A Versatile Tool for Mobility and Interaction Measurements in Pharmaceutical Research". *Pharmaceutical Research* **16**, 1153 - 1162 (1999).

[Mikr] Mikrut J.M., Dutta P., Ketterson J.B. and MacDonald R.C. "Atomic-Force and Fluorescence Microscopy of Langmuir-Blodgett Monolayers of L-a-dimyristoylphosphatidic acid". *Physical Review B* **48**, 14479 - 14487 (1993).

[Mill] Miller C., Cuendet P. and Grätzel M. "K+ Sensitive Bilayer Supporting Electrodes". *Journal of Electroanalytical Chemistry* **278**, 175 - 192 (1990).

[Milt] Milton J.G., Purkey R.M. and Galley W.C. "The Kinetics of Solvent Reorientation in Hydroxylated Solvents from the Exciting-Wavelength Dependence of Chromophore Emision Spectra". *Journal of Chemical Physics* **68**, 5396 - 5404 (1978).

[Mino] Minoura N., Koyano T., Koshizaki N., Umehara H., Nagura M. and Kobayashi K. "Preparation, Properties, and Cell Attachement/Growth Behaviour of PVA/Chitosan-Blended Hydrogels". *Materials Science and Engineering C* **6**, 275 - 280 (1998).

[Moel] Moellerfeld J., Prass W., Ringsdorf H., Hamazaki H. and Sunamoto J. "Improved Stability of Black Lipid Membranes by Coating with Polysaccharide Derivatives Bearing Hydrophobic Anchor Groups". *Biochimica et Biophysica Acta* **857**, 265 - 270 (1986).

[Möhw] Möhwald H. "Phospholipid and Phospholipid-Protein Monolayers at the Air/Water Interface". *Annual Reviews of Physical Chemistry* **41**, 441 - 476 (1990).

[Moor] Moore W.J. and Hummel D.O. (1973) *Physikalische Chemie,* De Gruyter, Berlin, New York.

[Mori] Morigaki K., Baumgart T., Jonas U., Offenhäusser A. and Knoll W. "Polymerization of Diacetylene Lipid Bilayers at the Solid/Liquid Interface and its Application to the Construction of Micropatterned Biomimetic Membranes". *in preparation* (2001a).

[Mori] Morigaki K., Baumgart T., Offenhäusser A. and Knoll W. "Structuring of Solid Supported Bilayer Lipid Membranes by Lithographic Polymerisation of a Diacetylene Lipid". *Angewandte Chemie* **113**, 184 - 186 (2001b).

[Muel] Mueller P., Rudin D.O., Tien H.T. and Wescott W.C. *Nature* **194**, 979 (1962).

[Mukh] Mukherjee S., Chattopadhyay A., Samanta A. and Soujanya T. "Dipole Moment Change of NBD Group upon Excitation Studied Using Solvatochromic and Quantum Chemical Approaches: Implications in Membrane Research". *Journal of Physical Chemistry* **98**, 2809 - 2812 (1994).

[Murm] Murmeister J.S., Olivier L.A., Reichert W.M. and Truskey G.A. "Application of Total Internal Reflection Fluorescence Microscopy to Study Cell Adhesion to Biomaterials". *Biomaterials* **19**, 307 - 325 (1998).

[Naum] Naumann C., Brumm T., Rennie A.R., Penfold J. and Bayerl T.M. "Hydration of DPPC Monolayers at the Air/Water Interface and its Modulation by the Nonionic Surfactant $C_{12}E_4$: A Neutron Reflection Study". *Langmuir* **11**, 3948 - 3952 (1995a).

[Naum] Naumann R., Baumgart T., Gräber P., Jonczyk A., Offenhaeusser A. and Knoll W. "Proton Transport through a Peptide-Tethered Bilayer Lipid Membrane by the H(+)-ATP Synthase from Chloroplasts Measured by Impedance Spectroscopy". *submitted to Biosensors & Bioelectronics* (2001).

[Naum] Naumann R., Jonczyk A., Kopp R., van Esch J., Ringsdorf H., Knoll W. and Gräber P. "Inkorporation von Membranproteinen in festkörperunterstützte planare Lipidfilme". *Angewandte Chemie* **107**, 2168 - 2171 (1995b).

[Naum] Naumann R., Schmidt E.K., Jonczyk A., Fendler K., Kadenbach B., Liebermann T., Offenhaeusser A. and Knoll W. "The Peptide-Tethered Lipid Membrane as a Biomimetic System to Incorporate Cytochrome C Oxidase in a Functionally Active Form". *Biosensors & Bioelectronics* **14**, 651 - 662 (1999).

[Negr] Negri M.R. and Bernik D.L. "Note: Critical Revision of Apparent Dielectric Constants Calculations in Lipid-Water Interfaces". *Journal of Colloid and Interface Science* **226**, 364 - 366 (2000).

[Neum] Neuman R.D., Park S. and Shah P. "Lateral Diffusion of Surfactant Monolayer Molecules Confined between Two Solid Surfaces". *Journal of Physical Chemistry* **98**, 12474 - 12477 (1994).

[Niss] Nissen J., Gritsch S., Wiegand G. and Rädler J.O. "Wetting of Phospholipid Membranes on Hydrophilic Surfaces - Concepts Towards Self-Healing Membranes". *European Biophysics Journal B* **10**, 335 - 344 (1999).

[Novo] Novotny I., Rhacek V., Tvarozek V., Nikolelis D.P., Andreou V.G., Siontorou C.G. and Ziegler W. "Stabilized Bilayer Lipid Membranes (BLMs) on Agar-Thin Film Electrode System Support". *Materials Science and Engineering C* **5**, 55 - 58 (1997).

[Novo] Novotny L. (1996), *PhD thesis,* ETH, Zürich.

[Offe] Offenhäusser A., Rühe J. and Knoll W. "Neuronal Cells Cultured on Modified Microelectronic Device Surface". *Journal of Vacuum Science and Technology A* **13**, 2606 - 2612 (1995).

[Offe] Offenhäusser A., Sprössler C., Matsuzawa M. and Knoll W. "Field-Effect Transistor Array for Monitoring Electrical Activity from Mammalian Neurons in Culture". *Biosensors & Bioelectronics* **12**, 819 - 826 (1997).

[Okah] Okahata Y., Ando R. and Kunitake T. "Phase Transition of the Bilayer Membrane of Synthetic Dialkyl Amphiphiles as Studied by Differential Scanning Calorimetry". *Berichte der Bunsen Gesellschaft für Physikalische Chemie* **85**, 789 - 798 (1981).

[Onsa] Onsager L.J. *Journal of the American Chemical Society* **58**, 1486 (1936).

[Osha] Oshanin G., Coninck J.D., Cazabat A.M. and Moreau M. "Dewetting, Partial Wetting, and Spreading of a Two-Dimensional Monolayer on Solid Surface". *Physical Review E* **58**, 20 - 23 (1998a).

[Osha] Oshanin G., De Coninck J.D., Cazabat A.M. and Moreau M. "Microscopic Model for Spreading of a Two-Dimensional Monolayer". *Journal of Molecular Liquids* **76**, 195 - 219 (1998b).

[Otsu] Otsuki S. and Adachi K. "Medium-Sensitive Fluorophore as a Moisture Probe in Polymer Film". *Polymer Journal* **26**, 343 - 348 (1994).

[Otte] Ottenbacher D., Jähnig F. and Göpel W. "A Prototype Biosensor Based on Transport Proteins: Electrical Transducers Applied to Lactose Permease". *Sensors and Actuators B* **13 - 14**, 173 - 175 (1993).

[Otte] Ottenbacher D., Kindervater R. and Gimmel P. "Developing Biosensor with pH-ISFET Transducers Utilizing Lipid Bilayer Membranes with Transport Proteins". *Sensors and Actuators B* **6**, 192 - 196 (1992).

[Papr] Paprica P.A., Baird N.C. and Petersen N.O. "Theoretical and Experimental Analysis of Optical Transitions of Nitrobenzoxadiazole (NBD) Derivatives". *Journal for Photochemistry and Photobiology A: Chemistry* **70**, 51 - 57 (1993).

[Pars] Parsegian V.A., Fuller N. and Rand R.P. "Measured Work of Deformation and Repulsion of Lecithin Bilayers". *Proceedings of the National Academy of Science USA* **76**, 2750 - 2754 (1979).

[Pase] Pasenkiewicz-Gierula M., Rog T., Kitamura K. and Kusumi A. "Cholesterol Effects on the Phosphatidylcholine Bilayer Polar Region: A Molecular Simulation Study". *Biophysical Journal* **78**, 1376 - 1389 (2000).

[Pere] Perera L., Essmann U. and Berkowitz M.L. "Role of Water in the Hydration Force Acting between Lipid Bilayers". *Langmuir* **12**, 2625 - 2629 (1996).

[Pete] Peters R. and Beck K. "Translational Diffusion in Phospholipid Monolayers Measured by Fluorescence Microphotolysis". *Proceedings of the National Academy of Science, USA* **80**, 7183 - 7187 (1983).

[Pett] Petty M.C. (1996) *Langmuir-Blodgett Films: An Introduction,* Cambridge University Press, New York.

[Pink] Pink D., Kühner M., Quinn B., Sackmann E. and Pham H. "Evidence for Domains in Deposited Lipid Bilayers". *Langmuir* **11**, 2696 - 2704 (1995).

[Pink] Pink D.A. "Theoretical Studies of Phospholipid Bilayers and Monolayers. Perturbing Probes, Monolayer Phase Transitions, and Computer Simulations of Lipid-Protein Bilayers". *Canadian Journal of Biochemistry and Cell Biology* **62**, 760 - 777 (1983).

[Pink] Pink D.A., Ramadurai K.S. and Powell J.R. "Computer simulation of lipid diffusion in a two-component bilayer. The effect of adsorbing macromolecules". *Biochimica et Biophysica Acta* **1148**, 197 - 208 (1993).

[Piss] Pissis P., Enders A. and Mimitz G. "Hydration Dependence of Molecular Mobility in Phospholipid Bilayers". *Chemical Physics* **171**, 285 - 292 (1993).

[Plan] Plant A.L. "Self-Assembled Phospholipid/Alkanethiol Biomimetic Bilayers on Gold". *Langmuir* **9**, 2764 - 2767 (1993).

[Ploe] Ploem J. S. (1975) In *Mononuclear Phagocytes in Immunity, Infection and Pathology*Blackwell, Oxford, pp. 405 - 421.

[Plow] Plowman T.E., Saavedra S.S. and Reichert W.M. "Planar Integrated Optical Methods for Examining thin Films and Their Surface Adlayers.". *Biomaterials* **19**, 341 - 355 (1998).

[Popp] Popper K. (1994) *Logik der Forschung,* J.C.B. Mohr, Tübingen.

[Pruc] Prucker O., Naumann C., Rühe J., Knoll W. and Frank C.W. "Photochemical Attachement of Polymer Films to Solid Surfaces via Monolayers of Benzophenone Derivatives". *Journal of the American Chemical Society* **121**, 8766 (1999).

[Rädl] Rädler J. (1993a), "Über die Wechselwirkung fluider Phospholipidmembranen mit Festkörperoberflächen", *PhD Thesis,* Technische Universität München, München.

[Rädl] Rädler J. and Sackmann E. "On the Measurement of Weak Repulsive and Frictional Colloidal Forces by Reflection Interference Contrast Microscopy". *Langmuir* **8**, 848 - 853 (1992).

[Rädl] Rädler J. and Sackmann E. "Imaging Optical Thicknesses and Separation Distances of Phospholipid Vesicles at Solid Interfaces". *Journal de Physique II France* **3**, 727 - 748 (1993b).

[Rädl] Rädler J., Strey H. and Sackmann E. "Phenomenology and Kinetics of Lipid Bilayer Spreading on Hydrophilic Surfaces". *Langmuir* **11**, 4539 - 4548 (1995a).

[Rädl] Rädler J.O., Feder T.J., Strey H.H. and Sackmann E. "Fluctuation Analysis of Tension-Controlled Undulation Forces between Giant Vesicles and Solid Substrates". *Physical Review E* **51**, 4526 - 4536 (1995b).

[Raed] Raedler J. and Sackmann E. "Functionalization of Solids by Ultrathin Soft Polymer Films and Polymer/Lipid Composites: Modeling of Cell Surfaces and Cell Recognition Processes". *Current Opinion in Solid State & Materials Science* **2**, 330 - 336 (1997).

[Ragu] Raguse B., Braach-Maksvytis V., Cornell B.A., King L.G., Osman P.D.D., Pace R.J. and Wieczorek L. "Tethered Lipid Bilayer Membranes: Formation and Ionic Reservoir Characterization". *Langmuir* **14**, 648 - 659 (1998).

[Rand] Rand R.P. and Parsegian V.A. "Hydration Forces between Phospholipid Bilayers". *Biochimica et Biophysica Acta* **988**, 351 - 376 (1989).

[Rau] Rau D.C., Lee B.K. and Parsegian V.A. *Proceedings of the National Academy of Science USA* **81**, 2621 - 2625 (1984).

[Rau] Rau D.C. and Parsegian V.A. *Science* **249**, 1278 - 1281 (1990).

[Rich] Richard P., Rigand J.-P. and Gräber P. *European Journal of Biochemistry* **193**, 921 (1990).

[Rieg] Riegler H. and Spratte K. "Structural Changes in Lipid Monolayers during the Langmuir-Blodgett Transfer due to Substrate/Monolayer Interactions". *Thin Solid Films* **210/211**, 9 - 12 (1992).

[Rieg] Riegler J.E. and LeGrange J.D. "Observation of a Monolayer Phase Transition on the Meniscus in a Langmuir-Blodgett Transfer Configuration". *Physical Review Letters* **61**, 2492 - 2495 (1988).

[Robe] Robertson S.K. and Bike S.G. "Quantifying Cell-Surface Interactions Using Model Cells and Total Internal Reflection Microscopy". *Langmuir* **14**, 928 - 934 (1998).

[Sack] Sackmann E. "Supported Membranes: Scientific and Practical Applications". *Science* **271**, 43 - 48 (1996).

[Sack] Sackmann E. (1997) In *Physics of Biological Systems: From Molecules to Species*, Vol. 480 (Ed, Flyvbjerg H.) Springer, Berlin.

[Sack] Sackmann E. and Tanaka M. "Supported Membranes on Soft Polymer Cushions: Fabrication, Characterization and Applications". *Tibtech* **18**, 58 - 64 (2000).

[Saff] Saffman P.G. "Brownian Motion in Thin Sheets of Viscous Fluid". *Journal of Fluid Mechanics* **73**, 593 - 602 (1975).

[Saha] Saha S. and Samanta A. "Photophysical and Dynamic NMR Studies on 4-Amino-7-nitrobenz-2-oxa-1,3-diazole Derivatives: Elucidation of the Nonradiative Deactivation Pathway". *Journal of Physical Chemistry A* **102**, 7903 - 7912 (1998).

[Salo] Salome L., Cazeils J., Lopez A. and Tocanne J. "Characterization of Membrane Domains by Frap Experiments at Variable Observation Areas". *European Biophysics Journal* **27**, 391 - 402 (1998).

[Sand] Sanders C.R. and Schwonek J.P. "An Approximate Model and Empirical Energy Function for Solute Interactions with a Water-Phosphatidylcholine Interface". *Biophysical Journal* **65**, 1207 - 1218 (1993).

[Saxt] Saxton M. "Lateral Diffusion in an Archipelago: Effects of Impermeable Patches on diffusion in a Cell Membrane". *Biophysical Journal* **39**, 165 - 173 (1982).

[Scar] Scarlata S., Gupta R., Garcia P., Keach H., Shah S., Kasireddy C.R., Bittman R. and Rebecchi M.J. "Inhibition of Phospholipase C-d1 Catalytic Activity by Sphingomyelin". *Biochemistry* **35**, 14882 - 14888 (1996).

[Scha] Schaub M., Wenz G., Wegner G., Stein A. and Klemm D. "Ultrathin Films of Cellulose on Silicon Wafers". *Advanced Materials* **5**, 919 - 922 (1993).

[Schm] Schmidt C., Mayer M. and Vogel H. "A Chip-Based Biosensor for the Functional Analysis of Single Ion Channels". *Angewandte Chemie International Edition in English* **39**, 3137 - 3140 (2000).

[Schn] Schneider G., Knoll W. and Sackmann E. "Preparation and Characterisation of Asymmetric Soap Films on Vertical Si/SiO_2-Interfaces". *Europhysics Letters* **1**, 449 - 454 (1986).

[Scri] Scriven L.E. *Chemical Engineering Science* **12**, 98 - 108 (1960).

[Sell] Selle C., Pohle W. and Fritzsche H. "FTIR Spectroscopic Features of Lyotropically induced Phase Transitions in Model Membranes". *Journal of Molecular Structure* **480 - 481** (1999).

[Shen] Shen W.W., Boxer S.G., Knoll W. and Frank C.W. "Polymer-Supported Lipid Bilayers on Benzophenone-Modified Substrates". *submitted to: Biomacromolecules* (2000).

[Shik] Shiku H. and Dunn R.C. "Direct Observation of DPPC Phase Domain Motion on Mica Surfaces under Conditions of High Relative Humidity". *Journal of Physical Chemistry B* **102**, 3791 - 3797 (1998).

[Shim] Shimoji S. "Numerical Analysis of the Spin-Coating Process". *Journal of Applied Physics* **66**, 2712 - 2718 (1989).

[Sike] Sikes H.D. and Schartz D.K. "A Temperature-Dependent Two-Dimensional Condensation Transition during Langmuir-Blodgett Deposition". *Langmuir* **13**, 4704 - 4709 (1997).

[Sike] Sikes H.D., Woodward J.T. and Schartz D.K. "Pattern Formation in a Substrate-Induced Phase Transition during Langmuir-Blodgett Transfer". *Journal of Physical Chemistry* **100**, 9093 - 9097 (1996).

[Sing] Singer S.J. and Nicholson G.L. "The Fluid Mosaic Model of the Structure of Cell Membranes". *Science* **175**, 720 - 731 (1972).

[Sinn] Sinner A. (1999), "Präparation und Charakterisierung von polymerunterstützten Lipiddoppelschichten auf planaren oxidischen Oberflächen unter dem Aspekt der Anwendbarkeit für die Sensorik", Technische Universität München, München.

[Sinn] Sinner A. and Offenhäusser A. "The Electrical Characterization of Supported Phospholipid Bilayers using Titanium/Titanium Oxide Microelectrodes". *Thin Solid Films* **327 - 329**, 758 - 761 (1998).

[Siro] Sirota E.B., Smith G.S., Safinya C.R., Plano R.J. and Clark N.A. "X-Ray-Scattering Studies of Aligned, Stacked Surfactant Membranes". *Science* **242**, 1406 - 1409 (1988).

[Smit] Smith D.P.E., Bryant A., Quate C.F., Rabe J.P., Gerber Ch. and Swallen J.D. *Proceedings of the National Academy of Science USA* **84**, 969 (1987).

[Smit] Smith L.M., McConnell H.M., Smith B.A. and Parce J.W. "Pattern Photobleaching of Fluorescent Lipid Vesicles Using Polarized Laser Light". *Biophysical Journal* **33** (1981).

[Soll] Solletti J.M., Botreau M., Sommer F., Brunat W.L., Kasas S., Minh Duc T. and Celio M.R. "Elaboration and Characterization of Phospholipid Langmuir-Blodgett Films". *Langmuir* **12**, 5379 - 5386 (1996).

[Söll] Söllner T., Whiteheart S.W., Brunner M., Erdjument B.H., Geromanos S. and P. "SNAP Receptors Implicated in Vesicle Targeting and Fusion". *Nature* **362**, 318 - 324 (1993).

[Sonn] Sonntag D. (1966) *Hygrometrie,* Akademie Verlag, Berlin.

[Soum] Soumpasis D.M. "Theoretical Analysis of Fluorescence Photobleaching Recovery Experiments". *Biophysical Journal* **41**, 95 - 96 (1983).

[Spin] Spinke J., Yang J., Wolf H., Liley M., Ringsdorf H. and Knoll W. "Polymer-Supported Bilayer on a Solid Substrate". *Biophysical Journal* **63**, 1667 - 1671 (1992).

[Spra] Spratte K., Chi L.F. and Riegler H. "Physisorption Instabilities during Langmuir Wetting". *Europhysics Letters* **25**, 211 - 217 (1994a).

[Spra] Spratte K. and Riegler H. "Steady State Morphology and Composition of Mixed Monomolecular Films (Langmuir Monolayers) at the Air/Water Interface in the Vicinity of the Three-Phase Line: Model Calculations and Experiments". *Langmuir* **10**, 3161 - 3173 (1994b).

[Sprö] Sprössler C. (1997a), "Extrazelluläre Signalableitung durch ein Sensorfeld mit Feldeffekttransistoren", *PhD Thesis,* Johannes Gutenberg Universität, Mainz.

[Sprö] Sprössler C., Richter D., Denyer M. and Offenhäusser A. "Long-Term Recording System Based on Field-Effect Transistor Arrays for Monitoring Electrogenic Cells in Culture". *Biosensors & Bioelectronics* **13**, 613 - 618 (1997b).

[Stel] Stelzle M., Weissmüller G. and Sackmann E. "On the Application of Supported Bilayers as Receptive Layers for Biosensors with Electrical Detection". *Journal of Physical Chemistry* **97**, 2974 - 2981 (1993).

[Ston] Stone H.A. and Ajdari A. "Hydrodynamics of Particles Embedded in a Flat Surfactant Layer Overlying a Subphase of Finite Depth". *Journal of fluid mechanics* **369**, 151-173 (1998).

[Stub] Stubbs C.D., Meech S.R., Lee A.G. and Phillips D. "Solvent Relaxation in Lipid Bilayers with Dansyl Probes". *Biochimica et Biophysica Acta* **815**, 351 - 360 (1985).

[Suzu] Suzuki T., Mizushima Y., Umeda T. and Ohashi R. "Further Biocompatibility Testing of Silica-Chitosan Complex Membrane in the Production of Tissue Plasminogen Activator by Epithelial and Fibroblast Cells". *Journal of Bioscience and Bioengineering* **88**, 194 - 199 (1999).

[Swal] Swalen J.D., Allara D.L., Andrade J.D., Chandross E.A., Garoff S., Israelachvili J., McCarthy T.J., Murray R., Pease R.F., Rabolt J.F., Wynne K.J. and Yu H. "Molecular Monolayers and Films". *Langmuir* **3**, 932 - 950 (1987).

[Take] Takeuchi H., Yamamoto H., Niwa T., Hino T. and Kawashima Y. "Enteral Absorption of Insulin in Rats from Mucoadhesive Chitosan-Coated Liposomes". *Pharmaceutical Research* **13**, 896 - 901 (1996).

[Tama] Tamada K., Kim S. and Yu H. "Lateral Diffusion of a Probe Lipid in Biphasic Phospholipid Monolayers: Liquid/Gas Coexistence Films". *Langmuir* **9**, 1545 - 1550 (1993).

[Tamm] Tamm L.K. and McConnell H.M. "Supported Phospholipid Bilayers". *Biophysical Journal* **47**, 105 - 113 (1985).

[Tanf] Tanford C. (1980) *The Hydrophobic Effect: Formation of Micelles and Biological Membranes,* Wiley, New York.

[Thea] Theato P. and Zentel R. "Stabilization of Lipid Bilayers on Surfaces through Charged Polymers". *J. M. S. - Pure and Applied Chemistry A* **36**, 1001 - 1015 (1999).

[Thom] Thomas J.L., Feder T.J. and Webb W.W. "Effects of Protein Concentration on IgE Receptor Mobility in Rat Basophilic Leukemia Cell Plasma Membranes". *Biophysical Journal* **61**, 1402 - 1412 (1992).

[Tibe] Tiberg F. and Cazabat A.-M. "Self-Assembly and Spreading of Non-Ionic Trisiloxane Surfactants". *Europhysics Letters* **25**, 205 - 210 (1994a).

[Tibe] Tiberg F. and Cazabat A.-M. "Spreading of Thin Films of Ordered Nonionic Surfactants". *Langmuir* **10**, 2301 (1994b).

[Troi] Troian S.M., Herbolzheimer E. and Safran S.A. "Model for the Fingering Instability of Spreading Surfactant Drops". *Physical Review Letters* **65**, 333 - 336 (1990).

[Troi] Troian S.M., Wu X.L. and Safran S.A. "Fingering Instability in Thin Wetting Films". *Physical Review Letters* **62**, 1496 - 1499 (1989).

[Tsuk] Tsukihara T., Aoyama H., Yamashita E., Tomizaki T., Yamaguchi H., Shinzawa-Itoh K., Nakashima R., Yaono R. and Yoshikawa S. "Structures of Metal Sites of Oxidized Bovine Heart Cytochrome c Oxidase at 2.8 A". *Science* **269**, 1069 - 1074 (1995).

[Uto] Uto M., Araki M., Taniguchi T., Hoshi S. and Inoue S. "Stability of an Agar-Supported Bilayer Lipid Membrane and its Application to a Chemical Sensor". *Analytical Sciences* **10**, 943 - 946 (1994).

[Vali] Valignat M.P., Voue M., Oshanin G. and Cazabat A.M. "Structure and Dynamics of thin Liquid Films on Solid Substrates". *Colloids and Surfaces A: Physicochemical and Engineering Aspects* **154**, 25 - 31 (1999).

[Vand] Vanderveen R.J. and Barnes G.T. "Water Permeation through Langmuir-Blodgett Monolayers". *Thin Solid Films* **134**, 227 - 236 (1985).

[Vaz] Vaz W.L.C., Clegg R.M. and Hallmann D. "Translational Diffusion of Lipids in Liquid Crystalline Phase Phosphatidylcholine Multibilayers. A Comparison of Experiment with Theory". *Biochemistry* **24**, 781 - 786 (1985).

[Vaz] Vaz W.L.C., Melo E.C.C. and Thompson T.E. "Translational Diffusion and Fluid Domain Connectivity in a two-Component, two-Phase Phospholipid Bilayer". *Biophysical Journal* **56**, 869 - 876 (1989).

[Verw] Verwey E.J.W. (1948) *Theory of the Stability of Lyophobic Colloids,* Elsevier, New York.

[Vill] Villette S., Valignat M.P., Cazabat A.M., Jullien L. and Tiberg F. "Wetting on the Molecular Scale and the Role of Water. A Case Study of Wetting Hydrophilic Silica Surfaces.". *Langmuir* **12**, 825 - 830 (1996).

[Vill] Villette S., Valignat M.P., Cazabat A.M., Schabert F.A. and Kalachev A. "Ultrathin Liquid Films. Ellipsometric Study and AFM Preliminary Investigations". *Physica A* **236**, 123 - 129 (1997).

[Volk] Volke F., Eisenblätter S., Galle J. and Klose G. "Dynamic Properties of Water at Phosphatidylcholine Lipid-Bilayer Surfaces as seen by Deuterium and Pulsed Field Gradient Proton NMR". *Chemistry and Physics of Lipids* **70**, 121 - 131 (1994).

[Voue] Voue M., Valignat M.P., Oshanin G. and Cazabat A.M. "Dissipation Processes at the Mesoscopic and Molecular Scale. The Case of Polymer Films". *Langmuir* **15**, 1522 - 1527 (1999).

[Wagg] Waggoner A.S. and Stryer L. "Fluorescent Probes of Biological Membranes". *Proceedings of the National Academy of Science* **67**, 579 - 589 (1970).

[Wagn] Wagner M.L. and Tamm L.K. "Tethered Polymer-Supported Planar Lipid Bilayers for Reconstitution of Integral Membrane Proteins: Silane-Polyethyleneglycol-Lipid as a Cushion and Covalent Linker". *Biophysical Journal* **79**, 1400 - 1414 (2000).

[Wals] Walsh C.B. and Franses E.I. "Thickness and Quality of Spin-Coated Polymer Films by Two-Angle Ellipsometry". *Thin Solid Films* **347**, 167 - 177 (1999).

[Webe] Weber T., Zernelman B.V., McNew J.A., Westermann B., Gmachl, Parlati F., Söllner T.H. and Rothman J.E. "SNAREpins: Minimal Machinery for Membrane Fusion". *Cell* **92**, 759 - 772 (1998).

[Wenn] Wennertroem H. "personal communication". (2001).

[Wied] Wieder H. (2000), "Festkörperunterstützte Lipid-Modellmembranen auf Gold zur Rekonstitution von Membranproteinen", *PhD thesis,* Johannes Gutenberg Universität, Mainz.

[Wieg] Wiegand G., Jaworek T., Wegner G. and Sackmann E. "Heterogeneous Surfaces of Structured Hairy-Rod Polymer Films: Preparation and Methods of Functionalization". *Langmuir* **13**, 3563 - 3569 (1997a).

[Wieg] Wiegand G., Jaworek T., Wegner G. and Sackmann E. "Studies of Structure and Local Wetting Properties on Heterogeneous, Micropatterned Solid Surfaces by Microinterferometry". *Journal of Colloid and Interface Science* **196**, 299 - 312 (1997b).

[Wieg] Wiegand G., Neumaier K.R. and Sackmann E. "Microinterferometry: Three-Dimensional Reconstruction of Surface Microtopography for Thin-Film and Wetting Studies by Reflection Interference Contrast Microscopy (RICM)". *Applied Optics* **37**, 6892 - 6905 (1998).

[Wilc] Wilchek M. and Bayer E.A. (1990) *Avidin-Biotin Technology,* Academic Press, London.

[Wolf] Wolff O. (1998), "Bestimmung des viskoelastischen Verhaltens dünner und ultradünner Polymerfilme mit Hilfe von Schwingquarzen", *PhD thesis,* Ruprecht-Karls-Universität, Heidelberg.

[Wong] Wong J.Y., Majewski J., Seitz M., Park C.K., Israelachvili J.N. and Smith G.S. "Polymer-Cushioned Bilayers. I. A Structural Study of Various Preparation Methods Using Neutron Reflectometry". *Biophysical Journal* **77**, 1445 - 1457 (1999a).

[Wong] Wong J.Y., Park C.K., Seitz M. and Israelachvili J. "Polymer-Cushioned Bilayers. II. An Investigation of Interaction Forces and Fusion Using the Surface Forces Apparatus". *Biophysical Journal* **77**, 1458 - 1468 (1999b).

[Wüst] Wüstneck R., Wüstneck N., Grigoriev D.O., Pison U. and Miller R. "Stress Relaxation Behaviour of Dipalmitoylphosphatidylcholine Monolayers Spread on the Surface of a Pendant Drop". *Colloids and Surfaces B: Biointerfaces* **15**, 275 - 288 (1999).

[Yami] Yaminsky V., Nylander T. and Ninham B. "Thermodynamics of Transfer of Amphiphiles between the Liquid-Air Interface and a Solid Surface - Wetting Tension Study of Langmuir-Blodgett Films". *Langmuir* **13**, 1746 - 1757 (1997).

[Yasu] Yasuda T., Okuno T. and Yasuda H. "Contact Angle of Water on Polymer Surfaces". *Langmuir* **10**, 2435 - 2439 (1994).

[Yate] Yates D.E., Levine S. and Healy T.W. "Site-Binding Model of the Electrical Double Layer at the Oxide/water Interface". *Journal of the Chemical Society Faraday Transactions I* **70**, 1807 - 1818 (1974).

[Zaum] Zaumseil J., Wittstock G., Bahrs S. and Steinrücke P. "Imaging the Activity of Nitrate Reductase by Means of a Scanning Electrochemical Microscope". *Fresenius Journal of Analytical Chemistry* **367**, 352 - 355 (2000).

[Zieg] Ziegler J. (2000), "Schichtpräparation und Charakterisierung von Wellenleitern aus Polymeren", Johannes Gutenberg Universität, Mainz.

[Zieg] Ziegler W., Gaburjakova J., Gaburjakova M., Sivak B., Rehacek V., Tvarozek V. and Hianik T. "Agar-Supported Lipid Bilayers - Basic Structures for Biosensor Design. Electrical and Mechanical Properties". *Colloids and Surfaces A: Physicochemical and Engineering Aspects* **140**, 357 - 367 (1998).